Peripheral Quantitative Computed Tomography (pQCT)-based Finite Element Modelling And Its Application in Different Populations

Hongyuan Jiang

ORCID identifier: 0000-0003-0297-1671

Doctor of Philosophy

July 2020

Faculty of Medicine, Dentistry and Health Sciences

Department of Medicine, Royal Melbourne Hospital

Submitted in total fulfilment for the degree of Doctor of Philosophy at the University of Melbourne

ABSTRACT

Background:

Dual energy X-ray absorptiometry (DXA), as the most established tool for the assessment of bone fragility, has limitations in identifying individuals with increased fracture risk. Peripheral quantitative computed tomography (pQCT) can provide additional information about bone fragility compared with DXA alone. The three-dimensional data acquired by peripheral quantitative computed tomography are a potential source to generate finite element analysis (FEA) models to further estimate bone mechanical properties.

Aims:

This doctoral project aimed to establish a FEA model based on pQCT data (pQCT-FEA) and to investigate its role in the assessment of bone fragility in three populations: older patients with low-trauma fracture, women following surgical menopause and young women with type 1 diabetes mellitus (T1DM).

Methods:

This project consisted of four parts. In the first study, FEA models were established using distal radius pQCT cross-sections and were validated against forearm failure load obtained from mechanical testing in laboratory. In the second study, variables of DXA, standard pQCT and pQCT-FEA were compared between older patients with low-trauma fracture and controls. Their ability to classify the two groups were also examined. In the third study, bone loss was examined

between women who received and who did not receive hormone therapy following risk reducing bilateral salpingo-oophorectomy (RRBSO) and controls. In the fourth study, comparison was made in DXA, standard pQCT and pQCT-FEA variables between young women with T1DM and age-, height- and weight-matched controls.

Results:

For Study 1, high coefficient of determination (highest $r^2 = 0.86$) was observed between pQCT-FEA stiffness variables and forearm failure load. For Study 2, there were significant difference in pQCT-FEA stiffness variables between fracture patients and controls. Enhanced area under the receiver operating characteristic curve (AUROC) was found in pQCT-FEA stiffness variables in both females (0.83 for shearing stiffness) and males (0.81 for bending stiffness) compared with DXA variables (0.71 and 0.62, respectively, for total hip areal bone density). For Study 3, an average 14.1% decrease was observed in bending stiffness by pQCT-FEA in women who did not receive hormone therapy following surgical menopause. Although DXA can also detect bone loss over the 24 months follow up, the change was smaller (up to 6.0% at the femoral neck). At the 24 months visit, pQCT-FEA variables differ between women following surgical menopause and controls. For Study 4, no difference was observed in DXA measurements between young women with T1DM ($p \geq 0.08$) although there was a trend towards lower aBMD at the lumbar spine in T1DM subjects than in controls after adjustment for confounders ($p = 0.053$). Significantly lower stiffness by pQCT-FEA was detected in young women with T1DM.

Conclusions:

pQCT-FEA has good ability to predict bone failure load obtained from mechanical testing, which facilitates its application in clinical settings. It can provide additional information about bone strength deficits in patients with fragility fracture, women following surgical menopause and young women with T1DM. These findings warrant future study using pQCT-FEA for the assessment of bone fragility in other populations.

DECLARATION

This is to certify that:

i. the thesis comprises only my original work towards the PhD except where indicated in the preface,

ii. due acknowledgement has been made in the text of all other material used,

iii. the thesis is fewer than 100 000 words in length, exclusive of tables, maps, bibliographies and appendices

Hongyuan Jiang

PREFACE

This thesis contains published work and work that is written de novo and specifically for the thesis. With the exception of Appendix 2, I am the primary author responsible for the planning, execution and preparation of all the work presented and contributed approximately 80 – 90% of the content. I have listed all co-authors on the title page of relevant thesis chapters. I am the first author of the publication included as Appendix 1. The work based on Appendix 1 was performed when I was pursuing the degree of Master of Biomedical Science with the University of Melbourne and led directly to my research work when pursuing the degree of PhD. I am the second author of the publication included as Appendix 2 which was completed during my study for this degree of PhD and this is noted on the title page of that section.

In addition to recognising the contribution of my doctoral supervisors, Emeritus Prof John D Wark, Dr Dale L Robinson, A/Prof Christopher J Yates, Prof Peter VS Lee to this thesis, I would like to acknowledge the following collaborators who contributed to the work presented:

Chapter 4	Matthew McDonald, Saija A Kontulainen, James D Johnston
Chapter 6	Efrosinia O Krejany, Martha Hickey
Chapter 7	Alison Nankervis, Suzanne M Garland, Emma T Callegari, Sarah Price
Appendix 1	Alexandra Gorelik, Ashwini Kale, Qichun Song
Appendix 2	Qichun Song

ACKNOWLEDGEMENTS

This thesis would not have been possible without the support of many individuals.

Foremost I would like to thank my supervisors: Emeritus Professor John D Wark, my primary supervisor, who willingly offered a young man an opportunity into the field of bone and mineral research when I approached him five year ago; who provided fully professional supervision but also encouraged me to explore research questions myself; his help during the last few years to me was not only academic but also personal. And Dr Dale L Robinson, my co-supervisor, whose expertise guided a layman of engineering into a new domain; this work would not have been achievable without his constantly and patiently technical support. I would also like to thank other co-supervisors, Associate Professor Christopher J Yates, who facilitated recruitment of the primary fracture cohort and offered intellectual input into many aspects of the sub-studies; and Professor Peter VS Lee, who provided me unconditional access to the essential engineering facilities in his department. When looking back over my PhD life, I felt grateful for the support and encouragement they have offered, and it was my fortune and honour to be their students.

I would also like to express my gratitude to my collaborators of each sub-study: Mr Matthew McDonald, Professor Saija Kontulainen and Professor James D Johnston for the validation study (Chapter 4); Ms Efrosinia O Krejany and Professor Martha Hickey for the study on women with surgical menopause (Chapter 6); Dr Emma T Callegari, Dr Sarah Price, Associate Professor Alison Nankervis and Professor Suzanne M Garland for the study on young women with T1DM (Chapter 7).

I gratefully acknowledge the funding received from the China Scholarship Council (CSC, reference: CSC201608240003) and the University of Melbourne that provided living allowances and tuition fee waiver for me to conduct this doctoral project in the far south away from my home country.

I would also like to say a heartful thank you to my Mum and Dad for believing in me and encouraging me to follow my dreams. Thank you for providing unconditional support during my pursuing the PhD degree.

I owe my deepest gratitude to my wife, Yang, for her affection, encouragement, understanding and patience that enables me to fulfil ambitions that would otherwise remain dreams. Your accompany has been the best gift I have ever received.

Finally, I would like to dedicate this thesis to my my little princesses, Luna and Mika, who came into my life during production of this work. You have made me stronger, better and more fulfilled than I could have ever imagined. Thank you for being my honey and I love you more than three thousand.

PUBLICATIONS ARISING FROM THIS THESIS

Original papers published

CHAPTER 4, published by Bone on 28 August 2019: Jiang H, Robinson DL, McDonald M, Lee PVS, Kontulainen SA, Johnston JD, Yates CJ, Wark JD. Predicting experimentally-derived failure load at the distal radius using finite element modelling based on peripheral quantitative computed tomography cross-sections (pQCT-FE): a validation study. Bone, 2019; 129: 115051. doi: 10.1016/j.bone.2019.115051

CHAPTER 5, published by Osteoporosis International on 13 November 2019: Jiang H, Robinson DL, Yates CJ, Lee PVS, Wark JD. Peripheral quantitative computed tomography (pQCT)-based finite element analysis provides enhanced diagnostic performance in identifying non-vertebral fracture patients compared with dual energy X-ray absorptiometry. Osteoporosis International, 2020; 31(1): 141-151. doi: 10.1007/s00198-019-05213-1

CHAPTER 7, published by Journal of Clinical Densitometry on 28 May 2020: Jiang H, Robinson DL, Nankervis A, Garland SM, Callegari ET, Price S, Lee PVS, Wark JD. Bone measures by dual energy x-ray absorptiometry and peripheral quantitative computed tomography in young women with type 1 diabetes mellitus. Journal of Clinical Densitometry, 2020; in press. doi: 10.1016/j.jocd.2020.05.009

APPENDIX 2, published by Biomechanics and Modeling in Mechanobiology on 6 October 2018: Robinson DL, Jiang H, Song Q, Yates C, Lee PVS, Wark JD. The application of finite element modelling based on clinical pQCT for classification of fracture status. Biomechanics and Modeling in Mechanobiology, 2019; 18(1): 245-260. doi: 10.1007/s10237-018-1079-7

Original Papers Submitted for Publication And Currently Under Review

CHAPTER 6, submitted to Osteoporosis International on 23 February 2020: Jiang H, Robinson DL, Yates CJ, Lee PVS, Krejany EO, Hickey M, Wark JD. Loss of bone density and bone strength following premenopausal bilateral oophorectomy: Results from a prospective study (WHAM Study).

Conference Abstracts

Jiang H, Robinson DL, Lee PVS, Yates CJ, Wark JD. Peripheral quantitative computed tomography based finite element modelling (pQCT-FE) in the classification of fracture patients. American Society of Bone and Mineral Research Annual Meeting, Montreal Canada, 2018. (ASBMR young investigator travel grant)

Jiang H, Robinson DL, Yates CJ, Lee PVS, Hickey M, Wark JD. Bone loss following risk reducing bilateral salpingo-oophorectomy in women with increased risk for breast and ovarian cancer: preliminary results from WHAM study. Australian and New Zealand Bone and Mineral Society Annual Scientific Meeting, Queenstown New Zealand, 2018. (Christopher & Margie Nordin Young Investigator Poster Award finalist; ANZBMS young investigator travel grant)

Jiang H, Robinson DL, McDonald M, Kontulainen S, Johnston JD, Lee PVS, Wark JD. Prediction of distal radius failure load using finite element modelling of peripheral quantitative computed tomography (pQCT-FE): a validation study. American Society of Bone and Mineral Research Annual Meeting, Denver USA, 2017.

Robinson DL, Song Q, Jiang H, Hickey M, Lee PVS, Wark JD. Enhanced fracture risk classification based on finite element modelling of clinical tibia pQCT. The 17th Congress of the International Society of Biomechanics, Brisbane Australia, 2017. (oral presentation)

Robinson DL, Song Q, Jiang H, Lee P, Wark JD. Finite element analysis based in pQCT imaging to improve assessment of fracture risk. American Society of Bone and Mineral Research Annual Meeting, Atlanta USA, 2016.

TABLE OF CONTENTS

LIST OF TABLES

LIST OF FIGURES

ABBREVIATIONS

25-OHD	Twenty-five-hydroxyvitamin D
aBMD	Areal bone mineral density
ALT	Alanine aminotransferase
ANOVA	Analysis of variance
AP-1	Activator protein-1
AUROC	Area under the receiver operating characteristic curve
bCTX	beta-carboxy-terminal cross-linking telopeptide of type 1 collagen
BDU	Bone densitometry unit
BMC	Bone mineral content
BMD	Bone mineral density
BMI	Body mass index
BMU	Basic multicellular unit
BRCA	breast-cancer susceptibility gene
BS	Bone surface
BSI	Bone strength index
BS/BV	Bone surface ratio
BTM	Bone turnover marker
BUN	Blood urea nitrogen
BV	Bone volume
BV/TV	Bone volume ratio
CI	Confidence interval
Crt BMC	Cortical bone mineral content (measured by pQCT)

Crt CSA	Cortical cross-sectional area (measured by pQCT)
Crt Thk	Cortical thickness (measured by pQCT)
Crt vBMD	Cortical volumetric bone mineral density (measured by pQCT)
CSA	Cross-sectional area
CSMI	Cross-sectional moment of inertia
CT	Computed tomography
Ct.BMD	Cortical bone mineral density (measured by HR-pQCT)
Ct.Po	Cortical porosity
Ct.Th	Cortical thickness (measured by HR-pQCT)
CV	Coefficient of variation
DM	Diabetes mellitus
DPA	Dual photon absorptiometry
DXA	Dual energy X-ray absorptiometry
EndoC	Endosteal circumference (measured by pQCT)
FE	Finite element
FEA	Finite element analysis
FEM	Finite element modelling
F_{exp}	Experimental failure load
FN aBMD	Femoral neck areal bone mineral density (measured by DXA)
FRAX®	Fracture Risk Assessment Tool
FTIR	Fourier transform infrared
GGT	Gamma-glutamyl transferase
HBA1c	Glycated hemoglobin

HDLC	High-density lipoprotein cholesterol
HLA	Human leukocyte antigen
HNPCC	Hereditary nonpolyposis colorectal cancer
HPLC	High pressure liquid chromatography
HR	Hazard ratio
HR-MRI	High-resolution magnetic resonance imaging
HR-pQCT	High-resolution peripheral quantitative computed tomography
HT	Hormone therapy
HU	Hounsfield unit
IGF-1	Insulin like growth factor-1
ISCD	International Society for Clinical Densitometry
ITS	Individual trabecular segmentation
$\mathbf{k_{bend}}$	Bending stiffness (calculated by pQCT-FEA)
$\mathbf{k_{comp}}$	Compression stiffness (calculated by pQCT-FEA)
$\mathbf{k_{shear}}$	Shearing stiffness (calculated by pQCT-FEA)
$\mathbf{k_{torsion}}$	Torsion stiffness (calculated by pQCT-FEA)
LDLC	Low-density lipoprotein cholesterol
LS aBMD	Lumbar spine areal bone mineral density (measured by DXA)
MCSA	Muscle cross-sectional area (measured by pQCT)
µCT	Micro computed tomography
µFE	Micro finite element
MDen	Muscle density (measured by pQCT)
MRI	Magnetic resonance imaging

MrOS	Osteoporotic Fractures in Men study
NF- κB	Nuclear factor κB
NHANES	National Health and Nutrition Examination Survey
NHMRC	National Health and Medical Research Council
NIH	National Institutes of Health
OPG	Osteoprotegrin
OR	Odds ratio
P1NP	Procollagen type 1 N propeptide
PBM	Peak bone mass
PeriC	Periosteal circumference (measured by pQCT)
PMMA	Polymethylmethacrylate
POI	Premature ovarian insufficiency
pQCT	Peripheral quantitative computed tomography
pQCT-FE	Peripheral quantitative computed tomography-based finite element
pQCT-FEA	Peripheral quantitative computed tomography-based finite element analysis
PTH	Parathyroid hormone
QALY	Quality-adjusted life years
QCT	Quantitative computed tomography
QUS	Quantitative ultrasound
r^2	Coefficient of determination
RANK	Receptor activator of nuclear factor κB
RANKL	Receptor activator of nuclear factor κB ligand
RR	Relative risk

RRBSO	Risk-reducing salpingo-oophorectomy
RUNX2	Runt-related transcription factor 2
S_{bend}	Bending strength (calculated by pQCT-FEA)
S_{comp}	Compression strength (calculated by pQCT-FEA)
SD	Standard deviation
SPA	Single photon absorptiometry
S_{shear}	Shearing strength (calculated by pQCT-FEA)
SSI	Stress strain index
SSI_p	Polar stress strain index
$S_{torsion}$	Torsion strength (calculated by pQCT-FEA)
SV	Scout view
SXA	Single X-ray absorptiometry
T1DM	Type 1 diabetes mellitus
T2DM	Type 2 diabetes mellitus
Tb.BMD	Trabecular bone mineral density (measured by HR-pQCT)
Tb.N	Trabecular number
Tb.Sp	Trabecular separation
Tb.Th	Trabecular thickness
TGF β	Transforming growth factor β
TH aBMD	Total hip areal bone mineral density (measured by DXA)
TNF-α	Tumour necrosis factor-α
To.Ar	Total bone area (measured by HR-pQCT)
To.BMD	Total bone mineral density (measured by HR-pQCT)

Tot BMC	Total bone mineral content (measured by pQCT)
Tot CSA	Total cross-sectional area (measured by pQCT)
Tot vBMD	Total volumetric bone mineral density (measured by pQCT)
Trb BMC	Trabecular bone mineral content (measured by pQCT)
Trb CSA	Trabecular cross-sectional area (measured by pQCT)
Trb vBMD	Trabecular volumetric bone mineral density (measured by pQCT)
TSH	Thyroid stimulating hormone
TV	Total volume
UK THIN	United Kingdom Health Improvement Network
vBMD	Volumetric bone mineral density
VIF	Variance inflation factor
WB aBMD	Whole-body areal bone mineral density (measured by DXA)
WB BMC	Whole-body bone mineral content (measured by DXA)
WHAM	What Happens After Menopause study
WHO	World Health Organization
YFHI	Young Female Health Initiative study

Chapter 1

Introduction

Clinical assessment of bone fragility is based on dual energy x-ray absorptiometry (DXA) in clinical settings although it has limitations in identifying individuals with increased fracture risk. This thesis describes a novel yet relatively simple finite element modelling (FEM) framework based on peripheral quantitative computed tomography (pQCT) cross-sectional images and its application in different populations.

A literature review is first presented in Chapter 2 to discuss the background information of bone biomechanics and biology, current assessment tools of bone strength, limitations of DXA, strengths of pQCT and the feasibility of using pQCT-based finite element analysis (FEA; pQCT-FEA) as a complementary or even alternative tool for the assessment of bone fragility in clinical settings. Current utility of finite element analysis in the assessment of bone fragility is also discussed in this chapter, followed by current knowledge of bone fragility from different clinical aspects including osteoporosis, surgical menopause and type 1 diabetes.

A validation study of pQCT-FEA against mechanical tests of cadaveric forearms is detailed in Chapter 3. Bone strength and stiffness estimates calculated from pQCT-FEA was compared with bone failure load obtained in the laboratory in this study. Chapter 3 is a chapter by publication, the data of which has been published in the journal Bone.

In Chapter 4, the diagnostic performance of the pQCT-FEA technique was examined by comparing finite element (FE) variables with DXA variables in distiguishing older patients with low-trauma fracture from healthy controls. This chapter is a chapter by publication, the data of which has been published in the journal Osteoporosis International.

The FEM framework is utilised in the following chapters. Chapter 6 examined bone health following surgical menopause caused by risk-reducing salpingo-oophorectomy (RRBSO) and the role of hormone therapy (HT) in preserving bone density and bone strength among women who had undergone this procedure. This chapter is a chapter by publication and is under review by the journal Osteoporosis International when this thesis is submitted.

Bone health of young adult women with type 1 diabetes mellitus (T1DM) was examined and compared with age-, height- and weigh-matched controls in Chapter 7. This chapter is a chapter by publication and is under review by the journal Calcified Tissue International when this thesis is submitted.

Finally, in Chapter 8, a brief summary is concluded for the potential use of pQCT-FEA for the assessment of bone fragility in clinical settings. Future research directions are also proposed in this chapter.

This thesis, as a whole, is an extension of a research project conducted during my degree of Master of Science with the University of Melbourne, which explored the role of standard pQCT variables in the diagnosis of osteoporosis (Appendix 1). Together with the current thesis for the degree of Doctor of Philosophy, the work is believed to contribute to the understanding of bone fragility with the application of pQCT and pQCT-FEA.

Table 1.1 shows the structure of this thesis briefly.

Table 1.1 The brief structure of this thesis

Chapter	Description
Chapter 1 Introduction	This chapter aims to provide a clear structure of the thesis for potential readers
Chapter 2 Literature review	This chapter provides background information on: (1) basic knowledge of bone mechanics and bone biology, (2) various tools for assessment of bone fragility, and (3) bone fragility in osteoporosis, surgical menopause and T1DM
Chapter 3 Aims and methods	This chapter describes research aims of the thesis and general methodology applied in each study
Chapter 4 Validation study	This chapter by publication validated pQCT-FEA models used in the following chapters by comparing pQCT-FEA variables with bone failure load obtained from cadaveric mechanical tests
Chapter 5 Fracture study	This chapter by publication compared the diagnostic performance of pQCT-FEA in older patients with low-trauma fracture with healthy controls
Chapter 6 WHAM study	This chapter by publication examined bone health RRBSO and the effect of HT using DXA, standard pQCT and pQCT-FEA variables
Chapter 7 T1DM study	This chapter by publication examined bone health in young adult women with T1DM using DXA, standard pQCT and pQCT-FEA variables
Chapter 8 Summary	This chapter summarises findings from studies above and discusses potential future research directions using pQCT-FEA
Appendices	Appendix 1 is the work on the role of standard pQCT variables in the understanding of bone fragility during my Master of Science. Appendix 2 is the preliminary work on pQCT-FEA addressed in Chapter 5.

Chapter 2

Literature review

2.1 Bone mechanical properties and the biological basis

2.1.1 Introduction

The human skeletal system provides structural support of the body and protection of the internal organs and serves as a primary reservoir to maintain mineral homeostasis (1). Bone is considered as a solid structure that breaks to failure (i.e. fracture) when external forces go beyond its loading limit, in which the basic functioning of the human skeleton will be impacted with potentially catastrophic consequences. Mechanical properties of whole-bone as a solid structure are dependent on two aspects: material and structure (2). From a clinical perspective, doctors and medical scientists are investing considerable efforts in developing novel technology for the assessment of bone fragility and new therapeutics to prevent fracture in different populations. These efforts are based on, at least in part, the knowledge of basic mechanical properties of bone and are applied in the fields of biomechanics and orthopaedics, as well as research on bone fragility. In this section of the literature review, background information on bone mechanical properties is discussed from first a material and then a structural perspective. As bone is arranged hierarchically from macro scale to micro scale and then to molecular scale biologically, this part of the literature review will also discuss the related biological background in this order.

This section is not intended to provide an extended review on our current understanding of basic science but aims to introduce relevant background knowledge on biomechanics and biology that applies in the utility of the finite element analysis (FEA) based on pQCT, which is the main topic of this thesis. As pQCT scans appendicular skeleton, i.e. the radius, tibia and sometimes femur, discussion in this section mainly focuses on long bones that approximate a hollow cylindrical tube in biomechanics and biomechanical engineering (3 - 5).

2.1.2 Stress and strain

When we discuss material properties of bone, structural factors are 'normalised out' to reflect bone's intrinsic characteristics. In engineering, stress (σ) and strain (ε) are defined to normalize the geometric design which also contributes to the strength of a whole-bone (2). Stress is defined as the external force applied per unit area of a material (Equation 1), which is quantified in the unit of N/m^2 (i.e. Pascal).When an external force is applied on a long bone, one can imagine two types of stress acting on the surface of small cubes (or 'elements' as in finite element models which will be discussed later) in the structure: normal stress perpendicular to the surface and shear stress tangential to the surface (Figure 2.1).

$$\sigma = \frac{F}{A} \tag{1}$$

where σ is stress, F is the external force applied, A is cross sectional area of the material

Strain describes as the deformation of material, relative to its initial size. Two types of strain may be calculated, normal strain defined as the change in length per unit length, or shear strain which is defined by the change in angle of a shape from its unloaded geometry (Figure 2.2). Equations 2 – 4 show the calculation of strains in different situations.

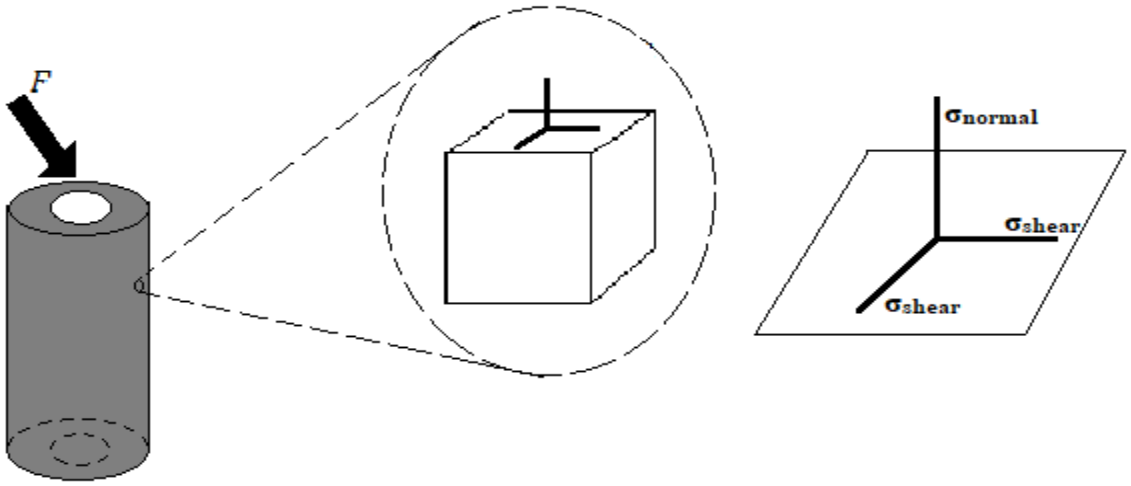

Figure 2.1. Normal and shear stress. F: the external force acting on the long bone, σ_{normal}: normal stress, σ_{shear}: shear stress

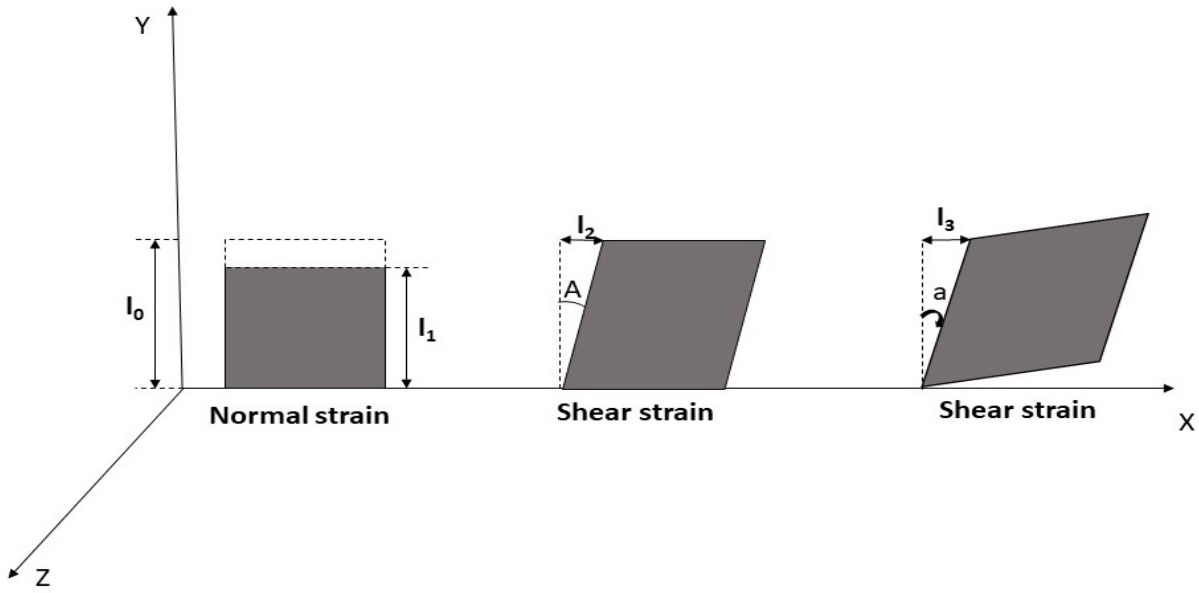

Figure 2.2. Normal and shear strains. In the three situations, deformations are along with X-, Y- and Z-axis, respectively. l_0: the original length of the material, l_1: the length of the material after the deformation is along the Y-axis, l_2: the replacement of the material along the X-axis, A: the deformational angle along the X-axis, l_3: the replacement along the Z-axis, a: the deformational angle along the Z-axis. Calculation of strains is shown in Equation 2 – 4.

$$\varepsilon = \frac{l_1 - l_0}{l_0} \quad (2)$$

where ε is strain, l_1 is the length of the material after the deformation is along the Y-axis, *l_0 is the original length of the material*

$$\varepsilon = \frac{l_2}{l_0} = tan\ A \quad (3)$$

where ε is strain, l_2 is the replacement of the material along the X-axis, *l_0 is the original length of the material, A is the deformational angle along the X-axis*

$$\varepsilon = \frac{l_3}{l_0} = tan\ a \quad (4)$$

where ε is strain, l_3 is the replacement along the Z-axis, *l_0 is the original length of the material, a is the deformational angle* along the Z-axis

2.1.3 Young's modulus

A stress-strain curve can be obtained by plotting stress against strain to directly show the mechanical properties of a material (Figure 2.3). As shown in the figure, there are two parts of the curve: the linear part (elastic phase) and the non-linear part (plastic phase). The point that divides the two phases (point A in Figure 2.3) is called yield point. When stress exceeds the yield stress, the material deforms plastically (i.e. the material cannot recover to its original length after the external force is removed, which contrasts with elastic deformation,

where the material is able to recover to its original length after the external force is removed). When the external force continues, the material will then reach a point where a catastrophic fracture occurs (failure point, point B in Figure 2.3). In the elastic phase of bone material, stress and strain have a linear correlation that complies with the Hooke's law, which identifies a constant slope for each elastic material (most solids are elastic material) (6). This constant for each material is defined as elastic modulus or Young's modulus (*E*). Young's modulus is an intrinsic property of solid material (7).

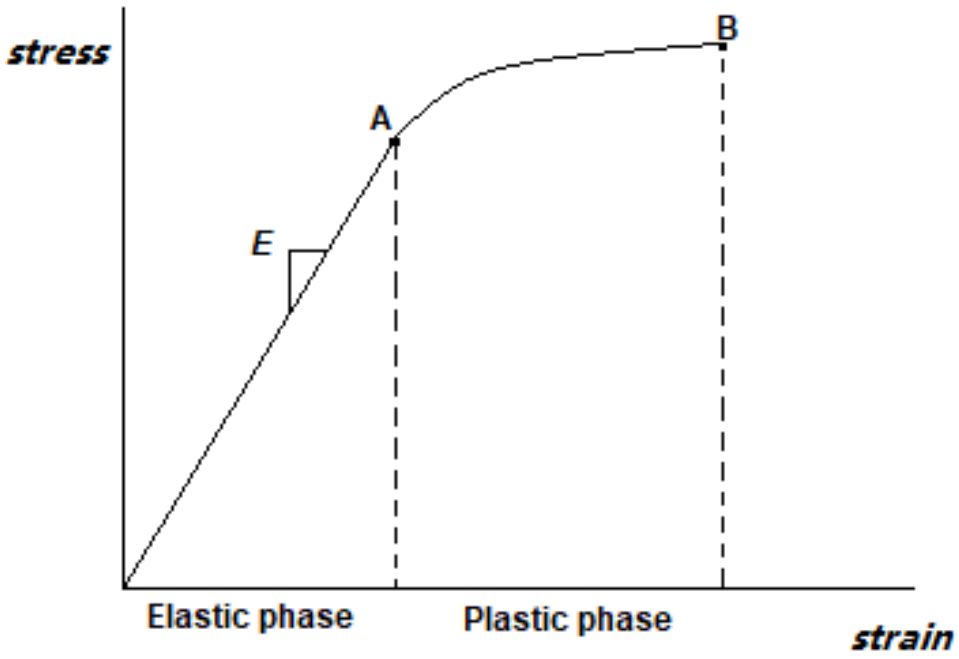

Figure 2.3. Stress strain curve of bone. A: yield point, B: failure point, E: elastic modulus or Young's modulus, which is the slope of the elastic phase

2.1.4 Whole-bone strength and stiffness

Whole-bone mechanical properties depend not only on intrinsic material characteristics but also on structural factors (2). Similar to solid material properties, mechanical properties of solid structure can also be reflected by certain plots. A load-deformation plot is obtained by plotting external load against deformation of the structure (Figure 2.4). Similarly, two phases (elastic phase and plastic phase) make up the curve.

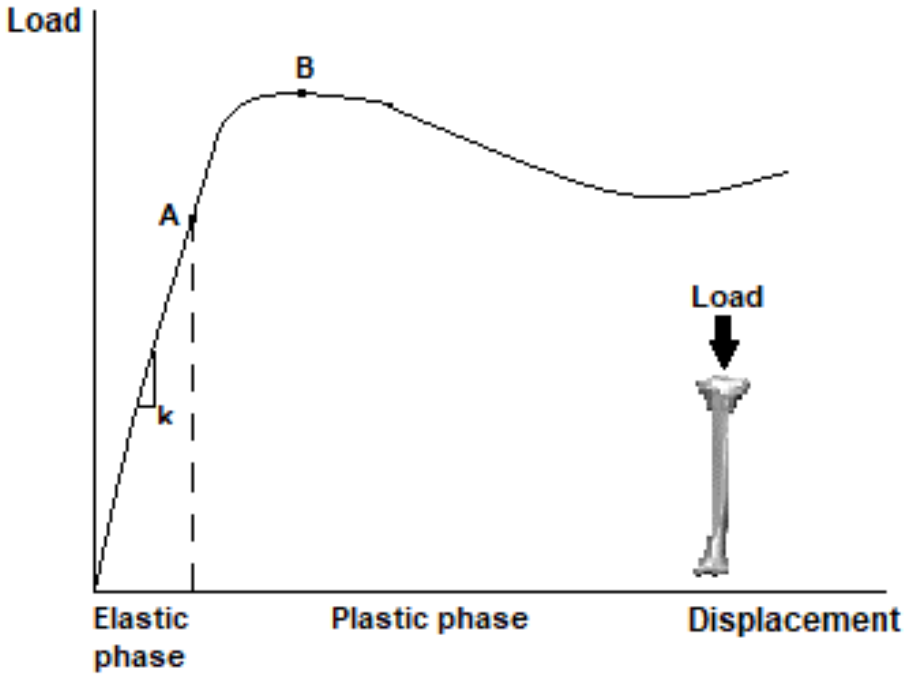

Figure 2.4. Load-deformation curve of the tibia. A: yield point, B: failure point, *k*: stiffness of the tibia.

At the elastic phase, bone (the tibia as in Figure 2.4) deforms elastically when the external load does not exceed the yield point of the tibia. Load and displacement have a linear correlation with each other. The slope is defined as the whole-bone stiffness (*k*). At the plastic phase after the external load exceeds the yield load, beyond which irreversible plastic

deformation occurs, the slope of curve begins to decrease (8). The point dividing the two phases is the yield point (point A in Figure 2.4). Failure point is the point when a catastrophic fracture occurs (point B in Figure 2.4). The definition of the structure strength is tricky as either yield load or failure load can be called structure strength depending on the situations where the name is used. However, whole-bone strength is often referred to failure load in biomechanics (2). The structure stiffness is defined as the external load needed to the deform a certain extent of the structure within the elastic phase (Equation 5).

$$k = \frac{Load}{Displacement} \tag{5}$$

where k is the structure stiffness

When an external force is applied to a structure, the change in shape is usually in three dimensions. For example, as shown in Figure 2.5, when a long bone is compressed longitudinally, it becomes shorter along with the direction of the force applied but wider perpendicular to the force. In biomechanics, Poisson's ratio is defined to describe the ratio of transversal change to longitudinal change (Equation 6). Poisson's ratio is an intrinsic material property. The Poisson's ratio of bone is about 0.3 (9).

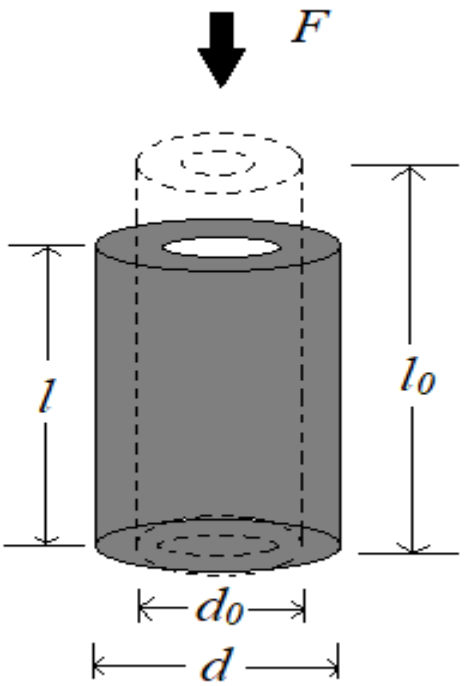

Figure 2.5. A diagram showing how Poisson's ratio is calculated. *F*: external force applied, d_0: original diameter of the cross section, *d*: diameter of the cross section after the external force is applied, l_0: original length, *l*: length after the external force is applied

$$Poisson'sratio = \frac{\Delta d}{\Delta l} = \frac{d-d_0}{l_0-l} \quad (6)$$

where Δd is the transversal change in cross-sectional diameter, Δl is the longitudinal change in length, d is the diameter of the cross section after the external force is applied, d_0 is the original diameter of the cross section, l_0 is the original length, l is the length after the external force is applied

From an engineering perspective, stiffness and strength are two components reflecting different aspects of mechanical behaviour. While strength measures how much stress can be

applied to an object before it deforms permanently, stiffness is an indicator of the tendency for an object to return to its original form after being subjected to a force. Therefore, a strong object can be either stiff or elastic. However, when we talk about bone, difference between stiffness and strength has been observed to be less. Mechanical testing has shown strong correlations between bone stiffness and bone strength at both structural and tissue levels (10 - 15), especially in axial loading of compression and tension of long bones (15, 16). Although the strong correlations varied between different ages, skeletal sites and species (17, 18), these findings enlighten future studies using stiffness for the assessment of bone strength, since strength is somewhat difficult to obtain (this will be discussed in Section 2.5) even in computational simulations. In fact, simulated bone stiffness is widely used to assess bone mechanical properties in current FEA research (19 - 21).

2.1.5 Different loading modes

The aforementioned structural mechanical properties of bone specifically describe axial compression. In the real world, a combination of different loads e.g. compression, tension, shearing, bending and torsion applies to whole-bone (Figure 2.6). The skeleton exhibits differences in response to different loadings due to variations in the spatial distribution of bone mass and arrangements of cortical and trabecular bone (22 - 24). Therefore, variations in strength and stiffness may be observed at different skeletal sites under different loads (25 - 28). For example, cortical bone resists compressive loads more than bending or shearing loads (9, 26, 29, 30). On the other hand, trabecular bone behaves less predictably due to its structural characteristics (25, 31 - 33). In summary, the whole-bone mechanical reaction to various loads is very complex; therefore, simplification is needed to provide practical ways to assess bone strength and stiffness from a clinical perspective.

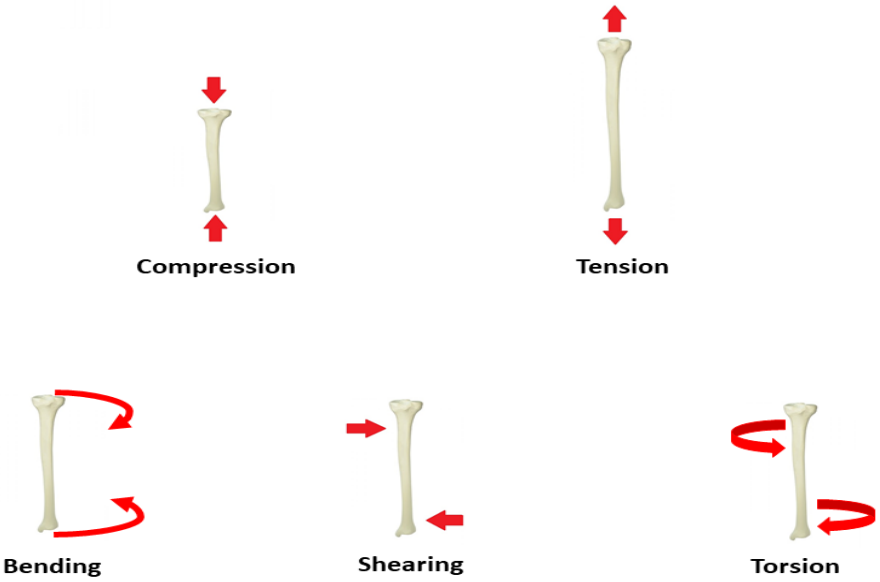

Figure 2.6 Different load cases at the tibia

2.1.6 Cortical and trabecular bone

The functions of the human skeletal system are based on its composition and organization that are optimized for the daily loads we experience (34). There are two types of bone in the healthy mature skeleton at a tissue level: cortical bone and trabecular bone, that contribute differently to the whole-bone strength (35, 36). Cortical bone is the compact part of the skeleton (Figure 2.7), which has higher density and less porosity than trabecular bone. It forms the shaft of a long bone and constitutes most of the bone mass of healthy adults' appendicular skeleton (37, 38). Trabecular bone is the spongy part with lower density and more porosity that fills in the distal or proximal ends of long bones (Figure 2.7). Although accounting for only about 20% of whole-bone mass, trabecular bone is more metabolically active than cortical bone due to its large surface that is subject to bone remodelling (39). Trabecular bone is designed in the form of an interconnected porous network by units of

individual trabeculae, which presents struts and plates of bone matrix. Although trabeculae are sometimes in a well-organized form of orthogonal arrays to act as a ‘buffer zone’ and to transfer loading to the stronger cortical shell at long bones (40), they are arranged more randomly than cortical bone more often (41).

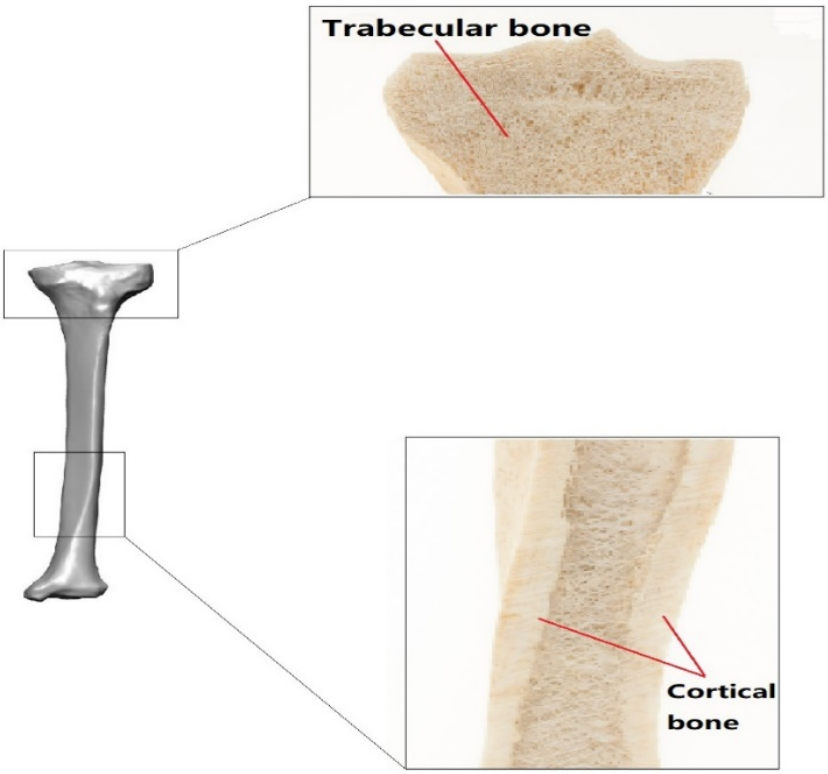

Figure 2.7. Cortical and trabecular compartments of the tibia. As shown in the figure, cortical is more compact than trabecular bone. Trabecular has more pores that are connected with each other and are filled with bone marrow.

It is a long-held notion that bone fragility is largely associated with trabecular bone loss after menopause. As discussed above, trabecular bone has more porous structure providing a large

surface for metabolism; therefore, it changes promptly with ageing and certain medical conditions than cortical bone (42, 43). This is evidenced by the fact that trabecular bone is compromised more than cortical bone in menopausal vertebrae Observed both in laboratory and in clinical settings (44 - 49). However, this conception has been changing recently (37, 50), especially at the appendicular skeleton, where the incidence of low-trauma fracture is reported to be much higher than of central skeleton in older patients (51, 52). Cortical bone is considered to have less opportunity than trabecular bone to be remodelled due to its design although it contributes up to 80% of bone mass (37). However, increased porosity has been observed at the intracortical surface in older osteoporotic patients (53, 54). This is of great clinical importance as up to 90% of longitudinal compression load is born by the cortical shell in long bones (55, 56). Although the role of cortical porosity in compromising bone strength still needs to be confirmed with more evidence, these findings suggest that cortical bone may contribute more than trabecular bone to long bone strength. Therefore, separate analysis of cortical and trabecular compartments of bone may enhance our understanding of bone fragility in future studies.

From a histological level, both cortical and trabecular bone are comprised of two kinds of bone tissue. Lamellar bone is a well-organized, stress-oriented bone tissue that usually forms mature bone, while woven bone is poorly-organized with collagen fibrils arranged randomly. Woven bone is seen in immature bone, fracture callus or pathological bone. The difference in structure decides their different mechanical behaviours. Lamellar bone is strong and stiffer than woven bone, while woven bone is more flexible. These characteristics of lamellar and woven bone together contribute to the final mechanical performance of whole-bone.

Table 2.1 Summarized characteristics of lamellar bone and woven bone

	Lamellar bone	Woven bone
Presence	Mature bone	Immature bone, fracture healing, pathological bone e.g. Paget's disease
Structure characteristics	Lamellae: well organized, stress-oriented, parallel to collagen fibrils	Poorly organized, collagen fibrils randomly arranged
Formation	Slow, remodelled from woven bone	Quick
Mechanical properties	Stronger, stiffer	Weaker, more flexible
Osteocyte number	Less	More

2.1.7 Cortical geometry

As discussed above, the intrinsic material properties of human skeleton are relatively stable. Variations in bone geometry are therefore important in determining whole-bone mechanical behaviour (57). For example, a bigger bone is stronger than a smaller bone. This is not only intuitively correct but is also supported by scientific evidence (58, 59). Although from a topology perspective, the shapes of bones are conservative between individuals, the sizes of bone may vary to a greater extent. When a long bone is assumed as a hollow cylindrical tube, its geometric characteristics are shown to be associated with bone strength and fracture incidence (32, 60, 61). A higher incidence of fracture has been observed in males with thinner cortical shell than with thicker one (62), which suggests cortical thickness is positively

correlated with bone strength (63, 64). Variations in bone strength between different ethnic groups and sexes have also been explained by cortical cross-sectional area (CSA) (65, 66). The cross-sectional diameter is an important factor that influences how much the bone can bear external loading. Its role in maintaining skeletal integrity is reported to be more important than bone mass, which is reflected by a higher magnitude in resistance to bending load (67, 68).

Figure 2.8 shows the cross-sectional cortical geometry parameters of a long bone. The essence of bone geometry is the spatial distribution of bone mass, which is influenced by many factors, e.g. genes, loading stimuli, ageing, developmental stage, disease states (40). Long bones are designed in an efficient way to resist daily loads applied on them. With a given amount of bone mass, bone's ability to resist compression load that is in the direction aligned with its long axis depends on its CSA. Therefore, long bones with larger CSA (and larger diameter) can resist greater compression loads (57). In bending or torsion loads, this ability depends on how far away bone mass is distributed from long bone's geometric centre, or cross-sectional moment of inertia (CSMI, Figure 2.8). Generally, with a given CSA, long bones with larger CSMI resist greater bending or torsion loads (40). This, again, is positively correlated with cortical diameter.

As early as in 1980, Thompson noted age-related cortical bone loss involved cortical thinning and increased cortical porosity (69). Although an age-related increase in periosteal diameter has been observed, a net cortical thickness loss is confirmed due to gradual bone mass loss (70). At the spine, cortical thickness only slightly decreases with aging due to the cortical shell at this site being very thin itself (71). At the femoral neck, an annual decrease of 6.4%

in cortical thickness was reported at its superioposterior octant, where the highest stress occurs in a sideway fall (72). At the radius and the tibia, changes in cortical dimensions with aging are more quantified by pQCT and HR-pQCT. MacDonald et al reported 31% and 24% decreases in cortical thickness between age 20 – 90 years at the radius and the tibia, respectively, while the increases in cortical porosity were 167% and 259%, respectively (73). However, Nicks et al did not find any difference in cortical thickness between subjects with a mean age of 41 years and 63 years although a higher cortical porosity was highlighted in the older group (92% and 28% for women and men, respectively) (74). Although more details still need exploration about the specific patterns cortical dimensions change with aging, one thing seems sure for now that cortical thinning and cortical porosity increase with aging.

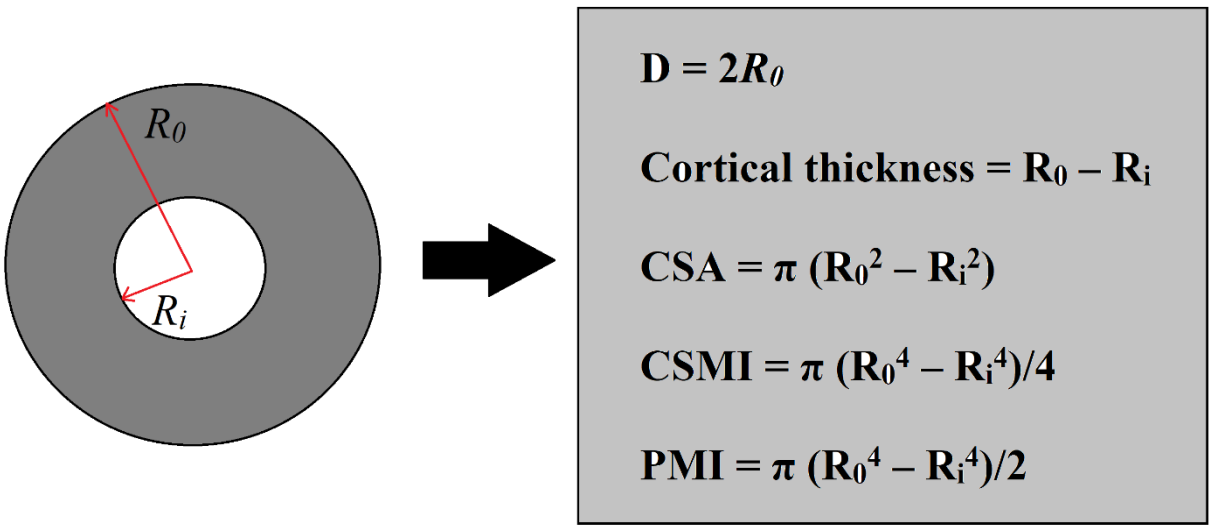

Figure 2.8 Cortical geometry parameters. A long bone approximates a hollow cylindrical tube thus the cross section is considered as circular. R0: cross-sectional perimeter of the cortical shell, Ri: cross-sectional perimeter of the hollow circle, D: cortical diameter, CSA: cross-sectional area, CSMI: cross-sectional moment of inertia, PMI: polar moment of inertia

2.1.8 Trabecular microstructure

Trabecular microstructure *i.e.* the size and spatial distribution, rods and plates, perforation and connectivity of trabeculae also contributes to the whole-bone strength and stiffness, especially at sites where it is trabecular-rich, *e.g.* vertebral body or epiphysis of long bones (75). Osteoporosis in ageing is not only a consequence of decreased bone mass, but, more importantly, also of disrupted trabecular microstructure. This is reflected in the definition of osteoporosis by the National Institutes of Health, which emphasizes compromised trabecular microstructure as a crucial basis for bone fragility (76). Experiments in sheep have shown that up to 70% of the femur's ability to resist axial compression load can be explained by trabecular microstructural properties (77). The resistance of trabeculae to different loads varies and depends on many factors among which the orientation of trabeculae plays an important role (78). The human vertebral body can bear more compression load that is along with trabeculae's vertical orientation compared to load that is antero-posteriorly or laterally directed (75, 79). In the ageing vertebral body, the decrease in transverse-arranged trabeculae is observed to be greater than in vertical-arranged trabeculae (80). Although trabeculae are arranged relatively randomly as discussed previously, the change in their arrangement due to ageing seems to fit for vertebra's mechanical needs. During the process of ageing, individual trabeculae become thinner (*i.e.* more struts, less and thinning plate structure, and more trabecular perforation) progressively. This leads to lower trabecular volume and CSA, reduced trabecular number, thickness and connectivity, and increased trabecular separation. All the deterioration contributes to compromised bone strength independent of cortical change (81).

Before the advent of high-resolution devices that are able to provide bone macrostructural and microstructural measurements in vivo, our understanding of bone fragility at the clinical level was largely limited to bone mass and bone density, which are only part of the whole story. Although bone biopsy enables the examination of more details, this invasive test was not widely applied even at that time. New analysis methods are now exploring more details on these factors which we ignored previously. More details of bone macrostructure and microstructure will be discussed in the following sections of this literature review.

2.1.9 Bone remodelling

The skeleton is a dynamic organ that is metabolically active. Bone remodelling is the process of removal of older bone and replacement with new bone to maintain its mechanical performance, as well as calcium and phosphorus homeostasis (82, 83). Three types of bone cells are involved in the process of remodelling. Osteoclasts are multinucleated cells originating from the monocyte macrophage lineage (84). They are the only known cells that resorb bone. Osteoblasts are mononuclear, cuboidal cells that differentiate from mesenchymal precursor cells. They produce the organic matrix of bone by synthesis and secretion of type 1 collagen and assist in making the newly-produced bone mineralized (85). Osteocytes make up most of the cells in the skeleton. They are derived from osteoblasts trapped in lacunae which have completed the task of bone formation. Osteocytes have long dendritic processes that extend into channels of bone matrix. Together, they form the lacunar-canalicular network that senses mechanical or chemical stimuli and transfers the signal to initiate bone remodelling process (86, 87). After osteocytes activate the remodelling process, osteoclasts are recruited to the site where bone resorption is started (88). Following the end of resorption, osteoblasts migrate to the cavities left by osteoclasts and begin to form new matrix which is

called osteoid. The newly formed matrix has more organic components and less mineral than mature bone matrix until it becomes mineralized under the regulation of several pathways, among which phosphoprotein kinases, alkaline phosphatase and vitamin D work together to assist in the deposition of hydroxyapatite crystals (89, 90). In the whole procedure, osteoclasts and osteoblasts work together in a basic multicellular unit (BMU) to make sure all steps are sequential (91). Normal bone remodelling is a highly-ordered process regulated by various hormones and proteins, both systemically and locally (82). This process of self-adaptation enables homeostasis of bone from a cellular level. More importantly, it stabilizes the whole-bone structure from a macrostructural aspect and prepares the whole-bone for further mechanical loading.

Bone remodelling replaces portions of the skeleton to maintain its mechanical performance under varying loading conditions. In contrast to remodelling, bone modelling refers to the process of independent actions of osteoclasts (bone formation) or osteoblasts (bone resorption) to ‘customise’ the shape and size of bone (92). Therefore, this process is continuous and prolonged without BMU formed. However, it should be noted that many orthopaedists and bone scientists refer to both modelling and remodelling activities as ‘remodelling’, which should be kept in mind in certain situations (91). Main differences between modelling and remodelling are summarised in Table 2.2.

Table 2.2 Summarised differences between bone modelling and remodelling

	Bone modelling	**Bone remodelling**
Definition	Reshaping and/or resizing of bone	Replacement portions of the skeleton
Cells involved	Independent actions of osteoclasts or osteoblasts	Sequential, combined actions of osteoclasts, osteoblasts and osteocytes
Outcome	Change of bone's size, shape, or both	Does not usually affect size and shape
Rate	Greatly reduced after skeletal maturity	Occurs throughout life, although substantially reduced after skeletal maturity too
Process	Continuous and prolonged	Episodic, with each episode having a definite beginning and ending

2.1.10 Collagen and mineral

When bone is studied at a molecular level, it is comprised of organic and mineralized components. Type I collagen is the primary organic component and accounts for one quarter of bone weight. Apatite in the form of hydroxyapatite accounts for up to 65% of bone weight. The rest is water, either in a free or bound form with other molecules. The characteristics of the three components are summarized in Table 2.3.

Table 2.3 Composition of whole-bone from a molecular level

Component	Site of specific molecule	Volume (%)
Water, 10%	Bound	60-80 [a]
	Free	20-40 [a]
Organic matrix, 25%	Collagen	90
	Non-collagenous proteins	10
Apatite mineral, 65%	In gaps between collagen ends	28
	Intrafibrillar	58
	Interfibrillar	14

[a] The precise ratio of bound and unbound water depends on a number of factors, including age

Many factors related to these components influence the mechanical behaviour of bone. Collagen fibrils are considered to strengthen bone. It has been observed that fracture incidence is higher at the tibia with reduced collagen composition (93). Moreover, the cross-linked bond structure between adjacent fibrils has been proved to resist high compression loading (94). In osteoporotic animal models, abnormal collagen fibrils which are arranged randomly are observed (95). In osteoporotic patients, a decrease in mean collagen fibril diameter is associated with compromised bone strength (41). Variations in fibril spacing may also contribute to bone fragility (96). In addition, a recent rat study suggested that degenerated apatite orientation tested by X-ray diffraction analysis and collagen orientation tested by birefringence analysis are associated with decreased Young's modulus tested by nanoindentation at the lumbar spine following ovariectomy (97).

Bone mineral is important to bone mechanical behaviours. In fact, it is the basis of clinical assessment of bone fragility due to its high absorption of X-ray. The amount of hydroxyapatite correlates positively with bone stiffness. In other words, over-mineralized bone can resist greater forces from a microcrack, but once a microcrack occurs, less energy is needed to break the bone to failure; and vice versa (98). This creates a dilema of whether more bone minerals are better for the maintenance of bone mechanical behaviour. Indeed, patients with fragility fracture are found to be either under-mineralized or over-mineralized (99). This dilemma also underlies the concern of atypical femoral fracture in osteoporotic patients treated by long-term antiresorptive drugs (100).

2.2 Assessment of bone mechanical behaviour

2.2.1 Introduction

Assessment of bone strength can be based on measurements of almost any aspect discussed previously. In clinical settings, assessment of bone strength and fracture risk is mainly based on DXA, which is the most-established tool for the diagnosis of osteoporosis recognised by both the World Health Organization (WHO) and International Society for Clinical Densitometry (ISCD). Other X-ray-based imaging modalities, such as quantitative computed tomography (QCT), pQCT and high-resolution pQCT (HR-pQCT) are also used in clinical settings and scientific studies. Non-X-ray-based imaging modalities e.g. magnetic resonance imaging (MRI) and quantitative ultrasound (QUS) are also available in the assessment of bone fragility. While these techniques provide non-invasive measurements of a range of variables in vivo, mechanical testing directly breaks whole-bone or part of a whole-bone and obtains mechanical properties in laboratory-based settings. Other invasive methods which provide measurements of other aspects that contribute to whole-bone mechanical behaviour are also discussed here in this section. All in all, these techniques provide various options for the determination of bone mechanical properties in different settings for different purposes. Each technique has advantages and disadvantages in application. Certain combinations of them may improve our understanding of bone fragility in certain situations.

2.2.2 Mechanical testing

Mechanical testing directly measures biomechanical properties, either of whole-bone or of localised properties within the bone (3, 101). Yield or failure load of bone is obtained from different testing configurations. Strain gauges attached to a bone surface are used to record strain at certain points. Compression, bending and torsion testing are widely used in

biomechanical experiments with bone of either human or animal origin. Regardless of testing modes, specimens need to be prepared and stored before testing. In most situations, fresh frozen specimens are stored in 0.9% saline solutions or fresh specimens embalmed in formalin solutions before testing. Although embalmed bone specimens can be kept longer for future use due to the ability of formalin to reduce microbiological infections, this preservation method has limitations in preserving the mechanical properties of bone. The amidogen of polypeptides in bone can connect with menthol molecules to increase collagen fibril crosslinks (102) which are important factors influencing whole-bone mechanical behaviour, as discussed previously. Decreased Young's modulus, yield stress and increased yield strain have been observed in formalin-fixed bone tissue compared with fresh frozen bone tissue (103, 104), especially when bone is stored at a higher temperature than 4 °C or for longer than 4 weeks (105). Fresh frozen specimens have been reported to preserve bone mechanical properties (106), therefore are recommended in order to improve accuracy in mechanical testing (107). Dry specimens are used for mechanical tests at times (108 - 110). While increasing the friction between specimens and testing plates thus ensuring specimens being held tightly, use of dry specimens has been reported to exaggerate the experimental stiffness compared to hydrated specimens (108, 111, 112). More importantly, free water is a crucial component of bone and contributes to the final mechanical behaviour of whole-bone. Therefore, results from mechanical testing using dry specimens should be interpreted with caution.

Mechanical testing can be performed either on whole-bone or bulk tissue excised from whole-bone, or even tiny tissue specimens from bone biopsy (101, 113). Whole-bone testing is the most direct way to obtain the structural performance by loading a whole-bone or a major part of whole-bone to failure. Structural stiffness, failure load and energy to failure can

be obtained from whole-bone testing. Bulk tissue specimen testing investigates material characteristics of bone by ruling out whole-bone geometric factors; however, microstructural confounders such as cortical porosity or trabecular orientation may still impact the obtained measurements (67). Excised specimens from either cortical or trabecular bone are prepared to cylindrical or cuboidal structure of several millimetres in scale from which apparent elastic modulus and yield stress can be obtained (18, 114). Indentation is a method that can measure material mechanical properties from an even finer scale (e.g. microindentation for individual trabeculae or osteons, or nanoindentation for individual lamellae) (115, 116). Generally, this engineering method uses hard-tipped material as a rigid indenter and presses the indenter into bone tissue with a given force; therefore, material stiffness can be calculated from the area of the imprint. This technique is traditionally applied ex vivo; however, in vivo microindentation has emerged in clinical studies recently (117), which may provide a good prospect for direct clinical assessment of bone mechanical properties in the future.

Different testing modes are applied in mechanical testing of bone. Compression testing is usually used for whole-bone mechanical behaviour of the vertebrae or bulk tissue specimens from cortical or trabecular bone at other skeletal sites (106). In a typical compression test, whole-bone or bulk tissue is fixed in the testing machine with two platens (Figure 2.9). While the bottom platen stays stationary during the test, the compressing platen loads the specimen with a vertical compressive force. Compression testing is widely used in testing the mechanical properties of vertebrae due to the comparable loading mode they are exposed to in daily life (67). Compression testing is also of clinical importance at certain long bone sites, *e.g.* the distal radius or proximal femur (118, 119).

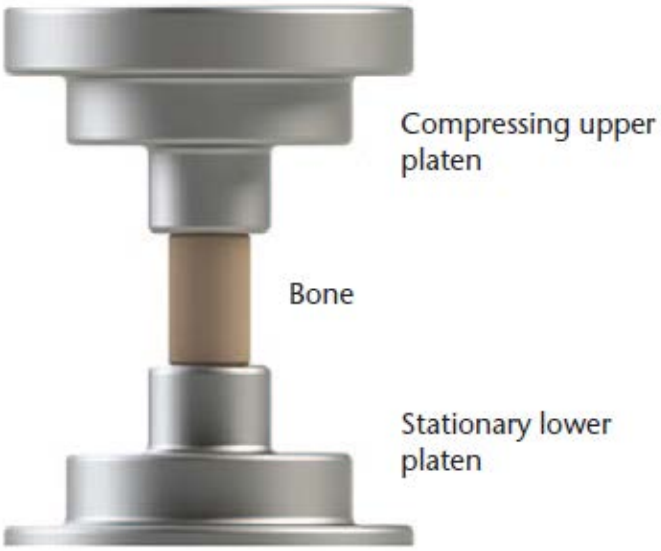

Figure 2.9 A typical compression test setup. As shown in this schematic, the bottom platen stays stationary when load is applied to the specimen from the upper platen.

Bending tests are the most widely-used method for whole-bone testing. There standard bending test setups: the three-point and four-point bending tests. In both tests, the whole-bone is supported by two supports. In three-point testing, load is applied by one prong located at the opposite surface of the specimen at a point corresponding to the exact middle point of the two supports (Figure 2.10 A) (3, 120), while in four-loading testing, loads are applied by two prongs located at the same side as in the three-point testing. The distances from the two prongs to the middle point of the two supports are equal (Figure 2.10 B) (1). As one can easily point out, the three-point test will create high shearing stress about the loading point (121). The four-point bending test ensures a uniform bending moment between the two loading points (3, 121); however, the three-point bending test is more widely used in mechanical experiments because it is easier to achive uniform contact with the points contacting the bone.

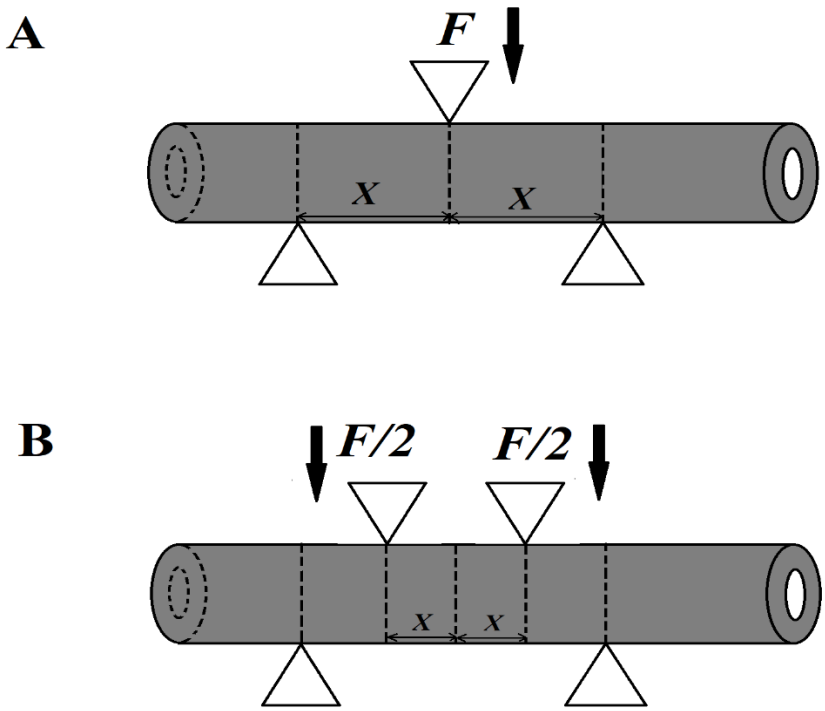

Figure 2.10 Diagrams showing the setup of three-point and four-point bending tests. A: three-point bending test; B: four-point bending test. F: the load applied to the long bone, X: the distance from the corresponding point to the middle of two supports to loading point(s).

In summary, mechanical testing provides direct insights into skeletal mechanical properties from a whole-bone level to a nano scale. Both structural and material characteristics can be obtained from various mechanical tests. Therefore, a choice should be made based on the research purpose since each testing method has advantages and disadvantages compared to others. However, it should be noted that all mechanical tests are conducted either ex vivo or invasively, which greatly limits their potential clinical application. Results from animal experiments or human cadaveric tests may be compared with results from clinical assessment

(which will be discussed in the following sections), but interpretation should be with caution due to the structural/biological differences of bone in vitro from tissues in vivo.

2.2.3 X-ray-based techniques

2.2.3.1 Introduction

In current practice, X-ray-based techniques are used for most of clinical tasks of bone strength assessment. DXA is the most established tool for the diagnosis of osteoporosis and assessment of fracture risk, although it has limitations in identifying individuals with increased fracture risk (122). Quantitative CT and pQCT provide both volumetric bone density and bone macro-geometric parameters that contribute to whole-bone strength. Over the past decades, HR-pQCT which enables assessment of bone micro-structure is developing popularity in clinical research. Micro-CT can also measure bone micro-structure but is limited to ex vivo studies. When X-ray travels through the scanned site, its attenuation is different for bone and soft tissue due to differences in their ability to absorb X-ray (123). This forms the basis of X-ray-based examinations. All the X-ray-based modalities above provide various options for the assessment of bone mechanical properties. The roles of DXA and pQCT for bone strength assessment will be discussed in the following two sections of this literature review. Here a brief review on QCT, HR-pQCT and micro-CT is provided.

2.2.3.2 Quantitative computed tomography

Quantitative CT uses a conventional clinical CT scanner to measure bone macro-geometric parameters as well as volumetric bone mineral density (vBMD) (124). As discussed above, the abilities of different tissues to absorb X-ray are different. X-ray attenuates more in bone tissue than in soft tissue. This forms the basis of an CT image of different densities, or CT

numbers. The CT number of a certain tissue is defined as the ratio of the difference in X-ray absorption between that tissue and water to the X-ray absorption of water (Equation 6). The CT number of water is therefore 0.

$$CT\ number = \frac{\mu_{tissue} - \mu_{water}}{\mu_{water}} * 1000 \quad (6)$$

where μ_{tissue} is the X-ray absorption coefficient of a certain tissue, μ_{water} is the X-ray absorption coefficient of water. The unite of CT number is Hounsfield unit (HU)

Unlike conventional CT that focuses more on tissue morphology *i.e.* size or shape of a certain tissue or focus, quantitative CT measures tissue characteristics by figures. Strictly speaking, the word 'quantitative' as in the name of QCT can mean any quantitative analysis from a CT image; however, the term QCT only refers to the quantification of bone density in current practice (125).

Linear correlation exists between CT number of bone and its apparent density (126). Although direct transformation from CT number to bone density is achievable and used in clinical research sometimes (127 -129), quantification of bone mineral density (BMD) is usually achieved by a calibration phantom of known density that is scanned with bone tissue at the same time in most cases. Most calibration phantoms are made of dipotassium phosphate (K_2HPO_4) or calcium hydroxyapatite [$Ca_5(PO_4)_3$], although other materials are also used. These phantoms are believed to have comparable ability to validate the quantitative analysis, although a higher coefficient of determination (r^2) with QCT results was reported in

the use of phantoms made of $Ca_5(PO_4)_3$ than of K_2HPO_4 in the same situation (*e.g.* scanner, peak voltage, tube current) (130).

During CT scanning, the X-ray source and detector rotate around the site of interest. Therefore, data acquired are three-dimensional and volumetric (130), which is an advantage over DXA and forms the basis of finite element analysis (these two aspects will be discussed in detail in the following sections). The resolution of QCT also enables separate analysis of cortical and trabecular compartments of bone tissue, although it is still not adequate for the assessment of bone microstructure (131). Compared to other X-ray-based techniques, QCT is the only modality that can provide in vivo volumetric measurements of the spine (101), which strengthens its utility at the central site.

Many studies have investigated the ability of QCT measures to predict bone mechanical properties. At the lumbar spine, Biggemann et al reported the r^2 between compression strength and vBMD to be 0.68 (132). One study by Ebbesen et al observed a similar r^2 between QCT vBMD and compression strength of the lumbar spine ($r^2 = 0.61$) (133). A greater correlation in females ($r^2 = 0.75$) than in males ($r^2 = 0.68$) was also noted (133). Comparable results were reported by Buckley et al; however, when they separately analysed the trabecular vBMD, they found much lower correlation ($r^2 = 0.17$) with compression strength, suggesting a major contribution of cortical bone to the final strength even at this trabecular-rich site (134). Nevertheless, the ability of integral vBMD to predict failure load of other loading modes was barely satisfactory. For example, in an anterior bending experiment of the lumbar spine, the integral vBMD only explained 18% of the final bending strength (135). When the investigators further took cross-sectional area of the endplate into

account, the r^2 was observed to increase slightly ($r^2 = 0.21$). Although this increase in r^2 by including geometric properties was much smaller than what was observed in Biggemann's study (r^2 increased from 0.68 to 0.91) (132), the results proved the importance of macro-structural measurements in the assessment of bone strength. This finding was supported by Buckley's study as well, where r^2 increased from 0.63 to 0.76 and from 0.17 to 0.42 for integral and trabecular vBMD, respectively, after inclusion of CSA (134). Quantitative CT measurements of the lumbar spine also provided acceptable prediction of failure strength of the appendicular skeleton. Moderate r^2 values of 0.57, 0.47 and 0.41 were reported between lumbar spine QCT (vBMD x CSA) and radius strength under three-point bending, axial compression and a fall-simulated configuration, respectively (118).

Quantitative CT is also used at the proximal femur, but analysis was more complex due to the irregular structure at this site. In a lateral impact loading experiment, r^2 between integral vBMD of total proximal femur region and failure load was reported to be 0.76 by Cheng et al (136). However, variations in r^2 of different sub-regions were observed, ranging 0.59 – 0.88 for femoral neck, trochanteric, intertrochanteric and Ward's regions. Further analysis of different cortical and trabecular measurements at the femoral neck and trochanteric region showed great variations in r^2 as well, with lowest r^2 with failure load observed in femoral neck cortical vBMD ($r^2 = 0.07$) and highest r^2 in trochanteric cortical area ($r^2 = 0.83$). Among femoral neck measurements, cortical area had the highest r^2 with femoral strength ($r^2 = 0.66$). This was comparable for trochanteric trabecular vBMD, the r^2 of which was 0.69. Cortical vBMD at trochanteric region was also observed to have low r^2 with femoral strength ($r^2 = 0.28$). However, Cheng reported r^2 of single vBMD or geometric variable in this study, whether a combination of vBMD and geometric parameter improved the ability of QCT to predict femoral strength was then answered in another study by Lang et al (137). In this

study, r^2 between integral vBMD of the whole proximal femur region and femoral strength from the fall loading configuration was observed to be 0.66. This value increased to 0.74 when minimal femoral neck CSA was considered. In fact, when the minimal neck CSA was included in the regression models, all r^2 of vBMD measures were observed to increase to some degree, with highest increase observed in femoral neck integral vBMD (from 0.48 to 0.70). The same findings were observed for a stance loading configuration from this study, although QCT measurements predicted failure load of the stance configuration better than of lateral impact loading on average. These findings suggest a combination of bone density and geometric variables improve the predictive ability of QCT and is therefore applied in later QCT studies (138 - 141).

In summary, QCT provides medium to good ability to predict bone strength, although it is primarily used at spine or proximal femur. Data are relatively limited on the role of central QCT measurements to predict appendicular skeletal strength, as well as on the role of QCT measurements of the peripheral sites since it is more commonly used at central sites. While QCT can provide volumetric BMD and geometric measurements, as well as separate analysis of cortical and trabecular bone, its resolution is not high enough to depict the trabecular microstructure and bone porosity which are important factors contributing to whole-bone strength as discussed in the previous section. On the other hand, the volumetric data acquired by QCT can be a source for finite element analysis. This will be discussed in Section 2.5.

2.2.3.3 High-resolution peripheral quantitative computed tomography

High-resolution pQCT has the same ability with QCT to provide vBMD measurements of bone and to separately analyse cortical and trabecular tissues. More importantly, it can assess

not only macro-structure but also micro-structure of bone. This strength results from its in-plane isotropic resolution of 85μm (the recent newer generation of HR-pQCT on the market has a resolution of 60 μm but most published studies have used the first-generation HR-pQCT) which enables analysis of individual trabeculae (142, 143). However, as a new technique, it faces problems of relatively long scanning time and high cost for procurement and maintenance. Therefore, it is still not as widely available as DXA and QCT currently.

HR-pQCT provides a variety of measurements of bone density, geometry and microstructure of total, cortical and trabecular bone (Table 2.4). Variance has been observed in the ability of different HR-pQCT variables of the vertebral to predict experimental failure load at central sites which was due to different testing configurations and whether in combination of other techniques (144 - 147). The ability of HR-pQCT variables at the appendicular sites to predict corresponding experimental failure load is of more clinical importance. In a compression experiment of the appendicular bone section, HR-pQCT To.BMD was found to correlate better with experimental stiffness and failure load at the tibia (r^2 = 0.53 and 0.66, respectively) than at the radius (r^2 = 0.30 and 0.35, respectively) (148). Ct.BMD was observed to have slightly higher r^2 than Tb.BMD at this site. For microstructural parameters in this study, Ct.Th had the highest r^2 with tibial and radius failure load (r^2 = 0.71 and 0.48, respectively). For the prediction of lateral compression failure load of the proximal femur, r^2 was reported to be 0.16 and 0.55 for radius and tibial HR-pQCT Po.BMD, respectively (149). In the studies above where the predictive ability of DXA was also assessed, some HR-pQCT measures had higher r^2 with bone mechanical strength or stiffness than DXA measures (144, 145, 147 – 149). However, most r^2 of HR-pQCT measures were still medium.

Table 2.4 HR-pQCT measurements, units and abbreviations

Measurements	Units	Abbreviations
Integral bone measurements		
Total bone mineral density	mg HA/cm^3	To.BMD
Total bone area	mm^2	Tt.Ar
Total volume	mm^3	TV
Bone volume	mm^3	BV
Bone surface	mm^2	BS
Bone volume ratio	%	BV/TV
Bone surface ratio	%	BS/BV
Cortical bone measurements		
Cortical bone mineral density	mg HA/cm^3	Ct.BMD
Cortical thickness	mm	Ct. Th
Cortical porosity	%	Ct. Po
Trabecular bone measurements		
Trabecular bone mineral density	mg HA/cm^3	Tb.BMD
Trabecular thickness	mm	Tb.Th
Trabecular separation	mm	Tb.Sp
Trabecular number	per mm	Tb.N

The biggest advantage of HR-pQCT over other techniques is that it is the only available tool for in vivo assessment of bone microstructure although this utility is limited to peripheral bones. Many validation studies of HR-pQCT microstructural parameters are available against

μCT measurements and good agreement between them was identified (150 - 159). One aspect that is not covered in this section is HR-pQCT-based micro FEA. The micro FEA by HR-pQCT will be discussed in Section 2.5. Although providing promising assessment for bone strength, HR-pQCT, as a relatively new technique, is not widely available currently due to high procurement and maintenance cost and long scanning and analysis time.

2.2.3.4 Micro computed tomography

Micro CT is widely used in animal experiments or human cadaveric studies to assess ex vivo bone microstructure due to its ultra-high in-plane resolution of less than 10 μm (160). It is also available for human bone biopsies. During μCT scanning, the specimen is rotating to different directions of the projected X-ray. Projective data at each direction are then reconstructed to form three-dimensional data (161). Although newer μCT scanners enable follow up of changes of bone microarchitecture in small living animals, the limited scanning space and requirements for small tissue volumes constrain their use in living humans (162, 163). Moreover, the increased resolution of μCT is achieved by extremely long scanning time and high radiation exposure (164, 165).

Micro CT parameters have been reported to correlate very well with bone mechanical properties obtained from animal experiments, with r^2 ranging from 0.81 to 0.90 against ultimate load (161). Although it is not practical for μCT to scan bone in vivo for human beings, ex vivo μCT data can be used to validate measurements assessed by other modalities e.g. HR-pQCT (see previous section).

2.2.4 Non-X-ray-based techniques

2.2.4.1 Magnetic resonance imaging

High-resolution MRI (HR-MRI) is another available imaging modality that provides three-dimensional structural data (166). While existing data showed poor to medium correlations between HR-MRI structural measurements and experimental failure load (r^2 ranging from 0.14 to 0.48) (167 - 169), these results correlated well with μCT measurements (r^2 ranging from 0.26 to 0.94) (170 - 173). The advantage of HR-MRI is that, by applying a magnetic field to hydrogen in water in tissues, it does not expose patients to ionizing radiation. However, the scanning time associated with HR-MRI is relatively long which limits its utility in clinical assessment of bone fragility, especially among older people or patients with fracture.

2.2.4.2 Quantitative ultrasound

Quantification of bone measurements by QUS is achieved by attenuation of sound waves through bone tissue (174). QUS directly measures sound wave velocity and broadband attenuation, both of which follow certain functions of bone density and microarchitectural properties (131, 174). Although QUS can be used at central sites e.g. spine or proximal femur (175, 176), applications of QUS is limited at calcaneus in most studies. QUS is not a X-ray-based examination thus does not expose patients to ionizing radiation. Newer QUS devices are designed with small dimension and are portable and ideal for community use (177). However, due to the indirect quantification of BMD, results obtained by QUS cannot compare with other modalities directly.

Results from ex vivo mechanical testing have shown medium to good correlations between bone failure load and QUS measurements (r^2 = 0.50 – 0.67 for sound velocity and r^2 = 0.37 – 0.64 for broadband attenuation) (178 - 180). In all these studies, QUS and mechanical testing were performed at the same sites. The ability of calcaneus QUS variables to predict bone strength at different sites was reported to be poor, with some prediction even poorer than DXA (138).

2.2.4.3 Other analysis of bone quality

Fourier transform infrared (FTIR) and Ramen spectroscopy analyse mineral and organic composition of bone tissue by characterizing certain absorption peaks on infrared or Raman spectrum (181, 182). These techniques examine tissue properties of bone biopsy specimen under an optical microscope. FTIR and Ramen spectroscopy measurements are found to identify more fracture patients than DXA alone (183). The invasive process of biopsy may hinder its wide application, however, newer Raman spectroscopy with an in vivo probe can be applied from skin surface (184).

Ashing analysis weighs bone mineral mass of a specimen directly by removing organic components at a very high temperature (185). However, this simple method takes neither heterogeneity of bone tissue nor microstructural variations into consideration (101).

Collagen maturity can be assessed by high pressure liquid chromatography (HPLC) (186). While examining minor alterations in collagen crosslinks, this technique also needs invasive biopsy to provide bone tissue.

2.2.5 Summary

In summary, many examinations are available to assess bone mechanical behaviour from various aspects. DXA is the most widely used technique for bone density testing, and its role in the assessment of bone strength and fracture risk will be discussed in the next section separately. Peripheral QCT, as the main topic of the current thesis, will also be discussed separately thereafter. Mechanical testing of different loading modes and configurations provides the most direct measurement of bone mechanical properties, but as a destructive process, it can only be used in the laboratory to validate other assessment methods. By adding a density phantom to existing all-purpose CT scanners, QCT has potentially wide use in clinical settings. However, its relatively high radiation exposure may be a concern for both patients and healthcare providers. HR-pQCT exposes patients to smaller amount of radiation and can assess bone microarchitecture in vivo, although its application is limited to peripheral sites. As a relatively new technique, its high cost may impede its wide utility, at least currently. As non-X-ray-based modalities, HR-MRI and QUS may improve our understanding of bone fragility together with conventional examinations, but more data are needed to validate their clinical use. Bone quality analysis including FTIR spectroscopy, Raman spectroscopy, ashing and HPLC provides insights into bone quality from a finer scale and may attract more attention for future research; however, they are not mainstream examinations currently.

2.3 Dual energy X-ray absorptiometry in the management of osteoporosis

2.3.1 Osteoporosis: definition and pathophysiology

In etymology, the word “osteoporosis” is formed by three parts (187). “osteo-” originating from the Greek word “osteon” means bone. “poros” originates from the Latin word “porus” and the Greek word “poros” and means a pore or minute opening. “osis” is word suffix expressing “state” or “condition”. Therefore, the direct message conveyed by the word “osteoporosis” is “a condition of bone with small pores”. The most recent definition of osteoporosis from a medical point of view is “a skeletal disorder characterized by compromised bone strength predisposing to an increased risk of fracture” by the US National Institutes of Health (NIH) (76). While emphasizing the consequence of osteoporosis, this definition does not tell the reason for compromised bone strength and consequent fragility fracture. The older version of this definition answers this by stating osteoporosis is “a systemic skeletal disease characterized by low bone mass and micro-architectural deterioration of bone tissue with a consequent increase in bone fragility and susceptibility to fracture” (188). This definition integrates change in bone quantity and quality in osteoporosis, as well as concerns about its consequence.

The basic pathophysiology of osteoporosis is the imbalance of bone formation and resorption. As discussed previously, bone is a dynamic organ where formation and resorption occur simultaneously to maintain homeostasis of bone tissue (82). The early decades of life are a bone accrual period when more bone is formed than resorbed until reaching peak bone mass (PBM) around the age of thirties (189, 190). After PBM is reached, bone mass is lost at a slow rate gradually until the age around fifty years when bone loss is increasingly fast (189, 190). This is an inevitable ageing process that is seen in both women and men. However,

women are found to be more vulnerable to osteoporosis with a three-fold ratio to men (191). This attributes to lack of estrogen resulting from menopause in women. Estrogen mediates bone remodelling by both promoting bone formation and suppressing bone resorption (192, 193). Serum estradiol level has been observed to correlate negatively with serum level of sclerostin, which is a Wnt signalling pathway inhibitor (194, 195). Wnt signalling is associated with the osteocyte's response to mechanical stress, which, in turn, activates osteoblast activity of bone formation (196). The inhibitory role of estrogen on bone resorption is, in part, by disturbing osteoclast differentiation from monocytes which is modulated by osteoblast activity (197). More importantly, estrogen also induces osteoclast apoptosis through the receptor activator of nuclear factor (RANK) κB signalling pathway (198, 199). Therefore, postmenopausal women are more susceptible to bone loss due to estrogen deprivation. The more detailed role of estrogen in osteoporosis will be discussed in a later section.

2.3.2 Diagnosis of osteoporosis

In clinical practice, the diagnosis of osteoporosis generally is based on areal bone mineral density (aBMD) determined by DXA (200). In the diagnostic criteria for osteoporosis established by WHO, a system based on the T-score, which is the difference between individual aBMD and reference (of healthy young adult individuals of the same sex) mean aBMD compared to reference standard deviation (SD) (Equation 7), is used to classify normal bone density, osteopenia and osteoporosis (Table 2.5). Patients with a T-score of no less than -1.0 are considered to have normal bone density. Osteoporosis is diagnosed with a T-score of no more than -2.5. Patients with a T-score in between are considered to have osteopenia. When an osteoporotic T-score is accompanied with a fragility fracture, severe

osteoporosis is diagnosed. The standard measurement sites are the lumbar spine, total hip or femoral neck.

$$T - score = \frac{Individual\ aBMD - Reference\ aBMD}{Reference\ SD} \quad (7)$$

where SD denotes for standard deviation

Table 2.5. World Health Organization diagnostic criteria for osteoporosis

Diagnosis	T-scores
Normal bone density	T-score ≥ -1.0
Osteopenia	-2.5 < T-score < -1.0
Osteoporosis	T-score ≤ -2.5
Severe osteoporosis	T-score ≤ -2.5 with fragility fracture

In practice, reference data used currently in the diagnostic criteria come from different sources (201). For the total hip and femoral neck, reference data are from Caucasian women aged 20 – 29 years obtained from the National Health and Nutrition Examination Survey (NHANES) III in the USA (202, 203). For the lumbar spine, local databases are used to generate normative data by each DXA manufacturer. The local references are also based on data of young women (201). This raises concerns about derivation of T-scores for individual patients from at least two aspects (204). The first concern is the application of female reference data to generate T-scores for males (205). T-scores of males generated from female reference would be higher than those generated from male reference due to the averagely

larger bone size of males compared to females (205). However, increasing data have shown a similar fracture rate between males and females with the same aBMD (203, 206 - 209). These results lay the basis for both WHO and ISCD to recommend use of young female reference data for males (210). The second concern is the influence of race and ethnicity on the generation of T-score, especially at the total hip and femoral neck, where a T-score is derived from Caucasian data. Difference in osteoporosis prevalence and fracture risk exists among different racial and ethnic groups (211). Therefore, using local ethnicity-specific reference data for generation of T-scores at the lumbar spine while uniform Caucasian reference data at the total hip and the femoral neck is tricky. While this reflects the necessity of more data for other ethnic groups rather than Caucasians, local ethnic normative data are accumulating in some regions (212 - 215). This is also reflected in the Fracture Risk Assessment Tool (FRAX®) by the University of Sheffield where ethnicity-specific data are used to calculate a ten-year absolute fracture risk (216).

2.3.3 Fragility fracture

Osteoporosis is a silent medical condition. This lies in the fact that fragility fracture, as the consequence of osteoporosis, is often the first sign that attracts the attention of patients and physicians (76). Osteoporotic fracture, or fragility fracture, is a serious complication of osteoporosis. It is usually defined as fracture resulting from minimal trauma, such as a fall from a standing height or less (217). Therefore, it is sometimes called low-trauma fracture. However, the description of “low-trauma’ itself is vague as it is sometimes difficult to quantify “low trauma” at least in clinical settings. Moreover, even in the situation of “high trauma”, patients with osteoporosis are more prone to sustain a fracture than healthy people (218). Therefore, it is recommended that characterization of osteoporotic fracture be

associated with fracture sites where a fracture is sustained with ageing and low bone mass (210, 218, 219).

Common sites for fragility fracture include the hip, the distal forearm and the vertebral body. Fragility fractures at other sites, such as the proximal humerus, the pelvis, the ribs, the distal femur and the tibia also occur among patients with osteoporosis. Hip fracture is the most severe complication of osteoporosis. This is reflected not only by the fact that more than half of the patients cannot gain total function rehabilitation after a hip fracture (220), but also by the high death rate within one year post hip fracture (221,222). The most common cause for an osteoporotic hip fracture is falling from a standing height, although a spontaneous hip fracture is also noted at times (223). A hip fracture occurs either at the femoral neck (transcervical or subcapital fracture) or at the trochanteric region (intertrochanteric fracture, which is more osteoporosis-related) (224).

Distal forearm fracture (typically a Colles' fracture) caused by a fall on the outstretched hand is the major fracture type in younger postmenopausal women (225). While this type of osteoporotic fracture usually does not require hospitalization and its prognosis is better than a hip fracture (226), the risk for a subsequent fragility fracture increases following a Colles' fracture (227, 228). Given the younger age when a forearm fracture is sustained, appropriate follow-up may improve prevention of a future fracture at an older age.

Vertebral fracture may be the most underestimated type although it is a strong predictor for a second fragility fracture not only of the spine but also of the hip and the forearm (227 - 229). This is because a vertebral fracture is often accompanied with a non-specific sign, back pain,

which is common in older people, thus does not come to clinical attention frequently (230, 231). In clinical practice, a vertebral fracture is diagnosed using a mophometric method on lateral plain X-ray by Genant et al, which classifies the severity of a vertebral fracture according to the height loss of the vertebral body (232).

2.3.4 Prevalence and burden

The prevalence of osteoporosis increases with an ageing population. There are variations in the reported prevalence worldwide. In Europe, about one fifth of women aged greater than 50 years are osteoporotic based on the WHO diagnostic criteria, while this figure is smaller in men, less than 10% (210, 233). Together, this summed up to 28 million people in Europe in 2010. In the USA, according to NHANES 2005-2010 data, the overall prevalence was 10.3% for osteoporosis and 43.9% for osteopenia, from which it was estimated that a total of 10.2 million people had osteoporosis and another 43.4 million had osteopenia in 2010 (191). In the Middle East, a cross-sectional study of 321 healthy women in 1999 observed a prevalence of 28% for osteoporosis and 38% for osteopenia among women aged over 50 years (234). In mainland China, it was reported the overall prevalence of osteoporosis was 16.1% for people aged over 40 years from a study in 2002 (235). The prevalence of osteoporosis in Hong Kong was a little higher than in mainland China, 24.9% in women aged over 50 years (236). In Taiwan, prevalence was very high from recent data. The overall prevalence in postmenopausal women was reported to be 41.3% (237). In Australia, the estimated prevalence of osteoporosis was 23% and 6% for women and men, respectively (238). According to the WHO diagnostic criteria, more than half of the Australian population will suffer from osteoporosis or osteopenia by 2022 (238, 239).

Serious public health concern about osteoporosis arises from the high incidence of fragility fracture. It was estimated that up to 30% of women and 20% of men worldwide would sustain a fragility fracture after the age of 50 years which accounted for an annual incidence of up to 9 million fractures (210, 225). Europe is characterized by a high annual fracture incidence, where most countries have an annual fracture incidence of more than 200 cases per 1,000,000 population (240). In Australia, it was reported by the Dubbo Osteoporosis Epidemiology Study group that 56% of Australian women and 29% of Australian men would have a residual lifetime risk of an osteoporotic fracture after age of 60 years (241).

Fragility fracture is associated with significant morbidity and mortality (242, 243). Most fragility fractures cause substantial pain and loss of function for a certain period or even the residual lifetime, although recovery and rehabilitation vary amongst fracture types. Fragility fracture not only affects an individual patient's life quality but also causes a great societal burden due to high costs associated. A meta-analysis (244) concluded that during the first year post a fragility fracture, medical expenditure related to hospitalization and rehabilitation was 2 - 6 times higher than before a fracture occurred and 2 - 4 times higher than in controls without fracture. Moreover, the societal burden is also reflected by quality-adjusted life years (QALY) lost. QALY is an indicator of both death and morbidity caused by a fragility fracture. QALY = 0 when one recovers from a fracture totally (*i.e.* no disability or life quality change). If one death happens as the result of fragility fracture, QALY = 1. QALY is quantified between 0 to 1 based on the impact of fracture on life quality. It was reported that QALY lost associated with osteoporotic fracture was 5.8 million worldwide and accounted for 0.83% of total global burden of non-communicable diseases (225). From the macroeconomic perspective, osteoporotic fracture cost 13.8 billion US dollars per annum in the USA (245), and 850 million pounds per annum in the UK (246). In Australia, 1.9 billion

Australian dollars were spent on direct costs of osteoporosis and osteoporotic fracture in 2007 (247), which led to osteoporosis being one of the nine National Health Priority Areas.

Due to the high prevalence and cost of fragility fracture, fracture liaison programs have been proposed for better management of fragility fracture (248 – 251). However, improved strategies for early screening and diagnosis, and prediction for fracture risk, are essential for appropriate osteoporosis management.

2.3.5 DXA: technical aspects

Dual energy X-ray absorptiometry is based on the method of X-ray spectrophotometry and applies two-dimensional projection technique to quantify areal BMD (aBMD) of patients. Before the wide application of DXA, single photon absorptiometry (SPA) was initially used for the determination of bone density (252). This technique detected attenuation of a greatly focused photon beam through the human body transmitted by single-energy radionuclides. There were two major weaknesses of SPA. First, while single energy radiation discriminated bone from soft tissue, it did not take into consideration variations in attenuation of the photon beam through different soft tissues. Therefore, a water bath was applied during a SPA scan to correct for variations in soft tissue thickness and composition (253). Moreover, the radionuclide photon source greatly impacted precision and resolution of the measurements and prolonged scanning time due to its physical decay (254). Although its successor, single X-ray absorptiometry (SXA) solved the second issue by replacement of the radionuclide source with a low radiation X-ray tube (255), correction for soft tissue variations was still an inconvenience until the introduction of dual photon absorptiometry (DPA) which also used a radionuclide source.

With the advent of DXA in the late-1980s, better quantification of bone mass enabled better understanding of bone fragility by solving the two issues discussed above (256, 257). DXA determines bone density using a low-dose X-ray tube with two energies. Generation of a dual energy X-ray spectrum is achieved by either X-ray absorption filters or voltage switching among commercial scanners used currently. An X-ray absorption filter made of certain material can divide polychromatic X-ray beam into high and low energy beams (258). The resultant two beams therefore have narrower spectral distribution than the original polychromatic X-ray beam from the X-ray tube. This helps reduce artefacts from beam hardening, a phenomenon of selective attenuation of low energy beam by the scanned tissue (259). Voltage switching is another way to produce X-ray beams of two energies by switching the X-ray tube between high and low voltage during scanning. The wider spectral distribution of X-ray beams by voltage switching than by absorption filters is therefore associated with greater beam hardening artefact, which needs to be eliminated by pixel calibration (260).

Early DXA scanners generated pencil beam X-ray to scan patients back and forth. Currently, most DXA scanners use a fan beam for a single sweep scanning across the patient. This greatly shortens scanning time and exposes patients to lower radiation does (254). Common sites scanned include the lumbar spine and the proximal femur (including the femoral neck) as the standard measurements for osteoporosis diagnosis. A forearm scan is sometimes needed when significant artefacts appear on the standard sites. After the scan is completed, an automated threshold algorithm is used to detect bone edge. Mean bone density is then calculated for all the bone pixels within the edge. Bone mineral content (BMC) can then be

obtained with bone density and the projected bone area. Quality assurance scanning of a phantom, either made by the manufacturer or generic, is needed to maintain the scanner's stability. Although different materials are used for a phantom by different manufacturers, the essential of a phantom should be the ability to simulate human tissue composition in real clinical scans (254).

2.3.6 Prediction of bone strength by DXA

The ability of DXA to predict bone failure load varied but generally poor to medium correlation was observed among studies. In a study by Cheng et al, vertebral aBMD measured by DXA was reported to explain 64% of variation in vertebral compression load (261). In another study by Perilli et al, poorer correlation was observed between vertebral compression failure and DXA aBMD and BMC (r^2 = 0.37 and 0.49, respectively) (262). The predictive ability of DXA was improved significantly by lateral vertebral scan in this study (r^2 = 0.70 and 0.82 for aBMD and BMC, respectively). The poor predictive ability of standard vertebral measurements of DXA was also observed in animal experiments, with r^2 reported to be only 0.35 with ultimate compression load (263). A large study by Eckstein et al involving specimens from 110 donors revealed site-specific differences in the predictive ability of DXA (264). In this study, DXA scans were performed on the lumbar spine, the proximal femur and the forearm for each cadaver. Mechanical testing was conducted on the vertebrae (compression loading), the bilateral femurs (vertical and side impact loading for each), the bilateral radius (fall configuration, axial compression loading, and three-point bending). While failure loads displayed great heterogeneity between sites (r^2 = 0.15 – 0.40) (which suggest variations exist between different skeletal sites although osteoporosis is considered as a systemic disease), the ability of DXA aBMD to predict bone failure load was the strongest

at the site scanned. For instance, vertebral aBMD accounted for 49% of variation in vertebral compression failure load, but for only 19% - 34% and 20% - 29% for different loading failure at the femur and the forearm, respectively. While total hip aBMD predicted up to 53% of variations in femur failure loads, its ability to predict vertebral and radius failure loads was relatively poor ($r^2 = 0.20 – 0.38$). At the radius, DXA aBMD of the radius was observed to have the highest r^2 with bending failure load of the mid-shaft ($r^2 = 0.79$), but this figure decreased to 0.44 in a falling configuration, which may suggest its poor predictive ability at this distal site.

2.3.7 Limitations of DXA

Strong correlation exists between bone mass and bone strength (265), thus using bone density to predict bone mechanical properties and fracture risk is the standard practice in clinical settings. Although widely used clinically for decades, debate about its limitations in fracture prediction is ongoing.

First, as a projection technique, DXA measures aBMD, which is the BMC in a projected area of bone (254). Although partly adjusted for bone length and width, aBMD does not take bone "depth" into consideration. This weakness makes aBMD susceptible to effects of variation in bone size (266). Therefore, the fracture risk will be overestimated in individuals with small bones and underestimated in those with large bones (267, 268). Great variations have been observed in bone macrostructure between different ethnic groups (269). This is one of the important considerations in the use of ethnicity-specific reference data to generate DXA T-scores (212, 213).

Similarly, DXA provides an integrated measurement of aBMD as it is unable to separate cortical and trabecular bone measures. This, for example, reduces the sensitivity of the technique to detect trabecular bone loss which occurs in early stages of osteoporosis (270). Moreover, the inadequate resolution of DXA images cannot detect changes in bone microstructure which contributes to whole-bone strength (271, 272).

Another weakness of DXA is that its measurements are sensitive to various artefacts including degenerative changes, e.g. osteoarthritis, prevalent vertebral fractures and extra-skeletal calcium deposition (273). Areal BMD of individuals with significant degenerative diseases, *e.g.* spondylosis, will increase, which will suggest an artificially lower fracture risk (274). This problem is especially common in the spine with ageing. Aortic calcification which is common in aged people may also falsely increase aBMD, which, in turn, will underestimate fracture risk.

The ability of aBMD to predict fracture is comparable to the use of blood pressure to predict stroke, and significantly better than serum cholesterol to predict myocardial infarction (275); however, DXA-measured aBMD has fair specificity but low sensitivity, *i.e.* aBMD can predict fracture risk but cannot identify individuals who will have a fracture. Many articles have reported that marked variations in the prevalence of fragility fractures were observed for a comparable aBMD determined by DXA (276 - 281). Indeed, the majority of patients presenting with fragility fracture have osteopenia by WHO criteria rather than osteoporosis on DXA examination (282 - 285), indicating the limited diagnostic sensitivity and predictive value of DXA. This weakness of DXA aBMD significantly limits its utility in initiating pharmacological therapy, leaving a large number of patients at risk of sustaining a new

fracture. Furthermore, the sensitivity of DXA is suboptimal to monitor treatment responses. It is argued that DXA cannot explain the observed changes in fracture risk during treatment (286, 287), which, on the other hand, may extend the treatment period of patients unnecessarily.

Above all, DXA only measures bone quantity that partly explains bone mechanical properties. Although advanced post-processing programs such as hip structure analysis or trabecular bone score have been developed to compensate for the limited ability of DXA in the prediction of bone strength and fracture (288, 289), the intrinsic weakness of DXA cannot be overcome. Currently, a few fracture assessment tools are available for the calculation of absolute fracture risk, e.g. FRAX® by the University of Sheffield (290), GARVAN fracture risk calculator by the Garvan Institute of Medical Research (291), QFracture® by ClinRisk Ltd. (292). Although many clinical factors are taken into consideration in these calculation tools, including age, sex, body mass index, ethnicity, previous fragility fracture, long term use of oral glucocorticoids, alcohol consumption, tobacco smoking, rheumatoid arthritis, hyperthyroidism, hyperparathyroidism, falls, parental history of hip fracture, DXA is still the only radiological measurement in all fracture prediction tools. Other modalities, e.g. QCT, pQCT, HR-pQCT, QUS, HR-MRI (293 - 295), may provide additional information compared to aBMD alone and may be applied in clinical settings. Due to the limitations of DXA, the utility of alternative methods for fracture risk assessment in addition to aBMD should be considered.

2.4 Peripheral QCT in the assessment of bone strength and fracture risk

2.4.1 Peripheral QCT: technical aspects

Peripheral QCT uses a dedicated, purpose-built CT scanner for the quantification of BMD of the forearm and the tibia (296). Like a standard whole-body CT scanner, pQCT also provides an image of total linear X-ray attenuation coefficient, the values of which are calibrated to the X-ray attenuation coefficient of a calcium hydroxyapatite phantom. The calibration ascribes an individual BMC value for every voxel of the pQCT image. Then the pQCT analysis software can calculate the volumetric BMD of selected regions of interest (297). To maintain the quality of this calibration process, the phantom needs to be scanned daily prior to scanning of patients or study subjects.

The radius and the tibia are the skeletal sites where pQCT often scans, although other skeletal sites can also be analyzed by pQCT, *e.g.* the ulna, the fibula or the femur (298). Sites measured by pQCT include a diaphyseal site where cortical measures are analyzed, and a metaphyseal site where trabecular measures are analyzed. The precise scanned sites are defined as percentage of the radius/tibia length from the distal to the proximal. Length is measured from the ulnar styloid process to the olecranon process at the forearm, and from the medial malleolus to the medial condyle at the tibia. The 4% site of the radius/tibia is the most measured site for trabecular bone, while various sites, *e.g.* the 20% (299, 300), the 33% (301), the 38% (302), the 50% (303, 304), the 65% (305, 306) or the 66% (307, 308) site, are scanned for cortical bone. Scans have been performed mostly on the non-dominant limb; however, the left limb (304, 309) or the right limb (310) was also studied. There is no agreement on the optimum measurement sites up to date (311, 312), therefore comparisons in pQCT variables are sometimes difficult between studies with different scanning sites. This is

one of concerns raised by ISCD to call for consistent scanning sites for pQCT, especially for the mid-shaft cortical measurements (125).

As with HR-pQCT, movement artefacts also impact image quality of pQCT, which in turn may produce invalid results or non-analyzable data. Movement artefacts presenting as streaking or discontinuity of bone tissue are normal in children or aged fracture patients (313). Although some remedial analyses are available to quantify movement artefacts as much as possible to permit an immediate decision whether to perform a re-scan (313, 314), prevention of movement artefacts still relies on technicians and patients/research subjects. A kind reminder by the technician before scanning would improve data validity.

Analysis of pQCT uses simplification of density threshold and peeling program to separate cortical and trabecular compartments recommended by the manufacturer (315). The density threshold for total area detection is set at 169 mg/cm^3 by default at the epiphyseal sites, while at 280 mg/cm^3 at the diaphyseal sites. At the epiphyseal sites, separation of trabecular compartments is achieved by either a threshold of 400 mg/cm^3, or 45% of total bone CSA. Separation of cortical compartments is not usually applied due to the thin cortical shell and limited endosteal border differentiation at the trabecular-rich sites (316, 317). At the diaphyseal sites, threshold for cortical separation is set at 710 mg/cm^3 by default. Different peeling assumptions may affect vBMD results. It was observed that, compared with threshold peeling mode, the 45% peeling mode yielded up to 24.9% lower vBMD in healthy people, while the figure was higher, as up to 44.9% in patients with spinal cord injury (318). The difference was even higher in people with low vBMD. Although these thresholds are recommended by the manufacturer, manual input for analysis configurations is also available

(317, 319 – 321). However, different thresholds and peeling configurations make inter-institutional comparison difficult; therefore, optimal configurations for different populations are needed for agreement.

Four categories of measures can be obtained by pQCT (Table 2.6): (1) bone mass parameters: bone mineral content and density, including total content/density (Tot BMC/vBMD), trabecular content/density (Trb BMC/vBMD), and cortical content/density (Crt BMC/vBMD); (2) bone geometric parameters, including total cross-sectional area (Tot CSA), trabecular CSA (Trb CSA), cortical cross-sectional area (Crt CSA), cortical thickness (Crt Thk), periosteal circumference (PeriC), endosteal circumference (EndoC); (3) bone strength parameters, including cross-sectional moment of inertia (CSMI), stress strain index (SSI), bone strength index (BSI); (4) muscle parameters, including muscle CSA (MCSA), muscle density (MDen).

2.4.2 Advantages of pQCT

Peripheral QCT has some advantages compared to DXA. First, it measures volumetric BMD. Instead of measuring bone density and bone mass in a projected two-dimensional plane as DXA, pQCT can monitor bone mineral density in a given volume due to the volumetric data acquired (322). Therefore, bone density determined by pQCT is a true physical density of bone tissue (in the unit of mg/cm^3) which is independent of bone size.

Second, as discussed above, pQCT can separately estimate trabecular and cortical compartments of bone (312) while DXA calculates an average or integral aBMD of

Table 2.6. Standard pQCT measurements

Parameter category	Parameter	Abbreviation
Bone mass	Total bone mineral content	Tot BMC
	Total volumetric bone mineral density	Tot vBMD
	Trabecular bone mineral content	Trb BMC
	Trabecular volumetric bone mineral density	Trb vBMD
	Cortical bone mineral content	Crt BMC
	Cortical volumetric bone mineral density	Crt vBMD
Bone geometry	Total cross-sectional area	Tot CSA
	Trabecular cross-sectional area	Trb CSA
	Cortical cross-sectional area	Crt CSA
	Cortical thickness	Crt Thk
	Periosteal circumference	PeriC
	Endosteal circumference	EndoC
Bone strength	Cross-sectional moment of inertia	CSMI
	Stress stain index	SSI
	Bone strength index	BSI
Muscle	Muscle cross-sectional area	MCSA
	Muscle density	MDen

the whole-bone only. Trabecular bone is about 8 times more metabolically active than cortical bone, and changes more quickly in response to time, many diseases and treatment than cortical bone (311). The ability of pQCT to discriminate between trabecular and cortical

compartments is advantageous since cortical and trabecular structures are differentially associated with fragility fracture (323).

Third, pQCT can also measure bone geometry allowing estimation of bone strength. Geometric parameters have a strong correlation with bone failure loads measured experimentally (59, 324 - 327). In postmenopausal women, bone geometry parameters are significantly different from those in young females (328). SSI assessed by pQCT, which reflects the mechanical competence of human bone, is based on the calculation of geometric parameters and has been recommended as a diagnostic indicator for osteoporosis or related bone-weakening diseases (303, 125, 329 - 334). In a study by Cointry et al, it was even argued that the mechanical competence of bone was mostly determined by those geometric parameters rather than BMD (335), while other studies found no evidence that geometric parameters performed better than BMD alone (318, 324, 326, 336 - 338). Although it is unclear which parameters contribute more to fracture prediction, it is likely that a combination of BMD and geometric parameters can improve fracture prediction compared to single variables.

As an X-ray-based modality, pQCT inevitably exposes patients to ionizing radiation; however, its associated radiation exposure is much lower than that of standard whole-body CT scanners (125). Peripheral QCT exposes patients to even lower radiation than DXA, whose radiation exposure is recognized as very low. For example, the effective dose is < 0.001 mSv for one pQCT scan at the wrist, compared to 0.0047 mSv for one DXA scan of the hip (339). Modalities such as HR-pQCT and MRI have equivalent radiation exposure to pQCT or no ionizing radiation exposure, respectively, but these modalities are not widely

available due to their expense and associated maintenance costs. Low radiation exposure associated with pQCT also gains its popularity in measurements for children and adolescents (312).

Satisfactory precision was observed in pQCT measures from previous studies (340 - 343). In a serial study by Wong et al, the short-term coefficient of variation (CV) ranged from 0.030 for Trb vBMD to 0.070 for Crt vBMD at the distal radius, and from 0.011 for Trb vBMD to 0.052 for Tot vBMD at the distal tibia (344). Better short-term precision was observed for pQCT compared to MRI and HR-pQCT in the series, which suggests better reproducibility of pQCT measures. Although another part of the series found higher long-term precision in HR-pQCT than in pQCT, this advantage was only significant for quantifying change where smaller effect sizes were expected. The authors recommended pQCT as a better modality for studies expecting larger effect changes (345).

Further, due to its ability to acquire volumetric data and to capture the distribution of density within bone, pQCT is a suitable source for FEA. FEA models have been reported as a good predictor of osteoporotic fracture at some bone sites, *e.g.* the spine and the hip (346, 347); however, few FEA models at the radius or the tibia using pQCT images have been developed. Thus, pQCT-based FEA models may be a research direction for the assessment of bone strength at the appendicular skeleton, which is the main purpose of this thesis.

Due to all these qualities, pQCT may therefore provide additional information compared to DXA for the assessment of bone strength and the prediction of fracture risk, and may contribute to the understanding of bone fragility in patients with fragility fracture.

2.4.3 Peripheral QCT in the prediction of bone mechanical properties

The radius is the most scanned site by pQCT. Lochmuller et al reported slightly stronger correlation of pQCT radius Crt vBMD than DXA distal radius aBMD against failure load of bending (r^2 = 0.83 vs 0.77), compression (r^2 = 0.62 vs 0.61) and falling configuration (r^2 = 0.42 vs 0.41) (326). Similar findings were reported in another falling configuration experiment by Muller et al, where r^2 was 0.48 for pQCT Crt vBMD vs 0.34 for DXA distal radius aBMD (59). However, BMC determined by both pQCT (r^2 = 0.72) and DXA (r^2 = 0.50) was found to have higher correlation with radius failure load than BMD. Ashe et al compared pQCT measurements with mechanical testing results of the radius with 10-degree inclination that mimics a falling fracture. Up to 81% of variation in radius failure load was explained by Tot BMC and Crt Thk separately, compared with 39% and 75% of DXA aBMD at the ultra-distal and distal radius, respectively. Generally, bone quantity parameters predicted failure load with medium to strong r^2 ranging from 0.51 (for Crt vBMD) to 0.81 (for Tot BMC). While Crt Thk and Crt CSA correlated strongly with failure load (r^2 = 0.81 and 0.77, respectively), polar SSI (SSI_p) and Tot CSA were found to correlate only poorly with failure load (r^2 = 0.47 and 0.12, respectively) (336).

The tibia is another site where pQCT is often applied. In a study by Kontulainen et al where correlation of compression and bending mechanical loads of the tibia was evaluated against pQCT measurements at multiple tibial sites, BSI and SSI at multiple sites (4%, 10%, 50% and 66% for BSI, 50% and 66% for SSI) were found to correlate strongly with both compression and bending failure load (r^2 = 0.60 – 0.85). For compression failure load, Tot BMC/aBMD had a stronger correlation than Trb BMC/vBMD (r^2 = 0.75/0.68 vs r^2 =

0.54/0.56, respectively). For bending failure load, Crt CSA was the best predictor at both 50% and 66% sites (r^2 = 0.86 and 0.80, respectively) (348). In another tibial bending experiment, r^2 between pQCT Crt CSA at the 25% tibia and failure load was observed to be 0.75, compared with 0.72 for cortical area determined by MRI and 0.74 for aBMD of tibial mid-shaft determined by DXA (349).

Correlations of pQCT Tot BMC at multiple sites against experimental failure load at the hip, which is a clinically important site, are relatively weak to medium (58). In both axial compression loading along the femoral long axis and side impact configuration, proximal Tot BMC was found to correlate best with femoral compression failure load with r^2 = 0.45 and 0.40, respectively. Total BMC at different sites of the radius and the tibia predicted only 30% - 44% and 27% - 41% of variations in each configuration, respectively. After including bone geometric parameters in each regression model, Tot BMC of the proximal femur was still the best predictor for compression failure load (r^2 = 0.54), while femoral neck Tot BMC became the best predictor for side impact failure load (r^2 = 0.60). Improvement was not significant for radius and tibia measurements though (r^2 = 0.33 – 0.40 for compression failure load and 0.32 – 0.42 for side impact failure load). In the next year after the previous data were published, the same research group reported further results on comparison of different imaging modalities in the prediction of femur failure load with a slightly larger sample size (138). In general, DXA measurements of different regions of the femur were found to perform better than pQCT measurements of the radius (pQCT tibial measurements were not reported in this study but were assumed to have similar correlation with femoral failure loads with the radius measurements as reported in the first study), with highest r^2 found for DXA femoral neck BMC to be 0.52 compared with 0.31 for pQCT Tot BMC of the 4% radius. However, it was also found that DXA of the radius yielded comparable r^2 (r^2 = 0.35) with pQCT radius

measures. Overall, results from these studies suggest at least for the prediction of proximal femoral strength, DXA measurements of proximal femur may perform better than pQCT radius and tibia measurements.

In a study by Weatherholt et al, pQCT measurement of the humerus was evaluated to predict humeral diaphysis torsional mechanical properties due to common spiral fracture at this site (350). SSI_p was found to correlate strongly with both maximum torque and torsional rigidity measured from the mechanical experiment (r^2 = 0.94 and 0.92, respectively). Cortical CSA (r^2 = 0.85 and 0.71, respectively) and Crt BMC (r^2 = 0.76 and 0.61, respectively) but not Crt Thk (r^2 = 0.50 and 0.35, respectively) were also found to have good correlation with these torsional mechanical properties. However, Crt vBMD did not show a statistically-significant correlation with the mechanical characteristics at this site. While results from this study may provide information about ex vivo performance of pQCT at the upper arm, in vivo application is greatly limited due to the relatively small scanning space for many people (315).

2.4.4 Peripheral QCT in the assessment of fracture risk

The role of standard pQCT measurements in discriminating patients with fracture from controls is somewhat controversial. Some studies reported good ability of standard pQCT measurements in differentiating fracture patients from controls without fracture. The AUROC and odds ratio (OR) per SD decrease were reported to range 0.63 – 0.70 and 1.56 – 2.17, respectively, for pQCT measurements at the 4% radius to distinguish patients with vertebral fracture from controls (351). Measurements of pQCT radius and tibia parameters also showed good ability to differentiate between patients with distal forearm fracture and controls without

fracture, as reported by Crockett et al (352). Drey et al reported higher OR for pQCT than for DXA measurements among older people with and without fracture (353). Longitudinal data from the Hertfordshire Cohort study showed a significant hazard ratio (HR) for incident fracture at any site associated with one SD decrease in pQCT parameters of the radius (ranging 1.24 – 1.91) and tibia (ranging 1.16 – 1.69) in women (354). Similar trends were also observed in men. After adjustment for DXA aBMD, the relationships were attenuated slightly but were still of statistical significance in both sexes. Another longitudinal study also concluded that there was a significant relationship between incident fracture and pQCT radius and tibia measurements in men, with HR ranging 1.4 – 2.2 and AUROC ranging 0.73 – 0.80 after adjustment for femoral neck aBMD (334).

Some studies reported comparable or lower ability of pQCT than DXA. Clowes et al reported comparable ability of DXA and pQCT to differentiate between women with major osteoporotic fractures (*i.e.* fracture of the forearm, the vertebrae, the hip or the humerus) and controls (355). The reported AUROC for DXA aBMD of the total hip [0.734, 95% confident interval (CI) (0.701 – 0.765)], the lumbar spine [0.727, 95% CI (0.695 – 0.758)] and the forearm [0.697, 95% CI (0.663 – 0.729)], respectively, was slightly higher than pQCT Tot vBMD [0.696, 95% CI (0.658 – 0.731)], Trb vBMD [0.685, 95% CI (0.648 – 0.721)] and Crt vBMD [0.663, 95% CI (0.625 – 0.700)] of the forearm but with no statistical significance. This trend was also seen in OR for different DXA and pQCT measurements. For hip fracture only, Augat et al observed higher AUROC of DXA aBMD at the femoral neck and the total hip (both = 0.80, no confidence interval reported) than of pQCT Tot vBMD (0.61), Trb vBMD (0.65), Crt vBMD (0.52), Crt Thk (0.56) and SSI_p (0.54) (356). For vertebral fracture only, Kroger et al reported better performance of DXA at both the spine and the femoral neck compared with pQCT radius vBMD in women (357). This was the same with DXA femoral

neck aBMD versus pQCT radius vBMD in men, but unexpectly was not the case for DXA spine aBMD versus pQCT radius vBMD (0.82 vs 0.91, respectively) which may be attributed to the small sample size of fracture patients in men.

Due to the inconsistency in the reported ability of pQCT for the assessment of fracture risk, Wong did a meta-analysis reporting the combined effect from published data at that time (358). The pooled analysis showed a combined OR of 1.44 [95% CI (1.38 – 1.51)] for Tot vBMD for the prediction of fracture of any type. Higher OR was calculated for Trb vBMD [1.50; 95% CI (1.45 – 1.56)] and Crt vBMD [1.77; 95% CI (1.69 – 1.85)], while lower OR was calculated for Crt Thk [1.25; 95% CI (1.07 – 1.46)]. The ORs varied with specific fracture site but ranged 1.25 – 1.95 generally. ORs for pQCT tibia measurements were not available due to small number of studies published at that time. While the limitation of this systematic review is lack of direct comparison with DXA, current knowledge at least backs up further exploration of pQCT in fracture risk assessment.

2.4.5 Summary

Peripheral QCT utilises a dedicated CT scanner for the determination of volumetric BMD at the appendicular skeleton. Its strength over DXA in separately analyzing cortical and trabecular compartments of bone and providing geometric assessment may enhance its clinical use. Many data are available so far supporting its high ability in predicting experimental failure load, differentiating people with and without fracture, as well as predicting incidental fracture. Although it does not surpass DXA in all measured sites or for all purposes, its role for clinical use warrants future study. Furthermore, due to the three-

dimensional data acquired by pQCT, finite element analysis based on pQCT images seems a potential research focus and is investigated in this thesis.

2.5 Finite element analysis for the assessment of bone fragility

2.5.1 Introduction

Fracture of bone is a multifactorial event (359). Intrinsically, decreased bone quantity, compromised bone quality including bone geometry, microarchitecture, mineralization, hydroxyapatite crystal characteristics, collagen characteristics, and weakened bone material properties contribute to the inability of bone to resist external forces applied on it. Extrinsically, high energy accidents and tendency to fall should also be considered (360). Assessments based on each specific aspect above have been developed for the estimation of bone strength, and statistical models combining some of these aspects are also available for calculation of fracture risk (101, 131, 290).

FEA is a mathematical and engineering method to determine the mechanical ability of a complex structure under external loading by assigning mechanical properties to each unit, or "element", in the modelling framework (361). Due to the solid mechanical characteristics of the human skeleton, FEA has gained wide application in the estimation of bone strength with the development and advancement of CT technology (347). Therefore, the ISCD endorsed its application in fracture risk assessment in their 2015 official positions (362). In this section, clinically-relevant basics and the application of FEA are reviewed from existing literature. Limitations and potential research directions are also discussed.

2.5.2 Finite element method basics

The principal of FEA is to reduce a complex structure into smaller, simple elements with known material mechanical properties (363). Therefore, estimation of whole-bone strength may be calculated by the combined mechanical behaviour of these finite elements under a

given external force. Basic mechanical background knowledge applied in FEA has been discussed in the first section of this literature review. Generally, a structure's mechanical properties can be reflected by its stiffness and yield or failure strength. With normalization of bone size (i.e. length or area), strain and yield or failure stress are obtained as material properties. Load-deformation and stress-strain curves depict the structural and material properties of bone. Both curves present an elastic phase where the Hooke's law applies and a plastic phase where irreversible changes occur beyond the yield point. These basic concepts in mechanical engineering are the basis for FEA.

Raw CT data are first segmented to isolate the region of interest, the bone, by either manual segmentation or automated software (364). Finite elements may be obtained by directly converting the voxels in CT data into a hexahedral mesh, also known as a voxel mesh, or by fitting an irregular mesh of hexahedral, tetrahedral or pentahedral elements to represent the volume of bone (365). As discussed in the previous section, the voxels of the CT image represent different attenuation coefficients of the tissue to absorb X-ray. Based on a bone density phantom, the X-ray attenuation is converted to apparent density of each voxel. The same method can also be applied to obtain tissue mechanical properties. However, the main weakness of the direct auto-transformation is the irregular surfaces which lead to difficulty in identifying where fracture would occur. Instead of hexahedral elements, tetrahedral or pentahedral elements are sometimes applied to produce smoother surfaces and more detailed fracture site of the evaluated structure (366 - 368). These tetrahedral or pentahedral elements have good ability to refine the fracture site, but they also increase elements greatly and need more manual input thus increasing processing time.

The ability of FEA to explore details of bone tissue depends on element size, which, in turn, is decided by the spatial resolution of CT image. In the human skeleton, the sizes of individual osteons and trabeculae are basically 0.2 mm and 80 – 150 μm, respectively (41). Micro CT and HR-pQCT have high spatial resolution which enables simulation of trabeculae and osteons. FEM generated from μCT and HR-pQCT images are therefore called micro FE (μFE) which denotes the ability of detailed analysis of individual trabeculae and osteons. While in QCT, and potentially pQCT, each voxel contains both osteons/trabeculae and bone marrow. FEM generated from QCT and pQCT images are therefore termed homogenized FE which denotes the determination of apparent mechanical properties of the mixed tissue. It should be noted that definitions of μFE and homogenized FE are not purely based on the spatial resolution of different CT techniques, but actually reflect whether FEA can assess details of osteons and trabeculae. Indeed, even for HR-pQCT with an in-plane resolution of 60 – 85 μm, bone volume is often exaggerated (153); therefore, homogenized FEA can be generated and performed as an alternative (365).

To predict the strength, failure criteria are applied in FE models. However, failure occurs when the external load goes beyond yield point, the termination of the elastic phase. Therefore, linear FEA investigates bone's elastic properties under a certain range of strains without detailing the failure stress occurring during the plastic phase. Nonlinear FEA can solve this problem by a sequence of mathematical linear approximations for the plastic phase (369). The requirement of multiple loading input sometimes results in extremely long processing time even on super computers. Although nonlinear FEA is still achievable for QCT-based homogenized FEA (370, 371), it is not suitable for μFEA models in population screening currently (365).

Failure criteria applied also limit the wide application of nonlinear FEA. Although simulation of the plastic phase is possible in nonlinear FEA, yield stress is needed as an input (372). However, most yield stresses applied in bone nonlinear FEA are directly from other solid materials (373 - 375). Differences in material characteristics between bone and other solid materials may make the calculated failure load invalid (375). Therefore, simplified criteria based on strain are applied in practice (376). For example, the most accepted failure criterion at the distal radius was proposed by Pistoia et al as 2% of bone tissue exceeding a strain of 0.007 (377).

2.5.3 Model validation

As with aBMD determined by DXA, bone mechanical properties calculated from FEA were compared with experimental data derived from mechanical testing for model validation. At the spine, FEA presented good ability to predict mechanical properties derived from experimental testing (134, 367, 368, 378 - 382). In a compression test of individual vertebral bodies of the lumbar spine by Crawford et al, strength and stiffness calculated from hexahedral homogenized QCT-based FEA explained 92% and 91% of variation in experimental compression strength, respectively, compared with 81% and 72% for QCT BMC and vBMD, respectively (378). Similarly, Buckley et al also reported outperformance of QCT-FEA over standard QCT measures in predicting experimental strength and stiffness in the thoracolumbar spine (134). In their study, while r^2 of FEA strength and stiffness against experimental strength were reported to be 0.80 and 0.81, the r^2 of total vBMD and trabecular vBMD were only 0.63 and 0.17, respectively. In another compression test of individual vertebral bodies of the thoracolumbar spine by Liebschner et al, stiffness

calculated from hexahedral homogenized QCT-based FEA predicted 81% and 79% of variation in experimental compression stiffness and strength, respectively (379). In their FEA model, they added a 0.35 mm thick layer of cortical shell with uniform material mechanical properties to achieve geometric accuracy. Although they did not compare FEA measures with QCT bone quantity measures directly, the inclusion of a thin cortical shell for spine FEA was accepted by many studies later (367, 380 – 382). For non-linear FEA of the spine, Imai et al reported a high r^2 between experimental and FEA yield loads ($r^2 = 0.90$), and between experimental and FEA failure loads ($r^2 = 0.96$) (368); however, Dall'Ara et al reported only medium correlation between experimental and FEA failure load ($r^2 = 0.49$) (383). In Dall'Ara's study, QCT BMC was observed to correlate better with the experimental failure load than FEA failure load ($r^2 = 0.70$). The reason may be that in this study, the loading plate was designed to rotate according to difference in resistance to loading of the anterior and posterior sides of the vertebral body. Therefore, after initial axial loading, the loading plate inclined to the weaker side. No data have been reported on the linear FEA under such loading configuration so far; therefore, it is unclear whether the finding of outperformance of QCT BMC over FEA was by chance.

At the proximal femur, FEA was reported to correlate strongly with experimental mechanical properties. Koivumaki et al reported up to 87% of variation in experimental failure load of fall configuration can be explained by FEA failure load (384). Comparable results were also reported by Nishiyama et al, of $r^2 = 0.81$ between FEA and experimental failure loads under fall configuration, and of $r^2 = 0.89$ between FEA and experimental stiffnesses (385). For stance load configuration, yield load of a linear FEA was reported to explain 89% of variation in experimental failure load (386). QCT FEA was reported to predict experimental mechanical properties of the proximal femur better than DXA. In a study by Dragomir-

Daescu et al, r^2 between FEA stiffness and experimental stiffness was 0.87, and was 0.85 between FEA yield load and experimental failure load (21). In comparison, r^2 of femoral neck aBMD and total hip aBMD were only 0.44 and 0.29 against experimental stiffness, and 0.78 and 0.71 against experimental failure load, respectively. QCT FEA also outperformed QCT BMC and vBMD measures at the proximal femur. In another study by Dall'Ara et al, QCT FEA failure load predicted 80% and 85% of variation in experimental failure loads of stance and fall loading, respectively, while the figures were 56% and 68% for QCT vBMD, and 69% and 70% for QCT BMC, respectively (371). QCT FEA stiffness predicted 82% and 74% of variation in experimental stiffness of stance and fall loading, respectively, while the figures were 31% and 61% for QCT vBMD, and 36% and 58% for QCT BMC, respectively. The superiority of FEA over standard QCT and DXA measurements was supported by results of Cody et al, who reported higher predictive ability of QCT FEA ($r^2 = 0.84$) than standard QCT ($r^2 = 0.66$) and DXA ($r^2 = 0.57$) measures for failure load under stance loading configuration (135). In a study comparing experimental failure load with yield load calculated from linear hexahedral FEA, Keyak et al reported the r^2 to be 0.94 (387). When they separately analysed stance and fall loading configurations, higher r^2 was observed for fall ($r^2 = 0.90$) than stance ($r^2 = 0.75$) loading configuration. The r^2 were also found to be higher than QCT bone quantity measures ($r^2 = 0.82$ for intertrochanteric BMC of fall loading and $r^2 = 0.61$ for sub-capital vBMD for stance loading). In another study comparing nonlinear and linear FEA models by Keyak, higher r^2 was observed for the nonlinear model ($r^2 = 0.93$) than for the linear model ($r^2 = 0.77$) under stance loading of the proximal femur (388). Later in a nonlinear tetrahedral FEA study by Bessho et al, strong correlations were observed between FEA and experimental yield loads under fall loading configuration ($r^2 = 0.89$), as well as between FEA and experimental failure loads ($r^2 = 0.96$) (389). However, for stance loading configuration, Miura et al reported only medium correlations between non-linear FEA and experimental

failure loads (r^2 = 0.62), and between non-linear FEA and experimental stiffnesses (r^2 = 0.55) (390). Overall, FEA at the proximal femur provided good predictive ability for mechanical properties obtained from experimental tests and outperformed standard QCT and DXA bone quantity measurements.

Over the past decade, most FEA at the radius was based on HR-pQCT due to its high resolution for detection of trabecular microstructure. Early in 2002, Pistoia et al used a laboratory HR-pQCT, the predecessor of the current commercial HR-pQCT scanners, to simulate radius fracture under different failure criteria (377). By applying a yield strain of 0.007 (391, 392), different percentages (1% - 7%) of bone tissue exceeding this strain were tested against experimental forearm compression loading. R^2 ranged 0.70 – 0.75 between yield load calculated from the linear μFE and experimental failure load. They concluded that using a 2% of bone tissue exceeding yield strain of 0.007 produced the best prediction (r^2 = 0.75), which was widely applied in studies later. Later in 2004, the investigators compared the same data with DXA and HR-pQCT measurements and confirmed better predictive ability of μFE than DXA and HR-pQCT for experimental failure load (393). Mueller et al challenged the failure criteria later by comparing the 2% volume with volumes ranging 0.5% - 15%, and with absolute volumes ranging 4 – 280 mm^3 (394). However, they observed comparable results with the 2% volume proposed by Pistoia et al. Indeed, most r^2 were slightly lower than r^2 of the 2% volume with exceptions of only a few cases. Micro FE also was found to predict bone strength of isolated radius (instead of whole forearm as in Pistoia's studies) with high r^2. Varga et al examined both linear and non-linear μFE against experimental properties. For linear μFE, r^2 of 0.96 was observed between μFE and experimental yield loads, and r^2 of 0.94 between μFE and experimental stiffnesses (395). For non-linear μFE, r^2 were reported to be 0.87 and 0.79, respectively, which were lower than

those of linear μFE (396). In a study by Varga et al later, they compared linear μFE and homogenized FEA against compression testing of radius specimen sections and found only slightly higher r^2 for μFE than homogenized FEA (397). R^2 between experimental and FEA stiffnesses were 0.96 and 0.95, and were 0.95 and 0.94 between experimental and FEA yield loads for μFE and homogenized FEA, respectively. With application of HR-pQCT, FEA have been observed to offer good prediction for mechanical properties at the distal radius (377, 391 – 401).

2.5.4 Clinical application of FEA

Quantitative CT- based FEA of the spine was reported to provide good discrimination of fracture patients from non-fracture controls. In a comprehensive study comparing standard DXA, QCT, HR-pQCT and QCT FEA variables among patients with low-trauma vertebral fracture and non-fracture controls conducted in the USA, Melton et al observed higher OR and AUROC for QCT FEA variables than for DXA and QCT variables (402). Vertebral fracture risk increased the most with one SD decrease of "outer" FEA compressive strength which was defined as the outer 2mm of the vertebral body in the FEA models [OR 2.5; 95% CI (1.3 – 4.8)], and of overall compressive strength of the vertebral body by FEA [OR 2.2; 95% CI (1.2 – 4.3)]. In comparison, ORs were 0.7 [95% CI (0.4 – 1.2)], 2.2 [95% CI (1.1 – 4.3)], 2.1 [95% CI (1.1 – 4.1)] and 1.1 [95% CI (0.6 – 2.0)] for DXA lumbar spine aBMD, QCT lumbar spine vBMD, QCT lumbar spine cortical thickness and HR-pQCT radius BV/TV, respectively. QCT FEA also showed better diagnostic performance than DXA, but only slight improvement was seen compared with standard QCT variables. AUROCs for the above variables were reported to be 0.81 and 0.80 compared with 0.75, 0.78, 0.79 and 0.75, respectively. Imai et al also reported the same superiority of QCT FEA over DXA and QCT

vBMD in a Japanese population (403). By applying a nonlinear FEA protocol (368, 369), FEA failure load was reported with an OR of 6.7 [95% CI (2.9 – 19.5)] compared with 1.8 [95% CI (1.1 – 3.3)] for DXA lumbar spine aBMD and 3.6 [95% CI (1.7 – 8.6)] for QCT lumbar spine vBMD. Similar results were also reported by studies of men in Europe (404, 405). Longitudinal data from the Osteoporotic Fractures in Men (MrOS) study reported HR of 9.6 [95% CI (3.9 – 14.9)] for QCT FEA of the spine (406). The HR reduced to 8.5 [95% CI (3.6 – 20.1)] after adjustment for age, race, BMI, geographic site. Although the adjusted HR was higher than DXA lumbar spine aBMD [3.4; 95% CI (2.1 – 5.4)], it was slightly lower than QCT lumbar spine vBMD [9.9; 95% CI (5.0 – 19.7)]. Overall, FEA at the spine seems to provide enhanced performance in differentiating fracture patients from non-fracture controls compared to DXA, but provides slightly better, or equivalent in some studies, prediction compared to standard QCT variables.

At the hip, differences in classifying patients with hip fracture and non-fracture controls between DXA, standard QCT and QCT FEA variables were observed to be smaller than at the spine. Nishiyama et al reported comparable AUROC for QCT FEA strength compared with QCT vBMD (0.89 vs 0.87, respectively) (407). Kopperdahl et al reported higher OR for FEA strength [6.3; 95% CI (4.0-10.0)] than for DXA femoral neck aBMD [3.7; 95% CI (2.6 – 5.3)] in women; however, the observed difference was of no statistical significance (405). The difference remained the same after adjustment for age and BMI (408). Qasim et al also higher but non-significant OR for FEA strength of fall loading configuration than for femoral neck aBMD in women [4.5; 95% CI (2.3 – 9.0) vs 3.1; 95% CI (1.8 – 5.3), respectively] (409). Comparable age-adjusted ORs were also observed in DXA total hip aBMD, QCT total hip vBMD and QCT FEA failure load by Amin et al, in both women [1.3; 95% CI (1.1, 1.5) vs 1.6 95% CI (1.1, 2.2) vs 1.3 ; 95% CI (1.0, 1.9)] and men [1.4; 95% CI (1.1, 1.8) vs 1.6;

95% CI (1.2, 2.2)] vs 1.5; 95% CI (1.1, 2.1)] (410). Longitudinal data from MrOS study reported similar finding between FEA strength and DXA total hip aBMD (411). While the unadjusted HRs for FEA hip strength and DXA total hip aBMD were 13.1 [95% CI (3.9, 43.5)] and 5.1 [95% CI (2.8, 9.2)], respectively, the gap in the adjusted HRs was much smaller [6.5; 95% CI (2.3, 18.3)] vs 4.4; 95% CI (2.1, 9.1), respectively]. The reason for the smaller difference between measurements may be, in part, that unlike the spine, the hip was not exposed to many artefacts as a result of degenerative conditions such as arthritis or aortic calcification. While DXA has difficulty deleting these artefacts from analysis, QCT segmentation can well separate them from further FEA. More importantly, hip fracture was caused by a falling more often than vertebral fracture, and neither DXA, QCT or FEA captured the risk of falling, which made the prediction similar at this site (365).

HR-pQCT-based μFEA was reported to have good ability to distinguish individuals with and without forearm fracture, but the associated fracture risk per SD decrease was not found to be superior to HR-pQCT geometric and microstructural variables, and even DXA aBMD in some studies. Boutroy et al reported that risk of wrist fracture in postmenopausal women increased 3.1-fold [95% CI (1.6, 6.2)] and 3.0-fold [95% CI (1.5, 6.0)] with each SD decrease in μFE stiffness and failure load, respectively, compared with 3.0-fold [95% CI (1.5, 5.9)] in DXA distal radius aBMD (412). However, decrease in μFE variables was not associated with higher wrist fracture risk than decrease in HR-pQCT radius Tot vBMD [OR 5.38; 95% CI (2.2, 13.3)] or Crt Thk [OR 5.14; 95% CI (2.2, 12.3)]. In another study, a 12% decrease in μFE failure load was observed between postmenopausal women with a recent radius fracture and non-fracture controls by Melton et al, which was associated with an OR of 1.8 [95% CI (1.3, 2.5)] (413). However, the decrease and OR of μFEA failure load were comparable with those of DXA distal radius aBMD [-12% difference, OR 1.9; 95% CI (1.4, 2.6)] and of

cortical thickness [-11% difference, OR 1.5; 95% CI (1.1, 2.1)]. AUROCs of these measurements were also similar (0.65 vs 0.65 vs 0.62, respectively). Findings were also observed in children. Maatta et al reported comparable OR associated with forearm low-trauma fracture for Crt Thk than for μFE failure load in both girls [7.0; 95% CI (2.0, 22.5) vs 4.3; 95% CI (1.6, 11.5)] and boys [1.82; 95% CI (0.98, 3.36) v 1.76; 95% CI (0.96, 3.20)], respectively (414). Farr et al reported μFE can differentiate young adults with childhood forearm fracture from non-fracture controls (415). In another study on premenopausal women with distal radius fracture by Rozental et al, μFE failure load of the tibia [2.14; 95% CI (1.32, 3.48)] was associated with slightly higher but non-significant OR than DXA distal radius aBMD [1.47; 95% CI (0.94, 2.29)], and μFE failure load of the radius [1.66; 95% CI (1.10, 2.50)] (416).

As the only modality that provides trabecular microstructural assessment, HR-pQCT is also used to study non-forearm fractures. Stiffness and failure load calculated from μFE of both the radius and the tibia were observed to differ between postmenopausal women with vertebral fracture and controls (417). In this study by Wang et al, OR of tibia stiffness [3.22; 95% CI (2.73, 4.16)] was higher than of radius stiffness [1.45; 95% CI (1.23, 1.66)], and of any other measures of HR-pQCT density, geometry or microstructure. Stiffness and failure load were also reported to differ between individuals with and without hip fracture (418). Zhu et al reported decreases of 12.5% and 12.7% for stiffness and failure load of radius μFE in patients with hip fracture, while the decreases were 16.9% and 16.5%, respectively, of tibia μFE. Radius stiffness and failure load were associated with OR of 2.26 [95% CI (1.04, 4.93)] and 2.35 [95% CI (1.05, 5.25)], respectively, compared with 2.15 [95% CI (1.08, 4.28)] for HR-pQCT radius Tot vBMD, and 2.64 [95% CI (1.06, 6.54)] for radius trabecular separation. Results of μFE were also reported for young people. In young girls, μFE failure load and

stiffness of the radius differed with an 8.7% and 9.4% decrease between girls with all-type fracture and controls, respectively (419). In young boys, μFE failure load and stiffness of the tibia but not the radius differed with a 5.8% decrease for both between boys with all-type fracture and controls (420). In young adult men, μFE failure load was associated with an OR of 1.2 [95% CI (1.0-1.4)] and 1.3 [95% CI (1.1-1.6)] of the radius and the tibia, respectively, for all-type fracture, compared with 1.3 [95% CI (1.1, 1.5)] for DXA radius aBMD (421). The ORs were still comparable when analysis was limited to radius fracture. Longitudinal data were also reported on HR-pQCT μFE in the prediction of fracture occurrence. Burt et al reported decreases of 12.4% (HR: 1.6) and 10.3% (HR: 1.7) in radius and tibia failure load, respectively, in postmenopausal women with major fragility fracture compared to controls (422). Szulc et al found 6.7% and 5.9% decreases in radius and tibia failure loads, respectively, in older men with osteoporotic fracture compared to controls (423). The decreases were associated with HRs of 1.62 [95% CI (1.30, 2.03)] and 1.79 [95% CI (1.44, 2.23)], respectively. Similar findings from longitudinal studies were also reported by Sonay-Rendu et al (424), Biver et al (425) and Ohlsson et al (426).

2.5.5 Limitations of FEA

Finite element analysis provides clinicians with assessment of bone strength and potentially improved discrimination of patients from controls and prediction of fracture. However, its clinical application has not been extended as for DXA. From a historical perspective, DXA has wider accessibility and lower radiation exposure than QCT. More importantly, it is the current basis for osteoporosis diagnosis although it has limitations in identifying individuals with increased fracture risk. FEA based on clinical all-purpose CT scanners has potential use for assessment of vertebral and hip strength in clinical settings. However, whether it should

be applied specifically for the purpose of bone densitometry is a dilemma. On the one hand, its inability to detect trabecular microstructure and its relatively high radiation exposure compared with DXA hinders its use as a dedicated densitometry tool. On the other hand, existing data did not demonstrate a greater superiority over DXA in fracture classification and prediction. This may partly be due to population heterogeneity observed in various studies, but may also stem from different processing configurations available for FEA. Therefore, future studies may focus more in detail on different populations and processing configurations. The same points are also argued for HR-pQCT. While resolution of HR-pQCT enables examination of trabecular microstructure, its application is limited to the peripheral skeleton in vivo. Although some studies reported HR-pQCT μFE variables differed clearly between fracture patients and controls, they did not show clear superiority over DXA and standard HR-pQCT variables. Moreover, pQCT, its counterpart with lower resolution, has wider accessibility than HR-pQCT. So far FEA has not been established specifically for pQCT, therefore, whether pQCT-based FEA provides comparable assessment for fracture risk is unknown. Overall, various FEA models have potential to provide additional information on bone fragility, but their defining role in clinical use still needs more investigation.

2.6 Bone fragility following surgical menopause

2.6.1 Ovarian cancer, risk factors and oophorectomy

Ovarian cancer is the eighth most common and potentially-lethal cancer in women (427, 428). It was estimated that there were 295,414 new cases and 184,799 deaths associated with ovarian cancer globally in 2018. Age-adjusted incidence and mortality were 7.0% and 3.8% in developed countries, and 5.7% and 4.0% in developing countries. The highest incidence was observed in Eastern and Northern Europe, and the lowest in Middle and Western Africa and Eastern Asia (429).

Ovarian tumours are heterogenous in histological origin, which is the basis for the WHO classification (430, 431). Although clear cell tumours and transitional cell tumours occur, epithelial tumour, including serous, mucinous, and endometrioid tumours, accounts for 90% of cases found in clinical settings (432).

Family history is the most important risk factor for ovarian cancer (429, 433, 434). Jervis et al reported 3.0-fold higher risk in individuals who had first-degree relatives with ovarian cancer compared with those who did not (434). The risk increased to 4.7 folds if the first-degree relative was diagnosed before 50 years, and to 3.6 folds if was diagnosed with serous tumour. Heredity of ovarian cancer is associated with breast-cancer susceptibility gene (BRCA) mutations, although the mutations are also observed in patients with no family history (435). BRCA1 gene located on the long arm of chromosome 17 and BRCA2 gene located on the long arm of chromosome 13, were first discovered in families with a high incidence of breast cancer (436). Both genes are involved in maintenance of genomic stability by repairing DNA double-strand breaks and regulating DNA transcription (437 – 439).

BRCA1 is also involved in oxidative stress regulation and ubiquitin ligase activity (440, 441). While the normal function of BRCA1 and 2 is crucial for tumour suppression, the specific mechanisms of BRCA1 and 2 mutations in development and progression of ovarian cancer remain unclear (442). Nevertheless, BRCA1 and 2 mutation carriers have a lifetime risk of 40% and 15% for developing ovarian cancer, respectively (443, 444).

Other hereditary factors also contribute to the development of ovarian cancer. Lynch syndrome or hereditary nonpolyposis colorectal cancer (HNPCC) accounts for 10 - 15% of hereditary ovarian cancer (445). Mutations of multiple genes responsible for repair of DNA mismatch errors are involved in Lynch syndrome, and most of those are mutations of mutL homolog 1 (MLH1) and mutS homolog 2 (MSH2) (446, 447). Lack of normal protein products of these genes causes microsatellite instability (the abnormally repeated nucleotides) to accumulate, which results in the occurrence of cancers including gastric, colon, rectal and ovarian cancer (448). Li-Fraumeni syndrome is a rare autosomal dominant disorder predisposing patients to various cancers, primarily breast cancer, brain cancer and sarcoma, in children and young adults (449). Ovarian cancer is also seen in patients with Li-Fraumeni syndrome although not as often as the tumours above. Mutation of tumour protein p53 (TP53) gene, one of the most important tumour-suppression gene, is involved in this syndrome (450 – 452). Mutations of many other genes, including RAD51, PALB2, CHEK2, Mre11, NBS11, RAD50, BARD1, BRIP1, WNT4, are also involved in certain stages of oncogenesis in ovarian cancer (429, 453 - 455).

Non-hereditary factors have also been associated with ovarian cancer. Two meta-analyses have concluded that there is a positive correlation between obesity and ovarian cancer risk

(456, 457). Another meta-analysis found greater adult height increases the risk (458). The risk increases in smoking women, and decreases after they quit smoking (459, 460). Late menarche is associated with increased risk for ovarian cancer (461, 462), while pregnancy, breastfeeding and additional births reduce the risk (462 - 464). Combined oral contraceptive pills has been shown to be negatively correlated with ovarian cancer risk (465), but menopausal hormone therapy increases the risk regardless of whether estrogen-only or combined hormones (466). Other factors have also been correlated with ovarian cancer risk, either positively (*e.g.* diabetes, pelvic inflammation, genital talcum powder use, sedentary time), or negatively (*e.g.* aspirin use, vitamin D supplementation); however, existing data on these factors are not adequate to reach a final conclusion (429).

Although some factors associated with ovarian cancer risk are modifiable, most of these risk factors, especially heredity, cannot be changed or are difficult to modify. Increasing availability of gene testing means that more women are aware of their high-risk status. However, current screening strategies cannot detect ovarian cancer at an early stage (467). In fact, the only effective intervention currently associated with reduced death risk among high-risk women is prophylactic ovariectomy or RRBSO (468, 469). Salpingo-oophorectomy is the surgical procedure to remove the ovaries and fallopian tubes for benign or malignant diseases. In women with high risk for ovarian cancer, RRBSO has been shown to be associated with an 80 – 85% reduction in the risk of ovarian cancer, and a 75 – 77% reduction in mortality (470, 471). However, since RRBSO is recommended at a premenopausal age, early surgical menopause following RRBSO may raise multiple health concerns, including menopausal syndrome, coronary heart disease, sexual dysfunction, dementia and compromised bone health (472 - 475), which need to be considered during clinical decision-making.

2.6.2 Estrogen effects on bone metabolism

Estrogen plays a major role in regulating bone metabolism in both women and men (193). Estrogen deprivation leads to increased activity of both bone resorption and bone formation (476). Since the effect is stronger for bone resorption than for bone formation, this leads to bone loss. Hormone replacement therapy in postmenopausal women has been proved to reduce bone resorption (477, 478). Changes in bone formation are somehow complicated though during hormone therapy: an initial increase has been observed when the therapy is started, followed by a long-term decrease (477). However, the decrease in bone resorption is greater than in formation, leading to increased bone density (479 – 481).

As discussed in Section 2.1, bone remodelling involves three types of bone cells: osteoclasts for resorption, osteoblasts for formation, and osteocytes for initiation of bone remodelling. The regulatory effects of estrogen are reflected by its interactions with all the three types of cells. The osteocyte is an important estrogen target cell in bone (482). Studies have found increased osteocyte apoptosis in biopsies of premenopausal women with estrogen deficiency (483). Consistent findings have also been observed in animal models (484, 485). The preventative role of estradiol in osteocyte apoptosis has been demonstrated by cytological studies (486). The prevention appears to link with multiple protein kinase activation working against Bcl-2 associated death promotor. Therefore, the anti-apoptosis effect of estrogen maintains the number of functional osteocytes, thus promoting bone remodelling.

Estrogen modulates bone remodelling also by direct and indirect interaction with osteoclasts. Osteoclasts have many estrogen receptors (487). By combining with these receptors, estrogen

induces osteoclast apoptosis by upregulating transforming growth factor β (TGF β) (488, 489). Estrogen also directly disturbs osteoclast differentiation by suppressing the activity of receptor activator of nuclear factor κB ligand (RANKL) and blocking transcription by activator protein-1 (AP-1) (198, 490 – 492). Estrogen also supresses RANKL production by T-cells. In bone, expansion of T-cells is associated with increased tumour necrosis factor-α (TNF-α), which is involved in osteoclast differentiation (493 – 495).

Three potential mechanisms may be involved in the regulation of bone formation by estrogen. First, estrogen has been shown to prolong osteoblast lifespan by disturbing its apoptosis through Src-ERK pathway (496). Second, animal studies have observed oxidative stress in bone attenuated osteoblastogenesis in estrogen deficiency. Therefore, estrogen may work in an inverse way to enhance bone formation (497 - 499). Third, estrogen deprivation has also been associated with enhanced activity of nuclear factor κB (NF- κB), and disturbed NF- κB activity was observed to alleviate bone loss following ovariectomized animals (500). This may be another potential mechanism by which estrogen preserves bone tissue.

In summary, the protective role of estrogen in bone involves its interaction with osteocytes, osteoclasts and osteoblasts. Estrogen has been shown to participate differently in the apoptosis of different bone cells. While it prolongs lifespan of osteocytes and osteoblasts, it induces osteoclast apoptosis. Estrogen also disturbs RANKL-induced osteoclast differentiation to reduce bone resorption. It potentially works against oxidative stress and NF-κB activity in osteoblasts, however, more research is needed to explore these mechanisms in detail.

2.6.3 Bone loss following surgical menopause

Due to the protective role of estrogen in bone health, and the estrogen deprivation following RRBSO in women with high risk of ovarian cancer, understanding of bone fragility in this population is of great clinical importance since many women undergoing RRBSO have not reached natural menopause before the surgery (501). However, it was reported that more than half of all patients had not received a bone density test 6 years after RRBSO (502, 503), which makes it particularly important to acquire data on bone fragility in this population.

A high prevalence of low bone density was observed in women undergoing RRBSO. Garcia et al reported that 12.1% of women following RRBSO had osteoporosis and 55.6% had osteopenia (503) according to the WHO criteria. Similarly, Cohen et al reported a high prevalence of osteoporosis (14%) and osteopenia (57%) in women undergoing premenopausal RRBSO with an average age of 56 years (504). Prevalence of low bone density did not differ between women undergoing premenopausal RRBSO and postmenopausal RRBSO (70% vs 72%, respectively). However, no control data were available in this study. Michelson et al reported higher prevalence of low bone density in women following RRBSO (8%) than in controls (3%), and no difference between premenopausal and postmenopausal RRBSO (both 13%) (505). Powell et al noted a prevalence of 72.5% for low bone density in women undergoing RRBSO compared with 55.0% in controls, although the difference was not statistically significant (506). In contrast to Cohen's results, a higher prevalence of low bone density was observed in women undergoing postmenopausal RRBSO than premenopausal RRBSO (82.1% vs 63.4%, respectively). Significant age difference existed between women undergoing premenopausal and postmenopausal RRBSO in these studies due to the study designs (44.7 vs 60.6 years in

Cohen's study, and 51 vs 62.5 years in Powell's study, respectively), which may confound the results. In addition, there was great heterogeneity in the hormone therapy provided, which made interpretation of the results difficult. In a study by Challberg et al, the investigators divided women following RRBSO into three groups with comparable ages based on hormone therapy use: no estrogen deprivation, estrogen deprivation of 1 – 23 months, and estrogen deprivation of more than 24 months (507). Higher prevalence of low bone density was found in the estrogen deprivation groups (40% for 1 – 23 months deprivation and 47% for more than 24 months deprivation) than in the non-deprivation group (16%).

Bone loss was observed following RRBSO in several retrospective studies. Hibler et al reported 8.5% and 5.7% decreases in aBMD at the lumbar spine and the hip, respectively, within 18 months following RRBSO, although no comparison was available between these women following RRBSO and healthy controls (508). Similar findings were reported by Kotsopoulos et al. Average annual decreases of 3.45%, 2.85% and 2.24% in aBMD at the lumbar spine, total hip and femoral neck, respectively, were observed in women undergoing premenopausal RRBSO during an average of 22 months follow up (509). When the analysis was separated according to hormone therapy following surgical menopause, less bone loss was found in hormone users than in non-hormone users (decrease of 2.0% vs 4.7% at the lumbar spine, of 1.4% vs 3.2% at the total hip, respectively). Bone loss was also observed in women undergoing postmenopausal RRBSO (0.8% at the lumbar spine, 0.7% at the femoral neck and 0.2% at the total hip) but was less than in premenopausal women. Fakkert et al compared bone density at 5 years post RRBSO with reference data (510). Z-scores were +0.01 and +0.15 for aBMD at the lumbar spine and the femoral neck, respectively. However, 13% of the subjects were postmenopausal at the time of surgery and they did not provide a separate analysis, which was a limitation of their data.

It should be acknowledged that all these studies were retrospective that are prone to bias. Since a randomised study on RRBSO would face ethical issues, non-randomised observational studies with prospective design and longitudinal follow-up are needed to help understand the impact on bone health in this population. Although two recent systematic reviews concluded that no difference in bone loss was observed between women with surgical menopause and natural menopause (472, 511), more valid interpretation should be obtained from prospective studies.In addition, among the published data, comparison with control group was not available due to the study designs. More importantly, only DXA was involved in the assessment of bone health in these studies, which may not reflect detailed changes in bone mechanical properties in this population. Therefore, other assessment tools should be applied in future studies.

2.7 Bone fragility in Type 1 diabetes mellitus

2.7.1 Incidence and prevalence of Type 1 diabetes mellitus

Diabetes mellitus (DM) is a medical condition defined by impairment of glucose metabolism, leading to high blood sugar, or hyperglycaemia (512, 513). There are two major types of diabetes. Type 1 diabetes mellitus (T1DM) is characterized by destruction of pancreatic beta cells leading to absolute insulin deficiency. T1DM is often called juvenile diabetes due to the many cases diagnosed at childhood or adolescence, but it can affect patients of all ages. This type accounts for 5% - 10% of all diabetes types. Type 2 diabetes mellitus (T2DM) is caused by weakened response of body to insulin leading to relatively inadequate insulin. As the most common type of diabetes, T2DM are diagnosed in adults most of the times although its prevalence in young people is increasing (514, 515).

According to the WHO data, global incidence of T1DM in children varied from 0.1/100,000 in China to 40.9/100,000 in Finland (516). The World Health Organization Multinational Project for Childhood Diabetes (517), or DIAMOND project, is a multicentral study conducted in 112 centres from 57 countries. The data were based on 43,013 T1DM cases from 740 million children aged less than 14 years during 1990 – 1999. Most Asian countries had a low incidence of less than 1/100,000 while high incidence was found in Europe and North America, averaging 20/100,000. The observed incidence increased with age. Children aged 10 – 14 years had 1.9 folds higher T1DM incidence than children aged 0 – 4 years, compared to 1.6 folds for children aged 5 – 9 years.

Another multicentre project reporting incidence as well as prevalence of T1DM is the SEARCH for Diabetes in Youth (SEARCH) study conducted in individuals aged less than 20

years in the USA (518). It was found that in 2002 – 2003, a total of 2561 diabetes cases led to an incidence of 24.3/100,000, among which up to 80% were T1DM cases (515). The 10 – 14 years group was observed to have the highest T1DM incidence (25.9/100,000), followed by the 5 – 10 years (22.1/100,000) and 15 – 19 years groups (13.1/100,000). The 0 – 4 years group had the lowest T1DM incidence (14.3/100,000) with no T2DM case found in this population. This trend was similar to findings from the DIAMOND project. Non-Hispanic white individuals were found with the highest incidence in all age groups (ranged 15.1 – 32.9 /100,000) compared the lowest incidence in American Indians in all age groups (ranged 4.1 – 8.0/100,000). Results from another part the SEARCH project estimated the prevalence of T1DM was 2280/100,000 in youths aged less than 20 years with similar distribution of age and ethnicity (514).

Globally, T1DM incidence was increasing by an annual rate of 2.8% from 1990 – 1999. During the last five years of the study period of the DIAMOND project, this rate was even higher (3.4%) (516). The increasing incidence was also observed in the SEARCH study. The incidence increased from 14.8/100,000 in 1978 – 1988 to 23.9/100,000 in 2002 – 2004, representing an annual increase of 2.3% among American young people (519). Data from EURODIAB project, another large multicentre study across 26 European countries and Israel (520), also showed an annual increase in T1DM incidence of 3.4% in Europe, with the highest increase observed in children aged 0 – 4 years (6.3%) (521). While these increases in T1DM incidence do not seem to be fully explained by genetic factors in the short term, data suggest that environmental factors may contribute to this trend (522 - 524).

2.7.2 Risk factors of Type 1 diabetes mellitus

Genetic factors contribute to susceptibility of T1DM. It was reported that individuals with a first-degree family member with T1DM had a 15 times higher risk of T1DM compared with the general population (525). Human leukocyte antigen (HLA), especially HLA class II, is the most important gene predisposing an individual to T1DM (526). It was reported that up to 95% of children with T1DM carried either or both of two major haplotypes in the HLA class II region (527).

As discussed above, T1DM is diagnosed mostly in young people and the incidence peaks at the ages of 10 – 14 years. Incidence of T1DM appears to decrease after the age of 16 years and stabilizes during 16 – 29 years (514 - 516, 521, 528 - 530). Race and ethnicity also affect incidence and prevalence of T1DM. While non-Hispanic white people were reported to have the highest rates of T1DM, Asians and Pacific Islanders were found to have relative low rates (531 - 536). Gender may also be a risk factor of T1DM. Although on average no difference in T1DM incidence and prevalence was observed between boys and girls across all ethnic groups (537), more boys than girls were found with T1DM among those of European origin (520, 538). This distinction was more significant in adults with a male-to-female ratio of more than 1.5 (539 – 542).

Birth month may also play a potential role in T1DM onset. Higher onset rates of T1DM were reported in spring than in fall or winter months (543 – 547). This phenomenon may be due to the seasonal effect of vitamin D on pancreatic cells and the immune system (548, 549). Nutrition *e.g.* milk consumption at early stage of childhood has also been associated with T1DM onset although the effects are not well understood and sometimes results are

conflicting (550 – 553). Wheat gluten and vitamin E were also reported to protect infants and children from T1DM onset (554 – 556).

Overall, individuals with T1DM were born with genetic susceptibility to autoimmune destruction of pancreatic β cells while various environmental factors work as triggers to the natural history of T1DM (557- 559). The process of compromised insulin secretion is gradual and progressive, and never reaches a net zero in some patients (560). This causes a marked gap between autoimmunity onset and symptomatic onset, which may be big in some patients. Moreover, it is still unclear to what degree of β cell destruction would lead to symptomatic onset. Historically, it was believed that symptoms of T1DM would not present until 80% - 90% of β cells were destroyed (561). However, more recent data suggest that the proportion should be up to 50% (562). This may explain the preclinical stage of T1DM where early serological alterations in amino-acids and autoantibodies are detected but insulin secretion can remain stable for a long time (557, 563 – 565). All in all, there are still much uncertainty about the roles of various genetic and environmental factors from autoimmune onset to clinical onset of T1DM, which remains a future research direction.

2.7.3 Bone fragility in Type 1 diabetes mellitus

Diabetes is associated with increased fracture risk (566 - 568). In a large population cohort study consisting of 30,394 participants with T1DM and 303,872 controls, Weber et al reported increased fracture risk in T1DM patients of all age groups (569). Their data from the United Kingdom Health Improvement Network (UK THIN) found HR for fracture were highest in women aged 40 – 49 years [2.03; 95% CI (1.73, 2.39)] and men aged 60 – 69 years [2.18; 95% CI (1.79 – 2.65)]. Lowest HRs were observed in both females [1.35; 95% CI

(1.12, 1.63)] and males [1.14; 95% CI (1.01, 1.29)] aged less than 20 years. A wider gap between young adults with and without T1DM was observed in females than in males. In addition, a statistically higher proportion of lower limb fracture (fractures of the femur, tibia, fibula, ankle and foot) was noted in participants with than without T1DM (39.3% vs 32% in females, and 31.1% vs 25.1% in males, respectively). HRs for hip fracture were 5.63 [95% CI (2.25, 14.11)] for women aged 30 – 39 years and 5.64 [95% CI (3.55, 8.97)] for men aged 60 – 69 years. Therefore, the high relative fracture risk observed in young adult females and the high proportion of lower extremity fracture in T1DM patients may need more research seeking underlying mechanisms. Shah et al reported higher fracture incidence in adults with than without T1DM (570). In this meta-analysis consisting of 27,300 T1DM cases and 4,364,125 controls, fracture incidences were 2,066 (7.6%) versus 136,579 (3.1%) for each group, respectively. Relative risk (RR) of all-site fracture from pooled analysis was 3.16 [95% CI (1.51, 6.63)] in T1DM patients compared with controls. When fracture sites were analysed separately, RRs for hip and vertebral fracture were 3.78 [95% CI (2.05, 6.98)] and 2.88 [95% CI (1.71, 4.82)], respectively.

There is inconsistency in DXA findings reported between individuals with and without T1DM. In females, some but not all studies reported lower aBMD in T1DM patients than in controls at the femoral neck (571 - 578) and the lumbar spine (578, 579). While many studies did not find any difference in aBMD between individuals with and without T1DM at either the femoral neck (580 - 584) or the lumbar spine (575 – 577, 580 - 584), several studies reported higher aBMD in T1DM patients than in controls at both the femoral neck (585) and the lumbar spine (571, 581, 585). In males, most studies did not find any difference in aBMD between individuals with and without T1DM at the femoral neck (573, 577, 579, 580, 582) and the lumbar spine (577, 579, 580, 582 - 584), while several studies reported lower aBMD

at the femoral neck (583) and the lumbar spine in T1DM patients (578, 579). A pooled analysis of some of these studies by Shah et al concluded that there was modestly lower aBMD at the femoral neck in T1DM patients while no statistical difference was found in aBMD at the lumber spine (566). Results from these studies contribute minimally to the observed high risk in T1DM patients, which makes further investigation of bone fragility necessary. In these studies, DXA was still the most applied tool for bone examination, which may be the reason for the gap.

Similar findings were also reported using serological examinations. Meta-analyses did not find any difference in serum calcium, phosphorus or parathyroid hormone levels (586) between T1DM patients and controls, while bone turnover markers (BTM) were modestly lower in T1DM patients than in controls (586, 587). Bone geometric measurements have provided more information about bone fragility in T1DM patients. Reduced cortical thickness and smaller cross-sectional area determined by QCT were observed at the intertrochanteric region of the proximal femur (588). Thinner cortical shell at the distal radius in T1DM patients was also detected by pQCT (589) and HR-pQCT (590). In the HR-pQCT study, however, no difference was observed in micro-structural parameters between T1DM patients and controls. This finding contrasts with results of a MR-MRI study, where the authors reported lower trabecular number and higher trabecular spacing at the proximal tibia in T1DM patients (591). Although these modalities may provide more insights into our understanding of bone fragility, there are not as much data as on DXA in T1DM patients, especially in young adults in the bone accrual period. Further research should be conducted in this population to gain more knowledge for the prevention and management of fractures in patients with T1DM.

Chapter 3

Research aims and general methods

3.1 Research aims

As outlined in the literature review, DXA detects only some of the determinants contributing to whole-bone strength, and therefore has limitations in identifying individuals with increased fracture risk. The ability of pQCT to measure volumetric bone density and to separately analyse cortical and trabecular compartments of bone enables it to provide additional information about bone fragility, especially at the appendicular skeleton. Furthermore, the three-dimensional data acquired can be used to generate FEA models providing estimates of bone mechanical properties in different populations with a higher fracture risk than general population. Therefore, the aims of this doctoral research are:

1. To validate pQCT-FEA against mechanical properties derived from cadaveric specimens
2. To investigate the diagnostic performance of pQCT-FEA in classifying older patients with fragility fracture and controls
3. To apply pQCT-FEA in the assessment of bone fragility in women following surgical menopause
4. To apply pQCT-FEA in the assessment of bone fragility in young adult women with T1DM

3.2 Study design, location, recruitment and ethics

Four sub-studies were conducted to address the research aims described above. For aim 1, a validation study was based on collaborative work between the University of Melbourne, Australia and the University of Saskatchewan, Canada (Chapter 4). Cadaveric forearm specimens were prepared, scanned and tested in the laboratory based at the Department of Biomedical Engineering, University of Saskatchewan. Peripheral QCT data were then transferred to the Department of Biomedical Engineering, University of Melbourne for FEA simulation. My work in this study included segmentation of the pQCT data for pQCT-FEA, as well as analysis and interpretation of the data, and writing the manuscript for publication.

For Aims 2 – 4, participant recruitment was based at the Parkville Biomedical Precinct, Australia (specifically, University of Melbourne, Royal Melbourne Hospital, Royal Women's Hospital). DXA and pQCT scans were performed and analysed at the Bone Densitometry Unit (BDU), Royal Melbourne Hospital. All pQCT-FEA simulations were generated and analysed at the Department of Biomedical Engineering, University of Melbourne.

The study addressing Aim 2 was cross-sectional, comparing variables from DXA, standard pQCT and pQCT-FEA between fracture patients and controls. Fracture patients were recruited from a multidisciplinary fracture liaison service involving endocrinology, orthopaedic surgery, emergency and radiology departments at the Royal Melbourne Hospital. All patients were either approached when attending an orthopaedic fracture clinic or endocrinology clinic or were referred by an endocrinologist or orthopaedic surgeon. Controls were recruited from multiple sources: (1) by talking with family members of fracture patients at the clinics; (2) targeted advertising posters and flyers at the hospital; (3) targeted

recruitment from the volunteer service team of the hospital; (4) electronic communications with community education programs for older people (University of the Third Age) in metropolitan Melbourne; (5) advertisement in the University of Melbourne staff and student notice systems. My work in this study included ethics application and research administration, recruiting all participants, performing DXA and pQCT scans for most participants, performing DXA, pQCT and pQCT-FEA analysis, analysing and interpreting data, writing the manuscript for publication.

The study for Aim 3 was part of the What Happens After Menopause (WHAM) study, a multinational prospective study on the effect of RRBSO on various health issues. Longitudinal data on bone outcomes were obtained from the Melbourne, Australia, site. Women with high risk of ovarian cancer who underwent RRBSO were recruited from multiple familial cancer and gynaecological oncology services and via targeted advertising though mainstream and electronic media by a study coordinator. Controls were recruited via mainstream and electronic advertising to the general public and by referring from high-risk participants. My work in this study included performing DXA and pQCT scans for most participants, performing DXA, pQCT and pQCT-FEA analysis, analysing and interpreting data, writing the manuscript for publication.

The study for Aim 4 was cross-sectional and was part of two large studies on young women's health conducted at the Royal Melbourne Hospital and the Royal Women's Hospital. The Safe-D study was a large, comprehensive project investigating the role of vitamin D in young Australian women's health. The Young Female Health Initiative (YFHI) was a comprehensive study investigating various aspects of young Australian women's health and

wellbeing. Bone health was one of the themes for both studies. Young females with T1DM and controls were recruited for these studies via Facebook. Females with T1DM were also recruited from the Young Adult Diabetes Service at the Royal Melbourne Hospital. My work in this study included performing DXA and pQCT scans for some of the participants, performing DXA, pQCT and pQCT-FEA analysis, analysing and interpreting data, writing the manuscript for publication.

All studies were conducted in accordance with the Declaration of Helsinki. Ethics approvals were obtained from respective institutions' research ethics committees. The study for Aim 1 was approved by the University of Saskatchewan Biomedical Research Ethics Board (ethics reference 09-96). The study for Aim 2 was approved by Melbourne Health Human Research Ethics Committee (ethics reference MH 2014.143). The study for Aim 3 was approved by the Melbourne Health Human Research Committee (ethics reference MH 2013.060), Royal Women's Human Research Ethics Committee (ethics reference RWH 12/50), and The Peter MacCallum Cancer Centre Human Research Ethics Committee (ethics reference HREC/12/PMCC/24). The study for Aim 4 was approved by Melbourne Health Human Research Ethics Committee (ethics reference MH 2013.007 and MH 2012.189) and Royal Women's Human Research Ethics Committee (ethics reference RWH 11/14).

3.3 DXA scanning and analysis

DXA scans were performed for participants in the studies for Aims 2 – 4. A fan beam densitometer (Horizon QDR4500A, Hologic Inc., Bedford, MA, USA) was used to scan all participants. All scans were performed in fast array mode. A quality control spine phantom with known bone density and content was scanned prior to any patient scan daily to ensure the reproducibility of the machine's results.

DXA scans were performed on the lumbar spine using the manufacturer's standard AP (anteroposterior) Lumbar Spine protocol, and on the hip using manufacturer's standard Left/Right Hip protocol. All participants were lying supine on the scanning table during scanning. For lumbar spine scans, both legs of participants were elevated using a cubic Hologic positioning cushion. For hip scans, a foot trap was used to stabilize and invert the leg being scanned. Scans were not performed on a participant's hip/lumbar spine where previous surgery had been performed *e.g.* hip arthroplasty, laminectomy, as in such situations artefacts would affect the analysis. A participant who had undergone DXA scans within recent 8 weeks was not scanned again. In such situations, his/her latest DXA data were used; however, in order to eliminate variations caused by different DXA machines and operators, only DXA scans performed at the BDU of the RMH City Campus were accepted.

The manufacturer's commercial software (version 9.10D) was used to analyse DXA scans and to obtain aBMD of the lumbar spine, the femoral neck and the total hip. For lumbar spine analysis, the horizontal boundaries of the four vertebrae of interest (L1-L4) were selected first. The analysis software then identified these vertebrae automatically based on the chosen protocol. If there was more than 1 SD difference between one vertebra and adjacent

vertebrae, either caused by local structure or metal/calcification artefeacts, or other defined/undefined medical conditions, that vertebra was excluded from analysis. For hip analysis, the investigator moved lines identifying the global region of interest. Bone tissue, as well as subregions, were outlined within the selected region.

3.4 Peripheral QCT scanning and analysis

An XCT 3000 pQCT scanner (Stratec Medizintechnik, Pforzheim, Germany) was used to scan all participants' tibia and/or radius in Studies 2 - 4. The working settings of the scanner are summarized in Table 3.1. Analysis of pQCT data was performed by the same investigator. Training was provided by an experienced technician, and regular inspection and supervision was also conducted to ensure reproducibility of analysis.

Participants were positioned on a dedicated scanning chair which can be rotated and moved orthogonally to the machine axis to bring the limb axis parallel to the machine axis. A leg or forearm holder enabled the limb scanned to be fixed in an appropriate position. A scout view (SV) scan was performed prior to the CT scan to ensure the correct scanning sites. During the SV scan the exact starting position of the measurement was defined. The software proposed automatically a reference line, which was the starting position of the measure in most cases. In cases where an automatic reference line was not positioned through the centre of the distal metaphysis surface, the operator defined it manually. Once the reference line was defined, the CT scan started. Scanning sites were the 4% and 66% sites of participants' non-dominant tibia and forearm. The length of the tibia/forearm was measured using a standard ruler provided by the manufacturer. In the tibia, length was defined as the distance from the medial malleolus to the superior margin of the medial condyle. In the forearm, length was defined as the distance from the ulna styloid process to the olecranon process. If a participant had a fracture on his/her non-dominant tibia/forearm, scans of the dominant tibia/forearm were performed. In situations where a participant had fractures of both tibias/forearms, scans were not performed on his/her tibia/forearm. In order to eliminate movement artefact, which had a

deleterious effect on the analysis process, all participants were educated to stay still during scanning.

Stratec commercial software (version XCT 5.50E) was used to perform pQCT analysis and to obtain various variables, including Tot vBMD, Trb vBMD, Crt vBMD, CSA, Crt Thk, SSI. In the analysis process, a specific region of interest containing bone tissue was determined automatically first. All voxels outside the bone (soft tissue) with lower attenuation coefficient than the selected threshold were removed within the region of interest. The function CALCBD was applied to yield the results for total, trabecular, and cortical-subcortical bone density and the cross-sectional area at the 4% site. CONTOUR mode was applied to define the way the outer contour of the bone was detected. A default threshold of 280 mg/cm^3 was applied in this mode. Separation of cortical and trabecular structure was obtained by the areal distribution of both bone structures using PEEL mode by applying a default threshold of 710 mg/cm^3. By default, 55% of the outer bone area was concentrically separated and defined as the subcortical region. The remaining 45% inner core was defined as trabecular bone. The function CORTBD was applied to calculate cortical density and area at the 66% site. The function SSI was used to calculate the bone strength with respect to torsion. The default threshold for SSI was 480 mg/cm^3. Polar stress strain index, which reflects the torsional bone strength, was obtained using this function.

In the study for Aim 1, pQCT scans were performed using an XCT 2000 pQCT scanner. The same scanning protocol applied for the scanning process.

Table 3.1 Working settings of Stratec XCT 3000

X-ray tube	
Voltage	60kV
Current	<0.3mA
Mean X-ray energy	42keV
Energy distribution after filtration	19keV
Detector	12 semiconductor detectors with amplifier
Mechanic	
Linear scan range	250mm
Scan time	6-15 s per translation
Rotation angle	180°
Rotation speed	13°/s
Maximum axial scan length	280mm
Axial scan speed	20-50mm/s
Central gantry opening	300mm
Image	
Slice thickness	2mm
Voxel size	0.4mm

3.5 Mechanical testing in the validation study

Detailed methods for mechanical testing settings are described in Chapter 4.

3.6 pQCT-FEA simulation

Detailed simulation procedures are described in Chapters 4 – 7 and Appendix 2.

Chapter 4

Predicting experimentally-derived failure load at the distal radius using finite element modelling based on peripheral quantitative computed tomography cross sections (pQCT-FE): a validation study

4.1 Predicting experimentally-derived failure load at the distal radius using finite element modelling based on peripheral quantitative compute tomography cross sections (pQCT-FE): a validation study

Authors and affiliations:

Hongyuan Jiang [a], Dale L. Robinson [b], Matthew McDonald [c], Peter V.S. Lee [b], Saija A. Kontulainen [e], James D. Johnston [c], Christopher J. Yates [a,d,f], John D. Wark [a,d, f]

[a] Department of Medicine, Royal Melbourne Hospital, University of Melbourne, Melbourne, Australia

[b] Department of Biomedical Engineering, University of Melbourne, Melbourne, Australia

[c] Department of Mechanical Engineering, University of Saskatchewan, Saskatoon, Canada

[d] Department of Diabetes and Endocrinology, Royal Melbourne Hospital, Melbourne, Australia

[e] College of Kinesiology, University of Saskatchewan, Saskatoon, Canada

[f] Bone and Mineral Medicine, Royal Melbourne Hospital, Melbourne, Australia

4.2 Abstract

Dual energy X-ray absorptiometry, the current clinical criterion method for osteoporosis diagnosis, has limitations in identifying individuals with increased fracture risk, especially at the distal radius. Peripheral quantitative computed tomography (pQCT) can provide volumetric bone density data, as well as information on bone geometry, which makes it possible to establish finite element (FE) models of the distal radius from which bone strength and stiffness can be calculated. In this study, we compared experimental mechanical failure load data of the forearm with pQCT- based FE (pQCT-FE) modelling properties. Sixteen cadaveric forearm specimens were experimentally loaded until failure. Estimated stiffness and strength variables of compression, shear, bending and torsion were calculated from pQCT-FE modelling of single cross-sections of 0.2 x 0.2 x 2.4 mm of the radius pQCT image. A moderate-to-strong coefficient of determination (r^2) was observed between experimental failure load and pQCT-FE variables. The highest r^2 was observed for bending stiffness ($r^2 = 0.83$). This study validates the use of pQCT-FE in the assessment of distal radius bone strength for future studies.

4.3 Introduction

The prevalence of osteoporosis and subsequent fragility fractures (*i.e.* a fracture resulting from a minimal trauma such as a fall from a standing height or less. All fracture refers to fragility fracture in the following paragraphs) is increasing worldwide mainly due to population ageing (592, 593). A key to reducing this great public health burden is to identify individuals with increased risk for compromised bone strength (*e.g.*, failure load, stiffness). The most established tool for the assessment of fracture risk is based on areal bone mineral density (aBMD) determined by dual energy x-ray absorptiometry (DXA), which is utilised in various algorithms for the calculation of absolute fracture risk (594 - 596). However, DXA has limitations in the assessment of bone strength. On one hand, as a projective technique, it does not take bone volume adequately into consideration; rather it provides an 'areal' bone mineral density (aBMD) in g/cm^2, which represents the bone mineral content within a projected area of bone. On the other hand, bone failure strength is determined not only by bone quantity, but also by how trabecular bone is spatially distributed (60), which is not represented well by conventional DXA measures. Previous studies have observed that DXA measurements only explain part of bone strength, with r^2 ranging from 0.31 – 0.56 between different DXA variables and failure load of the radius in falling configurations (324, 326, 377, 597). Therefore, alternate clinically-relevant fracture risk assessment strategies are needed at the distal radius.

Other than bone quantity, bone quality also contributes strongly to bone strength (32). As one aspect of bone quality, bone geometry *e.g.* bone size, cortical thickness, bone cross-sectional area *etc.* are closely associated with bone failure load and fracture occurrence (60, 61). Therefore, bone density and bone geometry together should contribute to the

understanding of bone strength. Peripheral quantitative computed tomography (pQCT), a CT scanner that is specifically used to image the radius and tibia, is able to measure bone geometry, e.g. bone cross-sectional area, second moment of inertia (I), cortical thickness, as well as volumetric bone mineral density (vBMD). All these pQCT properties should contribute to our understanding of bone fragility. Indeed, more patients with low-trauma fracture can be identified as high-risk for osteoporosis using conventional pQCT measures combined with DXA T-scores when compared with DXA measures alone (598). More recently, we established the potential of finite element analysis based on tibial pQCT images for the classification of fracture status in a clinical setting (599). As a large proportion of low-trauma fractures occur at the distal radius, pQCT was anticipated to be an ideal tool for the assessment of bone strength at this clinically-important site.

Due to the volumetric bone measurements acquired by pQCT, it is an ideal imaging modality to be utilised with FE modelling. Previously, FE models of sites of clinical interest e.g. vertebrae and femur, have been developed based on quantitative computed tomography (QCT) using a clinical CT scanner and bone density phantom (600, 601), or magnetic resonance imaging (MRI) scanner (602). During the past decade, FE models based on high-resolution pQCT (HR-pQCT) have also emerged in the assessment of the tibia or radius strength (603, 377, 399). While providing good prediction for bone strength, these modalities do have some drawbacks. QCT has relatively high radiation exposure to scan the whole spine or limb (125). While HR-pQCT has comparable radiation exposure with pQCT, it is time-consuming to scan and set up individual FE models from HR-pQCT images (604), as well as QCT images. While MRI does not expose the patients to radiation, its cost and prolonged imaging sequences limit its clinical use and applications in large populations and, more

importantly, the extremely short life-time of the MR signal for water bound to hard tissue, makes the quantification of cortical mineralization difficult (605).

Similarly, issues of long scanning time, relatively high radiation exposure and extended individual model set-up times exist for pQCT to scan the whole forearm, which makes it impractical in clinical settings. FE models based on single pQCT cross-sections may solve the aforementioned issues. pQCT is designed for measurement of the site where a distal radius fracture occurs (e.g., Colles' fracture) (606). This scanning location, together with its sufficient resolution for FE modelling and reasonable scanning time for one cross-section with low radiation exposure, makes pQCT a potentially-attractive choice as a data source for individually set-up FE models. Whilst not based on the whole radius properties, strength and stiffness predicted at a discrete location of a single pQCT cross-section may be proportional to the strength of the entire forearm, which may be utilised for more effective, yet rapid assessment of fracture risk.

In this study, we present a pQCT-derived FE analysis technique (pQCT-FE) to estimate bone strength and stiffness of individual cross-sections of the distal radius obtained from clinical pQCT images. For validation purposes, these strength and stiffness estimates were correlated against experimental testing of the forearm in loading configurations mimicking a Colles' fracture. We focus on distal radius fracture only here due to the fact that distal radius is a clinically-important site where a large proportion of fragility fractures was estimated to occur (225, 607). More importantly, fragility fracture is also an early sign of compromised bone strength and is associated with occurrence of further fracture (227, 608). Therefore, improvement in understanding bone fragility at this site may help identifying more patients

with osteoporosis at an earlier stage. We hypothesized that pQCT-FE properties could explain a large proportion of variance in the overall bone failure load, thus demonstrating the potential utility of this method for the assessment of bone fracture risk in vivo.

4.4 Methods

Information regarding specimen acquisition, preparation and mechanical testing is outlined in detail elsewhere (609, 610). Details are briefly summarized below.

Specimens

Twenty-one fresh human cadaver forearms (7 left, 14 right) from 21 female donors were obtained from an anatomical tissue bank. Specimens with no history of fracture or bone disease were selected. Donors' age at death was 81.7 ± 9.3 years, height was 161.4 ± 5.3 cm, weight was 58.9 ± 9.2 kg and body mass index (BMI) was 22.6 ± 3.2 kg/m^2. All specimens were kept intact, were fresh frozen at -20 °C, and thawed for imaging and mechanical testing. This study was approved by the University of Saskatchewan Biomedical Research Ethics Board.

Peripheral quantitative computed tomography scanning

A single 2.4 mm slice was acquired at the 4% site of the radius length, measured proximally to the distal articular surface, using an XCT 2000 pQCT scanner (Stratec Medizintechnik GmbH, Pforzheim, Germany) and our clinical scanning protocol (340). Radius length was measured from the proximal and lateral border of the head of the radius to the most distal point of the lateral margin of the styloid process of the radius. A scout view over the distal joint was performed from which a reference line at the medial tip of the distal endplate of the radius was set as the starting plane. An in-plane pixel size of 0.2 mm by 0.2 mm was obtained. Scanning speed was 10 mm/s. A commercial BMD phantom made by the scanner manufacturer was employed daily prior to scanning to maintain quality assurance.

Mechanical testing

After pQCT imaging, cadaveric forearms were prepared for mechanical testing. Soft tissue was removed from around the radius and ulna, then their midshafts were potted in polymethylmethacrylate (PMMA) according to the method proposed by Edwards and Troy (611). The potted forearm was clamped to the base of a servo-hydraulic material testing machine (MTS Bionix Servohydraulic Testing System), which compressed a flat plate attached to the piston against the outstretched palm of each specimen (609, 610). For the loading configuration, 21 specimens were positioned off-axially with 15^{o} dorsal inclination (612) and 3-6° radial inclination. The palm was set flat against the testing plate and perpendicular to the vertical loading axis.

Compression was conducted in displacement control to failure at a rate of 3 mm/s. Failure loads (F_{exp}, N) were calculated from the load-displacement curve, where failure load was defined as the maximum load on the load-displacement curve. The linear region for the stiffness calculation was identified by visual inspection and confirmed by manually fitting a linear regression curve ($r^2 > 0.99$) to the load-displacement curve.

Finite element analysis

All pQCT images were exported to Matlab software (2017a, Mathworks, Natick, MA, USA) for manual segmentation. A mesh of 0.2x0.2x2.4 mm elements was generated from segmentation, and then reconstructed in the axial plane to produce 0.2x0.2x0.2 mm elements. Each element (numbered i) was modeled as a linear elastic material with a Poisson's ratio of

0.3 and the respective apparent bone mineral density ($\rho_{app,i}$) and Young's modulus (E_i) calculated using Equations 1 and 2 (611, 612).

$$\rho_{app,i} = 1.484H_{f,i} - 48965 \quad (1)$$

$$E_i = 2875{\rho_{app,i}}^3 \quad (2)$$

where $\rho_{app,i}$, E_i and $H_{f,i}$ are the apparent bone mineral density (g/cm^3), Young's modulus (MPa) and the Hounsfield unit of each individual voxel i (HU), respectively.

Each voxel mesh was used to generate a FE model in Abaqus (V6.11, 2011, Simulia, Dassault Systemes, Providence, RI, USA), with each element represented by a fully-integrated 8 node hexahedron. The origin of the models was set as the density-weighted centroid (Equations 3 and 4), where the x- and y-axes were aligned with the minimum and maximum neutral axes, respectively, and the z-axis was normal to the cross-section.

$$\bar{x} = \frac{\sum E_i x_i a_i}{\sum a_i} \quad (3)$$

$$\bar{y} = \frac{\sum E_i y_i a_i}{\sum a_i} \quad (4)$$

where a_i is the area of voxel i. $\bar{x}$, $\bar{y}$ are the coordinates of the density-weighted centroid for the cross-section, and x_i, y_i represent the horizontal and vertical distance between voxel i and the density-weighted centroid.

Four loading cases were considered for all FE Models: axial compression, shear, bending, and torsion (Figure 4.1), each considered as a quasi-static simulation with the assumption of small deformation. Axial compression was simulated by a 0.01 mm displacement of the superior surface towards the inferior surface. Shear was simulated by a 0.01 mm

displacement of the superior surface in the direction of either the x- or y-axes. Bending was simulated by a 0.0001 radian rotation of the inferior surface about either the x- or y-axes (*i.e.*, cross-section neutral axes). Torsion was simulated by a 0.0001 radian rotation of the inferior surface about the z-axis.

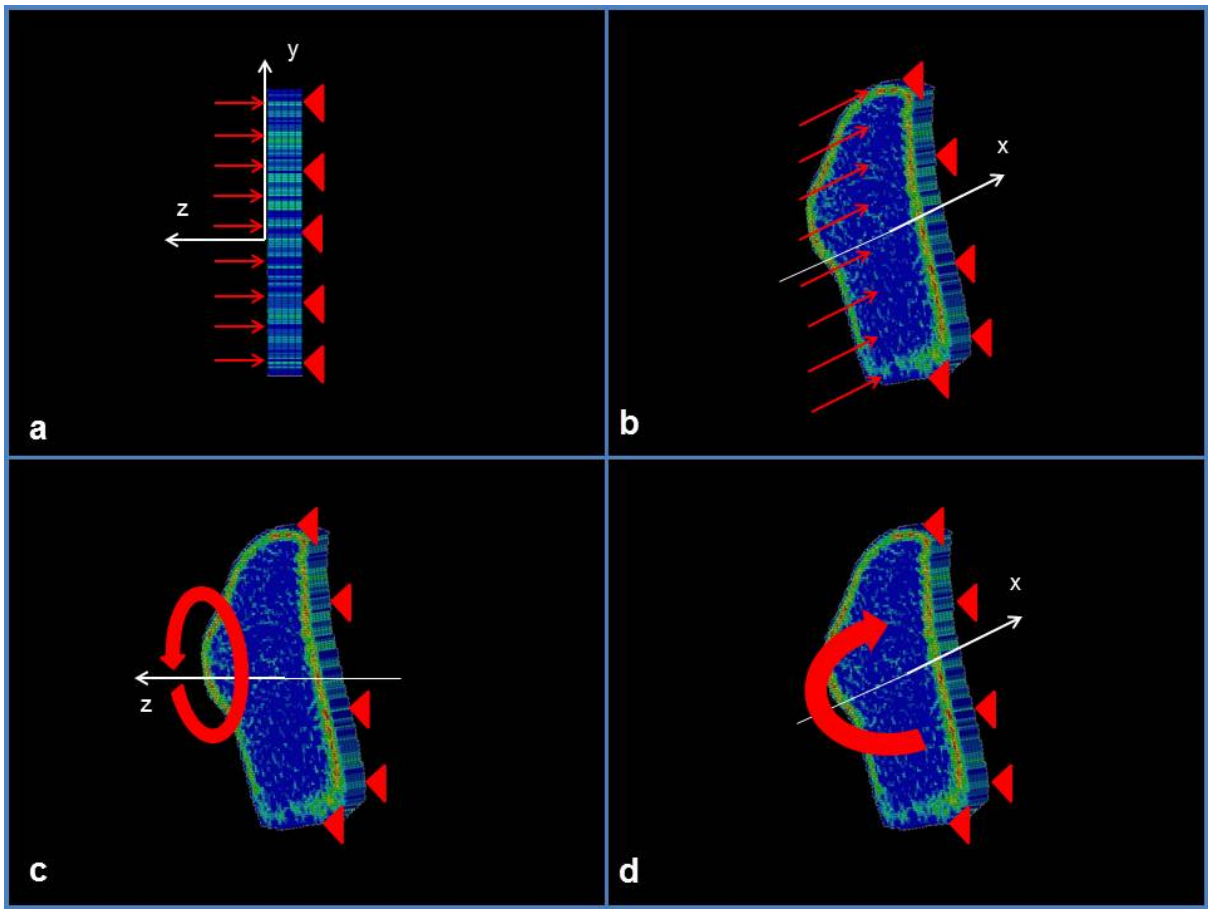

Figure 4.1 Four loading cases simulated in pQCT-FE model. Axial compression (a) was simulated by a 0.01 mm displacement of the superior surface towards the inferior surface. Shear (b) was simulated by a 0.01 mm displacement of the superior surface in the direction of either the x- or y-axes. Torsion (c) was simulated by a 0.0001 radian rotation of the inferior surface about the z-axis. Bending (d) was simulated by a 0.0001 radian rotation of the inferior surface about either the x- or y-axes (i.e., cross-section neutral axes).

Stiffness and strength were calculated for each loading case for each specimen. The reaction forces and moments predicted from the simulations were divided by the respective applied displacement or rotation to derive the compressive stiffness (k_{comp}), shear stiffness (k_{shear}), bending stiffness (k_{bend}), and torsional stiffness ($k_{torsion}$) of each cross-section. The bending and shear stiffness were each taken as the minimum value derived from the two neutral-axis directions. The minimum compressive and maximum tensile principal strains predicted for each simulation (ε_{max} and ε_{min}, respectively) were compared with compressive and tensile yield strains reported for the radius (1.10% and 0.66%, for compression and tension, respectively; 616) to derive a factor-of-safety. The factor-of-safety was multiplied by the respective reaction force or moment to derive the strength for compression (S_{comp}), shear (S_{shear}), bending (S_{bend}) and torsion ($S_{torsion}$), of each cross-section.

Statistical analysis

Descriptive data were expressed as mean ± 1.0 standard deviation (SD). A linear regression model was developed to correlate each pQCT-FE stiffness and strength variable with failure load (F_{exp}) measured from the mechanical testing, from which the coefficient of determination (r^2) was calculated. Additional regression models were also developed for each pQCT-FE variable after adjustment for age, *i.e.* set age and each pQCT stiffness/strength variable as independent factors while failure load as the dependent factor in the regression models. Level of significance for all analyses was set as $p<0.05$. All statistical analyses were performed using SPSS 22.0 (SPSS Inc., Chicago, IL, USA).

4.5 Results

After loading, 5 specimens did not experience a distal radius fracture and were excluded from further analysis. Alternate failure mechanisms included a scaphoid fracture (n=1) and midshaft fractures originating at the potting (n=4). They were excluded from analysis as pQCT scans were not obtained at these locations. Therefore, it would be incompatible for the FE model to attempt to predict the bone strength at these locations. Furthermore, these fractures do not represent a common type of fragility fracture, and were beyond the topic of this study.

Alternate failure mechanisms brought the sample to 16 specimens (609, 610). The mean ± SD age of this analysis sample was 81.6 ± 9.9 years. In terms of fracture types, the majority were Colles' type (n=14) combined with compressive-type fractures (n=2). A Colles' type fracture was defined as a transverse fracture ~25-40 mm to the radio-carpal joint, with evidence of dorsal displacement and angulation of the distal fragment, radial shortening, and loss of radial inclination and palmar tilt (614, 615). A compressive-type fracture was defined as a transverse fracture ~25-40 mm to the radio-carpal joint with evidence of radial shortening. Fracture classification was based upon visual assessment by a single researcher (MM). In terms of limb distribution, there were 5 left and 11 right limbs included in the analysis.

The pQCT-FE stiffness and strength properties of the cadaveric radii and the corresponding r^2 when regressed against the experimental failure load are summarised in Table 4.1, and visual representation of each regression is shown in Figure 4.2. Medium-to-strong r^2 values were observed for experimental failure load regressed against each of the FE-derived stiffness variables, which were r^2 = 0.66, 0.64, 0.83 and 0.82 for k_{comp}, k_{shear}, k_{bend} and $k_{torsion}$,

respectively (all $p < 0.01$). Similar trends for r^2 were found for experimental failure load regressed against FE-derived strength variables, where $r^2 = 0.56$, 0.46, 0.71 and 0.64 for S_{comp}, S_{shear}, S_{bend} and $S_{torsion}$, respectively (all $p < 0.01$). All r^2 tended to improve after regression models were adjusted for age, with highest $r^2 = 0.86$ and 0.79 for k_{bend} and S_{bend}, respectively.

Table 4.1 Means and SDs of pQCT-FEA variables and corresponding coefficients of determination (r^2) against failure load before and after adjustment for age. All correlations had a significance of $p<0.01$.

FEA variable	Mean ± SD	r^2	r_{adj}^2
k_{comp} (kN/mm)	198.0 ± 60.7	0.66	0.77
k_{shear} (kN/mm)	46.3 ± 16.2	0.64	0.77
k_{bend} (Nm/deg)	85.7 ± 31.3	0.83	0.86
$k_{torsion}$ (Nm/deg)	69.4 ± 27.3	0.81	0.85
S_{comp} (N)	3.5 ± 1.3	0.56	0.69
S_{shear} (10^2 N)	3.1 ± 1.1	0.46	0.67
S_{bend} (Nm)	4.1 ± 1.5	0.71	0.79
$S_{torsion}$ (Nm)	2.5 ± 1.0	0.64	0.77

k_{comp}, compression stiffness; k_{shear}, shear stiffness; k_{bend}, bending stiffness; $k_{torsion}$, torsion stiffness, S_{comp}, compression strength; S_{shear}, shear strength, S_{bend}, bending strength; $S_{torsion}$, torsion strength, r^2, coefficient of determination before adjustment for age; r_{adj}^2, coefficient of determination after adjustment for age.

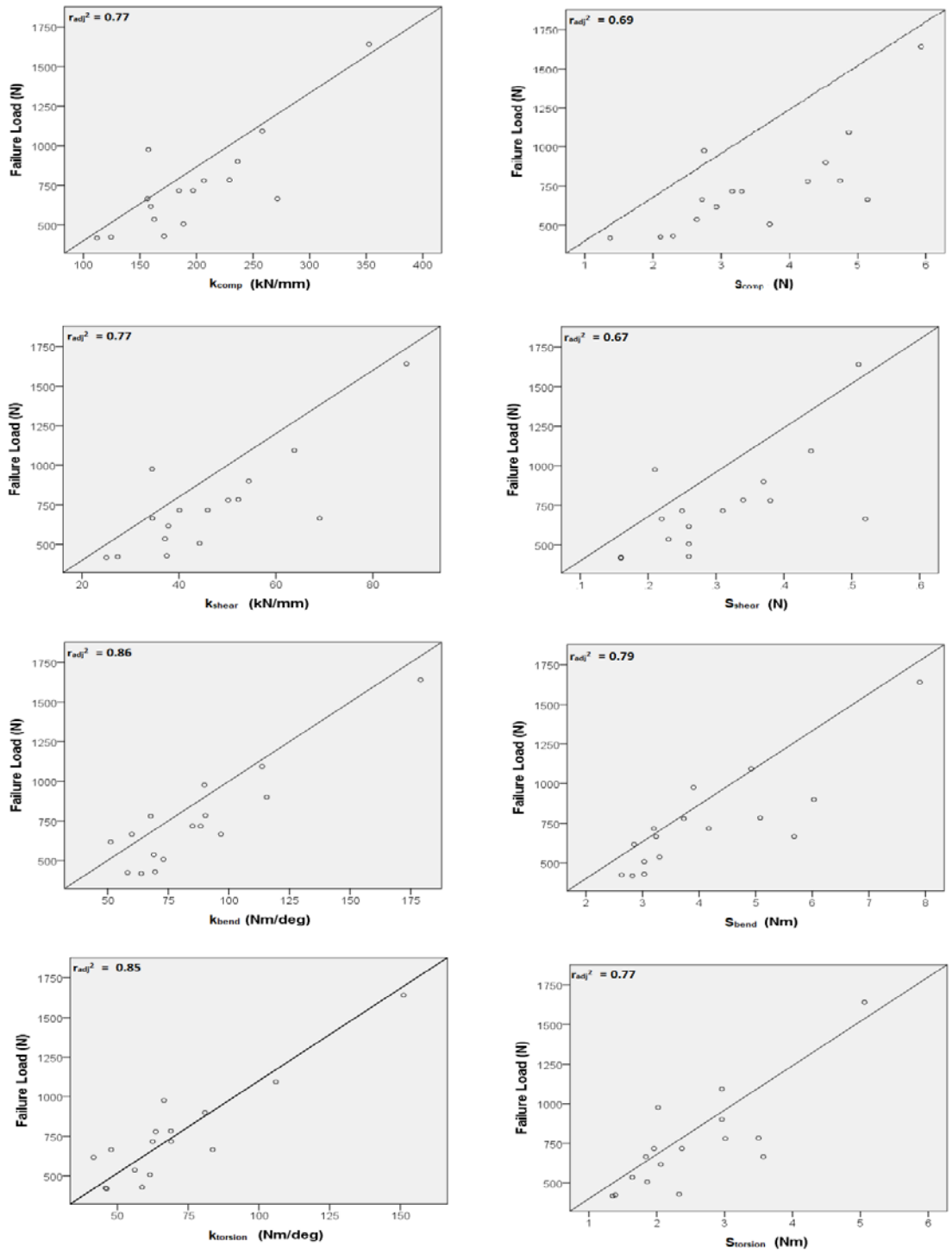

Figure 4.2 Scatter plots of pQCT-FE properties against experimental failure load. r^2: coefficient of determination before adjustment for age, r_{adj}^2: coefficient of determination after adjustment for age. k_{comp}: compression stiffness; S_{comp}: compression strength; k_{shear}: shear stiffness; S_{shear}: shear strength; k_{bend}: bending stiffness; S_{bend}: bending strength; $k_{torsion}$: torsion stiffness; $S_{torsion}$: torsion strength.

4.6 Discussion

Due to the great economic and societal burden of osteoporosis and the consequent fractures, and the limitations of DXA in identifying individuals with increased fracture risk, it is necessary to find a complementary tool providing information about bone strength additional to DXA. In this study, we sought to validate a pQCT-FE model that could be used to supplement assessment of bone strength using DXA alone. Medium to strong r^2 values were observed between experimental failure load and pQCT-FE properties, ranging from 0.64 – 0.83 for pQCT-FE stiffness variables, and 0.46 – 0.71 for pQCT-FE strength variables. Improvement in r^2 was also observed after the regression models were adjusted for age, with r_{adj}^2 ranging from 0.77 – 0.86 for pQCT-FE stiffness variables, and 0.64 – 0.79 for pQCT-FE strength variables. These r^2 were found to be higher than those between DXA radius variables and forearm fracture failure in mechanical testing with similar falling configurations, which were 0.31 – 0.56 from the literature (324, 326, 377, 597).

Among the pQCT-FE properties of the four load cases, bending properties had the highest contribution to variance in experimental failure load for both stiffness and strength variables, with r_{adj}^2 = 0.86 and 0.79, respectively. This was likely to be due to the imposed loading configuration, where the radius long axis was offset 15 degrees from the loading axis, thus imparting a combination of compression and bending on the radius. It may also explain why the pQCT-FE shearing properties accounted for the least variance in failure load among the four load cases since the off-axis compression is unlikely to generate a high shear load. This is pertinent to the real-world situation as Colles' fractures are believed to be the result of bending, rather than other types of loading vectors *i.e.* compression, torsion or shearing (616 – 618).

Areal BMD measured by DXA accounts for only part of the variance in bone failure load. The r^2 between bone failure load and aBMD differed in various studies but generally ranged between 0.34 – 0.64 at standard imaging sites (261 - 264). When it comes to the radius, DXA is reported to account for no more than 60% of variation in forearm strength. Higher r^2 was reported in the current study between radius mechanical failure load and pQCT-FEA stiffness, with highest r^2 of 0.86. These results suggest that our pQCT FE models provide improved bone strength assessment compared to previous estimates based on DXA.

More recently, micro FE (μFE) models based on HR-pQCT with voxel size of 85 μm, which enables depiction of the trabecular micro-structure of the radius and tibia, emerged in clinical research (399). Outputs from these models have demonstrated an improved ability to classify fracture status of patients compared to DXA (619), and good correlations have been observed when predicting experimental failure loads of cadaveric radii, with r^2 of 0.70 – 0.92 (377, 394, 395). Although these previous r^2 findings describe a different testing configuration to the off-axis loading in the current study, they provide insight into our understanding of bone fragility explained by different tools. In a study comparing HR-pQCT μFE and QCT FE which is based on volumetric data of similar resolution to pQCT in the prediction of femur failure load, HR-pQCT μFE predicted failure load similarly to QCT FE (r^2 = 0.86 vs r^2 = 0.84, respectively) (620). HR-pQCT has other drawbacks, such as exposing patients to slightly higher radiation than pQCT, and due to its higher resolution, it is time-consuming to process the large volume of imaging data in the FE analysis (604). More importantly, HR-pQCT, as a newer technique than pQCT, is not widely available due to its prohibitive cost.

This study has several limitations. Peripheral QCT images with a voxel size of 0.2 mm and slice thickness of 2.4 were obtained to generate a cross-sectional FE model for each specimen. Compared to the voxel size of HR-pQCT (85 µm) which can depict the micro-structure of the radius, the voxel size of pQCT (200 µm) is relatively large and is not precise enough to reflect the topology of individual trabeculae. However, this resolution appears to be sufficient to allow prediction of the variance in experimental failure load of the radius according to previous studies (21, 384, 387). In these studies, 0.25 - 1.08 mm voxels from QCT images were used to established FE models of the femur, and simplified trabeculae topology as a continuum FE mesh as in the current study was used with similar element sizes. Strong coefficients of determination were observed between these QCT FE variables and mechanical failure load in the laboratory, ranging from 0.74 – 0.90. Strong r^2 between pQCT-FEA variables and radius failure load in the current study support the argument that resolution of 0.2 mm voxels can explain a high proportion of the variance inf the whole-bone properties.

FE strength and stiffness were calculated from four loading cases in this study; however, a loading combination of compression, torsion, bending and shear occurs at the same time in vivo (50). The individual loading cases may be too idealised for the assessment of bone strength, but similar to the barrel analogy of Liebig's law of the minimum, where the shortest stave decides the capacity of a barrel with staves of unequal lengths, a bone's strength is limited by the weakest resistance of an idealised loading condition. This logic was reflected in previous studies, where the radius strength for fracture risk assessment was measured by idealised axial compression only (621). Indeed, we did not intend to calculate the real radius strength or stiffness from the pQCT-FE, rather we presented an idealized loading scenario that could be easily constructed, and it was assumed that strength and stiffness from one

cross-section would be proportional to the whole-bone failure under more complex loading configurations.

As discussed previously, bone quality contributes to bone strength (32, 622). Properties of bone quality other than bone geometry, *e.g.* degree of bone mineralization, hydroxyapatite crystal size and heterogeneity, collagen properties and osteocyte density are considered determinants of bone strength; however unfortunately, these bone properties are not available using standard pQCT imaging and require detailed analysis of bone biopsies. The feasibility of using bone biopsies to identify fracture risk is challenging as it is invasive and likely difficult to recruit otherwise healthy patients to undergo this procedure. The advantage of the current method is that it is readily available as it can be applied to existing clinical pQCT imaging methods.

Following the exclusion of 5 specimens for undesirable material behaviors during testing, there was a reduced number of specimens (n = 16), which would have lessened the statistical power of our analysis. However, the final sample size was sufficient for strong univariate correlations to be found in the models where r^2 was calculated. In addition, the mean age of donors in this study (82 ± 10 years) was greater than the average ages reported for forearm fracture (71 ± 15 years; 623, 624). However, after adjustment for age, improvement was observed in all correlations between experimental and pQCT-FE properties. This provides better prospect for the pQCT-FE models although sample size was limited. Further studies with a larger sample size may help improve the multivariate regression models.

In summary, we experimentally validated a pQCT image-based FE method for the assessment of bone strength at the clinically-relevant distal radius site. As much as 86% of variance in experimental radius failure load was explained by pQCT-FE properties. This FE model makes individual assessment of bone strength at a site with a propensity for osteoporotic fracture more accessible by using a widely-available device with reasonable scanning time and low radiation. Future research may focus on this technique's role in differentiating patients with increased fracture risk from the healthy in clinical settings.

4.7 Acknowledgements

We thank all study donors who bequeathed their bodies for medical science. We wish to acknowledge Dr. Chantal Kawalilak, Nima Ashjaee and Amy Bunyamin for assistance with mechanical testing and specimen preparation.

Declarations of interest: none.

Funding: This work was supported by the Natural Sciences and Engineering Research Council of Canada (NSERC Discovery Grant RGPIN-2016-05301, SK) and Saskatchewan Health Research Foundation (SHRF Establishment Grant 2632, JDJ). HJ was funded under a joint PhD scholarship by China Scholarship Council (funding reference: CSC201608240003) and the University of Melbourne.

Ethical approval: This study involves use of human cadaver and was approved by the University of Saskatchewan Biomedical Research Ethics Board (Ethics number 09-96).

4.8 Additional discussion

This section is not published along with Sections 4.1 – 4.7 but aims to discuss the improved age-adjusted r^2 between FEA variables and experimental variables. In the pQCT-FEA analysis, assignment of Young's modulus to each element was based on conversion from CT number, which, in turn, was dependent on the quantity of bone mass at the scanned site. While the FE models also took bone macro-geometry information into account during the analysis, other properties, e.g. bone microstructure, organic composition, which have strong correlations with age, contribute to the mechanical performance of bone as discussed in Section 2.1. Therefore, the improvement in the ability of pQCT-FEA variables to predict experimental failure load while adjusting for age indicates the importance of integral analysis of bone mechanical performance. However, it is acknowledged that the range of age distribution was relatively narrow; therefore, how well the model would be improved is uncertain in younger population, which warrants future research.

Chapter 5

Peripheral quantitative computed tomography (pQCT)-based finite element analysis provides enhanced diagnostic performance in identifying non-vertebral fracture patients compared with dual energy x-ray absorptiometry

5.1 Peripheral quantitative computed tomography (pQCT)-based finite element analysis provides enhanced diagnostic performance in identifying non-vertebral fracture patients compared with dual energy x-ray absorptiometry

Authors and affiliations:

Hongyuan Jiang [a], Dale L Robinson [b], Christopher J Yates [a,c,d], Peter VS Lee [b], John D Wark [a,c,d]

[a] Department of Medicine, Royal Melbourne Hospital, University of Melbourne

[b] Department of Biomedical Engineering, University of Melbourne

[c] Bone and Mineral Medicine, Royal Melbourne Hospital

[d] Department of Diabetes and Endocrinology, Royal Melbourne Hospital

5.2 Abstract

SUMMARY Due to limitations of the predominant clinical method for diagnosing osteoporosis, an engineering model based on a dedicated CT scanner for bone density and structure was applied in fracture patients and controls. Improved diagnostic performance was observed, which supports its potential use in future research and clinical practice.

INTRODUCTION Dual energy x-ray absorptiometry (DXA), the predominant clinical method for diagnosing osteoporosis, has limitations in identifying individuals with increased fracture risk. Peripheral quantitative computed tomography (pQCT) provides additional information and can be used to generate finite element (FE) models from which bone strength properties can be estimated. We investigated the ability of pQCT-FE properties to distinguish peripheral low-trauma fracture patients from healthy controls, by comparison with DXA and standard pQCT.

METHODS One hundred and eight fracture patients (77 females aged 67.7 ± 7.9 years, 31 males aged 69.7 ± 8.9 years) were recruited from a hospital fracture liaison service. One hundred and twenty healthy community controls (85 females aged 69.8 ± 8.5 years, 35 males aged 68.9 ± 7.2 years) were recruited.

RESULTS Significant differences between groups were observed in pQCT-FE properties, especially at the 4% tibia site. Fracture odds increased most per standard deviation decrease in pQCT-FE at this location [shear stiffness estimate, k_{shear}, in females, OR = 10.34, 95% CI (1.91, 43.98); bending stiffness estimate, k_{bend}, in males, OR = 8.32, 95% CI (4.15, 33.84)]. Area under the receiver operating characteristics curve (AUROC) was observed to be highest with pQCT-FE properties at 4% the tibia site. In females, this was 0.83 for the pQCT-FE variable k_{shear}, compared with 0.72 for DXA total hip bone density (TH aBMD) and 0.76 for pQCT tibia trabecular density (Trb vBMD); in males, this was 0.81 for the pQCT-FE variable

k_{bend} at the 4% tibia site, compared with 0.62 for TH aBMD and 0.71 for Trb vBMD. There were significant differences in AUROC between DXA and pQCT-FE variables in both females ($p = 0.02$) and males ($p = 0.03$), while no difference was observed in AUROC between primary pQCT and pQCT-FE variables.

CONCLUSIONS pQCT-FE modeling can provide enhanced diagnostic performance compared with DXA and, given its moderate cost, may be useful in clinical settings.

5.3 Introduction

The prevalence of osteoporosis is increasing due to population ageing worldwide (191). Being a “silent” disease, osteoporosis may not attract the attention of patients and primary health care practitioners until a fragility fracture occurs. It has been estimated that one third of women and one fifth of men will sustain a fragility fracture after age 50 years (210), which is a great societal burden associated with high morbidity, mortality and healthcare expenditure. Although many modifiable risk factors for bone fragility have been identified previously, better screening, case-finding and monitoring strategies are still needed given the intrinsic limitations of dual energy x-ray absorptiometry (DXA) (625).

Although DXA is considered the clinical criterion method for osteoporosis diagnosis, almost seventy percent of patients who had recently sustained a low-trauma fracture were diagnosed with osteopenia or normal bone density based on DXA measurements at our institution (588). This misclassification is due in part to the technique itself which projects the region of interest into a two-dimensional plane. This data acquisition from a projective x-ray technique does not take bone “depth” into account, thus making results susceptible to artifacts related to different bone sizes. DXA also fails to capture other bone geometric information including cortical thickness which has been closely correlated to bone fragility (60). In addition, DXA is performed routinely at central sites *i.e.* the lumbar spine and the proximal femur in clinical practice, while a large proportion of fragility fractures occur at more peripheral sites *e.g.* the distal forearm (210), where fracture is an early indication of bone fragility (626).

Peripheral quantitative computed tomography (pQCT) provides both volumetric bone density and bone geometry measurements which correlate well with bone mechanical properties at

multiple peripheral sites (59, 348, 350). These variables can differentiate between people with and without prevalent fractures (352), and are associated with fracture occurrence during follow-up in both women and men (334, 627). Therefore, pQCT has a potential role in improving our understanding of bone fragility compared to using DXA alone (598). Finite element (FE) analysis is a computational method that can provide non-invasive assessment of bone strength in vivo. FE models based on quantitative computed tomography (QCT) images of either the vertebral body or proximal femur have provided estimates of bone strength that correlate strongly with cadaveric fracture loads (383, 385), and these correlations were reported to be higher than those of bone mineral density (BMD) measured by DXA (383, 140). FE models of cadaveric forearm or tibia using either QCT or pQCT were established previously (611, 628, 629). Whilst these studies showed good correlation between FE properties and fracture failure load, the models were time-consuming to build and imparted considerable radiation to image the entire bone or joint, thus limiting their use in clinical settings. Since it is designed for measurement at the appendicular skeleton, pQCT is a potentially suitable source for FE analysis at peripheral sites with its volumetric data acquisition, spatial distribution of bone density and comparable resolution with QCT. Moreover, pQCT instruments can be acquired and operated at quite moderate cost.

In this current study, we aimed to evaluate the ability of a clinically-relevant, pQCT-based FE model (pQCT-FE) to estimate bone strength in patients with recent fragility fractures and age-matched controls, and to compare the diagnostic characteristics of DXA, pQCT and pQCT-FE variables.

5.4 Methods

Participants

Two groups of participants were recruited for this study. The fracture group was recruited from a fracture liaison service involving multiple disciplines at a tertiary hospital, which improves uptake of osteoporosis intervention guidelines in a cost-effective way (250). The control group was recruited through electronic and paper-based advertisements from multiple sources, including members of a community education program (University of the Third Age), staff, volunteers, visitors and contacts of the University of Melbourne and the Royal Melbourne Hospital.

General inclusion criteria for both groups were: (1) aged 50 years or above; (2) English-speaking or has an English-speaking family member or friend available; (3) consent to participate in this study and be able to attend a study visit at the Royal Melbourne Hospital. Specific inclusion criteria for the fracture group were: (1) had sustained at least one low-trauma fracture, *i.e.* a fracture caused by minimal trauma such as a fall from a standing height or less, within 3 months prior to a study visit; (2) for patients with two or more fractures, there were at least one radius and one tibia without a fracture history or other relevant pathology and available for measurement. Specific inclusion criterion for the control group was: reported no prior history of osteoporosis, low bone density or low-trauma fracture.

General exclusion criteria for both groups were: (1) prior diagnosis of osteoporosis; (2) prolonged (>3 months) use of osteoporosis therapy, including bisphosphonates, denosumab, selective ostrogen receptor modulators, hormone replacement therapy in the past 2 years; (3) prior therapy with teriparatide or strontium ranelate; (4) other medical conditions which may

affect bone health, *e.g.* hyperthyroidism, hyperparathyroidism, Crohn's disease, diabetes, Cushing Syndrome; (5) currently taking or have recently taken medications which may affect bone health, *e.g.* glucocorticoid agents, anti-epilepsy drugs, heparin.

Verbal and written informed consent were obtained from each participant after they were provided with detailed information about the study. This study was approved by Melbourne Health Human Research Ethics Committee (ethics approval number MH 2014.143).

DXA scanning and analysis protocol

Standard clinical scans of the lumbar spine (L1 – L4) and the right hip were performed using a fan-beam densitometer (Horizon QDR 4500A, Hologic Inc., Bedford, MA, USA). In cases where participants had a right-sided hip replacement or fracture, the left hip was scanned. DXA scans were performed in array mode and were analysed using the manufacturer's commercial software (v 9.10D). Variables of interest included areal bone mineral density (aBMD) of the lumbar spine (LS aBMD), the total hip (TH aBMD) and the femoral neck (FN aBMD). The 12-month precision of the scanner for the Hologic spine phantom was 0.39% for aBMD.

pQCT scanning and analysis protocol

Scans of the non-dominant radius and tibia were performed using an XCT 3000 pQCT scanner (Stratec Medizintechnik, Pforzheim, Germany) at both the 4% and 66% sites along the limb length. Length was measured from the ulna styloid process to the olecranon process at the forearm, and from the base of the medial malleolus to the superior margin of the medial

condyle at the tibia. In fracture patients whose non-dominant radius/tibia sustained a fracture, the dominant side was scanned. A scout scan was performed to identify the correct starting line, which was taken as the distal articular surface of the radius or tibia. A single slice at each site was acquired with an in-plane resolution of 0.4 x 0.4 mm and a slice thickness of 2 mm. Scanning speed was 10 mm/s. The manufacturer's commercial software (version XCT 5.50E) was used to analyse pQCT images for standard pQCT variables. Variables of interest included total volumetric bone mineral density (Tot vBMD), trabecular volumetric bone mineral density (Trb vBMD) and trabecular cross-sectional area (Trb CSA) at the 4% site, and cortical volumetric bone mineral density (Crt vBMD), cortical thickness (Crt Thk) and polar stress-strain index (SSIp) at the 66% site.

FE model properties

Detailed methodology of the pQCT-FE models was described elsewhere (599). Briefly, all pQCT images were exported to MATLAB (version R2016b, Mathworks, Natick, MA, USA), where manual segmentation was performed. A mesh of 0.4 x 0.4 x 2 mm elements was generated from segmentation, and then re-sliced in the z-direction to produce a mesh of 0.4 x 0.4 x 0.4 mm elements. The Young's modulus was calculated using an established equation for the tibia (630) and the radius (611), and was assigned to each element. Each voxel mesh was then used to generate a FE model in Abaqus (version 6.11, Simulia, Dassault Systems, Providence, RI, USA).

Four loading cases were considered for all FE Models (Figure 5.1): axial compression, shear, bending, and torsion. Axial compression was simulated by a 0.01 mm displacement of the superior surface towards the inferior surface (Figure 5.1, a). Shear was simulated by a 0.01

mm displacement of the superior surface in the direction of either the x- or y-axes (Figure 5.1, b). Bending was simulated by a 0.0001 radian rotation of the inferior surface about either the x- or y-axes (i.e., cross-section neutral axes, Figure 5.1, c). Torsion was simulated by a 0.0001 radian rotation of the inferior surface about the z-axis (Figure 5.1, d). The reaction forces and moments predicted from the simulations were divided by the respective applied displacement or rotation to derive the compressive, shear, bending and torsional stiffness (k_{comp}, k_{shear}, k_{bend} and $k_{torsion}$, respectively) of each cross-section. The bending and shear stiffness were each taken as the minimum value derived from the two neutral-axis directions.

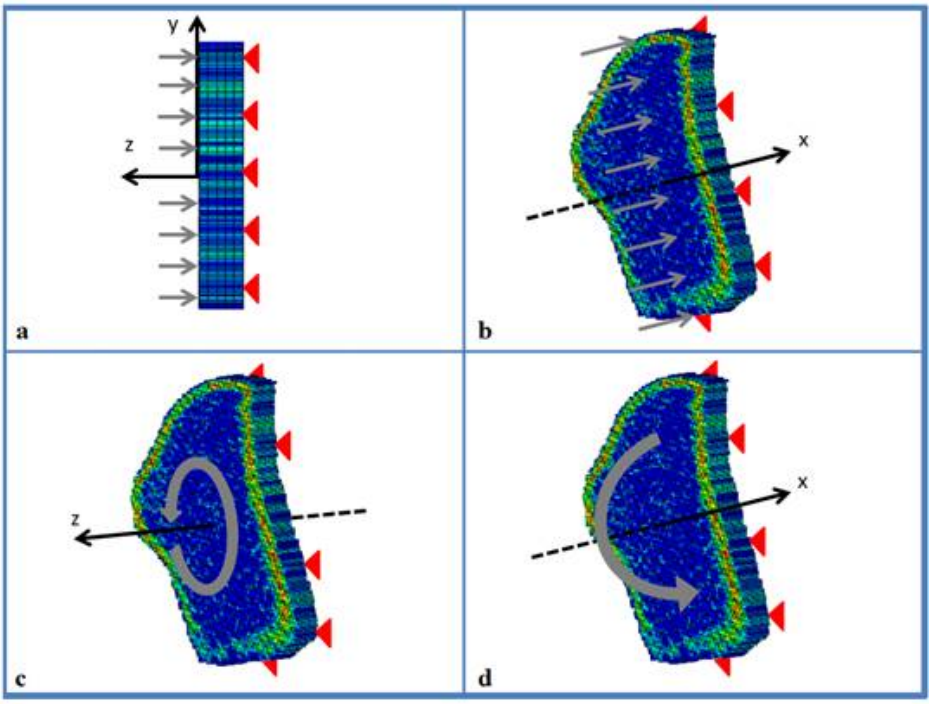

Figure 5.1 Loading cases of pQCT-FE. Figures show examples of 4% radius. a. Axial compression loading case. Grey arrows applied displacement of 0.01 mm in the negative z direction. b. Shear loading case. Grey arrows applied displacement of 0.01 mm in either positive x direction or positive y direction. c. Torsion loading case. Grey arrow applied rotation of 0.0001 radians about z-axis. d. Bending loading case. Grey arrow applied rotation of 0.0001 radians about either x- or y-axis.

Other data collected

An ethics-approved questionnaire was used to collect other information from participants. The information included date of birth, sex, height, weight, fracture details/history, comorbidities, related medical history, and risk factors for osteoporotic fracture according to the FRAX® algorithm (https://www.sheffield.ac.uk/FRAX).

Statistical analysis

Descriptive statistics were expressed as mean ± 1.0 standard deviation (SD). Difference between groups was assessed using a two-sample t-test for variables that were normally distributed, or the Kolmogorov-Smirnov test for variables that were not normally distributed. Multivariate linear regression models were established to compare means between groups while adjusting for age, height and weight. To identify multicollinearity between variables, multivariate linear regression models were established for each group of variables including DXA, pQCT radius/tibia, pQCT-FE stiffness of 4/66% radius/tibia, from which variance inflation factors (VIFs) were derived for each variable. Age, height and weight were included in each model. Collinearity was assumed with a VIF > 5 (631).

For all DXA variables, and pQCT and pQCT-FE variables that varied significantly between the control and fracture groups, a binary logistic regression was established to evaluate their relationship with fracture status. All logistic regression models were adjusted for confounding

factors including age, height and weight. Results of logistic regression models were expressed as odds ratio (OR) per SD decrease of the respective variable and its 95% confidence interval (95% CI). In the case of variables determined to be collinear according to the VIFs, only the variable with the highest average OR was included in the analysis.

Specificity, sensitivity and area under the receiver operating characteristics (AUROC) curve were obtained from the logistic regression models to show the ability of each predictor to classify between fracture patients and controls. The significance of differences between the AUROCs of key DXA, pQCT and pQCT-FE variables (*i.e.* those with highest AUROC value in each group of DXA, standard pQCT amd pQCT-FE variables) was determined using the method by Delong et al (632), which is a non-parametric method based on U-statistics from which the test statistic follows a χ^2 distribution. All statistical analyses were performed in SPSS (version 25, SPSS Inc., Chicago, IL, USA). All significance levels were set as $p < 0.05$.

5.5 Results

One hundred and eight fracture patients (77 females, 31 males) and 120 controls (85 females, 35 males) were recruited into this study (Table 5.1). No significant difference was observed in age, height, weight, BMI, sex or radius/tibia length between the fracture patients and controls. Among fracture risk factors, no difference between groups was observed in alcohol consumption. The fracture group had a higher rate of smoking than the control group ($p = 0.01$). More fracture patients were found to have rheumatoid arthritis than controls ($p = 0.03$), and their parental hip fracture incidence was also greater ($p = 0.01$). For fracture patients, the average interval between fracture and the study visit (mean ± SD) was 56.6 ± 13.2 days. Most fractures sustained were non-vertebral. Colles' fractures accounted for the major proportion of all fractures (60.7%), followed by lower leg (13.9%) and humerus (9.0%) fractures (Table 5.1).

A difference between the fracture group and the control group was observed in TH aBMD but not in DXA aBMD variables at other sites; however, the difference was not significant after adjustment for age, height, weight and sex (Table 5.2). Several standard pQCT variables differed between groups before adjustment for age, height, weight and sex, but the only variables with significant difference between groups after adjustment were Trb vBMD at both the radius and the tibia ($p = 0.01$ and 0.02 for the radius and the tibia, respectively). No pQCT-FE variables differed between groups at the 4% radius site. At the 66% radius site, k_{comp} and k_{bend} were lower in the fracture patients than in the controls after adjustment for age, height, weight and sex ($p = 0.04$ and 0.03, respectively). At the 4% tibia site, all pQCT-FE variables differed between groups before adjustment for age, height, weight and sex; although the differences were not statistically significant for k_{bend} and $k_{torsion}$ after adjustment for age, height, weight and sex. At the 66% tibia

site, all pQCT-FE stiffness variables except $k_{torsion}$ differed between groups before and after adjustment for age, height weight and sex. Similar results in different DXA, pQCT and pQCT-FE variables were observed between groups when females and males were analysed separately (Tables 5.3 and 5.4).

Age, height and weight did not exhibit collinearity with each group of DXA, pQCT and pQCT-FE variables in any of the regression models, with all corresponding VIF < 5 (Table 5.2). Collinearity, however, was identified with other predictors in each. Among DXA variables, the highest VIF was found with TH aBMD (VIF = 5.1). For standard pQCT variables, radius tot vBMD (VIF = 11.0) and tibia SSI_p (VIF =16.0) had the highest collinearity with other standard pQCT variables. Strong collinearity with high VIF values was observed in all groups of pQCT-FE properties indicating strong correlations among the stiffness estimates of the four loading cases at the same site, especially between k_{comp} and k_{shear} (*e.g.* at 4% tibia, VIF = 641.8 and 598.6, respectively). Similar trends were observed when females and males were analysed separately (Tables 5.3 and 5.4).

The ability of each DXA, standard pQCT and pQCT-FE property to classify between fracture and control groups (*i.e.* OR, specificity, sensitivity and AUROC derived from the logistic regression models) in all participants, and females and males separately is shown in Table 5.5. In the pooled analysis, odds of fracture increased 1.53-fold per SD decrease in DXA TH aBMD [95% CI (1.01, 2.15)]. Odds of fracture increased more per SD decrease of tibia Trb vBMD and 4% tibia k_{shear}, which were 7.64 [95% CI (1.92, 26.51)] and 9.13 [95% CI (1.87, 31.36)],

respectively. The highest AUROC was observed with 4% tibia k_{shear}, which was 0.79 [95% CI (0.74, 0.84)], compared with 0.69 [95% CI (0.62, 0.75)] for TH aBMD and 0.74 [95% CI (0.68, 0.80)] for tibia Trb vBMD. Specificity and sensitivity were 66.7% and 78.7% for 4% tibia k_{shear}, compared with 76.7% and 54.8% for TH aBMD, respectively. Pairwise comparisons (Figure 5.2; Table 5.6) of AUROC for the three key variables (DXA TH aBMD, tibia Trb vBMD and 4% tibia k_{shear}) showed that the AUROC of k_{shear} was higher than TH aBMD ($p = 0.02$). No difference in AUROC was observed between tibia Trb vBMD and TH aBMD, nor between 4% tibia k_{shear} and tibia Trb vBMD.

In females, odds of fracture increased 1.52-fold per SD decrease in DXA TH aBMD [95% CI (1.01, 2.16)]. Higher ORs were observed for standard pQCT and pQCT-FE properties, which were greatest for tibial Trb vBMD [OR = 8.15, 95% CI (1.78, 39.72)] and k_{shear} at 4% tibia [OR = 10.34, 95% CI (1.91, 43.98)], respectively. Among all variables, the highest AUROC was found with k_{shear} at 4% tibia, which was 0.83 [95% CI (0.77, 0.89)] compared with 0.72 [95% CI (0.64, 0.79)] for DXA TH aBMD and 0.76 [95% CI (0.68, 0.82)] for tibia Trb vBMD. Specificity and sensitivity for k_{shear} at 4% tibia were 79.2% and 69.4%, compared with 72.4% and 52.7% for DXA TH aBMD, respectively. Pairwise comparisons (Figure 5.2; Table 5.6) of AUROC for the three primary variables (DXA TH aBMD, tibia Trb vBMD and 4% tibia k_{shear}) showed that AUROC of k_{shear} was higher than TH aBMD ($p = 0.02$). No difference in AUROC was observed between tibia Trb vBMD and TH aBMD ($p = 0.4$). There was a trend that AUROC of k_{shear} was higher than that of tibia Trb vBMD with a $p = 0.07$.

For male participants, odds of fracture increased 1.55-fold per SD decrease in DXA TH aBMD [95% CI (1.02, 2.07)]. Higher ORs were observed for standard pQCT and pQCT-FE properties, which were greatest for tibia Trb vBMD [OR = 6.58, 95% CI (2.43, 10.70)] and k_{bend} at 4% tibia [OR = 8.32, 95% CI (4.15, 33.84)], respectively. Among all variables, the highest AUROC was found with k_{bend} at 4% tibia, which was 0.81 [95% CI (0.70, 0.90)] compared with 0.62 [95% CI (0.49, 0.74)] for DXA TH aBMD and 0.71 [95% CI (0.59, 0.82)] for tibia Trb vBMD. Specificity and sensitivity for k_{bend} at 4% tibia were 80.0% and 74.2%, compared with 65.7% and 64.5% for DXA TH aBMD, respectively. Pairwise comparisons (Figure 5.2; Table 5.6) found higher AUROC for 4% tibia k_{bend} than for TH aBMD ($p = 0.03$). No difference in AUROC was observed either between standard pQCT and DXA variables or between pQCT-FE and standard pQCT variables.

Table 5.1 Characteristics of study participants

	Fracture (n = 108)	Control (n = 120)	p
Age (years, mean ± SD)	68.3 ± 8.2	69.5 ± 8.1	0.27
Height (cm, mean ± SD)	165.6 ± 8.3	166.2 ± 6.3	0.54
Weight (kg, mean ± SD)	74.9 ± 13.7	72.2 ± 12.8	0.13
BMI (kg/m^2, mean ± SD)	27.4 ± 5.2	26.5 ± 4.4	0.16
Sex (female, n, %)	77 (71.3%)	85 (70.8%)	0.94
Radius length (mm, mean ± SD)	229.6 ± 25.2	232.0 ± 27.0	0.49
Tibia length (mm, mean ± SD)	352.1 ± 19.9	355.4 ± 21.1	0.23
Fracture risk factors (n, %)			
Smoking	17 (15.7%)	7 (5.8%)	0.01
Alcohol	15 (13.9%)	11 (9.2%)	0.26
Rheumatoid arthritis	13 (12.0%)	5 (4.2%)	0.03
Parental hip fracture	17 (15.7%)	7 (5.8%)	0.01
Interval between fracture and study visit (days, mean ± SD)	56.6 ± 13.2		
Fracture site *			
Radius/ulna	74		
Hand	4		
Humerus	11		
Tibia/fibula	17		
Ankle/foot	6		
Femur	6		
Pelvis	2		
Rib	1		
Spine	1		

* 13 patients (7 females and 6 males) had fracture of more than one site: 6 females with two fracture sites and 1 female with three fracture sites, 6 males with two fracture sites

Table 5.2 Comparison of different properties between the fracture and control groups in all participants. Variance inflation factors (VIFs) were calculated for the properties of each modality [a]. Values are expressed as mean ± 1.0 SD.

	Fracture group (n=108)	Control group (n=120)	p	p_{adj} [b]	VIF
DXA properties					
LS aBMD (g/cm^2)	1.00 ± 0.14	1.04 ± 0.18	0.06	0.17	2.6
TH aBMD (g/cm^2)	0.90 ± 0.15	0.95 ± 0.17	0.02	0.13	5.1
FN aBMD (g/cm^2)	0.75 ± 0.11	0.77 ± 0.13	0.21	0.27	5.0
Standard pQCT radius properties					
Tot vBMD (mg/cm^3)	281.75 ± 61.17	282.46 ± 55.61	0.93	0.97	11.0
Trb vBMD (mg/cm^3)	164.92 ± 46.08	182.03 ± 36.47	<0.01	0.01	7.3
Trb CSA (mm^2)	178.45 ± 39.34	187.27 ± 31.69	0.06	0.11	3.5
Crt vBMD (mg/cm^3)	1123.77 ± 57.94	1139.88 ± 49.45	0.02	0.07	5.7
Crt Thk (mm)	2.26 ± 0.35	2.39 ± 0.33	<0.01	0.09	3.9
SSI_p (mm^3)	256.87 ± 54.54	266.91 ± 51.24	0.15	0.21	10.8
Standard pQCT tibia properties					
Tot vBMD (mg/cm^3)	264.56 ± 52.02	278.38 ± 52.52	0.05	0.22	12.7
Trb vBMD (mg/cm^3)	205.63 ± 48.20	223.47 ± 44.13	<0.01	0.02	6.9
Trb CSA (mm^2)	527.82 ± 77.57	541.31 ± 76.32	0.19	0.47	3.7
Crt vBMD (mg/cm^3)	1120.72 ± 42.38	1129.94 ± 39.18	0.09	0.14	5.1
Crt Thk (mm)	4.01 ± 0.80	4.16 ± 0.68	0.13	0.29	3.9
SSI_p (mm^3)	2248.76 ± 394.44	2369.36 ± 397.11	0.02	0.17	16.0
pQCT-FE properties (4% radius)					
k_{comp} (kN/mm)	39.47 ± 22.23	45.46 ± 26.79	0.07	0.11	92.1
k_{shear} (kN/mm)	9.92 ± 5.44	10.92 ± 6.06	0.19	0.28	107.5
k_{bend} (Nm/deg)	20.99 ± 12.12	23.51 ± 14.26	0.15	0.33	18.7
$k_{torsion}$ (Nm/deg)	16.87 ± 8.83	18.52 ± 10.97	0.22	0.29	25.1
pQCT-FE properties (66% radius)					
k_{comp} (kN/mm)	196.85 ± 58.97	221.41 ± 71.53	<0.01	0.04	374.2
k_{shear} (kN/mm)	56.61 ± 17.72	64.10 ± 17.87	<0.01	0.07	354.7
k_{bend} (Nm/deg)	36.62 ± 10.58	48.75 ± 22.17	<0.01	0.03	6.9
$k_{torsion}$ (Nm/deg)	28.98 ± 11.78	32.41 ± 12.42	0.03	0.06	8.5
pQCT-FE properties (4% tibia)					
k_{comp} (kN/mm)	1017.10 ± 285.44	1224.70 ± 345.70	<0.01	<0.01	641.8
k_{shear} (kN/mm)	275.12 ± 88.98	356.84 ± 106.06	<0.01	0.01	598.6
k_{bend} (Nm/deg)	1866.48 ± 713.26	2163.96 ± 677.60	<0.01	0.06	11.7
$k_{torsion}$ (Nm/deg)	1251.59 ± 398.72	1525.70 ± 481.82	<0.01	0.05	14.9
pQCT-FE properties (66% tibia)					
k_{comp} (kN/mm)	3402.49 ± 652.90	3681.22 ± 648.68	<0.01	0.03	971.5
k_{shear} (kN/mm)	1015.76 ± 193.17	1113.30 ± 197.80	<0.01	0.04	827.1
k_{bend} (Nm/deg)	2524.93 ± 1043.97	2768.08 ± 1143.02	0.02	0.04	5.2
$k_{torsion}$ (Nm/deg)	2461.42 ± 572.77	2578.14 ± 563.71	0.12	0.19	5.3

p values with statistical significance are highlighted in bold.

[a] Age, height and weight were also included in each regression model and all VIFs for them were lower than 5.

[b] p values for comparison between groups after adjusted for age, height and weight

Table 5.3 Comparison of different properties between the fracture and control groups in females. Variance inflation factors (VIFs) were calculated for the properties of each modality [a]. Values are expressed as mean ± 1.0 SD.

	Fracture group (n=77)	Control group (n=85)	p	p_{adj} [b]	VIF
DXA properties					
LS aBMD (g/cm^2)	0.97 ± 0.16	1.01 ± 0.19	0.15	0.12	2.3
TH aBMD (g/cm^2)	0.87 ± 0.17	0.91 ± 0.19	0.16	0.06	5.2
FN aBMD (g/cm^2)	0.73 ± 0.11	0.74 ± 0.14	0.62	0.58	5.5
Standard pQCT radius properties					
Tot vBMD (mg/cm^3)	269.01 ± 59.53	274.01 ± 59.83	0.60	0.59	11.1
Trb vBMD (mg/cm^3)	157.85 ± 40.04	171.82 ± 37.64	0.02	0.04	7.0
Trb CSA (mm^2)	165.95 ± 39.31	171.72 ± 32.85	0.31	0.26	3.3
Crt vBMD (mg/cm^3)	1121.14 ± 57.52	1133.49 ± 50.99	0.15	0.15	5.7
Crt Thk (mm)	2.13 ± 0.31	2.21 ± 0.29	0.09	0.11	3.2
SSI_p (mm^3)	218.95 ± 46.64	232.98 ± 50.19	0.07	0.12	10.6
Standard pQCT tibia properties					
Tot vBMD (mg/cm^3)	249.12 ± 47.21	260.85 ± 52.32	0.14	0.22	12.4
Trb vBMD (mg/cm^3)	201.65 ± 50.78	217.02 ± 46.55	0.05	0.02	5.6
Trb CSA (mm^2)	510.87 ± 77.45	521.65 ± 80.10	0.39	0.42	3.2
Crt vBMD (mg/cm^3)	1116.81 ± 44.88	1125.25 ± 42.18	0.22	0.15	5.0
Crt Thk (mm)	3.85 ± 0.87	3.99± 0.74	0.27	0.30	2.7
SSI_p (mm^3)	1988.09 ± 344.34	2082.12 ± 370.32	0.10	0.10	12.7
pQCT-FE properties (4% radius)					
k_{comp} (kN/mm)	35.59 ± 23.24	41.15 ± 27.89	0.17	0.31	87.6
k_{shear} (kN/mm)	8.85 ± 5.63	9.66 ± 6.42	0.40	0.41	103.4
k_{bend} (Nm/deg)	19.37 ± 11.70	20.67 ± 13.58	0.52	0.52	18.9
$k_{torsion}$ (Nm/deg)	15.05 ± 8.71	16.26 ± 10.26	0.42	0.51	28.7
pQCT-FE properties (66% radius)					
k_{comp} (kN/mm)	183.92 ± 62.08	210.14 ± 55.70	<0.01	<0.01	391.2
k_{shear} (kN/mm)	51.16 ± 18.82	58.45 ± 16.85	0.01	0.03	369.0
k_{bend} (Nm/deg)	30.45 ± 10.69	43.10 ± 22.40	<0.01	<0.01	5.1
$k_{torsion}$ (Nm/deg)	25.68 ± 12.29	28.73 ± 9.14	0.07	0.11	8.3
pQCT-FE properties (4% tibia)					
k_{comp} (kN/mm)	959.53 ± 303.77	1174.33 ± 354.41	<0.01	<0.01	660.5
k_{shear} (kN/mm)	262.94 ± 86.22	324.58 ± 100.55	<0.01	0.02	632.3
k_{bend} (Nm/deg)	1797.17 ± 722.72	2025.54 ± 687.87	0.04	0.09	12.3
$k_{torsion}$ (Nm/deg)	1123.50 ± 369.69	1382.32 ± 482.97	<0.01	0.02	15.8
pQCT-FE properties (66% tibia)					
k_{comp} (kN/mm)	3322.82 ± 704.61	3635.64 ± 662.08	<0.01	0.03	1055.2
k_{shear} (kN/mm)	955.52 ± 209.22	1045.87 ± 194.13	<0.01	<0.01	1029.8
k_{bend} (Nm/deg)	2401.94 ± 922.49	2798.71 ± 919.13	0.01	0.04	5.4
$k_{torsion}$ (Nm/deg)	2369.67 ± 567.23	2465.15 ± 553.91	0.28	0.32	5.5

p values with statistical significance are highlighted in bold.

[a] Age, height and weight were also included in each regression model and all VIFs for them were lower than 5.

[b] p values for comparison between groups after adjusted for age, height and weight.

Table 5.4 Comparison of different properties between the fracture and control groups in males. Variance inflation factors (VIFs) were calculated for the properties of each modality [a]. Values are expressed as mean ± 1.0 SD.

	Fracture group (n=31)	Control group (n=35)	p	p_{adj} [b]	VIF
DXA properties					
LS aBMD (g/cm^2)	1.07 ± 0.09	1.12 ± 0.14	0.09	0.17	5.9
TH aBMD (g/cm^2)	0.97 ± 0.09	1.03 ± 0.12	0.03	0.047	3.7
FN aBMD (g/cm^2)	0.79 ± 0.10	0.83 ± 0.11	0.13	0.23	2.9
Standard pQCT radius properties					
Tot vBMD (mg/cm^3)	313.41 ± 65.15	302.97 ± 45.52	0.45	0.39	10.5
Trb vBMD (mg/cm^3)	182.49 ± 58.66	206.84 ± 34.54	0.04	0.046	8.1
Trb CSA (mm^2)	209.49 ± 39.43	225.03 ± 29.64	0.07	0.12	5.2
Crt vBMD (mg/cm^3)	1130.29 ± 59.00	1155.41 ± 46.99	0.06	0.08	6.2
Crt Thk (mm)	2.57 ± 0.44	2.81 ± 0.43	0.03	0.09	8.1
SSI_p (mm^3)	351.06 ± 70.72	349.31 ± 55.18	0.91	0.98	11.7
Standard pQCT tibia properties					
Tot vBMD (mg/cm^3)	302.92 ± 62.57	320.94 ± 54.51	0.22	0.31	16.5
Trb vBMD (mg/cm^3)	215.51 ± 40.94	239.12 ± 39.00	0.02	0.04	12.3
Trb CSA (mm^2)	569.91 ± 77.88	589.04 ± 68.60	0.29	0.31	6.9
Crt vBMD (mg/cm^3)	1130.44 ± 35.25	1141.34 ± 31.97	0.19	0.22	5.2
Crt Thk (mm)	4.40 ± 0.57	4.58 ± 0.51	0.18	0.19	7.7
SSI_p (mm^3)	2896.22 ± 499.36	3066.93 ± 466.64	0.16	0.25	15.9
pQCT-FE properties (4% radius)					
k_{comp} (kN/mm)	49.09 ± 19.45	55.91 ± 24.74	0.22	0.20	109.5
k_{shear} (kN/mm)	12.59 ± 4.92	13.98 ± 5.29	0.28	0.21	115.7
k_{bend} (Nm/deg)	25.02 ± 13.13	30.39 ± 16.19	0.15	0.27	16.9
$k_{torsion}$ (Nm/deg)	21.39 ± 9.13	24.02 ± 12.84	0.35	0.19	19.0
pQCT-FE properties (66% radius)					
k_{comp} (kN/mm)	228.96 ± 50.25	248.78 ± 101.95	0.16	0.14	288.3
k_{shear} (kN/mm)	70.16 ± 14.55	77.82 ± 20.64	0.09	0.12	302.7
k_{bend} (Nm/deg)	51.94 ± 10.30	62.47 ± 22.26	0.02	<0.01	10.2
$k_{torsion}$ (Nm/deg)	37.19 ± 10.38	41.33 ± 18.38	0.27	0.20	9.7
pQCT-FE properties (4% tibia)					
k_{comp} (kN/mm)	1160.10 ± 232.63	1347.02 ± 333.88	0.01	0.04	512.7
k_{shear} (kN/mm)	305.37 ± 95.62	435.20 ± 121.34	<0.01	0.045	488.6
k_{bend} (Nm/deg)	2038.64 ± 688.71	2500.11 ± 671.93	0.01	0.02	9.6
$k_{torsion}$ (Nm/deg)	1569.73 ± 434.2	1873.90 ± 493.01	0.01	0.06	12.7
pQCT-FE properties (66% tibia)					
k_{comp} (kN/mm)	3600.37 ± 498.44	3791.91 ± 634.15	0.18	0.15	751.4
k_{shear} (kN/mm)	1165.39 ± 144.75	1277.05 ± 212.09	0.02	0.06	683.5
k_{bend} (Nm/deg)	2631.71 ± 811.73	3106.54 ± 969.12	0.04	0.045	6.7
$k_{torsion}$ (Nm/deg)	2689.32 ± 586.57	2852.53 ± 602.94	0.27	0.21	4.2

p values with statistical significance are highlighted in bold.

[a] Age, height and weight were also included in each regression model and all VIFs for them were lower than 5.

[b] p values for comparison between groups after adjusted for age, height and weight.

Table 5.5 Odds ratio, specificity, sensitivity and area under receiver operating curve (AUROC) of receiver operative curve derived for key variables

	OR (95% CI)	Specificity (%)	Sensitivity (%)	AUROC (95% CI)
	All participants			
LS aBMD	1.26 (1.04, 1.66)	74.1	61.4	0.64 (0.56, 0.74)
TH aBMD	1.53 (1.01, 2.15)	76.7	54.8	0.69 (0.62, 0.75)
FN aBMD	1.19 (0.91, 1.60)	75.0	57.0	0.61 (0.54, 0.69)
Radius Trb vBMD	3.01 (0.92, 4.57)	70.2	61.4	0.70 (0.60, 0.79)
Tibia Trb vBMD	7.64 (1.92, 26.51)	76.7	62.0	0.74 (0.68, 0.80)
k_{bend} (66% radius)	5.84 (0.99, 7.23)	69.7	63.2	0.73 (0.64, 0.80)
k_{shear} (4% tibia)	9.13 (1.87, 31.36)	66.7	78.7	0.79 (0.74, 0.84)
k_{bend} (66% tibia)	5.23 (1.85, 15.37)	74.1	65.8	0.78 (0.70, 0.86)
	Females			
LS aBMD	1.23 (1.04, 1.59)	71.0	62.5	0.65 (0.58, 0.74)
TH aBMD	1.52 (1.01, 2.16)	72.4	52.7	0.72 (0.64, 0.79)
FN aBMD	1.15 (0.80, 1.66)	74.5	52.1	0.62 (0.55, 0.70)
Radius Trb vBMD	3.28 (0.89, 4.85)	67.4	62.2	0.70 (0.60, 0.78)
Tibia Trb vBMD	8.15 (1.78, 39.72)	65.9	75.3	0.76 (0.68, 0.82)
k_{bend} (66% radius)	5.95 (0.96, 9.39)	71.2	62.2	0.71 (0.64, 0.77)
k_{shear} (4% tibia)	10.34 (1.91, 43.98)	79.2	69.4	0.83 (0.77, 0.89)
k_{bend} (66% tibia)	6.04 (1.71, 18.51)	74.5	62.2	0.78 (0.70, 0.86)
	Males			
LS aBMD	1.49 (1.06, 1.89)	65.7	67.7	0.61 (0.52, 0.71)
TH aBMD	1.55 (1.02, 2.07)	65.7	64.5	0.62 (0.49, 0.74)
FN aBMD	1.21 (0.99, 1.52)	67.7	64.5	0.57 (0.50, 0.66)
Radius Trb vBMD	2.16 (1.02, 3.22)	74.3	77.4	0.73 (0.60, 0.83)
Tibia Trb vBMD	6.58 (2.43, 10.70)	74.3	64.5	0.71 (0.59, 0.82)
k_{bend} (66% radius)	3.27 (2.71, 3.82)	74.2	67.7	0.78 (0.65, 0.89)
k_{bend} (4% tibia)	8.32 (4.15, 33.84)	80.0	74.2	0.81 (0.70, 0.90)
k_{bend} (66% tibia)	4.64 (2.37, 7.09)	65.7	67.7	0.80 (0.72, 0.88)

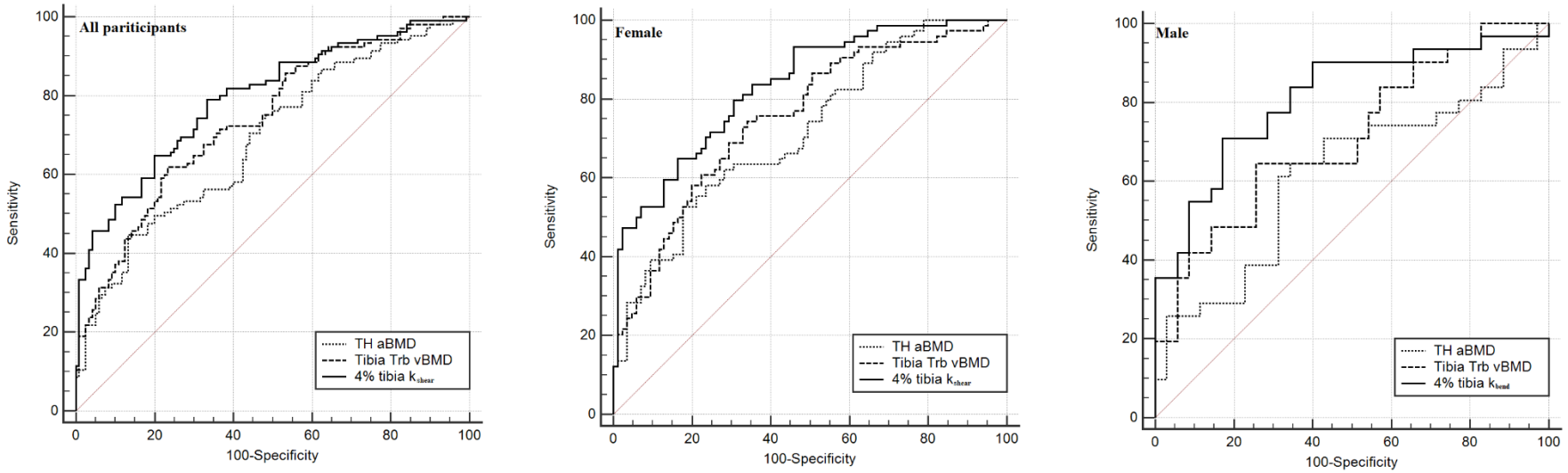

Figure 5.2 Comparisons of AUROC of primary variables in all participants, females and males.

Table 5.6 Pairwise comparison of AUROC of primary variables in females and males

	Mean difference	95% CI	p
	All participants		
Tibia Trb vBMD – TH aBMD	0.05	(-0.03, 0.13)	0.21
k_{shear} 4% tibia – TH aBMD	0.11	(0.02, 0.20)	0.02
k_{shear} 4% tibia – Tibia Trb vBMD	0.05	(-0.03, 0.14)	0.19
	Females		
Tibia Trb vBMD – TH aBMD	0.03	(-0.05, 0.12)	0.42
k_{shear} 4% tibia – TH aBMD	0.11	(0.02, 0.21)	0.02
k_{shear} 4% tibia – Tibia Trb vBMD	0.08	(-0.01, 0.17)	0.07
	Male		
Tibia Trb vBMD – TH aBMD	0.09	(-0.09, 0.27)	0.32
k_{bend} 4% tibia – TH aBMD	0.19	(0.02, 0.36)	0.03
k_{bend} 4% tibia – Tibia Trb vBMD	0.10	(-0.06, 0.26)	0.21

5.6 Discussion

This study evaluated whether pQCT-derived FE modeling provided improved discrimination between non-vertebral, low-trauma fracture patients with predominantly peripheral fractures and age-matched controls. Peripheral QCT scans of the radius and the tibia were performed on patients with recent non-vertebral, low-trauma fracture and age-matched healthy controls. The fracture group consisted primarily of ambulatory care patients with limb fractures; therefore, as expected, they were relatively young compared with patients presenting with spine and hip fractures. Thus, our pQCT findings are likely to reflect bone fragility at the relevant peripheral sites in this age group. Peripheral QCT can differentiate the cortical and trabecular compartments of bone, which is advantageous as the two types of bone change differently in response to ageing, bone diseases and treatment (633). In this study, pQCT-FE variables were found to have enhanced diagnostic performance compared with DXA and statistically comparable diagnostic performance with standard pQCT variables. By incorporating the BMDs across these different compartments in FE models, we hypothesized that predictions of bone stiffness may be used to better discriminate between fracture patients and healthy controls compared to DXA.

QCT-based FE modelling has been used in clinical studies to assess bone strength of the proximal femur and spine due to its strong predictive ability for fracture failure load (383, 385). In the last decade, a dedicated peripheral CT scanner with higher image resolution and voxel size emerged in clinical research. High-resolution pQCT (HR-pQCT) of the latest generation can achieve voxel sizes of 61 µm which enables depiction of the microstructure of the radius and the tibia. While micro FE (µFE) generated from HR-pQCT images has good ability to discriminate between fracture patients and controls (412), and is associated with

fracture occurrence during follow-up (424), there are several drawbacks with this technique when used in clinical settings. It is time-consuming to scan, set up and analyse an FE model for individual patients from HR-pQCT images (3 to 10 hours;604); hence, it is not efficient for fracture risk screening or diagnosing osteoporosis in a clinical setting. The amount of time required to setup QCT-based FE analysis is similarly problematic. Whilst HR-pQCT scanners expose patients to slightly greater radiation than for pQCT (634), the difference is negligible considering the minimal radiation dose associated with either scanning system. HR-pQCT provides considerably more bone structural information than pQCT. However, HR-pQCT scanners present increased procurement and maintenance costs compared to pQCT, which might restrict their widespread clinical use. Hence, we thought it worthwhile to evaluate the possible role of pQCT in enhancing the recognition of bone fragility in clinical settings. In our experience, pQCT-FE from single cross-sections solves each of these issues. Better diagnostic ability than DXA was achieved with simpler set up, thus shorter time to scan patients and to set up individual pQCT-FE models, with lower radiation exposure and cost. As a dedicated tool for the measurement of clinically-relevant sites with several practical advantages, pQCT-FE may play a complementary role in future clinical studies assessing bone health.

Significant differences between groups were observed in pQCT-FE properties, especially at the 4% tibia site, and in some standard pQCT properties. While trabecular or cortical vBMD differed statistically between fracture patients and healthy controls, no difference was identified in SSI_p, the bone strength index reported to be a good measure of bone strength and a good predictor for fracture (348). Fracture odds increased by 10.34 [95% CI (1.91, 43.98)] and 10.17 [95% CI (1.60, 42.21)] fold per SD decrease in pQCT-FE properties, and were only 1.52 [95% CI (1.01, 2.16)] and 1.74 [95% CI (1.02, 2.37)] with DXA aBMD measures

in females and males, respectively. pQCT-FE properties also had higher diagnostic ability than DXA with AUROC of 0.83 vs 0.72 ($p = 0.02$) in females, and that of 0.81 vs 0.62 in males. This strength was also with improvement in specificity (79.2% vs 72.4% in females, 80.0% vs 65.6% in males) and sensitivity (69.4% vs 52.7% in females, 74.2% vs 64.5% in males). The pQCT-FE variables with highest AUROC were observed at the 4% tibia site, although the specific loading variable differed between females (k_{shear}) and males (k_{bend}). However, since pQCT-FE variables at the same site had high VIFs thus correlated strongly with each other, the difference was not considered to imply different mechanical performance between females and males. Overall, pQCT-FE models improved clinical performance in the identification of patients with increased fracture risk compared with DXA.

The best fracture discrimination was observed for pQCT-FE variables at the trabecular-rich site in the tibia. It should be noted that while pQCT-FE variables are computed from both trabecular and cortical bone, their relative contributions will depend on the site; hence, the pQCT-FE variables at the distal site will be more influenced by trabecular bone than at the proximal site. Since the pQCT-FE variables provided the greatest fracture discrimination at the distal tibia, the trabecular bone should be considered of greater importance for classification of peripheral appendicular fractures.

Among the standard pQCT and pQCT-FE variables, better performance was generally observed for variables obtained at the tibia compared to the radius. At the 4% tibia site, all pQCT-FE properties differed significantly between groups with the highest OR for fracture and highest AUROC to classify fracture patients from healthy controls. This finding contrasts with peripheral clinical fracture locations, where more fractures occur at the distal radius

compared to the distal tibia. Many studies utilizing DXA have confirmed that scans of one specific site predict fracture of that site better than scans of other sites do. The finding from the current study is unexpected considering most fractures were forearm fractures. However, we do note similar findings by Sornay-Rendu et al (627) utilizing HR-pQCT between patients with mixed fractures and controls. In their study, none of the radius variables differed between groups after adjustment for radius aBMD, while several tibia variables remained statistically significant including both total and trabecular density at the distal tibia, cortical thickness and trabecular thickness. Furthermore, OR per SD decrease were also higher for tibia variables than for radius variables in this study. This may be due to variations in radius morphology and bone density across the population (635), which makes this site less sensitive to identify a fracture risk threshold. Indeed, we noticed higher coefficients of variance in radius variables than in the tibia from previous studies conducted at different centres using pQCT (636 -638) or HR-pQCT (639 -641), especially variables at distal site. Another possibility is that movement of the radius due to breathing and upper body movement may have affected imaging at this site to a greater degree than the distal tibia. The controls may have represented a more physically-active cohort compared to the fracture patients, which may have contributed to greater bone density, particularly at the tibia, and a better preservation of balance thus reducing their risk of falls and fracture (642). In addition, it may also result from the mixed fracture types in the studied population. However, even in patients with distal radius fracture only, pQCT-measured tibia variables still seem to have comparable ability to discriminate between fractures and controls (352).

A key limitation in the FE models was that the loading and boundary conditions in the simulations were artificial compared to daily loading of the radius and the tibia in vivo, where a loading combination of all cases occurs simultaneously (643). The logic for adopting these

loading cases in the pQCT-FE models is that a bone's strength is proportional to its weakest resistance for an idealised loading condition. Indeed, this assumption has been adopted extensively in HR-pQCT-based μFE models where idealised axial compression was used to assess fracture risk (644). Nevertheless, these idealized loading conditions when combined with the thin cross-sectional geometry of the FE models would have led to bone stiffness predictions that differed from those encountered in vivo. Hence, the bone stiffnesses predicted in the current study are only proportional to whole-bone fracture load applicable for comparing relative differences between cohorts of patients rather than assessing the absolute stiffness of bone for an individual.

pQCT has an inferior spatial resolution compared to HR-pQCT, thus provides limited information about bone micro-structure. This limitation of pQCT might restrict its wide research utility where knowledge of microstructure is required. However, comparable AUROC was reported in studies investigating the diagnostic ability of HR-pQCT and μFE in distinguishing controls from either patients with radius fracture (645) or with mixed low-trauma fractures (646). The degree to which HR-pQCT and μFE can improve the diagnostic performance directly compared with pQCT-FE in identifying fracture patients is still uncertain. Future studies are needed to confirm whether comparable diagnostic ability can be achieved using the relatively low-resolution pQCT scanner considering its lower procurement and maintenance costs.

Due to lack of thoracolumbar X-ray/vertebral fracture assessment, there is still a possibility that a sub-group of controls had asymptomatic vertebral fracture. We acknowledge that this is a limitation of the study, and might reduce rather than exaggerate the apparent differences in

FEM measures between fracture and non-fracture individuals. It is estimated that nearly 70% of vertebral fractures are missed in community in clinical practice (647). While improving diagnosis rate of asymptomatic vertebral fracture remains difficult, we do notice that osteoporotic vertebral fracture is more prevalent for ages greater than those seen in the current study (648). In addition, recruiting strategies were applied to eliminate the impact of vertebral fracture as much as possible. Subjects were screened for symptoms such as chronic back pain or loss of height on a self-reported questionnaire. As a proportion of vertebral fractures result from prolonged use of glucocorticoid agents, “currently taking or have recently taken glucocorticoid agents” was one of the general exclusion criteria for both groups.

DXA measurements of the forearm were not available in this study. DXA measurement of the 1/3 radius predicts wrist fracture better than central DXA measurements, therefore, the subsequent inability to relate pQCT and pQCT-FE to DXA values at similar anatomic site is another limitation of this study, especially for the reported population in whom a majority had forearm fractures. However, the ability of both distal radius and central DXA to predict all types of fragility fracture is comparable (649). The study by Amiri et al (650) reported good linear correlation between radius and central DXA results, which suggests that the trends in the central DXA results would remain similar if radius DXA measurements were used. The aim of the current study was to compare the pQCT-FE method with the most-accepted DXA measurements used for osteoporosis and fracture risk assessment in clinical practice, which both the WHO and ISCD recommend as central DXA. However, inclusion of radius DXA measurements and their comparisons to pQCT and pQCT-FE measures would provide additional information on the application of this novel yet simple technology and would be of added research interest.

In summary, pQCT-based FE models were applied together with standard pQCT and DXA properties to distinguish patients with recent non-vertebral fragility fracture from healthy controls. Improved diagnostic ability was observed for pQCT-FE, but not primary pQCT variables, compared with DXA properties in both females and males, although no statistical difference was observed in AUROC between primary pQCT and pQCT-FE variables. These results may provide an enhanced assessment for bone fragility in clinical settings considering the limitations of DXA, which is the most established modality currently. This study also strongly supports the rationale for future longitudinal studies with follow-up data for fracture risk assessment using pQCT-FE analysis. Recognizing and quantifying bone fragility before a major osteoporotic fracture occurs may bring considerable clinical benefits. Therefore, the potential clinical impact of applying this technology warrants exploration.

5.7 Acknowledgements

The authors would like to thank all subjects for their participation in this study, and the University of the Third Age for providing assistance in participant recruitment. We acknowledge Dr Ashwini Kale for performing DXA and pQCT scans, Mr Richard Farrugia for coordinating the fracture liaison service from which all fracture patients were recruited and Associate Professor Andrew Bucknill for his strong support of recruitment at the fracture liaison service. HJ is funded with a joint PhD scholarship by China Scholarship Council (funding reference: CSC201608240003) and the University of Melbourne.

Conflict of interest: Hongyuan Jiang, Dale L Robinson, Christopher J Yates, Peter VS Lee, and John D Wark declare that they have no conflict of interest.

5.8 Additional discussion

This section is not published along with Sections 5.1 – 5.7 but aims to discuss two additional points.

The FRAX® is a tool calculating an individual's absolute fracture risk based on clinical risk factors as well as DXA FN aBMD (651). Country-specific algorithms have been developed from epidemiological studies in Europe, North America, Asia and Australia (652). While providing improved fracture prediction over DXA T-scores alone, FRAX® does not take bone geometry, micro-structure, organic composition into account and DXA is still the only imaging modality considered in the models. In addition, performance of FRAX® has been reported to vary in different populations (653 – 656) and application of FRAX® to be barely satisfactory in premenopausal women (657, 658). In addition, FRAX® has also been criticised for lack of validation data for men (659). While this study did not manage to compare the pQCT-FEA modelling with FRAX®, such a project in the future would provide more information on the potential clinical use of the FE method.

Among pQCT and pQCT-FEA variables, the strongest discriminative values between fracture and controls groups were generally found at the 4% tibia. While possible explanation has been discussed in Section 5.6, it is aimed to extend one of the potential reasons here. The control group may represent a more physically active population in this study. Therefore, weight bearing activity may contribute to the significant findings at the 4% tibia. In a randomized controlled study, Evans et al reported increased Trb vBMD at the 4% tibia in young people following an aerobic training group (660) while no changes in Crt vBMD at both the 38% and 66% tibia. However, following sub-regional analysis of the mid-shaft

revealed increases in Crt vBMD at the medial side but not the lateral side, which led to the insignificant findings in apparent Crt vBMD. In another study by Rantalainen et al, the investigators found slightly lower Crt vBMD at the mid-shaft of tibia in young people doing impact exercise compared with controls (661). However, sub-regional analysis of the mid-shaft suggest Crt vBMD at this site was not modulated by exercise. In postmenopausal women, a meta-analysis by Polidoulis et al showed that lower extremity exercise improved both Trb vBMD at the distal tibia and Crt vBMD at the mid-shaft (662). Unfortunately, detailed information on physical activity and weight-bearing exercise was not available in the current study. The discriminative findings in Trb vBMD at the 4% tibia were consistent with the Evans study although whether there was sub-regional difference in Crt vBMD was unclear. The Rantalainen study recruited young adults with years of training, which may be one reason for the significant findings in mid-shaft tibia Crt vBMD. This was also supported in the Polidoulis meta-analysis that longer duration of exercise led to more significant changes in Crt vBMD at the tibial shaft.

Chapter 6

Loss of bone density and bone strength following premenopausal bilateral oophorectomy: Results from a prospective controlled study (WHAM Study)

6.1 Loss of bone density and bone strength following premenopausal bilateral oophorectomy: Results from a prospective controlled study (WHAM Study)

Authors and Affiliations:

Hongyuan Jiang [a], Dale L Robinson [b], Peter VS Lee [b], Efrosinia O Krejany [c], Christopher J Yates [a,d,e], Martha Hickey [c], John D Wark [a,d,e,]

[a] Department of Medicine, Royal Melbourne Hospital, University of Melbourne

[b] Department of Biomedical Engineering, University of Melbourne

[c] Department of Obstetrics and Gynaecology, University of Melbourne and Royal Women's Hospital

[d] Bone and Mineral Medicine, Royal Melbourne Hospital

[e] Department of Diabetes and Endocrinology, Royal Melbourne Hospital

6.2 Abstract

PURPOSE This prospective study investigated bone health in women following premenopausal oophorectomy.

METHODS Dual energy x-ray absorptiometry (DXA), peripheral quantitative computed tomography (pQCT) and pQCT-based finite element analysis (pQCT-FEA) were used to assess bone health between systemic hormone therapy (HT) users and non-users after premenopausal risk-reducing bilateral salpingo-oophorectomy (RRBSO) compared to premenopausal controls over 24 months follow up.

RESULTS Mean age at RRBSO was 42.4±2.6 years (n=30) and 40.2 ± 6.3 years in controls (n=42) and baseline bone measures were similar between groups. At 24 months after RRBSO, areal bone mineral density (aBMD) at the lumbar spine, tibial volumetric cortical density (Crt vBMD) and tibial bending stiffness (k_{bend}) had decreased by 4.7%, 1.0% and 12.1% respectively (all $p < 0.01$). Tibial Crt vBMD and k_{bend} were significantly lower after RRBSO than in controls at 24 months ($p < 0.01$ and $= 0.04$, respectively). In non-HT users, significant losses in lumbar spine (5.8%), total hip (5.2%) and femoral neck (6.0%) aBMD, tibial Crt vBMD (2.3%) and k_{bend} (14.8%) were observed at 24 months (all $p < 0.01$). HT prevented losses in k_{bend}, tibial Crt vBMD and aBMD, except for modest 2.3 % loss at the lumbar spine ($p = 0.01$).

CONCLUSION This is the first prospective, controlled study of bone health following RRBSO or premenopausal oophorectomy for any indication. It demonstrates substantial loss of bone density and bone strength, with bone loss not fully prevented by systemic HT. These findings may inform decision-making about RRBSO and clinical management following premenopausal oophorectomy.

6.3 Introduction

Approximately one in 400 women in the general population carries a gene mutation that confers an elevated risk of ovarian cancer (663). With the growing availability of gene testing more women are aware of their high-risk status. For BRCA mutation carriers, the only intervention shown to reduce risk of death from ovarian cancer is risk-reducing bilateral salpingo-oophorectomy (RRBSO) (468, 469). Recommended timing of RRBSO depends on gene mutation status, and personal and family cancer history, but is generally before age 45 years and this will induce surgical menopause. Although RRBSO is potentially-lifesaving, concerns about the consequences of surgical menopause mean that uptake continues to be suboptimal (664).

Premature loss of estrogen following premenopausal oophorectomy may increase the risk of osteoporosis and fracture, but prospective data are lacking. Also, whether systemic hormone therapy (HT) preserves bone density and bone strength is uncertain. Whilst two recent systematic reviews reported no significant differences in bone loss following premenopausal oophorectomy compared to natural menopause (472, 511), prospective data are very limited. Understanding the impact of premenopausal oophorectomy on bone health is of clinical importance to inform prevention and management of the growing population of women undergoing RRBSO or premenopausal oophorectomy for other clinical indications (501).

Published evidence addressing changes in bone density, osteoporosis and fracture risk following RRBSO is based on retrospective and cross-sectional data. These findings suggest that bone mineral density (aBMD) at the lumbar spine is reduced by up to 8% and at the hip by up to 5.7% within two years post-surgery (508, 509). Moreover, the prevalence of

osteopenia and osteoporosis is increased following premenopausal oophorectomy compared to natural menopause and the general population of similar age (504, 506, 507). A systematic review (510) reported comparable aBMD and fracture prevalence following RRBSO compared to the general population but was limited to retrospective studies with increased risk of bias. This has limited the development and implementation of clinical practice guidelines following RRBSO with potential negative consequences of this growing patient group (509). Prospective controlled studies are needed to inform the consequences of RRBSO for bone health and to preserve bone health in this population.

Bone loss with consequent fractures is associated with high morbidity, mortality and societal burden (665). Published data suggest that bone health is often overlooked following RRBSO. A retrospective study reported that less than 50% of women had bone mineral density (BMD) measured after RRBSO and up to 70% of those tested had osteopenia or osteoporosis by WHO criteria (503). Estimates of fracture risk based on measurements of BMD are used commonly in clinical settings (666). Dual energy x-ray absorptiometry (DXA) is currently the most established modality to measure BMD. However, the ability of DXA to predict increased fracture risk is limited (667). More than 50% of women with low trauma fractures do not meet WHO criteria for osteoporosis (284). Peripheral quantitative computed tomography (pQCT) measures volumetric bone mineral density (vBMD) independently of bone size and includes specific measures of cortical and trabecular density. It also provides bone geometric parameters allowing estimation of bone strength. Moreover, imaging data from pQCT cross-sections can be used to establish finite element analysis (FEA) models which predict bone mechanical failure well (668) and help discriminate fracture patients from non-fracture controls (599, 669). Therefore, pQCT and pQCT-FEA may improve the

estimation of bone strength compared with DXA to enhance fracture prediction in at-risk populations.

What Happens After Menopause (WHAM) is a multicenter, prospective study of RRBSO compared to age-matched control women addressing multiple health outcomes, including sexual function, menopausal symptoms, quality of life, mood, sleep quality, cardiovascular disease, metabolic and bone health (670). This is the first prospective controlled study of BMD and bone strength after premenopausal oophorectomy and the first to describe the impact of systemic HT on bone health in this population. The aim of the project is to prospectively compare BMD measures and bone strength indices at baseline through to 24-months' follow-up between premenopausal women undergoing RRBSO and age-matched premenopausal controls who retain their ovaries. We also measure the impact of systemic HT on BMD and bone strength by DXA, pQCT and pQCT-based FEA. We hypothesized that RRBSO would lead to a significant reduction in BMD and bone strength, but that systemic HT would maintain bone health at 24 months.

6.4 Methods

Study design

Premenopausal women at high inherited risk of ovarian cancer due to mutations in the BRCA1/2 gene or family history, planning RRBSO (RRBSO group) and premenopausal aged-matched controls (control group) planning to retain their ovaries over 24 months were recruited for this study. Detailed study design has been described elsewhere (670). Multiple bone variables were measured using DXA at baseline (within 3 months after RRBSO), and at 12- and 24-months post RRBSO with additional pQCT at selected study sites at baseline and 24 months. Demographic information, fracture risk factors, vitamin supplements and oral contraceptive use were collected prior to the surgery for the RRBSO group or following eligibility screening for the control group. Following RRBSO, use of HT and dose was decided on a clinical basis by the patients' treating doctors. Timepoints for collecting this information included pre-baseline, baseline, 6 months, 12 months and 24 months. In this report, we present findings from the Melbourne, Australia, site, where pQCT and customized FEA data have been collected.

The study was conducted in accordance with the Declaration of Helsinki. Ethics approval was obtained from the respective human research ethics committee at the Royal Melbourne Hospital (ethics reference: MH2013.060), the Royal Women's Hospital, Melbourne (ethics reference: RWH12/50) and the Peter MacCallum Cancer Centre (ethics reference: HREC/12/PMCC/24).

Participant recruitment

Premenopausal women at high inherited risk of ovarian cancer were recruited through clinical services including familial cancer and gynecological oncology and via targeted advertising through mainstream and electronic media. Controls were recruited via mainstream and electronic advertising to the general public and by snowballing techniques, which refers to recruitment of new participants by the referral of existing participants.

Inclusion criteria for RRBSO group:

(1) age 18 – 50 years inclusive
(2) regular menstrual cycles (if uterus intact)
(3) no vasomotor symptoms (hot flushes or night sweats)
(4) early follicular phase serum FSH ≤ 15 IU/L (if not taking hormonal contraception)
(5) early follicular phase serum estradiol > 100 pmol/L (if not taking hormonal contraception)
(6) confirmed elevated risk of developing breast/ovarian cancer (i.e. either confirmed carrier of BRCA1/2, BRIP1, RAD51C or Lynch syndrome gene mutation, or based on family history.
(7) planning to undergo RRBSO within the recruitment period

Exclusion criteria for RRBSO group:

(1) previous bilateral salpingo-oophorectomy
(2) taking anti-estrogen endocrine therapy in the previous 3 months
(3) pregnant, lactating or within 3 months of pregnancy
(4) undiagnosed abnormal vaginal bleeding
(5) non-English speakers or unable to provide informed consent

Inclusion criteria for the control group:

(1) the same inclusion criteria (1) – (5) as RRBSO group

(2) not planning to undergo oophorectomy or planning pregnancy in the next 2 years

(3) not menopausal at the end of the 24 months follow-up

Exclusion criteria for controls were the same as for the RRBSO group.

DXA scanning and analysis protocol

Standard clinical DXA scans of the lumbar spine (L1 – L4) and the right hip were performed using a fan-beam densitometer (Horizon QDR 4500A, Hologic Inc., Bedford, MA, USA) at baseline, 12M and 24M. Each scan was performed in array mode and analysed using the manufacturer's commercial software (v 9.10D). Variables of interest included areal bone mineral density (aBMD) of the lumbar spine (LS aBMD), the total hip (TH aBMD) and the femoral neck (FN aBMD). The 12-month precision of the scanner for the spine phantom was 0.36% for aBMD and 0.57% for bone mineral content. Classification of baseline bone health status was based on T-scores that were defined as the number of standard deviations (SD) from the mean BMD of reference data of young healthy population of the same race. A z-score > -1.0 was defined as normal bone density and ≤ -2.5 as osteoporosis.

Peripheral QCT scanning and analysis protocol

Axial pQCT images of the non-dominant tibia were acquired using an XCT 3000 pQCT scanner (Stratec Medizintechnik, Pforzheim, Germany) at 4% and 66% of the tibia length, measured from the base of the medial malleolus to the superior margin of the medial condyle at baseline and 24M. A scout scan was performed to identify the correct starting line, defined

as the distal articular surface of the tibia. A single axial image was acquired at both the 4% and 66% sites, each with an in-plane resolution of 0.4 x 0.4 mm and a slice thickness of 2 mm. Scanning speed was 10 mm/s. The manufacturer's commercial software (version XCT 5.50E) was used to analyse pQCT images for standard pQCT variables. Variables of interest included trabecular volumetric bone mineral density (Trb vBMD) at the 4% site, and cortical volumetric bone mineral density (Crt vBMD), cortical thickness (Crt Thk) and polar stress-strain index (SSIp) at the 66% site.

Peripheral QCT-finite element analysis (pQCT-FEA) properties

Peripheral QCT cross-sections at the 4% tibia site were used to establish the pQCT-FEA models. This site was chosen because pQCT-FEA at the distal site has been found to correlate well with failure load at the appendicular skeleton (668) and to improve osteoporosis classification in older patients with low-trauma fracture (599, 669). Detailed methodology of the models was described elsewhere (599). Briefly, all pQCT images were exported to MATLAB (version R2016b, Mathworks, Natick, MA, USA), where manual segmentation was performed. A mesh of 0.4 x 0.4 x 2 mm elements was generated from segmentation, and then re-sliced in the z-direction to produce a uniform mesh of 0.4 x 0.4 x 0.4 mm elements. The Young's modulus was calculated using an established equation (613, 630) and assigned to each element. Each voxel mesh was then used to generate a FEA model in Abaqus (version 2017, Simulia, Dassault Systems, Providence, RI, USA).

Four loading cases were considered for all FEA models (Figure 3 of reference 599): axial compression, shear, bending, and torsion. Axial compression was simulated by a 0.01 mm displacement of the superior surface towards the inferior surface. Shear was simulated by a

0.01 mm displacement of the superior surface in the direction of either the x- or y-axes. Bending was simulated by a 0.0001 radian rotation of the inferior surface about either the x- or y-axes (i.e., cross-section neutral axes). Torsion was simulated by a 0.0001 radian rotation of the inferior surface about the z-axis. The reaction forces and moments predicted from the simulations were divided by the respective applied displacement or rotation to derive the compressive stiffness (k_{comp}), shear stiffness (k_{shear}), bending stiffness (k_{bend}), and torsional stiffness ($k_{torsion}$) of each cross-section. The bending and shear stiffness were each taken as the minimum value derived from the two neutral-axis directions.

Statistical analysis

Descriptive statistics were expressed as mean ± standard deviation (SD). Differences between the RRBSO and control groups were compared using two-sample t-tests if data were normally distributed, or the Kolmogorov-Smirnov test if they were not normally distributed. Paired t-tests were used to investigate changes from baseline to 12M for DXA variables, and from baseline to 24M for DXA, standard pQCT and pQCT-FEA variables. One-way analysis of variance (ANOVA) was used to compare changes in different bone variables during follow-up between RRBSO women who took HT (either estrogen-only or combined estrogen and progestin HT) at any time during the 24-month follow up (HT group), those who did not take HT at any point over the 24-month follow up period (non-HT group) and controls.

To investigate the influence of systemic HT use on bone health after RRBSO, linear regression models were used to determine the relationship between percentage change in the bone variables (dependent factors) and HT (independent factor, where HT use was set as a binary variable). To investigate the influence of HT type (estrogen-only or combined

estrogen and progestin) and duration on bone health, linear regression models were used to determine the relationship between percentage change in DXA, standard pQCT or pQCT-FEA variables (dependent factors) and HT type [independent factor, where hormone use was set as a binary variable (either estrogen only or combined HT)] or HT duration (independent factor, continuous data expressed as percentage of follow-up days). All regression models were adjusted for age, height and weight. All statistical analyses were performed using SPSS (version 25, SPSS Inc., Chicago, IL, USA). All significance levels were set as $p < 0.05$.

6.5 Results

A total of 72 participants completed baseline, 12- and 24-month follow-up (RRBSO group n = 30, control group n = 42). Following RRBSO, 17 (56.7%) women took systemic HT at any time during the 2-year follow up (HT group) and 13 (43.3%) did not take HT at any time point (non-HT group). In HT users, the average dosage of estradiol was 50mcg/day. Ten (58.8%) participants took estrogen-only HT (following hysterectomy) and seven (41.2%) took combined HT (estrogen and progestin) and 14 (82.4%) used HT for more than 75% of the follow-up period. The sample size provided 99%, 80% and 99% power to detect medium to large effect sizes (Cohen's f = 0.98, 0.37 and 0.63, respectively) in percent change of LS aBMD, Crt vBMD and k_{bend} from baseline to 24M in the ANOVA at a 0.05 significance level.

Baseline characteristics

No significant differences were observed between the RRBSO and control groups in age, height, weight or body mass index (BMI) at the baseline bone density visit (all $p \geq 0.08$, Table 6.1). There weas no baseline difference between the two groups in fracture risk factors as applied in the FRAX® fracture risk calculator (664) (all $p \geq 0.18$; Table 6.2). There was no significant difference in use of vitamin D or calcium supplements ($p = 0.16$) or hormonal contraception use ($p = 0.27$) at baseline. Twenty (66.7%) and 26 (61.9%) participants had normal baseline aBMD measured by DXA in the RRBSO and control groups, respectively (Table 6.1). No differences were observed between groups in bone density (*i.e.* normal aBMD, osteopenia, osteoporosis) at baseline ($p = 0.90$). The mean ± SD interval from surgery to the baseline bone density visit for the RRBSO group (HT and non-HT groups combined) group was 61.6 ± 24.2 days. The intervals for HT and non-HT groups were 63.2 ± 25.7 and

59.5 ± 22.1 days, respectively (p = 0.68). Comparing between HT, non-HT and control groups, the only baseline factor that differed between groups was parental history of hip fracture. Two HT users but no controls or non-HT users reported parental history of hip fracture (p = 0.04).

BMD and bone strength at baseline, 12 months and 24 months follow-up

No difference between the RRBSO (HT and non-HT groups combined) and control groups was observed in any of the DXA, pQCT or pQCT-FEA variables at baseline (all $p \geq 0.10$, Table 6.2). No DXA variables differed significantly at 12M (all $p \geq 0.07$) or 24M (all $p \geq 0.09$) between the combined RRBSO group and control group. At 24M, tibial Crt vBMD (1134.27 ± 29.92 vs 1153.46 ± 25.76 mg/cm^3, $p < 0.01$) and k_{bend} (1927.08 ± 533.39 vs 2227.78 ± 649.15 Nm/deg, p = 0.04) were significantly lower after RRBSO than in controls, respectively. No other standard pQCT or pQCT-FEA variables differed between the combined RRBSO and control groups at 24M (all $p \geq 0.10$). ANOVA and pairwise comparisons showed no differences in DXA measure between HT users, non-HT users and controls at either 12M or 24M (all $p \geq 0.08$; data not shown). At 24M, tibial cortical density was higher in controls (1157.46 ± 25.76 mg/cm^3) compared to HT users (1139.76 ± 29.54; p = 0.03) and non-HT users (1125.78 ± 29.83; $p < 0.01$).

Changes from baseline to 24 months in DXA measures

At 24 months, there was a statistically significant reduction in aBMD at the lumbar spine in HT users compared to baseline measures. The mean decrease in aBMD was 2.3% at the lumbar spine (mean change -0.02 ± 0.03 g/cm^2, p = 0.01, Table 3, Figure 1) in HT users but no significant changes in aBMD were seen at the total hip or the femoral neck (both $p \geq$

0.50). In non-HT users, there were significant decreases in aBMD at the lumbar spine of 5.8% (mean change -0.08 ± 0.04 g/cm^2, $p < 0.01$), at the total hip of 5.2% (mean change -0.05 ± 0.04 g/cm^2, $p < 0.01$) and at the femoral neck of 6.0% (mean change -0.06 ± 0.04 g/cm^2, $p < 0.01$). No significant changes in any of the aBMD measures were observed in the controls (all $p \geq 0.61$). ANOVA and pairwise comparisons showed that changes in DXA variables at 24 months between HT users, non-HT users and controls were significantly different. Non-HT users demonstrated greater decreases in aBMD than HT users and controls at the lumbar spine, total hip and femoral neck (all $p \leq 0.01$). Changes in the three groups at 12 months were similar to those found at 24 months (data not shown).

Changes from baseline to 24 months in pQCT and pQCT-FEA measures

At 24 months, no significant changes from baseline were observed in HT users and controls (all $p \geq 0.42$), while there was a mean decrease of 2.3% in Crt vBMD (mean change -26.85 ± 25.74 mg/cm^3, $p < 0.01$) and of 14.8% in k_{bend} (mean change -348.27 ± 168.98 Nm/deg, $p < 0.01$) for non-HT users (Table 6.3, Figure 6.1). ANOVA and pairwise comparisons showed that changes in pQCT and pQCT-FEA variables at 24 months between HT users, non-HT users and controls were significantly different. Non-HT users had significantly greater loss of tibial Crt vBMD and k_{bend} than HT users and controls (Table 6.3).

Systemic hormone therapy and bone outcomes

Following RRBSO in HT and non-HT users combined, the mean decreases in primary bone variables from baseline to 24M were 4.7% for LS aBMD, 1.0% for tibial Crt vBMD and 12.1% for k_{bend} (all $p < 0.05$, Table 6.4). Linear regression models demonstrated that use of systemic HT following RRBSO mitigated bone loss at the LS aBMD by 5.8% [95% CI (3.5,

8.1)] and Crt vBMD by 2.2% [95% CI (0.6, 3.8)], and loss of bone strength (k_{bend}) by 14.1% [95% CI (6.2, 22.0)]. These effects were independent of age, height and weight. Amongst HT users, no differences were observed according to type of HT used (*i.e.* either estrogen-only or combined HT, oral or transdermal therapy) on DXA measures, standard pQCT or pQCT-FEA measure (all $p \geq 0.17$). The effects of HT on bone health were not associated with duration of HT use (all $p \geq 0.09$).

Table 6.1 Participant background information at baseline*

	RRBSO group (n = 30)	Control group (n = 42)	p
Age (years)	42.4 ± 3.6	40.2 ± 6.3	0.08
Height (cm)	164.4 ± 5.7	166.0 ± 7.1	0.30
Weight (kg)	74.1 ± 14.7	70.3 ± 16.5	0.31
BMI (kg/m^2)	27.4 ±5.2	25.4 ± 4.8	0.09
Current smoking (n, %)	2 (6.7%)	1 (2.4%)	0.57
Alcohol 3 or more units/day (n, %)	0	1 (2.4%)	>0.99
Previous LTF (n, %)	0	0	
Parental fractured hip (n, %)	2 (6.7%)	0	0.18
Rheumatoid arthritis (n, %)	0	0	
Glucocorticoids use (n, %)	0	0	
Secondary osteoporosis (n, %)	1 (3.3%)	0	0.42
Vitamin D/calcium supplements (n, %)	10 (33.3%)	7 (16.7%)	0.16
Hormonal contraceptive use (n, %)	5 (16.7%)	13 (31.0%)	0.27
DXA diagnosis (n, %)			0.90
Normal aBMD	20 (66.7%)	26 (61.9%)	
Low bone mass	9 (30.0%)	14 (33.3%)	
Osteoporosis	1 (3.3%)	2 (4.8%)	
Interval from surgery to baseline BMD visit (days)	61.6 ± 24.2		

Results expressed as mean ± SD or number of case (percentage of case)

BMI: body mass index, **LTF**: low-trauma fracture, **DXA**: dual energy x-ray absorptiometry, **BMD**: bone mineral density, **RRBSO**: risk-reducing salpingo-oophorectomy

* All data in this table were collected pre-surgery except for age, height, weight, BMI and

DXA data which were collected within 3 months of surgery

Table 6.2 DXA variables at baseline, 12 months and 24 months, standard pQCT and pQCT-FEA variables at baseline and 24 months, and changes at 12M and 24M within and between groups

	RRBSO group (n=30)	Control group (n = 42)	p
DXA variables			
LS aBMD (g/cm^2)			
Baseline	1.06 ± 0.15	1.09 ± 0.14	0.39
12M	1.03 ± 0.15	1.09 ± 0.13	0.07
24M	1.02 ± 0.15	1.08 ± 0.14	0.09
TH aBMD (g/cm^2)			
Baseline	0.95 ± 0.12	0.95 ± 0.13	>0.99
12M	0.92 ± 0.13	0.95 ± 0.13	0.34
24M	0.93 ± 0.13	0.95 ± 0.13	0.52
FN aBMD (g/cm^2)			
Baseline	0.87 ± 0.12	0.85 ± 0.11	0.47
12M	0.85 ± 0.12	0.86 ± 0.12	0.73
24M	0.85 ± 0.12	0.85 ± 0.12	>0.99
Standard pQCT variables			
Trb vBMD (mg/cm^3)			
Baseline	236.26 ± 35.35	232.14 ± 28.69	0.59
24M	235.21 ± 37.90	228.27 ± 28.88	0.38
Crt vBMD (mg/cm^3)			
Baseline	1145.08 ± 27.07	1155.20 ± 23.60	0.10
24M	1134.27 ± 29.92	1153.46 ± 25.76	**< 0.01**
Crt Thk (mm)			
Baseline	4.06 ± 0.62	4.11 ± 0.57	0.72
24M	4.03 ± 0.63	4.07 ± 0.64	0.79
SSI_p (mm^3)			
Baseline	2419.59 ± 455.31	2334.96 ± 465.83	0.45
24M	2376.74 ± 462.88	2304.67 ± 580.54	0.57
pQCT-FEA variables			
k_{comp} (kN/mm)			
Baseline	1334.32 ± 278.47	1323.20 ± 279.83	0.87
24M	1231.70 ± 268.85	1324.44 ± 283.02	0.17
k_{shear} (kN/mm)			
Baseline	365.33 ± 78.95	360.36 ± 78.21	0.79
24M	337.45 ± 76.87	361.74 ± 78.27	0.20
k_{bend} (Nm/deg)			
Baseline	2215.03 ± 556.47	2172.05 ± 639.68	0.77
24M	1927.08 ± 533.39	2227.78 ± 649.15	**0.04**
$k_{torsion}$ (Nm/deg)			
Baseline	1540.91 ± 374.98	1496.15 ± 449.98	0.66
24M	1443.80 ± 375.63	1529.25 ± 458.92	0.40

Results expressed as mean ± SD. **Baseline**: within 3 months of oophorectomy for RRBSO group, **RRBSO**: risk-reducing salpingo-oophorectomy, **DXA**: dual energy x-ray absorptiometry, **pQCT**: peripheral quantitative computed tomography, **pQCT-FEA**: pQCT-based finite element analysis, **LS**: lumbar spine, **TH**: total hip, **FN**: femoral neck, **aBMD**: areal bone mineral density, **Trb**: trabecular, **Crt**: cortical, **vBMD**: volumetric bone mineral density, **CSA**: cross-sectional area, **Thk**: thickness, **SSI_p**: polar stree-strain index, **k_{comp}**: compression stiffness, **k_{shear}**: shearing stiffness, **k_{bend}**: bending stiffness, **$k_{torsion}$**: torsional stiffness

Table 6.3 Changes in primary variables at 24 months follow-up and comparisons within and between the HT, non-HT and control groups

Changes	HT group (n = 17)			Non-HT group (n = 13)			Control group (n =42)				
	Mean change	% change	p_{pair-t}	Mean change	% change	p_{pair-t}	Mean change	% change	p_{pair-t}	p_{ANOVA}	$p_{pairwise}$
LS aBMD	-0.02 ± 0.03	-2.3	**0.01**	-0.08 ± 0.04	-5.8	**<0.01**	-0.05×10^{-2} ± 0.02	-0.1×10^{-2}	0.76	**<0.01**	**<0.01;<0.01;<0.01**
TH aBMD	0.05×10^{-1} ± 0.03	0.5	0.50	-0.05 ± 0.04	-5.2	**<0.01**	0.02×10^{-1} ± 0.03	0.2	0.61	**<0.01**	**<0.01**; 0.73; **<0.01**
FN aBMD	-0.01×10^{-1}± 0.03	-0.3	0.90	-0.06 ± 0.04	-6.0	**<0.01**	0.01×10^{-1} ± 0.03	0.1	0.84	**<0.01**	**<0.01**; 0.69; **0.01**
Crt vBMD	-2.29 ± 17.56	-0.2	0.60	-26.85 ± 25.74	-2.3	**<0.01**	-1.70 ± 13.60	-0.1	0.42	**<0.01**	**<0.01**; 0.91; **<0.01**
k_{bend}	-29.43 ± 192.84	-0.3	0.54	-348.27 ± 168.98	-14.8	**<0.01**	21.08 ± 218.0	1.7	0.53	**<0.01**	**<0.01**; 0.48; **<0.01**

LS: lumbar spine, **TH**: total hip, **FN**: femoral neck, **aBMD**: areal bone mineral density, **Crt vBMD**: cortical volumetric bone mineral density, **k_{bend}**: bending stiffness, **HT**: hormone therapy, **non-HT**: non-hormone therapy, **p_{pair-t}:** p value for changes during follow-up within each group, **p_{ANOVA}**: p value for comparison of changes over follow-up between the HT, non-HT and control groups, **$p_{pairwise}$**: p value for pairwise comparison of changes for ANOVA, in the order of HT vs non-HT, HT vs control, non-HT vs control

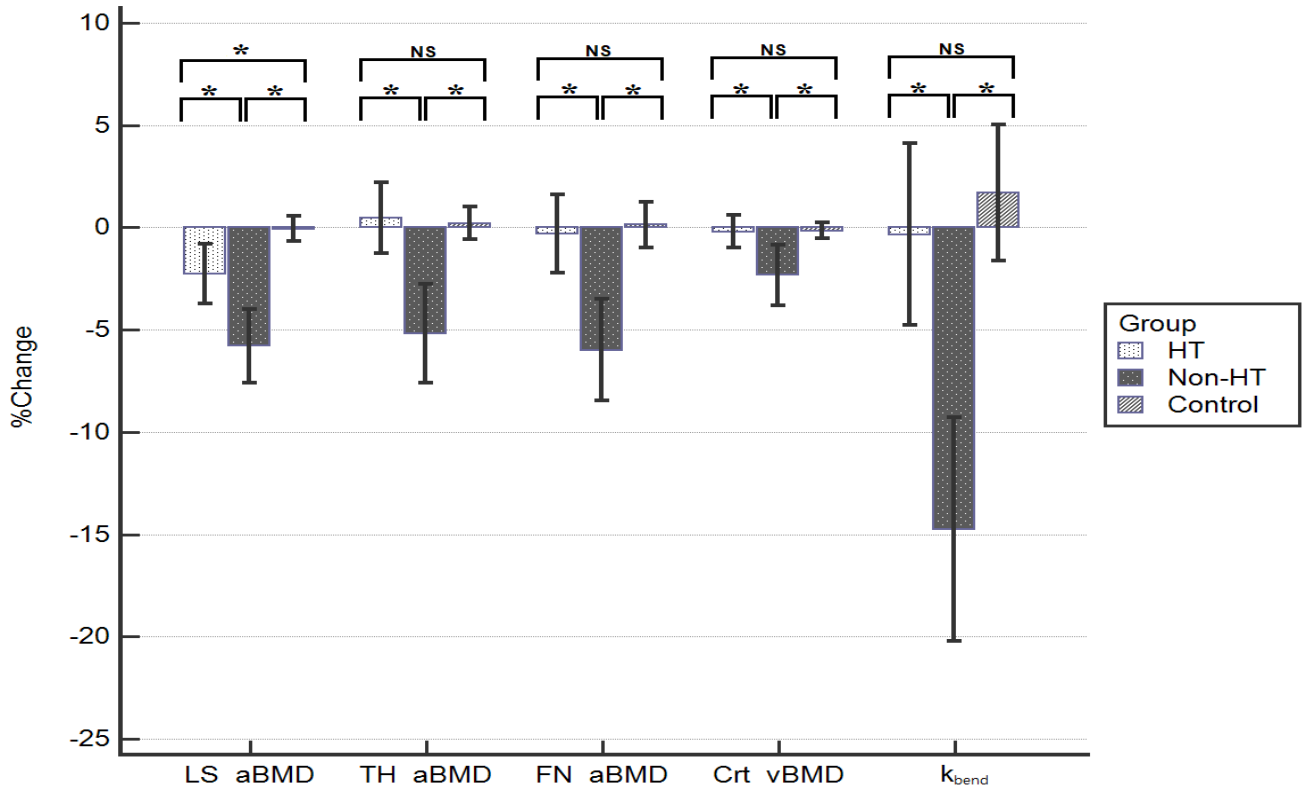

Figure 6.1 Percent change in primary bone variables from baseline to 24 months and pairwise comparisons between groups. Negative values indicate a decrease in the variables relative to its baseline value. Error bars represent 95% CI for the mean changes. *****: $p < 0.05$, **NS:** non-significant. **HT**: hormone therapy group, **non-HT**: non-hormone therapy group, **LS**: lumbar spine, **TH**: total hip, **FN**: femoral neck, **aBMD**: areal bone mineral density measured by DXA, **Crt vBMD**: cortical volumetric bone mineral density measured by pQCT, $\mathbf{k_{bend}}$: bending stiffness calculated using pQCT-FEA

Table 6.4 Means and SDs of percent of change in primary bone variables from baseline to 24M in RRBSO group (n = 30), and coefficients and 95% CIs of the linear regression models

	LS aBMD	**Crt vBMD**	**k_{bend}**
Change% (24M – baseline)	-4.7 ± 4.0 **	-1.0 ± 0.9 **	-12.1± 10.8 **
β (95% CI)			
Hormone therapy use	5.8 (3.5, 8.1) **	2.2 (0.6, 3.8) *	14.1 (6.2, 22.0) **
Hormone type	1.4 (-2.0, 4.9)	0.3 (-1.7, 2.2)	-5.4 (-17.0, 6.3)
Hormone duration	6.7 (-0.7, 14.1)	0.8 (-3.8, 5.5)	9.8 (-20.6, 40.3)

All regression models adjusted for age, height and weight

* $p < 0.05$ ** $p < 0.01$

SD: standard deviation, **RRBSO**: risk-reducing salpingo-oophorectomy, **CI**: confidence interval, **baseline**: within 3 months of RRBSO, **LS aBMD**: lumbar spine areal bone mineral density, **Crt vBMD**: cortical volumetric bone mineral density, **k_{bend}**: bending stiffness

6.6 Discussion

Use of systemic HT has sharply declined globally following concerns about its potential risks, particularly breast cancer (672). However, the benefits of HT for fracture prevention are well established and whilst HT is considered to be safe and confer overall benefits for most high-risk women following RRBSO, uptake is only around 50% in the majority of published studies (472). In addition, concerns about bone loss contribute to suboptimal uptake of RRBSO at the recommended age in at-risk women despite the proven benefits for morbidity and mortality from ovarian cancer (501). To our knowledge, this is the first prospective controlled study of bone outcomes following RRBSO and the effect of post-operative systemic HT on bone health. Our findings show that RRBSO led to significant loss of bone density by DXA and pQCT, and of bone strength by pQCT-FEA at 24 months compared with baseline. Bone density at the lumbar spine, and cortical density and bending stiffness at the tibia decreased by 4.7%, 1.0% and 12.1%, respectively, compared to baseline in the 2 years following RRBSO. The reporting of FEA parameters in this study is novel and the magnitude of loss in bending stiffness was substantial: it is similar to the deficit seen in a low-trauma fracture cohort compared with controls (669) and therefore is highly likely to be clinically significant.

Systemic HT is thought to prevent bone loss following early menopause, but the optimal dose and duration required to maintain bone in younger postmenopausal women is uncertain (475). Specifically, it is uncertain whether younger women require higher estrogen doses to preserve bone health. Most women at high risk of ovarian cancer are also at increased risk of breast cancer and whilst short-term HT appears to be safe (673), women and their clinicians generally wish to minimize exogenous hormone exposure. Whilst HT at average doses of

around 50 mcg/day (equivalent to 1mg oral estradiol) prevented bone loss at the lumbar spine by 5.8%, of tibial cortical density by 2.2% and in tibial bending stiffness by 14.1%, there was still a significant loss of bone density at the lumbar spine at 24 months after RRBSO compared to controls, suggesting that higher estrogen doses may be indicated in these patients. However, the amount of bone loss (2.3% at 24 months) was modest and of uncertain clinical significance. Consistent with existing evidence (665) we observed accelerated loss of bone density in non-HT users compared with HT users and age-matched controls. However, these data need to be interpreted with caution because of small sample size, variation in dose and delivery of HT used, and risk of bias due to the observational study design. Larger studies are needed to confirm how different delivery systems and doses of HT impact on bone health following RRBSO. Moreover, ongoing follow-up is required to help understand the potential clinical relevance of the small but significant amount of bone loss at the lumbar spine in HT users at 24 months.

Our finding that RRBSO led to a decrease in bone density and an index related to bone strength confirms and extends published data from cross-sectional and retrospective data (508, 665). A novelty and strength of our study is the inclusion of a prospective control group to account for the effects of age on bone health measures. Because bone measures did not change in controls over the follow-up period, we can be confident that the changes we observed were attributable to the intervention (RRBSO).

Whilst bone density was reduced after RRBSO in both HT and non-HT uses, we found no overall difference in DXA variables at 12M or 24M between RRBSO and control groups. This observation may represent the limitations of DXA in identifying individuals with

increased fracture risk whereby clinically relevant deficits in bone strength may occur without corresponding deficits in DXA aBMD (284). Alternatively, this may reflect the limitations of our study design and sample size, as indicated by the high SD observed.

The addition of pQCT provided additional information on bone strength that may not be detected with DXA, such as the significant decrease in cortical volumetric density (but not trabecular volumetric density) after RRBSO, particularly in non-HT users. Trabecular bone is considered more metabolically active, thus responds to stimuli and changes more quickly than cortical bone in most circumstances (39). Our findings suggest that RRBSO may reduce cortical bone more rapidly than trabecular bone, consistent with preclinical studies demonstrating increased cortical porosity in ovariectomised mice (674). Kawalilak et al (675) observed significant loss (mean 14.6%) in tibial cortical density measured by high-resolution pQCT (HR-pQCT) in naturally menopausal women not taking anti-resorptive medication over one-year follow-up ($p < 0.01$) but no change in trabecular density ($p = 0.39$). Future research should include a focus on the underlying mechanism of this heterogeneity. Comprehensive evaluation of bone health after RRBSO should include additional modalities rather than DXA alone.

Using pQCT-FEA to assess the changes in bone stiffness under different mechanical loading conditions is a further strength of our study. We found significant decreases in pQCT-FEA stiffness variables over follow-up in non-HT users. Greater decreases in all pQCT-FEA variables were observed in non-HT users compared to HT users or controls. Together with this, cross-section-based FEA work, pQCT provides additional information beyond DXA into changes in volumetric bone density, bone geometry and bone stiffness in this population. We

chose FEA variables at the 4% site to estimate bone mechanical properties as they had good correlations with bone failure load (668) and better diagnostic performance for bone fragility than at the mid-shaft (599, 669). Concerns may be raised about use of torsion or bending load cases at this site, it should be noted that these simplified load cases based on pQCT cross-sections only provide estimation of whole-bone mechanical behavior under complicated loadings. This logic has been widely used in the assessment of bone strength using SSI_p (335, 350) or HR-pQCT-based micro FEA (412, 644). Moreover, our results have shown bending stiffness at the 4% site has changed over the follow up, thus reflecting a change in the bone distribution at this site. Although whether this change reflects reductions in the entire bone strength due to bending failure is unknown, our previous study did observe lower bending stiffness at the 4% site did actually correlated with reduced bone strength for the radius (668).

Clinical guidelines consistently recommend systemic HT after early menopause until around age 50 years in all women without contraindications and prevention of osteoporosis is a leading driver for this recommendation (676, 677). Consistent with previously published data, uptake of systemic HT was relatively low in this high-risk population (678, 679). Although data from younger (under age 40 years) women with premature ovarian insufficiency (POI) suggest that higher estrogen doses might be needed to maintain bone health in younger women (680), there is very little evidence to guide dose or duration of HT use following RRBSO (675). HT may increase the risk of breast cancer, even in younger postmenopausal women (age 40-49) (672) and more evidence is needed informing the optimum dose and duration of HT following RRBSO to allow younger postmenopausal women to weigh up the risks and benefits of HT. Our findings are consistent with retrospective studies (507) reported lower DXA measures in non-HT users compared to HT users after RRBSO (16% vs 47%). However, confounding factors such as age, height and weight were not considered. Our data

were reassuring that HT preserves lumbar spine aBMD, tibial Crt vBMD and bending stiffness by 5.8%, 2.2% and 14.1% regardless of age at RRBSO, type of HT (estrogen only or combined) or duration of HT use. However, most HT users (82.4%, n = 14) in this study were taking HT for at least 75% of the 2 year follow up period.

A limitation of our study is that biochemical markers of bone turnover were not included. Retrospective data suggests that premenopausal oophorectomy may elevate bone turnover markers compared with preoperative levels (681) and with controls (682, 683). Although relationships between other serum biochemical markers, e.g. 25-OHD, parathyroid hormone, and natural menopause have been investigated extensively over the past decades (684, 685), there are no prospective studies of premenopausal oophorectomy. In addition, we did not consider the potential effects of other medication apart from HT on bone outcomes because of limited sample size. A further limitation is that the baseline DXA and pQCT measures were performed on average two months after RRBSO due to the Australian Medicare rebate policy for DXA. However, these indices are not thought to change over a two-month period following oophorectomy.

In conclusion, we have shown that DXA-measured lumbar spine aBMD decreased by 4.7% by 24 months after RRBSO, with decreases of 1.0% and 12.1% in pQCT-measured tibial cortical volumetric density and bending stiffness using FEA. While DXA measures did not differ between the RRBSO and control groups, tibial cortical density and bending stiffness were significantly lower after RRBSO compared to age-matched controls at 24M. Hormone therapy was found to alleviate but not to fully prevent bone loss, irrespective of age at RRBSO. Neither HT type nor duration of HT use modified this protective effect, but more

data are required to validate this finding. While DXA can detect longitudinal decreases in bone mineral measures, pQCT and pQCT-based FEA appear to provide more information comparing women undergoing RRBSO and their age-matched controls.

6.7 Acknowledgements

We thank all study participants for their contribution to this study. We wish to acknowledge Dr Ashwini Kale for performing DXA and pQCT scans. We thank Dr Gillian Mitchell, Associate Professor Bettina Meiser and Dr Mary-Ann Davey for their contributions in the design of the WHAM study. MH is funded by an Australian Government National Health and Medical Research Council (NHMRC) Practitioner Fellowship (reference: APP1058935). The study was funded by NHMRC Project Grant to MH and JDW (reference: APP1048023). HJ was funded by a joint PhD scholarship by China Scholarship Council (reference: CSC201608240003) and the University of Melbourne.

6.8 Additional data

Due to limit on words and tables of the publication, data were not shown on comparison in DXA variables between HT, non-HT and control groups, which is now shown in Table 6.5.

Table 6.5 Comparison in DXA variables at baseline, 12M and 24M

	HT group (n = 17)	Non-HT group (n=13)	Control group (n = 42)	p
LS aBMD (g/cm^2)				
Baseline	1.07 ± 0.17	1.05 ± 0.11	1.09 ± 0.14	0.81
12M	1.04 ± 0.18	0.99 ± 0.09	1.09 ± 0.13	0.08
24M	1.04 ± 0.18	0.97 ± 0.09	1.08 ± 0.14	0.06
TH aBMD (g/cm^2)				
Baseline	0.94 ± 0.13	0.96 ± 0.11	0.95 ± 0.13	0.90
12M	0.93 ± 0.15	0.90 ± 0.11	0.95 ± 0.13	0.49
24M	0.94 ± 0.14	0.91 ± 0.12	0.95 ± 0.13	0.64
FN aBMD (g/cm^2)				
Baseline	0.86 ± 0.13	0.88 ± 0.11	0.85 ± 0.11	0.71
12M	0.85 ± 0.14	0.84 ± 0.09	0.86 ± 0.12	0.88
24M	0.86 ± 0.14	0.83 ± 0.09	0.85 ± 0.12	0.75

Chapter 7

Bone measures by dual energy x-ray absorptiometry and peripheral quantitative computed tomography in young women with type 1 diabetes mellitus

7.1 Bone measures by dual energy x-ray absorptiometry and peripheral quantitative computed tomography in young women with type 1 diabetes mellitus

Authors and Affiliations:

Hongyuan Jiang [1], Dale L Robinson [2], Alison Nankervis [1,3,4], Suzanne M Garland [5,6,7], Emma T Callegari [1], Sarah Price [4], Peter VS Lee [2], John D Wark [1,8,4*]

[1] Department of Medicine, Royal Melbourne Hospital, University of Melbourne, Melbourne, Australia

[2] Department of Biomedical Engineering, University of Melbourne, Melbourne, Australia

[3] Diabetes Service, Royal Women's Hospital, Melbourne, Australia

[4] Department of Diabetes and Endocrinology, Royal Melbourne Hospital, Melbourne, Australia

[5] Centre for Women's Infectious Diseases Research, Royal Women's Hospital, Melbourne, Australia

[6] Department of Obstetrics and Gynaecology, University of Melbourne, Melbourne, Australia

[7] Infection & Immunity, Murdoch Children's Research Institute, Melbourne, Australia

[8] Bone and Mineral Medicine, Royal Melbourne Hospital, Melbourne, Australia

7.2 Abstract

BACKGROUND Understanding bone fragility in young adult females with type 1 diabetes mellitus (T1DM) is of great clinical importance since the high fracture risk in this population remains unexplained.

METHODS This study aimed to investigate bone health in young adult T1DM females by comparing relevant variables determined by dual energy X-ray absorptiometry (DXA), peripheral quantitative computed tomography (pQCT) at the tibia and pQCT-based finite element analysis (pQCT-FEA) between T1DM subjects (n = 21) and age-, height- and weight-matched controls (n = 63).

RESULTS Tibial trabecular density (lower by 7.1%; 228.8 ± 33.6 vs 246.4 ± 31.8 mg/cm3, p = 0.02) and cortical thickness (lower by 7.3%; 3.8 ± 0.5 vs 4.1 ± 0.5 cm, p = 0.03) by pQCT were significantly lower in T1DM subjects than in controls. Tibial shear stiffness by pQCT-FEA was also lower in T1DM subjects than in controls at both the 4% site (by 17.1%; 337.4 ± 75.5 vs 407.1 ± 75.4 kN/mm, p < 0.01) and 66% site (by 7.9%; 1113.0 ± 158.6 vs 1208.8 ± 161.8 kN/mm, p = 0.03). These differences remained statistically significant after adjustment for confounding factors. No difference between groups was observed in DXA-determined variables (all p $\geqslant$ 0.08), although there was a trend towards lower aBMD at the lumbar spine in T1DM subjects than in controls after adjustment for confounders (p = 0.053).

CONCLUSIONS These novel findings elicited using pQCT and pQCT-FEA suggest a clinically-significant impact of T1DM on bone strength in young adult females with T1DM. Peripheral QCT and pQCT-FEA may provide more information than DXA alone on bone

fragility in this population. Further longitudinal studies with a larger sample size are warranted to understand the evolution and causes of bone fragility in young T1DM females.

7.3 Introduction

The incidence of Type 1 diabetes Mellitus (T1DM) has been increasing over the last century (513). T1DM is associated with compromised bone strength at a later stage of life, which is reflected by an increase of over 6-fold in hip fracture risk compared with the general population (568, 686). Although much evidence is available on change in bone density measured by dual energy X-ray absorptiometry (DXA) in children, adolescents and older people, data are relatively limited in young adult, especially in young adult females. Weber et al. observed a large gap in fracture incidence between young T1DM patients aged 10 – 20 years and controls in females but not in males (569). Higher proportion of lower extremity fractures compared to other fractures in T1DM patients was also noted in this study.

Areal bone mineral density (aBMD) measured by DXA is a well-established indicator of bone strength; however, DXA sometimes failed to identify osteoporosis in children and adolescents with T1DM, although a negative impact of hyperglycemia on the skeletal system was seen in this population (687). Other technologies may contribute to our understanding of bone fragility in T1DM (688). Peripheral quantitative computed tomography (pQCT) can provide additional information about bone fragility due to its ability to analyze cortical and trabecular compartments of bone separately, and to capture more details on bone geometry. Furthermore, the 3-dimensional imaging data acquired can be used to generate finite element analysis (FEA) models for estimation of bone strength and stiffness (668) and to differentiate patients with increased fracture risk from controls (599, 669). More importantly, pQCT may be a better tool for the assessment of bone fragility than DXA due to the higher proportion of lower extremity fractures observed in this young population (569). In this study, we aimed to compare multiple

variables including blood analytes, DXA, pQCT and pQCT-based FEA (pQCT-FEA) in young females with T1DM with age-, height- and weight-matched controls.

7.4 Methods

Participant recruitment

Two groups of participants were recruited from two studies of young women's health in Australia: the YFHI and Safe-D studies (689, 690). The T1DM group was recruited from the Young Adult Diabetes Service at the Royal Melbourne Hospital, Australia and targeted social media advertising on Facebook. The control group was recruited through target advertising on Facebook.

Inclusion criteria of the T1DM group were: (1) females aged 16 – 25 years; (2) with T1DM of at least 12 months' duration; (3) living in Victoria, Australia, and able to attend a 3-hour study visit at the Royal Melbourne Hospital; (4) with no known history of medical conditions which may affect their bone health other than T1DM, including coeliac disease, eating disorder, inflammatory bowel disease, hyperthyroidism, hyperparathyroidism; (5) with no long term use of medication affecting bone health, including glucocorticoids, anti-epilepsy drugs. Exclusion criteria for the T1DM group were: (1) pregnant or breastfeeding at the time of the study visit; (2) having a significant medical or psychiatric condition.

Data were available from 620 apparently healthy participants recruited for the Safe-D and the YFHI studies. Among the participants, age-, height- and weight-matched controls for the current analysis were selected as per the following criteria: (1) age, height and weight within ± 1 years, 5 cm and 5 kg, respectively, of each T1DM participant; (2) with no known history of medical conditions which may affect their bone health, including osteoporosis, coeliac disease, eating

disorder, inflammatory bowel disease, hyperthyroidism, hyperparathyroidism; (3) with no long term use of medication affecting bone health, including glucocorticoids, anti-epilepsy drugs; (4) with no significant medical or psychiatric condition. The three best-matched eligible controls were selected for each case to enable a case-control ratio of 1:3.

Study questionnaire

Demographics, socioeconomic status, lifestyle factors, physical activity levels, dietary data were collected through online questionnaires (691), the link of which was emailed to all participants of the Safe-D and YFHI studies.

Pathology tests

Participants fasted for at least 8 hours before phlebotomy. Renal function, liver function, serum calcium, lipids, glucose and insulin levels were measured using an Abbott Architect platform (Abbott Diagnostics, Abbott Park, IL, USA). Twenty-five-hydroxyvitamin D (25 OHD), thyroid stimulating hormone (TSH) and parathyroid hormone (PTH) were measured using a chemiluminescent microparticle immunoassay (Abbott Diagnostics, Abbott Park, IL, USA). Glycated hemoglobin (HBA1c) level was measured on an Ultra Affinity HPLC system using an affinity chromatography assay (Royal Melbourne Hospital, Parkville, Australia). Serum levels of bone turnover markers (BTMs) were measured on a Cobas system (Roche Diagnostics, Basel, Switzerland) using the Elecsys beta-carboxy-terminal cross-linking telopeptide of type 1 collagen (bCTX) and procollagen type 1 N propeptide (P1NP) immunoassays.

DXA scanning and analysis protocol

Standard clinical scans of the lumbar spine (L1 – L4), the hip and the whole body were performed using a fan-beam densitometer (Horizon QDR 4500A, Hologic Inc., Bedford, MA, USA). DXA scans were performed in array mode and were analyzed using the manufacturer's commercial software (v 9.10D). Variables of interest included aBMD of the lumbar spine (LS aBMD), total hip (TH aBMD) and femoral neck (FN aBMD). Whole-body scan variables of interest included whole-body aBMD (WB aBMD), whole-body bone mineral content (WB BMC). The 12-month precision of the scanner for the spine phantom was 0.36% for aBMD and 0.57% for bone mineral content.

Peripheral QCT scanning and analysis protocol

Scans of the non-dominant tibia were performed using an XCT 3000 pQCT scanner (Stratec Medizintechnik, Pforzheim, Germany) at both 4% and 66% of the tibia length. Tibia length was measured from the base of the medial malleolus to the superior margin of the medial condyle. The dominant tibia was scanned for any participant who had previously sustained a fracture to their non-dominant tibia. A scout scan was performed to identify the correct starting line. A single slice at each site was acquired with an in-plane resolution of 0.4 x 0.4 mm and a slice thickness of 2 mm. The manufacturer's commercial software (version XCT 5.50E) was used to analyze pQCT images for standard pQCT variables. Variables of interest included total volumetric bone mineral density (Tot vBMD), trabecular volumetric bone mineral density (Trb vBMD), trabecular cross-sectional area (Trb CSA) at the 4% site, and cortical volumetric bone

mineral density (Crt vBMD), cortical thickness (Crt Thk), polar stress-strain index (SSIp), muscle cross-sectional area (MCSA) and muscle density (MDen) at the 66% site.

Peripheral QCT-FEA modelling

Peripheral QCT cross-sections at the 4% and 66% tibial sites were used to establish the pQCT-FEA models (599, 669). Four loading cases were considered for all FEA models (Figure 3 of reference 599): axial compression, shear, bending, and torsion. Axial compression was simulated by a 0.01 mm displacement of the superior surface towards the inferior surface. Shear was simulated by a 0.01 mm displacement of the superior surface in the direction of either the x- or y-axes. Bending was simulated by a 0.0001 radian rotation of the inferior surface about either the x- or y-axes (i.e., cross-section neutral axes). Torsion was simulated by a 0.0001 radian rotation of the inferior surface about the z-axis. The reaction forces and moments predicted from the simulations were divided by the respective applied displacement or rotation to derive the compressive stiffness (k_{comp}), shear stiffness (k_{shear}), bending stiffness (k_{bend}), and torsional stiffness ($k_{torsion}$) of each cross-section.

Statistical analysis

Distribution of each variable was tested for normality using both Shapiro-Wilk test and visual inspection of Q-Q plot. Descriptive statistics were expressed as mean ± standard deviation (SD) if data were normally distributed or median (Q1, Q3) if data were not normally distributed. Logistic regression models were applied to compare differences between T1DM and control groups with the participant group set as the binary dependent variable, and each variable of

interest considered in independent regressions. To adjust for potential confounding factors, any participant characteristics and blood analyte variables that varied significantly between the T1DM and control groups were included as confounders when comparing the DXA, pQCT and pQCT-FE variables. To identify collinearity amongst the confounders, variance inflation factors (VIFs) were calculated from a multivariate regression using the confounders as predictors and any unrelated property as the dependent variable. For sets of confounders found to be collinear (VIF > 5.0), the variable with the lowest p-value according to its respective logistical regression, as well as taking into account its biological meaning and/or clinical relevance, was included in the logistical regression for each DXA, pQCT and pQCT-FE variable. Following adjustment for confounders, collinearity was also tested for any bone measurement variables that showed a significant difference between the T1DM and control groups. All statistical analyses were performed using SPSS (version 25, SPSS Inc., Chicago, IL, USA). The significance level was set as $p < 0.05$.

7.5 Results

Twenty-one young women with T1DM were recruited. With a case-control ratio of 1:3, 63 age-, height- and weight-matched healthy, non-diabetic young women were selected and included in the analysis. Mean ages of the T1DM and control groups were 22.5 ± 2.3 years and 22.4 ± 2.3 years, respectively. There was no difference in age, height, weight or BMI between groups (all $p \geqslant 0.5$, Table 7.1). No difference was observed in ethnicity, socioeconomic status, education level, physical activity levels, lifestyle factors, daily vitamin D or calcium intake/supplementation between groups (all $p \geqslant 0.4$). No difference was observed in oral contraceptive use between groups ($p = 0.5$) but age at menarche was delayed in T1DM subjects compared to controls (13.1 ± 2.0 vs 12.5 ± 1.6 years, $p = 0.02$). Among participants with T1DM, mean age when T1DM was diagnosed was 14.5 ± 5.6 years, with a mean duration of diabetes of 7.8 ± 6.0 years.

A significant difference was observed in serum albumin level between T1DM subjects and controls [39.0 (37.0, 41.0) vs 42.0 (39.0, 43.0) g/L, $p = 0.03$; Table 7.2] but the levels were within the reference range for both groups. No difference was observed in other renal or liver function tests, serum lipids, calcium, vitamin D, TSH or PTH levels (all $p \geqslant 0.07$). Serum glucose [8.3 (6.6, 11.2) vs 4.7 (4.5, 5.1) mmol/L, respectively], insulin (15.4 ± 8.8 vs 9.3 ± 3.7 mIU/ml, respectively) and HbA1c [59.0 (50.0, 62.0) vs 32.0 (30.0, 33.0) mmol/mol, respectively] levels were significantly higher in T1DM than in the control group (all $p < 0.01$). These diabetes-specific variables of T1DM subjects were above the respective reference ranges. For serum BTMs, no difference was observed in P1NP [47.1 (36.0, 75.3) vs 61.7 (49.4, 83.9)

μg/L, p = 0.1, respectively) or βCTX [0.381 (0.317, 0.506) vs 0.519 (0.385, 0.642) ng/ml, p = 0.2, respectively] levels between the T1DM and control groups. All BTMs levels were within the reference range.

Among demographic and clinical characteristics, and blood analyte variables with significant difference between groups, serum albumin, glucose, insulin and HbA1c levels were found to show strong collinearity with each other (all VIFs $\geqslant$ 5.0, Table 7.2). Since the significance of differences between the T1DM and control groups was similar for each of these variables (each p < 0.01), serum HbA1c level, which better represents long-term glycemic control, was included with age at menarche as a confounding factor when comparing DXA, standard pQCT and pQCT-FE variables between groups.

T1DM subjects had an average 7.1% lower Trb vBMD (228.8 ± 33.6 vs 246.4 ± 31.8 mg/cm^3, respectively, p = 0.02) and 7.3% lower Crt Thk (3.8 ± 0.5 vs 4.1 ± 0.5 mm, p = 0.03) than controls (Table 7.3). These differences remained statistically significant after adjustment for serum HbA1c level and age at menarche (both p = 0.02). No difference was observed in other standard pQCT variables including SSI_p between T1DM and control groups before or after adjustment for the confounders (all p $\geqslant$ 0.3).

Significant differences were observed in pQCT-FEA variables at both 4% and 66% tibia sites between the T1DM and control groups (Table 7.3). At the 4% tibia site, T1DM subjects had

significantly lower k_{comp}, k_{shear} and k_{bend} than controls (1258.4 ± 239.4 vs 1444.7 ± 364.5 kN/mm, p = 0.02; 337.4 ± 75.5 vs 407.1 ± 75.4 kN/mm, p < 0.01; 2017.8 ± 443.0 vs 2290.7 ± 557.2 Nm/deg, p = 0.04, respectively). The differences were 12.9%, 17.1% and 11.9%, respectively, and remained statistically significant after adjusting for serum HbA1c level and age at menarche (p = 0.02, p < 0.01 and p = 0.02, respectively). At the 66% tibia site, T1DM subjects had 7.9% lower ks_{hear} than controls (1113.0 ± 158.6 vs 1208.8 ± 161.8 kN/mm, respectively, p = 0.03) and this difference remained statistically significant after adjustment for confounders (p = 0.03).

There was no difference in DXA-measured aBMD variables of the lumbar spine or hip between groups (all $p \geqslant 0.08$; Table 7.3) although there was a trend towards lower LS aBMD in T1DM subjects than in controls after adjustment for serum HbA1c level and age at menarche (0.988 ± 0.088 vs 1.034 ± 0.105 g/cm^2, respectively, p = 0.054). No difference was observed between groups in either WB aBMD or WB BMC before (both $p \geqslant 0.3$) or after (both $p \geqslant 0.4$) adjustment for confounders.

Among the primary bone variables with adjusted significant difference between groups, strong collinearity was found between the pQCT-FE variables (VIF = 185.30, 164.67, 9.72 and 69.86 for k_{comp}, k_{shear}, k_{bend} at the 4% tibia site and kshear at the 66% tibia site, respectively; Table 3). No collinearity was observed in the DXA or standard pQCT bone variables examined. Since k_{shear} at the 4% tibia site had the most significant difference between the T1DM and control groups (p<0.01; both with and without adjustment for confounders), together with Crt Thk and

Trb vBMD, these were the only bone variables that were independent and that varied significantly between the T1DM and control groups.

Table 7.1 General characteristics of participants

Characteristic	T1DM (n = 21)	Control (n = 63)	p	VIF
Age (years)	22.5 ± 2.3	22.4 ± 2.3	0.8	
Height (cm)	165.0 ± 7.1	166.0 ± 6.4	0.5	
Weight (kg)	65.1 (58.9, 74.0)	64.8 (57.5, 73.0)	> 0.9	
BMI (kg/m2)	24.1 (21.8, 26.3)	23.5 (21.5, 26.3)	0.7	
Ethnicity			0.8	
European descent [n (%)]	16 (76.2)	45 (71.4)		
Non-European descent [n (%)]	5 (23.8)	18 (28.6)		
SEIFA	57.5 (34.0, 79.3)	62.1 (36.7, 81.0)	0.7	
Currently attending school or university [n (%)]	15 (71.4)	47 (74.6)	0.7	
Physical activity levels			0.5	
Minimal-low, [n (%)]	8 (38.1)	17 (27.0)		
Moderate-high, [n (%)]	13 (61.9)	46 (73.0)		
Vitamin D intake (µg/day)	1.2 (0.8, 1.7)	1.1 (0.4, 1.8)	0.4	
Calcium intake (mg/day)	797 ± 314	841 ± 368	0.7	
Current smoker [n (%)]	3 (14.3)	11 (17.5)	0.8	
Alcohol (g/day)	1 (0, 5)	3 (0, 9)	0.9	
Vitamin D supplementation [n (%)]	2 (9.5)	4 (6.3)	0.7	
Calcium supplementation [n (%)]	1 (4.8)	1 (1.6)	0.5	
Oral contraceptive use [n (%)]	9 (42.9%)	30 (47.6%)	0.5	
Age at menarche (years)	13.1 ± 2.0	12.5 ± 1.6	0.02	4.81
Age at T1DM diagnosis (years)	14.5 ± 5.6			
Duration of T1DM (years)	7.8 ± 6.0			

Values expressed as mean ± 1.0 standard deviation if data were normally distributed or median (Q1, Q3) if data were not normally distributed. **VIF**: variance inflation factor, **T1DM**: type 1 diabetes mellitus, **BMI**: body mass index, **SEIFA**: socioeconomic index for area

Table 7.2 Comparison of blood analytes between T1DM and control groups

Analyte	T1DM (n = 21)	Control (n = 63)	Reference range	p	VIF
Renal function					
Creatinine (μmol/L)	66.8 ± 7.1	62.4 ± 5.6	49 - 90	0.07	
BUN (mmol/L)	4.1 ± 1.3	4.0 ± 0.9	2.5 – 8.3	0.8	
Liver function					
Albumin (g/L)	39.0 (37.0, 41.0)	42.0 (39.0, 43.0)	35 – 50	0.03	5.10
ALT (IU/L)	16.0 (12.0, 22.0)	17.0 (14.0, 26.5)	< 35	0.3	
GGT (IU/L)	12.0 (9.0, 14.0)	14.0 (10.5, 18.5)	10 – 65	0.3	
Calcium and vitamin D					
Calcium (mmol/L)	2.4 ± 0.1	2.4 ± 0.1	2.1 – 2.6	0.2	
25OHD (nmol/L)	59.0 (42.0, 70.0)	57.0 (43.0, 80.0)	> 55	0.5	
Lipids					
Total Cholesterol (mmol/L)	5.0 (4.3, 5.5)	4.6 (4.1, 5.3)	2.6 – 6.9	0.3	
Triglycerides (mmol/L)	0.8 (0.6, 1.2)	0.8 (0.6, 1.1)	0.2 – 2.0	0.5	
HDLC (mmol/L)	1.5 (1.3, 2.1)	1.4 (1.2, 1.6)	0.9 – 2.4	0.2	
LDLC (mmol/L)	2.8 (2.4, 3.2)	2.8 (2.2, 3.3)	≤ 3.5	0.7	
Diabetes-specific					
Glucose (mmol/L)	8.3 (6.6, 11.2)	4.7 (4.5, 5.1)	3 – 6	< 0.01	9.52
Insulin (mIU/ml)	15.4 ± 8.8	9.3 ± 3.7	< 15	< 0.01	5.17
HbA1c (mmol/mol)	59.0 (50.0, 62.0)	32.0 (30.0, 33.0)	< 48	< 0.01	6.33
Thyroid and parathyroid					
TSH (mIU/L)	2.3 (1.3, 3.0)	1.9 (1.3, 2.5)	0.1 – 4.0	0.3	
PTH (pmol/L)	5.9 (3.7, 7.2)	5.6 (4.4, 7.4)	1.7 – 10.0	0.9	
BTM					
P1NP (μg/L)	47.1 (36.0, 75.3)	61.7 (49.4, 83.9)	27 – 131 [688]	0.1	
bCTX (μg/L)	0.4 (0.3, 0.5)	0.5 (0.4, 0.6)	0.2 – 1.0 [688]	0.2	

Values expressed as mean ± standard deviation if data were normally distributed or median (Q1, Q3) if data were not normally distributed. All reference ranges are based on local laboratory reference ranges except for P1NP and bCTX. **VIF**: variance inflation factor, **BUN**: blood urea nitrogen, **ALT**: alanine aminotransferase, **GGT**: Gamma-glutamyl transferase, **HDLC**: High-density lipoprotein cholesterol, **LDLC**: low-density lipoprotein cholesterol, **25OHD**: 25-hydroxyvitamin D, **TSH**: thyroid stimulating hormone, **PTH**: parathyroid hormone, **HbA1c**: hemoglobin A1c, **BTM**: bone turnover marker,**P1NP**: procollagen type 1 N-terminal propeptide, **bCTX**: beta C-terminal cross-linked telopeptide of type 1 collagen

Table 7.3 Comparison of DXA, standard pQCT and pQCT-FEA variables between T1DM and control groups

Measurement	T1DM (n = 21)	Control (n = 63)	p	p_{adj}	VIF
DXA					
LS aBMD (g/cm^2)	0.988 ± 0.088	1.034 ± 0.105	0.08	0.054	1.18
TH aBMD (g/cm^2)	0.908 ± 0.084	0.942 ± 0.128	0.2	0.2	
FN aBMD (g/cm^2)	0.844 ± 0.076	0.880 ± 0.120	0.3	0.4	
WB aBMD (g/cm$^{2)}$	1.012 ± 0.080	1.020 ± 0.092	0.8	0.7	
WB BMC (g)	1857.9 ± 222.1	1974.1 ± 291.2	0.3	0.4	
Standard pQCT					
Tot vBMD (mg/cm^3) [a]	313.7 ± 44.4	320.3 ± 36.9	0.5	0.3	
Trb vBMD (mg/cm^3) [a]	228.8 ± 33.6	246.4 ± 31.8	0.02	0.02	4.61
Trb CSA (mm^2) [a]	436.3 ± 77.0	447.1 ± 62.7	0.6	0.5	
Crt vBMD (mg/cm^3) [b]	1154.1 ± 19.4	1151.5 ± 23.1	0.6	0.7	
Crt Thk (mm) [b]	3.8 ± 0.5	4.1 ± 0.5	0.03	0.02	3.74
SSI_p (mm^3) [b]	2133.2 ± 413.0	2177.3 ± 416.2	0.5	0.6	
MCSA (mm^2) [b]	6158.3 ± 1068.3	6057.8 ± 925.1	0.5	0.6	
MDen (mg/cm^3) [b]	78.9 ± 3.6	79.2 ± 3.2	0.6	0.6	
pQCT-FEA					
4% k_{comp} (kN/mm)	1258.4 ± 239.4	1444.7 ± 364.5	0.03	0.02	185.30
4% k_{shear} (kN/mm)	337.4 ± 75.5	407.1 ± 75.4	< 0.01	< 0.01	164.67
4% k_{bend} (Nm/deg)	2017.8 ± 443.0	2290.7 ± 557.2	0.04	0.02	9.72
4% $k_{torsion}$ (Nm/deg)	1245.6 ± 270.9	1296.1 ± 259.1	0.1	0.1	
66% k_{comp} (kN/mm)	2494.5 ± 651.8	2444.7 ± 863.4	0.5	0.5	
66% k_{shear} (kN/mm)	1113.0 ± 158.6	1208.8 ± 161.8	0.03	0.03	69.86
66% k_{bend} (Nm/deg)	2412.8 ± 718.6	2447.6 ± 931.7	0.5	0.4	
66% $k_{torsion}$ (Nm/deg)	3606.9 ± 551.9	3759.6 ± 543.4	0.1	0.2	

Values expressed as mean ± standard deviation. **[a]** standard pQCT variables measured at the 4% tibia. **[b]** standard pQCT variables measured at the 66% tibia. **p_{adj}**: p value with adjustment for HbA1c level and age at menarche. **VIF**: variance inflation factor. **DXA**: dual energy X-ray absorptiometry, **pQCT**: peripheral quantitative computed tomography, **pQCT-FEA**: pQCT-based finite element analysis, **T1DM**: type 1 diabetes mellitus, **aBMD**: areal bone mineral density, **LS**: lumbar spine, **TH**: total hip, **FN**: femoral neck, **WB**: whole body, **BMC**: bone mineral content, **Tot vBMD**: total volumetric bone mineral density, **Trb vBMD**: trabecular volumetric bone mineral density, **Trb CSA**: trabecular cross-sectional area, **Crt vBMD**: cortical volumetric bone mineral density, **Crt Thk**: cortical thickness, **SSI_p**: polar stress-strain index, **MCSA**: muscle cross-sectional area, **MDen**: muscle density, **k_{comp}**: compression stiffness, **k_{shear}**: shear stiffness, **k_{bend}**: bending stiffness, **$k_{torsion}$**: torsion stiffness

7.6 Discussion

Our findings demonstrate abnormalities in novel markers of bone fragility and are likely to be clinically-important in young T1DM females. In this study, we reported diabetes- and osteoporosis-related clinical characteristics in young females with T1DM aged 17 – 26 years with an average period of 8 years since T1DM diagnosis, compared with findings in age-, height- and weight-matched healthy, non-diabetic controls. According to participant characteristics (i.e. average age at diagnosis and BMI) and blood analyte results, the studied subjects represented a typical young adult female T1DM population with good glycemic control (acceptable diabetes-specific pathology results). Investigations did not reveal evidence of diabetic complications, but long-term complications including retinopathy and neuropathy were not reported. No difference was found in DXA aBMD variables between T1DM subjects and matched controls although a trend towards lower aBMD at the lumbar spine was noted in T1DM subjects compared with controls. Young T1DM women had lower tibial trabecular vBMD and thinner tibial cortical shell than controls. Notably, SSIp, a standard pQCT-derived indicator of bone bending strength, did not differ between cases and controls. However, pQCT-FEA revealed several substantially-lower tibial stiffness measures which are good predictors for bone failure load (668). The major bone deficits are similar to those reported in an older cohort of patients recruited after sustaining low-trauma fractures (669). Therefore, the findings are likely to be clinically-important despite the relatively modest sample size of participants with T1DM.

Weber et al reported the relative risk for all fractures to be 1.35- to 1.76-fold higher in females with T1DM aged less than 30 years compared to non-diabetic controls (569). The elevated relative risk of fracture especially affected lower extremity fractures. For hip fracture alone,

although absolute risk was low, the relative risk was particularly high in young T1DM females, about 5-fold compared to their non-diabetic counterparts in this young population (569). As this age is a key stage for bone mass accumulation and bone structure maturation (692), understanding of bone fragility in this population is of great clinical importance.

In this reported population, average values of the routine biochemistry analytes were within laboratory reference ranges, which indicated no signs of diabetes-related complications. However, a lower albumin level and higher glucose, insulin and HbA1c levels were observed in T1DM subjects than in controls, which may reflect the effects of diabetes of average duration of 8 years. Although these differences usually would not raise clinical concern, their long-term cumulative effects may be one contributing factor to compromised bone health observed in the current study. While serum BTMs can reflect activities of bone remodelling more rapidly than DXA (693), the current study did not find any differences in P1NP or bCTX levels between groups. This finding is consistent with a recent systematic review on BTMs in children and adolescents with T1DM (694). Laboratory BTMs reference ranges based on data of premenopausal women were not used in this study. Indeed, wider local reference ranges (27 – 131 and 0.2 – 1.0 μg/L for P1NP and bCTX, respectively) are suggested due to variability in bone remodeling rate across this age range (695).

In a meta-analysis by Shah et al (696), data pooled from 16 studies showed modestly lower aBMD at the femoral neck and the lumbar spine in T1DM adults compared to controls. In another meta-analysis by Pan et al (697), significant differences in aBMD at the lumbar spine,

femoral neck and the total body were observed between young female T1DM subjects and controls aged less than 20 years. However, the included data were either of children and adolescents, or of adults aged older than 30 years. Moreover, neither study managed to perform subgroup analysis based on different age groups. More recent data on T1DM adolescents and young adults have revealed inconsistent results as well. Kaur et al reported lower WB BMC and WB aBMD in female adolescents with T1DM than in controls (698). Fuusager observed a negative effect of hyperglycemia on total body less head aBMD in T1DM adolescents, but these adolescents did not meet DXA criteria for osteoporosis (687). However, comparable LS aBMD in female adolescents with and without T1DM was reported by Helper-Stromberg et al (699). Madsen et al did not find any difference in total body less head aBMD between subjects with and without T1DM, although they did not divide groups based on gender (700). Abdalrahaman et al observed no difference in DXA-determined aBMD variables or MRI-determined bone microstructural variables in young adult women with and without T1DM (701). However, their analysis did not adjust for confounding factors e.g. age at menarche or HbA1c level.

Among standard pQCT variables, trabecular vBMD and cortical thickness were observed to be lower in young females with T1DM than in their non-diabetic counterparts. Trabecular bone is more metabolically active than cortical bone and it changes more quickly in response to many diseases and treatments (633). However, in another study comparing standard pQCT variables between T1DM adolescents/young adults and controls, the investigators did not find any difference in Trb vBMD (702). The inconsistency with the current study may be due to higher BMI observed in the T1DM females than in controls in the study by Roggen et al. Another possible explanation may be site-specific effects since Roggen et al examined the radius instead

of the tibia. Our finding of reduced tibial cortical thickness is consistent with a previous finding by Verroken et al, although their observation was made in middle-aged adults at the radius (589). As cortical thickness is a strong predictor of bone strength and resistance to fracture (50), the standard pQCT findings suggest bone strength may be already compromised by early adulthood in T1DM females.

Bone stiffness estimates assessed by pQCT-FEA indicated compromised bone stiffness which is strong predictor for bone failure load (668). Peripheral QCT FEA models based on tibial cross-sectional images can provide better diagnostic performance than DXA alone in determining bone fragility in women with low-trauma fracture (599, 669). From our previous data, the area under the receiver operating curve (AUROC) for identifying patients with low-trauma fracture increased from 0.69 for total hip DXA to 0.83 for the pQCT-FEA shear stiffness estimate at the 4% tibia (669). In the current study, stiffness estimates in different load cases were found to be 11.9 – 17.1% lower in T1DM subjects than in controls. These differences are likely to be of clinical significance considering our previous finding of comparable deficits in pQCT-FEA estimates between older individuals with low-trauma fracture and controls without fracture (669). This finding may also help to explain the high relative risk of hip fracture seen in young T1DM females compared with non-diabetic controls in this age range, and ultimately may validate non-pharmacological or pharmacological intervention on bone fragility at an early stage of life in T1DM subjects. It is acknowledged that these FEA variables calculated from pQCT cross-sections do not capture bone stiffness and bone strength of the whole tibia but are estimates of bone mechanical properties that are proportional to the failure load. This logic has been

applied in micro-FEA by high-resolution pQCT (HR-pQCT) (412), although the current technique is more widely available and saves considerable time both in acquisition and analysis.

While existing data are inconsistent in aBMD measures between T1DM subjects and healthy controls in different age ranges, and data in the current age range are scarce, our findings suggest that DXA alone provides limited information about bone fragility in a young adult female population within 10 years of T1DM onset. This consideration may be based, at least in part, on the fact that DXA has limitations in identifying individuals with increased fracture risk in an older population (667) due to its intrinsic technical weaknesses (703). Peripheral QCT and pQCT-FEA may be better tools for the assessment of bone fragility in this population.

Age at menarche and oral contraceptive use potentially influence bone health in young T1DM adolescents. T1DM is associated with delayed age at menarche in young females and this impact is even present with good glycemic control (704). A negative correlation has been observed between age at menarche and DXA-determined aBMD variables in adults by both epidemiological and genetic studies (705, 706), although more details need to be explored in T1DM patients. Young females using oral contraceptives have also been found to present lower aBMD than non-users (707). While our unadjusted analysis did not find significant differences in DXA aBMD variables between T1DM subjects and controls, a trend towards lower aBMD at the lumbar spine was observed in T1DM subjects compared with controls after adjustment for age at menarche. Therefore, the role of these confounding factors warrants further investigation in T1DM females.

One of the strengths of this current study is that an age-, height- and weight-matched control group was selected from two large databases of projects on young women's health in Australia. It is well-known that both age and body size have an influence on areal bone density (708), and controlling for these confounding factors by selecting age-, height- and weight-matched controls most likely eliminated the impact of age and body size on the results.

Although differences in pQCT and pQCT-FEA were observed between young T1DM females and controls in this cross-sectional study, longitudinal comparisons were not available due to the study design. Future studies should focus on longitudinal changes in DXA, pQCT and pQCT-FEA variables in this population, in particular, studies commencing from the time of T1DM diagnosis, as well as investigating fracture outcomes. Another limitation is the relatively small sample size for the T1DM females due to its low incidence in the population and compared to males (709). However, increased statistical power can be achieved by a case-to-control ratio of 1:3 while keeping a practical study budget by not going beyond 1:4 (710). Moreover, the magnitude of the deficits revealed in pQCT-FEA variables strongly support the validity of the findings.

In conclusion, this study provides novel and important insights into bone health in a female T1DM population in their early twenties within 10 years of T1DM onset and contributes to our understanding of bone fragility in this population by comparing them with age-, height- and weight-matched controls. DXA-measured aBMD variables did not differ between T1DM females and controls. However, this negative finding did not indicate healthy bones in these

young T1DM individuals as pQCT and pQCT-FEA demonstrated clear evidence of bone fragility compared with matched non-diabetic controls. The observed deficits in pQCT-FEA variables reflecting bone strength were large and likely to be of clinical significance. Future studies providing longitudinal DXA and pQCT data with a larger sample size and commencing soon after the diagnosis of T1DM are needed for a more detailed analysis and improved understanding of bone health in this population.

7.7 Acknowledgements

The authors thank all subjects for their participation in this study. We acknowledge Associate Professor Christopher J Yates for helpful discussion on the background information and analysis of this study, Dr Ashwini Kale for performing DXA and pQCT scans, and Ms Heather Robinson and Ms Adele Rivers for collecting data from many YFHI participants. The YFHI study was funded by the Australian National Health and Medical Research Council (NHMRC) program grant 568971. The Safe-D study was funded by NHMRC project grant APP1049065. HJ is funded with a joint PhD scholarship by China Scholarship Council (CSC201608240003) and the University of Melbourne, Australia.

7.8 Additional discussion

This section aims to discuss a few additional aspects after the first 7 sections was published.

Oral contraceptive use was not an exclusion for either group. Although there was no difference observed in oral contraceptive use between groups, its influence on bone health is complicated and warrants discussion in this section. Allali et al (711) reported no differences in DXA aBMD or BTMs between past oral contraceptive users and never users among postmenopausal women. However, sub-group analysis in this study showed that past oral contraceptive use was associated with decreased BTMs (osteocalcin and CTX) but not aBMD variables in this study. In another study on premenopausal women in their mid-twenties by Ott et al (712), current oral contraceptive users were reported to have lower bone resorption and formation markers than non-users (DXA aBMD did not differ between them). While in another study on adolescents and younger women by Scholes et al, oral contraceptive use was associated with DXA aBMD (713), which was in consistent with data from the Canadian Multicentre Osteoporosis Study (714). However, none of the available literature focused on oral contraceptive use in T1DM females, especially T1DM young females, which hindered further assumption of whether oral contraceptive use led to changes in bone variables to different degrees for the two groups in this study.

Detailed matching protocol was not described in the published sections. In the selection of matching, all T1DM cases were first listed followed by potentially matched candidates according the criteria in Section 7.4 in separare rows (i.e. one row for each case and the respective potential

matches). In this step, each case was followed by at least three matches. For those with three matches only, they were fit into Table 7.4 with the corresponding three matches. For those with more than three matches, their matches were selected by the order of weight, height and age that had the closest values with the cases' corresponding variables. When there was a repeated match with another case, a new match was sought in the matching candidate list. The final cases and matches are shown in Table 7.4.

The significant findings in standard pQCT and pQCT-FEA variables between groups could be associated with compromised muscle condition in T1DM cases. Muscle and bone have been studies as a functional unit recent year due to the mechanical and chemical interactions between them (715). Diabetic myopathy, characterised by decreased muscle mass and muscle strength (716, 717), has been considered as one of the diabetic complications due to the interrupted protein synthesis resulting from hyperglycemia and hypoinsulinemia (718). In a study on children and adolescents with T1DM, Bechtold et al observed lower bone cross-sectional area and muscle mass in prepubertal but not adolescent T1DM cases compared to reference data (719). However, no differences were observed in vBMD or muscle strength in all T1DM cases compared with reference. In another study, Maratova et al reported decreased muscle strength and Trb vBMD in T1DM cases compared to reference data (720). One possible explanation, as proposed by the authors, was that the skeletal impairment may be partly associated with insufficient stimulation of muscles due to diabetic myopathy. While data on muscle strength were not available in the current study, whether correlation exists between muscle strength and compromised bone density and bone strength still needs further exploration.

Table 7.4 Final matches for each case

T1DM case			Match 1			Match 2			Match 3		
Age	**Height**	**Weight**	**Age**	**Height**	**Weight**	**Age**	**Height**	**Weight**	**Age**	**Height**	**Weight**
17	168.5	65.4	17	167.7	62.5	17	171.0	63.1	17	168.6	66.0
18	157.0	59.7	18	158.6	58.2	17	158.7	56.6	18	157.5	60.5
20	177.8	65.0	21	178.8	69.0	21	179.6	64.0	19	176.0	66.5
20	163.5	53.4	20	160.5	53.2	20	161.5	55.0	19	164.7	52.7
21	161.9	54.0	21	161.4	54.0	21	161.5	53.6	21	164.0	56.7
21	158.5	60.6	22	158.4	64.0	21	160.0	60.2	20	162.0	59.8
22	163.0	65.2	21	160.3	67.6	22	161.8	66.1	22	164.8	63.0
22	149.7	57.7	21	153.3	61.9	22	149.5	56.4	23	154.5	56.0
23	159.7	91.1	22	164.2	94.5	23	161.7	96.0	24	164.4	86.1
23	167.8	75.8	22	167.2	74.0	23	166.9	75.9	23	167.6	73.0
23	163.3	62.8	23	166.2	64.8	23	161.7	65.6	23	164.0	60.2
23	165.1	73.2	22	164.8	72.1	22	165.6	75.2	23	162.1	72.0
23	167.5	65.1	23	166.0	67.7	23	170.2	64.7	23	169.9	63.2
24	153.4	55.7	25	155.4	51.3	25	157.4	52.0	24	156.6	54.5
24	164.3	93.4	25	169.2	95.5	24	169.0	90.6	23	167.5	95.4
24	174.0	74.8	24	173.4	72.0	24	172.1	73.5	24	173.0	75.8
24	173.3	58.4	23	172.2	57.4	23	170.7	61.4	24	176.1	57.5
25	164.6	83.8	24	168.0	86.0	25	167.9	83.9	25	168.2	81.5
25	173.0	59.4	24	174.0	56.8	25	171.0	57.2	25	175.4	58.4
25	165.0	66.7	25	167.3	69.7	25	167.8	65.6	25	166.8	66.8
26	173.7	71.9	25	169.8	75.5	25	174.3	73.0	25	176.5	68.2

Age, height and weight are expressed in the unit of year, cm and kg, respectively.

While this study finds compromised bone density, bone geometry and bone strength in young females with T1DM by pQCT and pQCT-FEA, the underlying mechanisms are multifactorial.

One major mechanism may be a suppressed bone formation caused by deficiency of insulin and insulin like growth factor-1 (IGF-1) in T1DM. Studies have confirmed poor bone formation in T1DM. In T1DM, deficiency of insulin and IGF-1 cause alterations in transcription of osteoblast promoting genes [e.g. Runt-related transcription factor 2 (RUNX2) that directs differentiation of mesenchymal cells into pre-osteoblasts and inhibits differentiation of mesenchymal cells into adipocytes and chondrocytes] resulting in decreased osteoblasts for bone formation (721, 722). In addition, hyperglycemia and inflammatory environments are also a toxic factor for osteoblast activity and survival (723). The effect of T1DM on osteoclasts and bone resorption is not as well-understood as on osteoblasts and bone formation. The most investigated signaling pathway in osteoclast differentiation and activation is RANK system (discussed in Section 2.6.2). Studies have shown that interaction between RANKL and osteoprotegrin (OPG), a decoy receptor of RANKL, results in increased osteoclast activity and bone resorption (724). This is supported by the finding of increased OPG expression in young T1DM cases (725). However, decreased OPG expression has been also reported in some animal models, which reflects the uncertainty existing in this mechanism (726). Furthermore, other studies have reported suppressed osteoclast differentiation under high glucose conditions in vitro (727, 728). All these findings together indicate that the RANK signaling system may not be the primary mechanism of bone effects throughout the course of T1DM that drives osteoclast activity, and new pathways need to be explored.

Chapter 8

Conclusions and future directions

8.1 Conclusions

Dual energy X-ray absorptiometry (DXA) is the most established tool for the assessment of bone strength in clinical practice and research, and is a key investigation in the diagnosis of osteoporosis currently. However, it only provides part of information about bone fragility, therefore has limitations in identifying individuals with increased fracture risk. The human skeleton is a hierarchical organ whose mechanical behaviour depends on multiple factors from organ level, to macrostructural and microstructural levels, finally to nano-structural level. Developments in modern technology enable examinations of all the hierarchical levels. Therefore, inclusion of other tests along with DXA may provide additional information about bone mechanical properties compared with DXA alone.

Peripheral QCT has the ability to determine volumetric bone density and to separately analyse cortical and trabecular compartments of bone. More promisingly, the three-dimensional data acquired by pQCT are a potential source for FEA, as the cases in QCT and HR-pQCT, the FEA of which has been proved to contribute to our understanding of bone fragility in different populations. Therefore, this doctoral project aimed to explore the role of pQCT-FEA in the assessment of bone fragility in both laboratory mechanical testing and clinical studies of three cohorts: older people with low-trauma fracture, women following surgical menopause as well as young women with T1DM.

In the first part of this project, the ability of pQCT-FEA of the radius to predict forearm fracture load obtained from mechanical testing was investigated. Up to 86% of variation in the failure

load can be explained by pQCT-FEA-calculated radius stiffness. This proportion was higher than the average proportion of DXA reported in the literature and comparable with that of HR-pQCT. Therefore, pQCT-FEA was potentially a tool to be used in clinical settings where assessment of bone strength is required. The promising finding facilitated its application in the following studies of this doctoral project.

The next three studies investigated the application of pQCT-FEA in three cohorts considered to have increased risk of fracture. In the second study, comparison was made in DXA, standard pQCT and PQCT-FEA variables between older people with low-trauma fracture and controls. Significant differences were observed in pQCT-FEA stiffness variables, as well as in Trb vBMD, between the two groups. However, this degree of difference was not observed in DXA aBMD variables. Further analysis found that the pQCT-FEA variables were associated with high OR for fracture status. Moreover, enhanced diagnostic ability (specificity, sensitivity and AUROC) was observed with pQCT-FEA variables compared with DXA alone in both females and males. On one hand, this study confirmed again the limitations of DXA in identifying individuals with increased risk of fracture; more importantly, these findings suggest pQCT-FEA may offer complementary information in this population and improve clinical management of osteoporosis patients.

In the third study, significant bone loss was detected by DXA, standard pQCT and pQCT-FEA variables in women who did not receive hormone therapy following surgical menopause. Up to a 14.8% decrease in pQCT-FEA variables was observed 24 months post-surgery in these subjects

compared with up to 6.0% in DXA aBMD. This difference was similar to the difference found between older patients with osteoporotic fracture and controls in the second study, which indicated a clinically-important change in these women. In addition, pQCT-FEA but not DXA measurements differed between women undergoing RRBSO and controls at the end of the two-year follow up, which means pQCT also seems to provide a more detailed assessment of bone strength in a cross-sectional setting.

The fourth study examined bone fragility in young adult females with T1DM compared with age-, height- and weight-matched controls. While DXA aBMD measurements did not detect any difference in between them, significant difference was observed in pQCT-FEA of the distal tibia. As a large proportion of lower limb fracture was found in young females with T1DM, findings from the fourth study provided a more direct assessment of bone mechanical characteristics at this site compared to central measurements of DXA. The pathogenesis of fracture risk in young people with T1DM is poorly understood, with inconsistent data being found with DXA. This provided a strong justification for investigating alternative measures of bone strength in this population.

In conclusion, this doctoral project provided insights in the application of pQCT-FEA as valid tool for the assessment of bone fragility considering the intrinsic limitations of DXA in clinical settings. Exploration of its utility in future studies is warranted.

8.2 General limitations

Other than the specific limitations discussed in each of sub-studies, there are a few general limitations to be acknowledged in this section.

Selection bias may have existed in the three sub-studies invloving a control group (Chapter 5, 6, 7). Ideally, selection of controls should be based on a random sample from the source population to eliminate selection bias when comparing differences between them and study cases (729). In chapter 5, recruiting sources were mainly based on community education programs (University of the Third Age) and people from the University of Melbourne and the Royal Melbourne Hospital. While community attendees and hospital volunteers were all retired people and were older than the rest of the control group, they were assumed to be more physically active than the general population at their age. The overall impact on the control group to represent the study population is uncertain, therefore, interpretation of the difference should be with caution. In Chapter 6, again, combined recruitment techniques of population advertising and snowballing were used. While controls by snowballing technique may have similar socioeconomic background or living environment with the intervention group (730), these factors may confound the difference between cases and controls from general advertising. In Chapter 7, both the T1DM group and the control group were recruited from two large cohorts on young women's health. Therefore, they may represent a young female population who pay attention to their health more than the general population. All in all, subjects and controls were generally well-matched for known relevant covariables and adjustments were made for potentially relevant differences, thus reducing the risk of bias between groups.

In Chapters 5 – 7, information about statistical power was not provided when each chapter was published/peer-reviewed by the respective journal. This information is important to describe what difference the observed samples could reliably reflect. In Chapter 5, the statistical power of TH aBMD, tibia Trb vBMD and k_{shear} at 4% tibia to detect differences between groups at the 5% significance level were 76.2%, 89.6% and 99.9%, respectively, which were not considered underpowered. In Chapter 6, the statistical power of LS aBMD, tibia Crt vBMD and 4% tibia k_{bend} to detect differences between RRBSO and control groups at 24 months at the 5% significance level were 53.0%, 88.4% and 69.4%, respectively. In Chapter 7, the statistical power of LS aBMD, tibia Trb vBMD and 4% tibia k_{shear} to detect differences between T1DM and control groups at the 5% significance level were 62.8%, 67.8% and 97.8%, respectively. Unfortunately, the statistical power for some outcomes was considered only moderate to detect differences between groups at 5% significance level, which means the risk of Type II error may increase. On the other hand, all studies explored novel outcomes so a priori estimates of power and sample size were not feasible. Future studies with larger sample size are therefore warranted to overcome this statistical issue.

A precision study on the pQCT-FEA models was not conducted at the time of thesis submission. Such a study has been conducted by my colleagues thereafter and reproducibility of pQCT-FEA is shown in Appendix 3.

8.3 Future directions

Based on the findings of this doctoral project, there are several directions for future research. The first potential lies in the methodology of pQCT-FEA itself. All FEA models were based on a thin cross-section of pQCT image; therefore, the calculated strength and stiffness were assumed to be proportionate with the real whole-bone mechanical properties. This logic is also reflected in the idealized load cases applied in the FEA simulations. In reality, a combination of all load cases occurs at the same time in vivo. Using separate load case to predict bone strength can only reflect the whole-bone strength but is never the real whole-bone strength. This logic has been widely used in FEA studies of QCT and HR-pQCT. A regression model involving all the load cases and concluding a more comprehensive variable may be developed in future studies.

Although strong correlation was observed between pQCT-FEA variables and bone failure load in the validation study, direct comparisons between the pQCT-FEA variables and DXA or HR-pQCT variables were not available, although the r^2 of pQCT-FEA in this study was higher than the reported r^2 of DXA and comparable with that of HR-pQCT. A more comprehensive study is therefore needed to see whether pQCT-FEA performs parallel to, if not better than, DXA and HR-pQCT under the same testing configuration.

Most of the fractures were peripheral fractures in the second study, which proved the value of pQCT-FEA in patients with non-vertebral fracture. However, hip and vertebral fractures account for a large proportion of osteoporotic fracture and are associated with worse clinical outcomes than peripheral fracture. Therefore, whether pQCT-FEA can provide the same diagnostic

performance in patients with central fractures is unclear. A further study exploring the role of pQCT-FEA in these patients is therefore warranted.

pQCT-FEA showed a good ability to detect long-term changes in women with surgical menopause in the third study. However, pQCT data were not available at 12 months follow-up or earlier. Therefore, its role in detecting short-term changes in bone mechanical behaviour is unknown. PQCT-FEA may be sensitive to subtle changes in bone mechanical properties, as reflected in the larger difference compared with the difference in DXA aBMD observed between respective groups in the second to the fourth studies, but this hypothesis needs further validation. In addition, recruitment of more subjects and extended follow-up is also needed due to the relatively small sample size in this study, as well as in the fourth study.

The cross-sectional design of the fourth study may limit further interpretation of bone fragility seen in young women with T1DM. Therefore, longitudinal comparison is needed for the comprehensive role of pQCT-FEA in this population. Heterogeneity existed in the gap between T1DM onset and the study time point, which may confound the findings. Future studies are also in need with comparable period of T1DM onset in this population.

As compromised bone strength has also been shown in many other populations, *e.g.* individuals with inflammatory bowel disease or end-stage renal disease, individuals taking glucocorticoid agents for an extended period or anti-epileptic drugs, individuals undergoing bariatric surgery,

application of pQCT-FEA can also used in these populations to compare with DXA and other modalities.

Sarcopenia has been associated with osteoporosis in recent studies (731). It is now considered that the two conditions should be recognised in association as osteosaropenia. Since the diagnostic criteria for sarcopenia still face challenges (732), and pQCT can also measure some muscle variables e.g. muscle density, muscle CSA, future studies may also focus on the role of pQCT and pQCT-FEA in the identification of osteosarcopenia and clinical implications of the association.

The clinical application of pQCT-FEA would be greatly facilitated with identification of one or several key pQCT-FEA variables that best distinguish between individuals with increased fracture risk and a general population. This would be an important future research direction as an extension of this PhD project. Comparison of key pQCT-FEA variables in each chapter is summarised in Table 8.1 for this purpose. Intuitively, kbend and kshear at the 4% tibia performed better than the rest of the pQCT-FEA variables but more detailed analysis are needed to confirm this assumption.

Table 8.1 Comparison between key pQCT-FEA variables in each chapter

Chapter	Key variable	Measured site	Key results
Chapter 4 **The validation study**	k_{bend}	4% radius	r^2 = 0.83 and 0.86 with experimental failure load, before and after adjustment for age, respectively
Chapter 5 **The FRACTURE study**	k_{shear}	4% tibia	29.7% lower in fracture patients than in controls; OR = 9.13 for a fracture fracture and AUROC = 0.79
Chapter 6 **The WHAM study**	k_{bend}	4% tibia	12.1% lower in RRBSO group than in control group at 24 months; identify as high as 14.8% loss in non-HT users in 24-month follow-up
Chapter 7 **The T1DM study**	k_{shear}	4% tibia	17.1% lower in T1DM cases than in controls; difference between groups was still significant after adjustment for confounders

Finally, to improve fracture prediction using pQCT and pQCT-FEA, large epidemiological studies recording detailed fracture event and fracture risk factors with DXA and pQCT measurements are therefore needed to develop more valid prediction models.

Chapter 9

References

1. Hall JE. Guyton and Hall Textbook of Medical Physiology. 13rd Edition. Saunders, Philadelphia, PA, 2015.
2. Martin RB, Burr DB, Sharkey NA, Fyhrie DP. Mechanical properties of bone. In: Skeletal tissue mechanics, Edition 2. Springer, New York, NY, 2015.
3. Sharir A, Barak MM, Shahar R. Whole-bone mechanics and mechanical testing. Vet J, 2008; 177(1): 8-17.
4. Oftadeh R, Perez-Viloria M, Villa-Camacho JC, Vaziri A, Nazarian A. Biomechanics and mechanobiology of trabecular bone: a review. J Biomech Eng, 2015; 137(1): 010802.
5. Ruffoni D, van Lenthe H. Finite element analysis in bone research: a computational method relating structure to mechanical function. In: Reference module in materials science and materials engineering. Elsevier, Amsterdam, Netherlands, 2005.
6. Turner CH. Bone strength: current concepts. Ann N Y Acad Sci, 2006; 1068: 429-446.
7. Wu D, Isaksson P, Ferguson SJ, Persson C. Young's modulus of trabecular bone at a tissue level: a review. Acta Biomater, 2018; 78: 1-12.
8. Linde F. Elastic and viscoelastic properties of trabecular bone by a compression testing approach. Dan Med Bull, 1994; 41(2): 119-138.
9. Shahar R, Zaslansky P, Barak M, Friesem AA, Currey JD, Weiner S. Anisotropic Poisson's ratio and compression modulus of cortical bone determined by speckle interferometry. J Biomech, 2007; 40(2): 252-264.
10. Saha S and Hayes WC, Tensile impact properties of human compact bone, J Biomech, 1976; 9: 243–251.
11. Turner CH, Yield behavior of bovine cancellous bone, J Biomech Eng, 1989; 111: 256–260.

12. Keller TS, Mao Z and Spengler DM. Young's modulus, bending strength, and tissue physical properties of human compact bone, J Orthop Res, 1990; 8: 592–603.
13. Zioupos P, Currey JD and Casinos A. Exploring the effects of hypermineralisation in bone tissue by using an extreme biological example. Connect Tissue Res, 2000; 41: 229–248.
14. Yeni YN and Fyhrie DP. Finite element predicted apparent stiffness is a consistent predictor of apparent strength in human cancellous bone tested with different boundary conditions. J Biomech, 2001; 34: 1649–1654.
15. Fyhrie DP and Vashishth D. Bone stiffness predicts strength similarly for human vertebral cancellous bone in compression and for cortical bone in tension. Bone, 2000; 26: 169–173.
16. Yeni YN, Dong XN, Fyhrie DP, Les CM. The dependence between the strength and stiffness of cancellous and cortical bone tissue for tension and compression: Extension of a unifying principle. Bio-Medical Materials and Engineering, 2004; 14(3): 303-310.
17. Patton DM, Bigelow EMR, Schlecht SH, Kohn DH, Bredbenner TL, Jepsen KJ. The relationship between whole-bone stiffness and strength is age and sex dependent. J Biomech, 2019; 83: 125-133.
18. Keaveny TM, Wachtel EF, Ford CM and Hayes WC. Differences between the tensile and compressive strengths of bovine tibial trabecular bone depend on modulus. J Biomech, 1994; 27: 1137–1146.
19. Martin H, Werner J, Andersen R, Schober H-C, Schmitz K-P. Noninvasive assessment of stiffness and failure load of human vertebrae from CT-data. Biomed Tech 1998;43:82–88.

20. Stein EM, Liu XS, Nickolas TL, Cohen A, Thomas V, McMahon DJ et al. Abnormal microarchitecture and reduced stiffness at the radius and tibia in postmenopausal women with fractures. J Bone Miner Res, 2010; 25: 2572–2581.
21. Dragomir-Daescu D, Op Den Buijs J, McEligot S, Dai Y, Entwistle RC, Salas C, Melton LJ 3rd, Benenet KE, Khosla S, Amin S. Robust QCT/FEA models of proximal femur stiffness and fracture load during a sideways fall on the hip. Ann Biomed Eng, 2011; 39: 742–755.
22. Yang P, Bruggemann G, Rittweger J. What do we currently know from in vivo bone strain measurements in humans? J Musculoskelet Neuronal Interact, 2011;11(1): 8-20.
23. Lynch ME, Main RP, Xu Q, Schmicker TL, Schaffler MB, Wright TM, ven der Meulen MC. Tibial compression is anabolic in the adult mouse skeleton despite reduced responsiveness with ageing. Bone, 2011; 49(3): 439-446.
24. Russo CR. The effects of exercise on bone. Basic concepts and implications for the prevention of fractures. Clin Cases Miner Bone Metab, 2009; 6(3): 223-228.
25. Beaupied H, Lespessailles E, Benhamou C-L. Evaluation of macrostructural bone biomechanics. Joint Bone Spine, 2007; 74(3): 233-239.
26. Li S, Demirci E, Silberschmidt VV. Variability and anisotropy of mechanical behavior of cortical bone in tension and compression. J Mech Behav Biomed Mater, 2013; 21: 109-120.
27. Guedes RM, Simoes JA, Morais JL. Viscoelastic behaviour and failure of bovine cancellous bone under constant strain rate. J Biomech, 2006; 39(1): 49-60.
28. Iyo T, Maki Y, Sasaki N, Nakata M. Anisotropic viscoelastic properties of cortical bone. J Biomech, 2004; 37(9): 1433-1437.

29. Bayraktar HH, Morgan EF, Niebur GL, Morris GE, Wong EK, Keaveny TM. Comparison of the elastic and yield properties of human femoral trabecular and cortical bone tissue. J Biomech, 2004; 37(1): 27-35.
30. Dong XN, Guo XE. The dependence of transversely isotropic elasticity of human femoral cortical bone porosity. J Biomech, 2004; 37(8): 1281-1287.
31. Seeman E. Age-and menopause-related bone loss compromise cortical and trabecular microstructure. J Gerontol Series A: Biol Sci Med Sci, 2013: glt071.
32. Fonseca H, Moreira-Goncalves D, Coriolano HJ, Duarte JA. Bone quality: the determinants of bone strength and fragility. Sports Med, 2014; 44(1): 37-53.
33. Gong H, Zhu D, Gao J, Lv L, Zhang X. An adaptation model for trabecular bone at different mechanical levels. Biomed Eng Online, 2010; 9: 32-49.
34. Einhorn TA. Bone strength: the bottom line. Calcif Tissue Int, 1992; 51(5): 333-339.
35. Ott SM. Cortical or trabecular bone: what's the difference? Am J Nephrol, 2018; 47(6): 373-375.
36. Iolascon G, Napolano R, Gioia M, Moretti A, Riccio I, Gimigliano F. The contribution of cortical and trabecular tissues to bone strength: insights from denosumab studies. Clin Cases Miner Bone Metab, 2013; 10(1): 47-51.
37. Bala Y, Zebaze R, Seeman E. Role of cortical bone in bone fragility. Curr Opin Rheumatol, 2015; 27(4): 406-413.
38. Zebaze RM, Ghasem-Zadeh A, Bohte A, Iuliano-Burns S, Mirams M, Price RI, Mackie EJ, Seeman E. Intracortical remodelling and porosity in the distal radius and post-mortem femurs of women: a cross-sectional study. Lancet, 2010; 375(9727): 1729-1736.

39. Jacobs CR. The mechanobiology of cancellous bone structural adaptation. J Rehabil Res Dev, 2000; 37(2): 209-216.
40. Cole JH, ven der Meulen MC. Whole-bone mechanics and bone quality. Clin Orthop Relat Res, 2011; 469(8): 2139-2149.
41. Martin RB, Burr DB, Sharkey NA, Fyhrie DP. Skeletal biology. In: Skeletal tissue mechanics, Edition 2. Springer, New York, NY, 2015.
42. Parfitt AM. Misconceptions: turnover is always higher in cancellous than in cortical bone. Bone 2002; 30: 807-809.
43. Pouilles JM, Tremollieres F, Ribot C. Spine and femur densitometry at the menopause: are both sites necessary in the assessment of the risk of osteoporosis? Calcif Tissue Int, 1993; 52: 344-347.
44. Hesp R, Arlot ME, Edouard C, Bradbeer JN, Meunier PJ, Reeve J. Iliac trabecular bone formation predicts radial trabecular bone density changes in type 1 osteoporosis. J Bone Miner Res, 1991; 6(9): 929-935.
45. Delmas PD, Fontanges E, Duboeuf F, Boivin G, Chavassieux P, Meunier PJ. Comparison of bone mass measured by histomorphometry on iliac biopsy and by dual photon absorptiometry of the lumbar spine. Bone, 1988; 9(4): 209-213.
46. Hui SL, Slemenda CW, Johnston CC, Appledorn CR. Effects of age and menopause on vertebral bone density. Bone Min, 1987; 2(2): 141-146.
47. Eastell R, Riggs BL, Wahner HW, O'Fallon WM, Amadio PC, Melton LJ 3rd. Colles' fracture and bone density of the ultradistal radius. J Bone Miner Res, 1989; 4(4): 607-613.

48. Eastell R, Wahner HW, O'Fallon WM, Amadio PC, Melton LJ 3rd, Riggs BL. Unequal decrease in bone density of lumbar spine and ultradistal radius in Colles' and vertebral fracture syndromes. J Clin Invest, 1989; 83(1): 168-174.
49. Melton LJ 3rd, Atkinson EJ, O'Fallon WM, Wahner HW, Riggs BL. Long-term fracture prediction by bone mineral assessed at different skeletal sites. J Bone Miner Res, 1993; 8(10): 1227-1233.
50. Augat P, Schorlemmer S. The role of cortical bone and its microstructure in bone strength. Age Ageing, 2006; 35 (S2): ii27-ii31.
51. Ioannidis G, Flahive J, Pickard L, Papaioannou A, Chapurlat RD, Saag KG, Silverman S, Anderson FA Jr, Gehlbach SH, Hooven FH, Boonen S, Compston JE, Cooper C, Diez-Perez A, Greenspan SL, Lacroix AZ, Lindsay R, Netelenbos JC, Pfeilschifter J, Rossini M, Roux C, Sambrook PN, Siris ES, Watts NB, Adachi JD; GLOW Investigators. Non-hip, non-spine fractures drive healthcare utilization following a fracture: the Global Longitudinal Study of Osteoporosis in Women (GLOW). Osteoporos Int, 2013; 24(1): 59-67.
52. Roux C, Wyman A, Hooven FH, Gehlbach SH, Adachi JD, Chapurlat RD, Comston JE, Cooper C, Diez-Perez A, Greenspan SL, Lacroix AZ, Netelenbos JC, Pfeilschifter J, Rossini M, Saag KG, Sambrook PN, Silverman S, Siris ES, Watts NB, Boonen S; GLOW investigators. Burden of non-hip, non-vertebral fractures on quality of life in postmenopausal women: the Global Longitudinal study of Osteoporosis in Women (GLOW). Osteoporos Int, 2012; 23(12): 2863-2871.
53. Sundh D, Nilsson AG, Nilsson M, Johansson L, Mellstrom D, Lorentzon M. Increased cortical porosity in women with hip fracture. J Intern Med, 2017; 281(5): 496-506.

54. Bjornerem A. The clinical contribution of cortical porosity to fragility fractures. Bonekey Rep, 2016; doi: 10.1038/bonekey.2016.77
55. Burghardt AJ, Kazakia GJ, Ramachandran S, Link TM, Majumdar S. Age- and gender-related differences in the geometric properties and biomechanical significance of intracortical porosity in the distal radius and tibia. J Bone Miner Res, 2010; 25(5): 983-993.
56. Holzer G, von Skrbensky G, Holzer LA, Pichl W. Hip fractures and the contribution of cortical versus trabecular bone to femoral neck strength. J Bone Miner Res, 2009; 24(3): 468-474.
57. Bouxsein ML, Karasik D. Bone geometry and skeletal fragility. Curr Osteoporos Rep, 2006; 4(2): 49-56.
58. Lochmuller EM, Groll O, Kuhn V, Eckstein F. Mechanical strength of the proximal femur as predicted from geometric and densitometric bone properties at the lower limb versus the distal radius. Bone, 2002; 30(1): 207-216.
59. Muller ME, Webber CE, Bouxsein ML. Predicting the failure load of the distal radius. Osteoporos Int, 2003; 14(4): 345-352.
60. Fonseca H, Moreira-Goncalves D, Vaz M, Fernandes MH, Ferreira R, Amado F, Mota MP, Duarte JA. Changes in proximal femur bone properties following ovariectomy and their association with resistance to fracture. J Bone Miner Metab, 2012; 30(3): 281-292.
61. Alele JD, Kamen DL, Hunt KJ, Ramsey-Goldman R. Bone geometry profiles in women with and without SLE. J Bone Miner Res. 2011; 26(11): 2719–26.

62. Taes Y, Lapauw B, Griet V, De Bacquer D, Goemaere S, Zmierczak H, Kaufman JM. Prevalent fractures are related to cortical bone geometry in young healthy men at age of peak bone mass. J Bone Miner Res, 2010; 25(6): 1433-1440.
63. Ammann P, Rizzoli R, Meyer JM, Bonjour JP. Bone density and shape as determinants of bone strength in IGF-I and/or pamidronate treated ovariectomized rats. Osteoporos Int. 1996; 6(3): 219–27.
64. Andreassen TT, Jorgensen PH, Flyvbjerg A, Orskov H, Oxlund H. Growth hormone stimulates bone formation and strength of cortical bone in aged rats. J Bone Miner Res, 1995; 10(7): 1057-1067.
65. Nelson DA, Pettifor JM, Barondess DA, Cody DD, Uusi-Rasi K, Beck TJ. Comparison of cross-sectional geometry of the proximal femur in white and black women from Detroit and Johannesburg. J Bone Miner Res, 2004; 19(4): 560-565.
66. Russo CR, Lauretani F, Seeman E, Bartali B, Bandinelli S, Di Iorio A, Guralnik J, Ferrucci L. Structural adaptations of bone loss in aging men and women. Bone, 2006; 38(1): 112-118.
67. Turner CH, Burr DB. Basic biomechanical measurements of bone: a tutorial. Bone, 1993; 14(4): 595-608.
68. Orwoll ES. Toward an expanded understanding of the role of the periosteum in skeletal health. J Bone Miner Res, 2003; 18(6): 949-954.
69. Thompson DD. Age changes in bone mineralization, cortical thickness, and Haversian cannal area. Calcif Tissue Int, 1980; 31(1): 5-11.
70. Smith Jr RW, Walker RR. Femoral expansion in aging women. Implications for osteoporosis and fractures. Henry Ford Hosp Med J, 1980; 28(2-3): 168-170.

71. Ritzel H, Amling M, Posl M, Hahn M, Delling G. The thickness of human vertebral cortical bone and its changes in aging and osteoporosis: a histomorphometric analysis of the complete spinal column from thirty-seven autopsy specimens. J Bone Miner Res, 1997; 12(1): 89-95.
72. Mayhew PM, Thomas CD, Clement JG, Loveridge N, Beck TJ, Bonfield W, Burgoyne CJ, Reeve J. Relation between age, femoral neck cortical stability, and hip fracture risk. Lancet, 2005; 366(9480): 129–135.
73. MacDonald HM, Nishiyama KK, Kang J, Hanley DA, Boyd SK. Age-related patterns of trabecular and cortical bone loss differ between sexes and skeletal sites: a population-based HR-pQCT study. J Bone Miner Res, 2011; 26(1): 50–62.
74. Nicks KM, Amin S, Atkinson EJ, Riggs BL, Melton LJ III, Khosla S. Relationship of age to bone microstructure independent of areal bone mineral density. J Bone Miner Res, 2012; 27(3): 637–644.
75. Galante J, Rostoker W, Ray RD. Physical properties of trabecular bone. Calcif Tissue Res, 1970; 5: 236–246.
76. NIH Consensus Development Panel on Osteoporosis Prevention, Diagnosis, and Therapy. Osteoporosis prevention, diagnosis, and therapy. JAMA, 2001; 285: 785-795.
77. Mittra E, Rubin C, Qin YX. Interrelationship of trabecular mechanical and microstructural properties in sheep trabecular bone. J Biomech, 2005; 38: 1229–1237.
78. Fields AJ, Lee GL, Liu XS, Jekir MG, Guo XE, Keaveny TM. Influence of vertical trabeculae on the compressive strength of the human vertebra. J Bone Miner Res, 2011; 26(2): 263-269.

79. Mosekilde L, Viidik A. Correlation between the compressive strength of iliac and vertebral trabecular bone in normal individuals. Bone, 1985; 6: 291–295.
80. Atkinson PJ. Variation in trabecular structure of vertebrae with age. Calcif Tissue Res, 1967; 1(1): 24-32.
81. Fields AJ, Eswaran SK, Jekir MG, Keaveny TM. Role of trabecular microarchitecture in whole-vertebral body biomechanical behavior. J Bone Miner Res, 2009; 24(9): 1523-1530.
82. Hadjidakis DJ, Androulakis II. Bone remodeling. Ann N Y Acad Aci, 2006; 1092: 385-396.
83. Katsimbri P. The biology of bone remodelling. Eur J Cancer Care (Engl), 2017; 26(6): doi: 10.1111/ecc.12740
84. Teitelbaum SL, Ross FP. Genetic regulation of osteoclast development and function. Nat Rev Genet, 2003; 4(8): 638-649.
85. Bianco P, Riminucci M, Gronthos S, Robey PG. Bone marrow stromal stem cells: nature, biology, and potential application. Stem Cells, 2001; 19(3): 180-192.
86. Rochefort GY, Pallu S, Benhamou CL. Osteocyte: the unrecognized side of bone tissue. Osteoporos Int, 2010; 21(9): 1457-1469.
87. Bonewald LF. Osteocytes as dynamic multifunction cells. Ann N Y Acad Sci, 2007; 1116: 281-290.
88. Vaananen HK, Zhao H, Mulari M, Halleen JM. The cell biology of osteoclast function. J Cell Sci, 2000; 113: 377-381.
89. Katsimbri P. The biology of normal bone remodeling. Eur J Cancer Care (Engl), 2017; 26(6).

90. Murshed M. Mechanism of bone mineralization. Cold Spring Harb Perspect Med, 2018; 8(12): pii a031229.
91. Martin RB, Burr DB, Sharkey NA, Fyhrie DP. Growth, modeling and remodeling of bone. In: Skeletal tissue mechanics, Edition 2. Springer, New York, NY, 2015.
92. Langdahl B, Ferrari S, Dempster DW. Bone modeling and remodeling: potential as therapeutics targets for the treatment of osteoporosis. Ther Adv Musculoskelet Dis, 2016; 8(6): 225-235.
93. Ding M, Dalstra M, Danielsen CC, Kabel J, Hvid I, Linde F. Age variations in the properties of human tibial trabeculae bone. J Bone Joint Surg Br, 1997; 79(6): 995-1002.
94. Banse X, Sims TJ, Bailey AJ. Mechanical properties of adult vertebral cancellous bone: correlation with collagen intermolecular cross-links. J Bone Miner Res, 2002; 17(9): 1621-1628.
95. Tzaphlidou M. Bone architecture: collagen structure and calcium/phosphorus maps. J Biol Phys, 2008; 34(1-2): 39-49.
96. Wallace JM, Orr BG, Marini JC, Holl MM. Nanoscale morphology of type 1 collagen is altered in the Brtl mouse model of osteogenesis imperfecta. J Struct Biol, 2011; 173(1): 146-152.
97. Ozasa R, Ishimoto T, Miyabe S, Hashimoto J, Hirao M, Yoshikawa H, Nakano T. Osteoporosis changes collagen/apatite orientation and Young's modulus in vertebral cortical bone of rat. Calfi Tissue Int, 2019; 104(4): 449-460.
98. Currey JD. Incompatible mechanical properties in compact bone. J Theor Biol, 2004; 231(4): 569-580.

99. Ciarelli TE, Fyhrie DP, Parfitt AM. Effects of vertebral bone fragility and bone formation rate on the mineralization levels of cancellous bone from white females. Bone, 2003; 32(3): 311-315.

100. Lloyd AA, Gludovatz B, Riedel C, Luengo EA, Saiyed R, Marty E, Lorich DG, Lane JM, Ritchie RO, Busse B, Donnelly E. Atypical fracture with long-term bisphosphonate therapy is associated with altered cortical composition and reduced fracture resistance. Proc Natl Acad Sci U S A, 2017; 113(33): 8722-8727.

101. Donnelly E. Methods for assessing bone quality. Clin Orthop Relat Res, 2011; 469: 2128-2138.

102. Hammer N, Voigt C, Werner M, Hoffman F, Bente K, Kunze H, Scholz R, Steinke H. Ethanol and formaldehyde fixation irreversibly alter bone's organic matrix. J Mech Behav Biomed Mater, 2014; 29: 252-258.

103. Morita K, Doi K, Oue H, Kajahara S, Hayashi K, Akagawa Y. Influence of formalin fixation on the implant stability quotient and mechanical characteristics of bone. Br J Oral Maxillofac Surg, 2013; 51(6): 550-554.

104. Wieding J, Mick E, Wree A, Bader R. Influence of three different preservative techniques on the mechanical properties of the ovine cortical bone. Acta Bioeng Biomech, 2015; 17(1): 137-146.

105. Zhang G, Wang S, Xu S, Guan F, Bai Z, Mao H. The effect of formalin preservation time and temperature on the material properties of bovine femoral cortical bone tissue. Ann Biomed Eng, 2019; 47(4): 937-952.

106. Linde F, Sorensen HC. The effect of different storage methods on the mechanical properties of trabecular bone. J Biomech, 1993; 26(10): 1249-1252.

107. Zhao S, Arnold M, Ma S, Abel RL, Cobb JP, Hansen U, Boughton O. Standardizing compression testing for measuring the stiffness of human bone. Bone Joint Res, 2018; 7(8): 524-538.

108. Samuel J, Park JS, Almer J, Wang X. Effect of water on nanomechanics of bone is different between tension and compression. J Mech Behav Mater, 2016; 57: 128-138.

109. Erivan R, Villatte G, Cueff R, Boisgard S, Descamps S. Rehydration improves the ductility of dry bone allografts. Cell Tissue Bank, 2017; 18(3): 307-312.

110. Pothuaud L, van Rietbergen B, Mosekilde L, Beuf O, Levitz P, Benhamou CL, Majumdar S. Combination of topological parameters and bone volume fraction better predicts the mechanical properties of trabecular bone. J Biomech, 2002; 35(8): 1091-1099.

111. Carter DR, Schwab GH, Spengler DM. Tensile fracture of cancellous bone. Acta Orthop Scand, 1980; 51(5): 733-741.

112. Bargren JH, Andrew C, Bassett L, Gjelsvik A. Mechanical properties of hydrated cortical bone. J Biomech 1974; 7(3): 239-245.

113. De Bakker CMJ, Tseng WJ, Li Y, Zhao H, Liu XS. Clinical evaluation of bone strength and fracture risk. Curr Osteoporos Rep, 2017; 15: 32-42.

114. Reilly DT, Burstein AH. The elastic and ultimate properties of compact bone tissue. J Biomech, 1975; 8: 393-405.

115. Oliver WC, Phar GM. Improved technique for determining hardness and elastic modulus using load and displacement sensing indentation experiments. J Mater Res, 1992; 7: 1564-1583.

116. Zysset PK. Indentation of bone tissue: a short review. Osteoporos Int, 2009; 20: 1049-1055.

117. Herrera S, Diez-Perez A. Clinical experience with microindentation in vivo in humans. Bone, 2017; 95: 175-182.

118. Lochmuller EM, Lill CA, Schneider E, Eckstein F. Radius bone strength in bending, compression, and falling and its correlation with clinical densitometry at multiple sites. J Bone Miner Res, 2002; 17(9): 1629-1638.

119. Zhang G, Qin L, Shi Y, Leung K. A comparative study between axial compression and lateral fall configuration tested in a rat proximal femur model. Clin Biomech (Bristol, Avon), 2005; 20(7): 729-735.

120. Goodyear SR., Aspden RM. Mechanical properties of bone ex vivo. Methods Mol Biol, 2012; 816: 555-571.

121. Oksztulska-Kolanek E, Znorko B, Michalowska M, Pawlak K. The biomechanical testing for the assessment of bone quality in an experimental model of chronic kidney disease. Nephron, 2016; 132(1): 51-58.

122. Bazzocchi A, Ponti F, Albisinni U, Battista G, Guglielmi G. DXA: technical aspects and application. Eur J Radiol, 2016; 85(8): 1481-1492.

123. Berger M, Yang Q, Maier A. X-ray imaging. In: Maier A, Steidl S, Christlein V, Hornegger J, editors. Medical imaging systems: an introductory guide. Springer, 2018.

124. Genank HK, Engelke K, Prevrhal S. Advanced CT bone imaging in osteoporosis. Rheumatology (Oxford), 2008; 47(S4): iv9-iv16.

125. Engelke K, Adams JE, Armbrecht G, Augat P, Bogado CE, Bouxsein ML, Felsemberg D, Ito M, Prevrhal S, Hans DB, Lewiecki EM. Clinical use of quantitative computed

tomography and peripheral quantitative computed tomography in the management of osteoporosis in adults: the 2007 ISCD Official Positions. J Clin Densitom, 2008; 11(1): 123-162.

126. Knowles NK, Reeves JM, Ferreira LM. Quantitative computed tomography (QCT) derived bone mineral density (BMD) in finite element studies: a review of the literature. J Exp Orthop, 2016; 3: 36.

127. Schreiber JJ, Anderson PA, Hsu WK. Use of computed tomography for assessing bone mineral density. Neurosurg Focus, 2014; 37(1): E4.

128. Link TM, Koppers BB, Licht T, Bauer J, Lu Y, Rummeny EJ. In vitro and in vivo spiral CT to determine bone mineral density: initial experience in patients at risk for osteoporosis. Radiology, 2004; 231(3): 805-811.

129. Schreiber JJ, Anderson PA, Rosas HG, Buchholz AL, Au AG. Hounsfield units for assessing bone mineral density and strength: a tool for osteoporosis management. J Bone Joint Surg Ann, 2011; 93(11): 1057-1063.

130. Quantitative computed tomography in assessment of osteoporosis. Semin Nucl Med, 1987; 17(4): 316-333.

131. Dhainaut A, Hoff M, Syversen U, Haugeberg G. Technologies for assessment of bone reflecting bone strength and bone mineral density in elderly women: a update. Womens Health (Lond), 2016; 12(2): 209-216.

132. Biggemann M, Hilweg D, Brinckmann P. Prediction of the compressive strength of vertebral bodies of the lumbar spine by quantitative computed tomography. Skeletal Radiol, 1988; 17(4): 264-269.

133. Ebbesen EN, Thomsen JS, Beck-Nielsen H, Nepper-Rasmussen HJ, Mosekilde L. Lumbar vertebral body compressive strength evaluated by dual-energy X-ray absorptiometry, quantitative computed tomography, and ashing. Bone, 1999; 25(6): 713-724.

134. Buckley JM, Loo K, Motherway J. Comparison of quantitative computed tomograph-based measures in predicting vertebral compressive strength. Bone, 2007; 40(3): 767-774.

135. Buckley JM, Cheng L, Loo K, Slyfield C, Xu Z. Quantitative computed tomphraphy-based predictions of vertebral strength in anterior bending. Spine (Phila Pa 1976), 2007; 32(9): 1019-1027.

136. Cheng XG, Lowet G, Boonen S, Nicholson PH, Brys P, Nijs J, Dequeker J. Assessment of the strength of proximal femur in vitro: relationship to femoral bone mineral density and femoral geometry. Bone, 1997; 20(3): 213-218.

137. Lang TF, Keyak JH, Heitz MW, Augat P, Lu Y, Mathur A, Genant HK. Volumetric quantitative computed tomography of the proximal femur: precision and relation to bone strength. Bone, 1997; 21(1): 101-108.

138. Lochmuller EM, Muller R, Kuhn V, Lill CA, Eckstein F. Can novel clinical densitometric techniques replace or improve DXA in predicting bone strength in osteoporosis at the hip and other skeletal sites? J Bone Miner Res, 2003; 18(5): 906-912.

139. Bousson V, Le Bras A, Roqueplan F, Kang Y, Mitton D, Kolta S, Bergot C, Skalli W, Vicaut E, Kalender W, Engelke K, Laredo JD. Volumetric quantitative computed tomography of the proximal femur: relationships linking geometric and densitometric variables to bone strength. Role for compact bone. Osteoporos Int, 2006; 17(6): 855-864.

140. Cody DD, Gross GJ, Hou FJ, Spencer HJ, Goldstein SA, Fyhrie DP. Femoral strength is better predicted by finite element models than QCT and DXA. J Biomech, 1999; 32(10): 1013-1020.

141. Bauer JS, Kohlmann S, Eckstein F, Mueller D, Lochmuller EM, Link TM. Structural analysis of trabecular bone of the proximal femur using multislice computed tomography: a comparison with dual X-ray absorptiometry for predicting biomechanical strength in vitro. Calcif Tissue Int, 2006; 78(2): 78-89.

142. Nishiyama KK, Shane E. Clinical imaging of bone microstructure with HR-pQCT. Curr Osteoporos Rep, 2013; 11(2): 147-155.

143. Cheung AM, Adachi JD, Hanley DA, Kendler DL, Davison KS, Josse R, Brown JP, Ste-Marie LG, Kremer R, Erlandson MC, Dian L, Burghardt AJ, Boyd SK. High-resolution peripheral quantitative computed tomography for the assessment of bone strength and structure: a review by the Canadian Bone Strength Working Group. Curr Osteoporos Rep, 2013; 11(2): 136-146.

144. Lu Y, Krause M, Bishop N, Sellenschloh K, Gluer CC, Puschel K, Amling M, Morlock MM, Huber G. The role of patient-mode high-resolution peripheral quantitative computed tomography indices in the prediction of failure strength of the elderly women's thoracic vertebral body. Osteoporos Int, 2015; 26(1): 237-244.

145. Maquer G, Lu Y, Dall'Ara E, Chevalier Y, Krause M, Yang L, Eastell R, Lippuner K, Zysset PK. The initial slope of the variogram, foundation of the trabecular bone score, is not or is poorly associated with vertebral strength. J Bone Miner Res, 2016; 31(2): 341-346.

146. Berlemann U, Ferguson SJ, Nolte LP, Heini PF. Adjacent vertebral failure after vertebroplasty. A biomechanical investigation. J Bone Joint Surg (Br), 2002; 84: 748-752.

147. Baround G, Nemes J, Heini P, Steffen T. Load shift of the intervertebral disc after vertebroplasty: a finite element study. Eur Spine J, 2003; 12(4): 421-426.

148. Zhou B, Wang J, Yu YE, Zhang Z, Nawathe S, Nishiyama KK, Rosete FR, Keaveny TM, Shane E, Guo XE. High-resolution peripheral quantitative computed tomography (HR-pQCT) can assess microstructural and biomechanical properties of both human distal radius and tibia: ex vivo computational and experimental validations. Bone, 2016; 86: 58-67.

149. Kroker A, Plett R, Nishiyama KK, McErlain DD, Sandino C, Boyd SK. Distal skeletal tibia assessed by HR-pQCT is highly correlated with femoral and lumbar vertebra failure load. J Biomech, 2017; 59: 43-49.

150. Tjong W, Kazakia GJ, Burghardt AJ, Majumdar S. The effect of voxel size on high-resolution peripheral computed tomography measurements of trabecular and cortical bone microstructure. Med Phys, 2012; 39(4): 1893-1903.

151. MacNeil JA, Boyd SK. Accuracy of high-resolution peripheral quantitative computed tomography for measurement of bone quality. Med Eng Phys, 2007; 29(10): 1096-1105.

152. Liu XS, Zhang XH, Sekhon KK, Adams MF, McMahon DJ, Bilezikian JP, Shane E, Guo XE. High-resolution peripheral quantitative computed tomography can assess microstructural and mechanical properties of human distal tibial bone. J Bone Miner Res, 2010; 25(4): 746-756.

153. Varga P, Zysset PK. Assessment of volume fraction and fabric in the distal radius using HR-pQCT. Bone, 2009; 45(5): 909-917.

154. Burghardt AJ, Kazakia GJ, Majumdar S. A local adaptive threshold strategy for high resolution peripheral quantitative computed tomography of trabecular bone. Ann Biomed Eng, 2007; 35(10): 1678-1686.

155. Nishiyama KK, Macdonald HM, Buie HR, Hanley DA, Boyd SK. Postmenopausal women with osteopenia have higher cortical porosity and thinner cortices at the distal radius and tibia than women with normal aBMD: an in vivo HR-pQCT study. J Bone Miner Res, 2010; 25(4): 882-890.

156. Buie HR, Campbell GM, Klink RJ, MacNeil JA, Boyd SK. Automatic segmentation of cortical and trabecular compartments based on a dual threshold technique for in vivo micro-CT bone analysis. Bone, 2007; 41(4): 505-515.

157. Waarsing JH, Day JS, Weinans H. An improved segmentation method for in vivo microCT imaging. J Bone Miner Res, 2004; 19(10): 1640-1650.

158. Liu XS, Shane E, McMahon DJ, Guo XE. Individual trabecular segmentation (ITS)-based morphological analysis of microscale images of human tibial trabecular none at limited spatial resolution. J Bone Miner Res, 2011; 26(9): 2184-2193.

159. Liu XS, Cohen A, Shane E, Stein E, Rogers H, Kokolus SL, Yin PT, McMahon DJ, Lappe JM, Recker RR, Guo XE. Individual trabeculae segmentation (ITS)–based morphological analysis of high-resolution peripheral quantitative computed tomography images detects abnormal trabecular plate and rod microarchitecture in premenopausal women with idiopathic osteoporosis. J Bone Miner Res, 2010; 25(7): 1496-1505.

160. Ito M. Assessment of bone quality using micro-computed tomography (micro-CT) and synchrotron micro-CT. J Bone Miner Metab, 2005; 23(Suppl): 115-121.

161. Metscher BD. MicroCT for comparative morphology: simple staining methods allow high-contrast 3D imaging of diverse non-mineralized animal tissues. BMC Physiol, 2009; 9: 11.

162. Johnson KA. Imaging techniques for small animal imaging models of pulmonary disease: micro-CT. Toxicol Pathol, 2007; 35(1): 59-64.

163. Johnson LC, Johnson RW, Munoz SA, Mundy GR, Peterson TE, Sterling JA. Longitudinal live animal microCT allows for quantitative analysis of tumor-induced bone destruction. Bone, 2011; 48(1): 141-151.

164. Judex S, Boyd S, Qin YX, Miller L, Muller R, Rubin C. Combining high-resolution micro-computed tomography with material composition to define the quality of bone tissue. Curr Osteoporos Rep, 2003; 1: 11-19.

165. Waarsing JH, Day JS, ven der Linden JC, Ederveen AG, Spanjers C, De Clerck N, Sasov A, Verhaar JA, Weinans H. Detecting and tracking local changes in the tibiae of individual rats: a novel method to analyse longitudinal in vivo micro-CT data. Bone, 2004; 34: 163-169.

166. Ho KY, Hu HH, Keyak JH, Colletti PM, Powers CM. Measuring bone mineral density with fat-water MRI: comparison with computed tomography. J Magn Reason Imaging, 2013; 37(1): 237-242.

167. Lammentausta E, Hakulinen MA, Jurvelin JS, Nieminen MT. Prediction of mechanical properties of trabecular bone using quantitative MRI. Phys Med Biol, 2006; 51: 6187-6198.

168. Hudelmaier M, Kollstedt A, Lochmuller EM, Kuhn V, Eckstein F, Link TM. Gender differences in trabecular bone architecture of the distal radius assessed with magnetic resonance imaging and implications for mechanical competence. Osteoporos Int, 2005; 16: 1124-1133.

169. Link TM, Vieth V, Langenberg R, Meier N, Lotter A, Newitt D, Majumdar S. Structure analysis of high resolution magnetic resonance imaging of the proximal femur: in vitro correlation with biomechanical strength and BMD. Calcif Tissue Int, 2003; 72: 156-165.

170. Liu XS, Zhang XH, Rajapakse CS, Wald MJ, Magland J, Sekhon KK, Adam MF, Sajda P, Wehrli FW, Guo XE. Accuracy of high-resolution in vivo micro magnetic resonance imaging for measurements of microstructural and mechanical properties of human distal tibial bone. J Bone Miner Res, 2010; 2039-2050.

171. Phan CM, Matsuura M, Bauer JS, Dunn TC, Newitt D, Lochmueller EM, Eckstein F, Majumdar S, Link TM. Trabecular bone structure of the calcaneus: comparison of MR imaging at 3.0 and 1.5 T with micro-CT as the standard of reference. Radiology, 2006; 239(2): 488-496.

172. Sell CA, Masi JN, Burghardt A, Newitt D, Link TM, Majumdar S. Quantification of trabecular bone structure using magnetic resonance imaging at 3 Tesla- calibration studies using microcomputed tomography as a standard of reference. Calcif Tissue Int, 2005; 76(5): 355-364.

173. Krug R, Carballido-Gamio J, Burghardt AJ, Kazakia G, Hyun BH, Jobke B, Banerjee S, Huber M, Link TM, Majumdar S. Assessment of trabecular bone structure comparing magnetic resonance imaging at 3 Tesla with high-resolution peripheral quantitative computed tomography ex vivo and in vivo. Osteoporos Int, 2008; 19(5): 653-661.

174. Roux C, Dougados M. Quantitative ultrasound in postmenopausal osteoporosis. Curr Opin Rheumatol, 2000; 12: 336-345.

175. Garra BS, Locher M, Felker S, Wear KA. Measurements of ultrasonic backscattered spectral centroid shift from spine in vivo: methodology and preliminary results. Ultrasound Med Biol, 2009; 35(1): 165-168.

176. Grimal Q, Grondin J, Guerard S, Barkmann R, Engelke K, Gluer CC, Laugier P. Quantitative ultrasound of cortical bone in the femoral neck predicts femur strength: results of a pilot study. J Bone Miner Res, 2013; 28(2): 302-312.

177. Krieg MA, Barkmann R, Gonnelli S, Stewart A, Bauer DC, Del Rio Barquero L, Kaufman JJ, Lorenc R, Miller PD, Oslzynski WP, Poiana C, Schott AM, Lewiecki EM, Hans D. Quantitative ultrasound in the management of osteoporosis: the 2007 ISCD Official Positions. J Clin Densitom, 2008; 11(1): 163-187.

178. Hakulinen MA, Day JS, Toyras J, Timonen M, Kroger H, Weinans H, Kiviranta I, Jurvelin JS. Prediction of density and mechanical properties of human trabecular bone in vitro by using ultrasound transmission and backscattering measurements at 0.2-6.7 MHz frequency range. Phys Med Biol, 2005; 50: 1629-1642.

179. Riekkinen O, Hakulinen MA, Toyras J, Jurvelin JS. Spatial variation of acoustic properties is related with mechanical properties of trabecular bone. Phys Med Biol, 2007; 52: 6961-6968.

180. Nicholson PH, Alkalay R. Quantitative ultrasound predicts bone mineral density and failure load in human lumbar vertebrae. Clin Biomech (Bristol, Avon), 2007; 22: 623-629.

181. Carden A, Morris MD. Application of vibrational spectroscopy to the study of mineralized tissues (review). J Biomed Opt, 2000; 5(3): 259-268.

182. Boskey A, Mendelsohn R. Infrared analysis of bone in health and disease. J Biomed Opt, 2005; 10(3): 031102.

183. Boskey A, Pleshko Camacho N. FT-IR imaging of native and tissue-engineered bone and cartilage. Biomaterials, 2007; 28(15): 2465-2478.

184. Bhattacharjee T, Kumar P, Maru G, Ingle A, Krishna CM. Swiss bare mice: a suitable model for transcutaneous in vivo Raman spectroscopic studies of breast cancer. Lasers Med Sci, 2014; 29(1): 325-333.

185. Edward JB, Benfer RA, Morris JS. The effects of drying ashing on the composition of human and animal bone. Biol Trace Elem Res, 1990; 25(3): 219-231.

186. Avery NC, Sims TJ, Bailey AJ. Quantitative determination of collagen cross-links. Methods Mol Biol, 009; 522: 103-121.

187. Osteoporosis. In: Online Etymology Dictionary. Retrieved from : https://www.etymonline.com/word/osteoporosis, accessed 23rd November 2019.

188. Anonymous. Consensus development conference: diagnosis, prophylaxis, and treatment of osteoporosis. Am J Med, 1993; 94(6): 646-650.

189. Drake MT, Clarke BL, Lewiecki EM. The pathophysiology and treatment of osteoporosis. Clin Ther, 2015; 37(8): 1837-1850.

190. Armas LA, Recker RR. Pathophysiology of osteoporosis: new mechanistic insights. Endocrinol Metab Clin North Am, 2012; 41(3): 475-486.

191. Wright NC, Looker AC, Saag KG, Curtis JR, Delzell ES, Randall S, Dawson-Hughes B. The recent prevalence of osteoporosis and low bone mass in the United States based on

bone mineral density at the femoral neck or lumbar spine. J Bone Miner Res, 2014; 29(11): 2520-2526.

192. Okman-Kilic T. Estrogen deficiency and osteoporosis. In: Dionyssiotis Y (ed). Advances in osteoporosis. IntechOpen, London, UK.

193. Khosla S, Melton LJ 3rd, Riggs BL. The unitary model for estrogen deficiency and the pathogenesis of osteoporosis: is a revision needed? J Bone Miner Res, 2011; 26(3): 441-451.

194. Miraz FS, Padhi ID, Raisz LG, Lorenzo JA. Serum sclerostin levels negatively correlate with parathyroid hormone levels and free estrogen index in postmenopausal women. J Clin Endocrinol Mateb, 2010; 95(4): 1991-1997.

195. Modder UI, Clowes JA, Hoey K, Peterson JM, McCready L, Oursler MJ, Riggs BL, Khosla S. Regulation of circulating sclerostin levels by sex steroids in women and men. J Bone Miner Res, 2011; 26(1): 27-34.

196. Armstrong VJ, Muzylak M, Sunters A, Zaman G, Saxon LK, Price JS, Lanyon LE. WNT/B-Catenin signaling is a component of osteoblastic bone cells' early responses to load-bearing and requires estrogen receptor alpha. J Biol Chem, 2007; 282(28): 20715-20727.

197. Torres AYP, Flores MV, Orozco L, Cruz RV. Molecular aspects of bone remodeling. In: Flores MV (ed). Topics in osteoporosis. Rijeka: InTech; 2013.

198. Shevde NK, Bendixen AC, Dienger KM, Pike JW. Estrogens suppress RANK ligand-induced osteoclast differentiation via a stromal cell independent mechanism involving c-Jun repression. Proc Natl Acad Sci USA, 2000; 97: 7829–34.

199. Martin-Millan M, Almeida M, Ambrogini E, Han L, Zhao H, Weinstein RS, Jilka RL, O'Brien CA, Manolagas SC. The estrogen receptor-alpha in osteoclasts mediates the protective effects of estrogens on cancellous but not cortical bone. Mol Endocrinol, 2010; 24(2): 323–34.

200. World Health Organization. Assessment of fracture risk and its application to screening for postmenopausal osteoporosis. Report of a WHO Study Group. World Health Organ Tech Rep Ser, 1994; 843: 1-129.

201. Watts NB, Leslie WD, Foldes AJ, Miller PD. 2013 International Society for Clinical Densitometry Position Development Conference: Task Force for Normative Databases. J Clin Densitom, 2013; 16(4): 472-481.

202. Looker AC, Wahner HW, Dunn WL, Calvo MS, Harris TB, Heyse SP, Johnston CC, Lindsay R. Updated data on proximal demure bone mineral levels of US adults. Osteoporos Int, 1998; 8: 468-489.

203. Kanis JA, McCloskey EV, Johansson H, Oden A, Melton LJ, Khaltaev N. A reference standard for the description of osteoporosis. Bone, 2008; 42: 467-475.

204. Binkley NC, Schmeer P, Wasnich RD, Lenchik L; International Society for Clinical Densitometry Position Development Panel and Scientific Advisory Committee. What are the criteria by which a densitometric diagnosis of osteoporosis can be made in males and non-Caucasians? J Clin Densitom, 2002; 5(Suppl): S19-S27.

205. Binkley N, Adler R, Bilezikian JP. Osteoporosis diagnosis in men: The T-score controversy revisited. Curr Osteoporos Rep, 2014; 12(4): 403-409.

206. De Laet CE, van Hout BA, Burger H, Weel AE, Hofman A, Pols HA. Hip fracture prediction in elderly men and women: validation in the Rotterdam study. J Bone Miner Res, 1998; 13(10): 1587-1593.

207. Langsetmo L, Leslie WD, Zhou W, Goltzman D, Kovacs CS, Prior J, Josse R, Olszynski WP, Davison KS, Anastassiades T, Towheed T, Hanley DA, Kaiser S, Kreiger N; CaMOS Research Group. Using the same bone density reference database for men and women provides a simpler estimation of fracture risk. J Bone Miner Res, 2010; 25(10): 2108-2114.

208. Looker AC. Femur neck bone mineral density and fracture risk by age, sex, and race of Hispanic origin in older US adults from NHANES III. Arch Osteoporos, 2013; 8(1-2): 141.

209. Kanis JA, Bianchi G, Bilezikian JP, Kaufman JM, Khosla S, Orwoll E, Seeman E. Towards a diagnostic and therapeutic consensus in male osteoporosis. Osteoporos Int, 2011; 22(11): 2789-2798.

210. Hernlund E, Svedbom A, Ivergard M, Compston J, Cooper C, Stenmark J, McCloskey EV, Jonsson B, Kanis JA. Osteoporosis in the European Union: medical management, epidemiology and economic burden. Arch Osteoporos, 2013; 8(1-2): 136.

211. Cauley HA. Defining ethnic and racial differences in osteoporosis and fragility fractures. Clin Orthop Relat Res, 2011; 469(7): 1891-1899.

212. Raef H, Al-Bugami M, Balharith S, Moawad M, El-Shaker M, Hussain A, Al-Shaikh A, Al-Badawi I. Updated recommendations for the diagnosis and management of osteoporosis: a local perspective. Ann Saudi Med, 2011; 31(2): 111-128.

213. Lee K-S, Bae S-H, Lee SH, Lee J, Lee DR. New reference data on bone mineral density and the prevalence of osteoporosis in Korean adults aged 50 years or older: the Korea National Health and Nutrition Examination Survey 2008-2010. J Korean Med Sci, 2014; 29(11): 1514-1522.

214. Ho-Pham LT, Nguyen UD, Pham HN, Nguyen ND, Nguyen TV. Reference ranges for bone mineral density and prevalence of osteoporosis in Vietnamese men and women. BMC Musculoskelet Disord, 2011; 12: 182.

215. Yu F, Xia W. The epidemiology of osteoporosis, associated fragility fractures, and management gap in China. Arch Osteoporos, 2019; 14(1): 32.

216. The University of Sheffield. FRAX: Fracture Risk Assessment Tool. Retrieved from: https://www.sheffield.ac.uk/FRAX/index.aspx, accessed 24th November 2019.

217. Melton LJ 3rd, Thamer M, Ray NF, Chan JK, Chesnut CH 3rd, Einhorn TA, Johnston CC, Raisz LG, Silverman SL, Siris ES. Fractures attributable to osteoporosis: report from the National Osteoporosis Foundation. J Bone Miner Res, 1997; 12: 16-23.

218. Sanders KM, Pasco JA, Ugoni AM, Nicholson GC, Seeman E, Martin TJ, Skoric B, Panahi S, Kotowicz MA. The exclusion of high trauma fractures may unserestimate the prevalence of bone fragility fractures in the community: the Geelong Osteoporosis Study. J Bone Miner Res, 1998; 13: 1337-1342.

219. Mackey DC, Lui LY, Cawthon PM, Bauer DC, Nevitt MC, Cauley JA, Hillier TA, Lewis CE, Barrett-Connor E, Cummings SR. High-trauma fractures and low bone mineral density in older women and men. JAMA, 2007; 298: 2381-2388.

220. Melton LH 3rd. Adverse outcomes of osteoporotic fractures in the general population. J Bone Miner Res, 2003; 18: 1139-1141.

221. Keene GS, Parker MJ, Pryor GA. Mortality and morbidity after hip fractures. BMJ, 1993; 307: 1248-1250.

222. Poor G, Atkinson EJ, O'Fallon WM, Melton LJ 3rd. Determinants of reduced survival following hip fractures in men. Clin Orthop Relat Res, 1995; 319: 260-265.

223. Melton LJ 3rd. Epidemiology of fractures. In Riggs BL, Melton LJ 3rd (ed). Osteoporosis: etiology, diagnosis, and management, 2nd edition. Lippinott-Raven Press, Philadelphia, 1995, 225-247.

224. Michaelsson K, Weiderpass E, Farahmand BY, Baron JA, Persson PG, Ziden L, Zetterberg C, Ljunghall S. Differences in risk factor patterns between cervical and trochanteric hip fractures. Swedish Hip Fracture Study Group. Osteoporos Int, 1999; 10: 487-494.

225. Johnell O, Kanis JA. An estimate of the worldwide prevalence and disability associated with osteoporotic fractures. Osteoporos Int, 2006; 17: 1726-1733.

226. Chrischilles EA, Butler CD, Davis CS, Wallace RB. A model of lifetime osteoporosis impact. Arch Intern Med, 1991; 151: 2026-2032.

227. Klotzbuecher CM, Ross PD, Landsman PB, Abbott TA, III, Berger M. Patients with prior fractures have an increased risk of future fractures: a summary of the literature and statistical synthesis. J Bone Miner Res, 2000; 15: 721-739.

228. Johnell O, Kanis JA, OdenA, Sernbo I, Redlund-Johnell I, Petterson C, De Laet C, Jonsson B. Fracture risk following an osteoporotic fracture. Osteoporos Int, 2004; 15: 175-179.

229. Johnell O, Oden A, Caulin F, Kanis JA. Acute and long-term increase in fracture risk after hospitalization for vertebral fracture. Osteoporos Int, 2001; 12: 207-214.

230. Ettinger B, Black DM, Nevitt MC, Rundle AC, Cauley JA, Cummings SR, Genant HK. Contribution of vertebral deformities to chronic back pain and disability. The Study of Osteoporotic Fractures Research Group. J Bone Miner Res, 1992; 7: 449-456.

231. Kanis JA, Johnell O, Oden A, Borgstrom F, Zethraeus N, De Laet C, Jonsson B. The risk and burden of vertebral fractures in Sweden. Osteoporos Int, 2004; 15: 20-26.

232. Genant HK, Jergas M, Palermo L, Nevitt M, Valentin RS, Black D, Cummings SR. Comparison of semiquantitative visual and quantitative morphometric assessment of prevalent and incident vertebral fractures in osteoporosis The Study of Osteoporotic Fractures Research Group. J Bone Miner Res, 1996; 11: 984-996.

233. Kanis JA, Johnell O, Oden A, Jonsson B, De Laet C, Dawson A. Risk of hip fracture according to the World Health Organization criteria for osteopenia and osteoporosis. Bone, 2000; 27: 585-590.

234. Ghannam NN, Hammami MM, Bakheet SM, Khan BA. Bone mineral density of the spine and femur in healthy Saudi females: Relation to vitamin D status, pregnancy, and lactation. Calci Tissue Int, 1999; 65: 23-8.

235. Li N, Ou P, Zhu H, Yang D, Zheng P. Prevalence rate of osteoporosis in the mid-aged and elderly in selected parts of China. Chin Med J, 2002; 115: 773-775.

236. Lau EM, Chung HL, Ha PC, Tang H, Lam D. Bone mineral density, anthropometric indices, and the prevalence of osteoporosis in northern (Beijing) Chinese and southern (Hong Kong) Chinese women- the largest comparative study to date. J Clin Densitometry, 2015; 18: 519-524.

237. Su FM, Liu DH, Chen JF, Yu SF, ChiuWC, Hsu CY, Ko CH, Tsai CC, Cheng TT. Development and validation of an osteoporosis self-assessment tool for Taiwan (OSTAi)

postmenopausal women-a sub-study of the Taiwan OsteoPorosis survey (TOPS). PLoS One, 2015; 10: e0130716.

238. Watts JJ, Abimanyi-Ochom J, Sanders K. Osteoporosis costing all Australians: A new burden of disease analysis- 2012 to 2022. Glebe, NSW: Osteoporosis Australia, 2013.

239. Australian Bureau of Statistics. Population projections, Australia, 2012 to 2101. ABS cat. no. 32220.02013. Belconnen, ACT: ABS, 2013.

240. Kanis JA, Oden A, McCloskey EV, Johansson H, Wahl DA, Cooper C, IOF Working group on Epidemiology and Quality of Life. A systematic review of hip fracture incidence and probability of fracture worldwide. Osteoporos Int, 2012; 23: 2239–2256.

241. Jones G, Nguyen T, Sambrook PN, Kelly PJ, Gilbert C, Eisman JA. Symptomatic fracture incidence in elderly men and women: the Dubbo Osteoporosis Epidemiology Study (DOES). Osteoporos Int, 1994; 4(5): 277-282.

242. Kanis JA. Diagnosis of osteoporosis and assessment of fracture risk. Lancet,2002; 359(9321): 1929-1936.

243. Svedbom A, Hernlund E, Ivergard M, Compston J, Cooper C, Stenmark J, McCloskey EV, Jonsson B, Kanis JA; EU review panel of IOF. Osteoporosis in the European Union: a compendium of country-specific reports. Arch of osteoporos, 2013; 8: 137.

244. Budhia S, Mikyas Y, Tang M Badamgarav E. Osteoporotic fractures: A systematic review of US healthcare costs and resource utilization. Pharmacoeconomics, 2012; 30(2), 147-170.

245. Hoerger TJ, Downs KE, Lakshmanan MC, Lindrooth RC, Plouffe L Jr, Wendling B, West SL, Ohsfeldt RL. Healthcare use among U.S. women aged 45 and older: total costs

and costs for selected postmenopausal health risks. J Womens Health Gend Based Med, 1999; 8(8), 1077-1089.

246. Royal College of Physicians of UK. Guidelines for the prevention and treatment of osteoporosis. London: Royal College of Physicians of UK, 1999.

247. University of Melbourne. (2007). The burden of brittle bones: Epidemiology, costs & burden of osteoporosis in Australia- 2007. Department of Medicine, Western Hospital, Footscray. Retrieved from: https://www.iofbonehealth.org/sites/default/files/PDFs/white_paper_australia-23-06-08.pdf. Accessed 24th December 2019.

248. Eisman JA, Bogoch ER, Dell R, Harrington JT, McKinney RE Jr, McLellan A, Mitchell PJ, Silverman S, Singleton, R, Siris E; ASBMR Task Force on Secondary Fracture Prevention. Making the first fracture the last fracture: ASBMR task force report on secondary fracture prevention. J Bone Miner Res, 2012; 27(10): 2039-2046.

249. Akesson K, Marsh D, Mitchell PJ, McLellan AR, Stenmark J, Pierroz DD, Kyer C, Cooper C; IOF Fracture Working Group. Capture the Fracture: a best practice framework and global campaign to break the fragility fracture cycle. Osteoporos Int, 2013; 24(8): 2135-2152.

250. Yates CJ, Chauchard MA, Liew D, Bucknill A, Wark JD. Bridging the osteoporosis treatment gap: performance and cost-effective of a fracture liaison service. J Clin Densitom, 2015; 18(2): 150-156.

251. Hagino H, Wada T. Osteoporosis liaison service in Japan. Osteoporos Sarcopenia, 2019; 5(3): 65-68.

252. Cameron JR, Sorenson J. Measurement of bone mineral in vivo: an improved method. Science, 1963; 142(3589): 230-232.

253. Adams JE. Single and dual energy X-ray absorptiometry. Eur Radiol, 1997; 7(1): 20-31.

254. Njeh CF, Shepherd JA. Absorptiometric measurement. In: Langton CM, Njeh CF (ed). The physical measurement of bone. Institutes of Physics Publishing Ltd, London, UK, 2004.

255. Kelly TL, Crane G, Baran DT. Single X-ray absorptiometry of the forearm: precision, correlation, and reference data. Calcif Tissue Int, 1994; 54(3): 212-218.

256. Cullum ID, Ell PJ, Ryder JP. X-ray dual-photon absorptiometry: a new method for the measurement of bone density. Br J Radiol, 1989; 62(739): 587-592.

257. Kelly TL, Slovik DM, Schoenfeld DA, Neer RM. Quantitative digital radiography versus dual photon absorptiometry of the lumbar spine. J Clin Endocrinol Metab, 1988; 67(4): 839-844.

258. Blake GM, Fogelman I. Technical principles of dual energy X-ray absorptiometry. Semin Nucl Med, 1997; 27(3): 210-218.

259. Park HS, Chung YE, Seo JK. Computed tomographic beam-hardening artefacts: mathematical characterization and analysis. Philos Trans A Math Phys Eng Sci, 2015; 373(2043): 20140388.

260. Blake GM, McKeeney DB, Chhaya SC, Ryan PJ, Fogelman I. Dual energy X-ray absorptiometry: the effects of beam hardening on bone density measurements. Med Phys, 1992; 19(2): 459-465.

261. Cheng XG, Nicholson PH, Boonen S, Lowet G, Brys P, Aerssen J, ven der Perre G, Dequeker J. Prediction of vertebral strength in vitro by spinal bone densitometry and calcaneal ultrasound. J Bone Miner Res, 1997; 12(10): 1721-1728.

262. Perilli E, Briggs AM, Kantor S, Codrington J, Wark JD, Parkinson IH, Fazzalari NL. Failure strength of human vertebrae: prediction using bone mineral density measured by DXA and bone volume by micro-CT.

263. Mi J, Li K, Zhao X, Zhao CQ, Li H, Zhao J. Vertebral body compressive strength evaluated by dual-energy X-ray absorptiometry and Hounsfield units in vitro. J Clin Densitom, 2018; 21(1): 148-153.

264. Eckstein F, Lochmuller EM, Lill CA, Kuhn V, Schneider E, Delling G, Muller R. Bone strength at clinically relevant sites displays substantial heterogeneity and is best predicted from site-specific bone densitometry. J Bone Miner Res, 2002; 17(1): 162-171.

265. Singer K, Edmondston S, Day R, Breidahl P, Price R. Prediction of thoracic and lumbar vertebral body compressive strength. Correlations with bone mineral density and vertebral region. Bone, 1995; 17(2), 167-174.

266. Zengin A, Prentice A, Ward KA. Ethnic differences in bone health. Front Endocrinol (Lausanne), 2015; 6: 24.

267. Duan Y, Parfitt AM, Seeman E. Vertebral bone mass, size, and volumetric density in women with spinal fractures. J Bone Miner Res, 1999; 14: 1796-1802.

268. Farr JN, Khosla S. Skeletal changes through lifespan- from growth to senescence. Nat Rev Endocrinol, 2015; 11(9): 513-521.

269. Danielson ME, Beck TJ, Lian Y, Karlamangla As, Greendale GA, Ruppert K, Lo J, Greenspan S, Vuga M, Cauley JA. Ethnic variability in bone geometry as assessed by hip

structure analysis: findings from the hip strength across the menopausal transition study. J Bone Miner Res, 2013; 28(4): 771-779.

270. Osterhoff G, Morgan EF, Shefelbine SJ, Karim L, McNamara LM, Augat P. Bone mechanical properties and changes with osteoporosis. Injury, 2016; 47(Suppl 2): S11-S20.

271. Ulrich D, van Rietbergen B, Laib A, Ruegsegger P. The ability of three-dimensional structural indices to reflect mechanical aspects of trabecular bone. Bone, 1999; 25: 55-60.

272. Kleerekoper M, Villanueva AR, Stanciu J, Sudhaker D, Parfitt AM. The role of three-dimensional trabecular microstructure in the pathogenesis of vertebral compression fracture. Calcif Tissue Int, 1985; 37: 594-597.

273. Garg MK, Kharb S. Dual energy X-ray absorptiometry: pitfalls in measurement and interpretation of bone mineral density. Indian J Endocrinol Metab, 2013; 17(2): 203-210.

274. Gregson CL, Hardcastle SA, Cooper C, Tobias JH. Friend or foe: high bone mineral density on routine bone density scanning, a review of causes and management. Rheumatology (Oxford), 2013; 52(6): 968-985.

275. Marshall D, Johnell O, Wedel H. Meta-analysis of how well measures of bone mineral density predict occurrence of osteoporotic fractures. BMJ, 1996; 312(7041): 1254-1259.

276. Arabi A, Baddoura R, Awada H, Khoury N, Haddad S, Ayoub G, El-Haji Fuleihan G. Discriminative ability of dual-energy X-ray absorptiometry sit selection in identifying patients with osteoporotic fractures. Bone 2007; 40(4): 1060-1065.

277. Briggs AM, Greig AM, Wark JD. The vertebral fracture cascade in osteoporosis: a review of aetiopathogenesis. Osteoporos Int, 2007; 18(5): 575-584.

278. Hordon LD, Raisi M, Aaron JE, Paxton SK, Beneton M, Kanis JA. Trabecular architecture in women and men of similar bone mass with and without vertebral fracture: I. Two-dimensional histology. Bone, 2000; 27(2): 271-276.

279. Jergas M, Breitenseher M, Gluer CC, Black D, Lang P, Grampp S, Engelke K, Genant HK. Which vertebrae should be assessed using lateral dual-energy X-ray absorptiometry of the lumbar spine? Osteoporos Int, 1995; 5(3): 196-204.

280. Legrand E, Chappard D, Pascaretti C, Duguenne M, Krebs S, Basle MF, Audran M. Trabecular bone microarchitecture, bone mineral density, and vertebral fracture in male osteoporosis. J Bone Miner Res, 2000; 15(1): 13-19.

281. McCreadie R, Goldstein SA. Biomechanics of fracture: is bone mineral density sufficient to assess risk. J Bone Miner Res, 2000; 15(12): 2305-2308.

282. Miller PD, Siris ES, Barrett-Connor E, Faulkner KG, Wehren LE, Abbott TA, Chen YT, Berger ML, Santora AC, Sherwood LM. Prediction of fracture risk in postmenopausal white women with peripheral bone densitometry: evidence from the National Osteoporosis Risk Assessment. J Bone Miner Res, 2002; 17(12): 2222-2230.

283. Schuit SC, van der Klift M, Weel AE, de Laet CE, Burger H, Seeman E, Hofman A, Uitterlinden AG, van Leeuwen JP, Pols HA. Fracture incidence and association with bone mineral density in elderly men and women: the Rotterdam Study. Bone, 2004; 195-202.

284. Siris ES, Miller PD, Barrett-Connor E, Faulkner KG, Wehren LE, Abbott TA, Berger ML, Santora AC, Sherwood LM. Identification and fracture outcomes of undiagnosed low bone mineral density in postmenopausal women: results from the National Osteoporosis Risk Assessment. JAMA, 2001; 286(22): 2815-2822.

285. Sornay-Rendu E, Munoz F, Garnero P, Duboeuf F, Delmas PD. Identification of osteopenic women at high risk of fracture: the OFELY study. J Bone Miner Res, 2005; 20(10): 1813-1819.

286. Delmas PD, Seeman E. Changes in bone mineral density explain little of the reduction in vertebral or nonvertebral fracture risk with anti-resorptive therapy. Bone 2004; 34(4): 599-604.

287. Li Z, Chines AA, Meredith MP. Statistical validation of surrogate endpoints: is bone density a valid surrogate for fracture? J Musculoskelet Neuronal Interact, 2004; 4(1): 64-74.

288. Ohnaru K, Sone T, Tanaka K, Akagi K, Ju Y-I, Choi H-J, Tomomitsu T, Fukunaga M. Hip structural analysis: a comparison of DXA with CT in postmenopausal Japanese women. Springerplus, 2013; 2: 331.

289. Silva BC, Leslie WD. Trabecular bone score: a new DXA-derived measurement for fracture risk assessment. Endocrinol Metab Clin North Am, 2017; 46(1): 153-180.

290. McCloskey EV, Johansson H, Oden A, Kanis JA. From relative risk to absolute fracture risk calculation: the FRAX algorithm. Curr Osteoporos Rep, 2009; 7(3): 77-83.

291. Van Geel TA, van den Bergh JP, Dinant GJ, Geusens PP. Individualizing fracture risk prediction. Maturitas, 2010; 65(2): 143-148.

292. Hippisley-Cox J, Coupland C. Derivation and validation of updated QFracture algorithm to predict risk of osteoporotic fracture in primary care in the United Kingdom: prospective open cohort study. BMJ, 2012; 344: e3427.

293. Adams JE. Advances in bone imaging for osteoporosis. Nat Rev Endocrinol, 2013; 9(1): 28-42.

294. Bauer JS, Link TM. Advances in osteoporosis imaging. Eur J Radiol, 2009; 71(3): 440-449.

295. D'Elia G, Caracchini G, Cavalli L, Innocenti P. Bone fragility and imaging techniques. Clin Cases Miner Bone Metab, 2009; 6(3): 234-246.

296. Ruegsegger P, Niederer P, Anliker M. An extension of classical bone mineral measurements. Ann Biomed Eng, 1974; 2(2): 194-205.

297. Gordon CC. Peripheral quantitative computed tomography and micro-computed tomography. In Langton CM, Njeh CF (ed). The physical measurement of bone. Institute of Physics Publishing Ltd, Bristol, Philadelphia, USA, 2004.

298. Horikoshi T, Endo N, Uchiyama T, Tanizawa T, Takahashi HE. Peripheral quantitative computed tomography of the femoral neck in 60 Japanese women. Calfi Tissue Int, 1999; 65(6): 447-553.

299. Binkley TL, Specker BL, Witting TA. Centile curves for bone densitometry measurements in healthy males and females aged 5-22 yrs. J Clin Densitom, 2002; 5(4): 343-353.

300. Pollock NK, Laing EM, Taylor RG, Baile CA, Hamrick MW, Hall DB, Lewis RD. Comparison of trabecular and cortical bone in late adolescent black and white females. J Bone Miner Metab, 2011; 29(1): 44-53.

301. Dowthwaite JN, Scerpella TA. Distal radius geometry and skeletal strength indices after peripubertal artistic gymnastics. Osteoporos Int, 2011; 22(1): 207-216.

302. Wetzeon RJ, Zemel BS, Shults J, Howard KM, Kibe LW, Leonard MB. Mechanical loads and cortical bone geometry in healthy children and young adults. Bone, 2011; 48(5): 1103-1108.

303. Ashby RL, Ward KA, Roberts SA, Edwards L, Mughal MZ, Adams JE. A reference database for the Stratec XCT-2000 peripheral quantitative computed tomography (pQCT) scanner in healthy children and young adults aged 6-19 years. Osteoporos Int, 2009; 20(8): 1337-1346.

304. Kontulainen SA, MacDonald HM, Mckay HA. Change in cortical bone density and its distribution differs between boys and girls during puberty. J Clin Endocrinol Metab, 2006; 91(7): 2555-2561.

305. Beccard R, Land C, Semler O, Frickle O, Remer T, Stabrey A, Schoenau E. Do bone mineral density, bone geometry and functional muscle-bone unit explain bone fractures in healthy children and adolescents? Horm Res Paediatr, 2010; 74(5): 312-318.

306. Ward KA, Roberts SA, Adams JE, Mughal MZ. Bone geometry and density in the skeleton of pre-pubertal gymnasts and school children. Bone, 2005; 36(6): 1012-1018.

307. Burt LA, Naughton GA, Greene DA, Ducher G. Skeletal differences at the ulna and radius between pre-pubertal non-elite female gymnasts and non-gymnasts. J Musculoskelet Neuronal Interact, 2011; 11(3): 227-233.

308. Moyer-Mileur LJ, Quick JL, Murray MA. Peripheral quantitative computed tomography of the tibia: pediatric reference values. J Clin Densitom, 2008; 11(2): 283-294.

309. Leonard MB, Elmi A, Mostoufi-Moab S, Shults J, Burnham JM, Thayu M, Kibe L, Wetzsteon RJ, Zemel BS. Effects of sex, race, and puberty on cortical bone and the functional muscle bone unit in children, adolescents, and young adults. J Clin Endocrinol Metab, 2010; 95(4): 1681-1689.

310. Heinonen A, Sievanen H, Kannus P, Oja P, Pasanen M, Vuori I. High-impact exercise and bones of growing girls: a 9-month controlled trial. Osteoporos Int, 2000; 11(12): 1010-1017.

311. Adams JE, Engelke K, Zemel BS, Ward KA; International Society of Clinical Densitometry. Quantitative computed tomography in children and adolescents: the 2013 ISCD Pediatric Official Positions. J Clin Densitom, 2014; 17(2): 258-274.

312. Fonseca A, Gordon CL, Barr RD. Peripheral quantitative computed tomography (pQCT) to assess bone health in children, adolescents, and young adults: a review of normative data. J Pediatr Hematol Oncol, 2013; 35(8): 581-589.

313. Blew RM, Lee VR, Farr JN, Schiferl DJ, Going SB. Standardizing evaluation of pQCT image quality in the presence of subject movement: qualitative versus quantitative assessment. Calcif Tissue Int, 94(2): 202-211.

314. Rantalainen T, Chivers P, Beck BR, Robertson S, Hart NH, Nimphius S, Weeks BK, McIntyre F, Hands B, Siafarikas A. Please don't move- evaluating motion artifact from peripheral quantitative computed tomography scans using textural features. J Clin Densitom, 2018; 21(2): 260-268.

315. Cervinka T, Giangregorio L, Sievanen H, Cheung AM, Craven BC. Peripheral quantitative computed tomography: review of evidence and recommendations for image acquisition, analysis, and reporting, among individuals with neurological impairment. J Clin Densitom, 2018; 21(4): 563-582.

316. Hangartner TN, Short DF. Accurate quantification of width and density of bone structures by computed tomography. Med Phys, 2007; 34: 3777-3784.

317. Ward KA, Adans HE, Hangartner TN. Recommendations for thresholds for cortical bone geometry and density measurement by peripheral quantitative computed tomography. Calcif Tissue Int, 2005; 77: 275-280.

318. Dudley-Javoroski S, Shields RK. Longitudinal changes in femur bone mineral density after spinal cord injury: effects of slice placement and peel mode. Osteoporos Int, 2010; 21(6): 985-995.

319. Veitch SW, Findlay SC, Ingle BM, Ibbotson CJ, Barrington A, Hamer AJ, Eastell R. Accuracy and precision of peripheral quantitative computed tomography measurements at the tibial metaphysis. J Clin Densitom, 2004; 7(2): 209-217.

320. Kontulainen S, Liu D, Manske S, Jamieson M, Sievanen H, McKay H. Analyzing cortical bone cross-sectional geometry by peripheral QCT: comparison with bone histomorphometry. J Clin Densitom, 2007; 10: 86-92.

321. Hangartner TN. Thresholding technique for accurate analysis of density and geometry in QCT, pQCT and microCT images. J Musculoskelet Neuronal Interact, 2007; 7: 9-16.

322. Engelke K, Libannati C, Liu Y, Wang H, Austin M, Fuerst T, Stampa B, Timm W, Genant HK. Quantitative computed tomography (QCT) of the forearm using general purpose spiral whole-body CT scanners: accuracy, precision and comparison with dual-energy X-ray absorptiometry. Bone, 2009; 45(1): 110-118.

323. Roux JP, Wegrzyn J, Arlot ME, Guyen O, Delmas PD, Chapurlat R, Bouxsein ML. Contribution of trabecular and cortical components to biomechanical behavior of human vertebrae: an ex vivo study. J Bone Miner Res, 2010; 25(2): 356-361.

324. Augat P, Iida H, Jiang Y, Diao E, Genant HK. Distal radius fractures: mechanisms of injury and strength prediction by bone mineral assessment. J Orthop Res, 1998; 16(5): 629-635.

325. Augat P, Reeb H, Claes LE. Prediction of fracture load at different skeletal sites by geometric properties of the cortical shell. J Bone Miner Res, 1996; 11(9): 1356-1363.

326. Lochmuller EM, Lill CA, Kuhn V, Schneider E, Eckstein F. Radius bone strength in bending, compression and falling and its correlation with clinical densitometry at multiple sites. J Bone Miner Res, 2002; 17(9): 1629-1638.

327. Louise O, Boulpaep F, Willnecker J, van den Winkel P, Osteaux M. Cortical mineral content of the radius assessed by peripheral QCT predicts compressive strength on biomechanical testing. Bone, 1995; 375-379.

328. Stathpoulos KD, Katsimbri P, Atsali E, Metania E, Zoubos AB, Skarantavos G. Age-related differences of bone mass, geometry and strength in treatment-naïve postmenopausal women. A tibia pQCT study. J Clin Densitom, 2011; 14(1): 33-40.

329. Ahlborg HG, Johnell O, Turner CH, Rannevik G, Karlsson MK. Bone loss and bone size after menopause. NEJM, 2003; 349(4): 327-334.

330. Kokoroghiannis C, Charopoulos I, Lyritis G, Raptou P, Karachalios T, Papaioannou N. Correlation of pQCT bone strength index with mechanical testing in distraction osteogenesis. Bone, 2009; 45(3): 512-516.

331. MacDonald H, Kontulainen S, Petit M, Janssen P, McKay H. Bone strength and its determinants in pre- and early pubertal boys and girls. Bone, 2006; 39(3): 598-609.

332. Martin DE, Severns AE, Kabo JM. Determination of mechanical stiffness of bone by pQCT measurements: correlation with non-destructive mechanical four-point bending test data. J Biomech, 2004; 37(8): 1289-1293.

333. Rauch F, Schonau E. Peripheral quantitative computed tomography of the proximal radius in young subjects- new reference data and interpretation of results. J Musculoskelet neuronal Interact, 2008; 8(3): 217-226.

334. Sheu Y, Zmuda JM, Boudreau RM, Petit MA, Ensrud KE, Bauer DC, Gordon CL, Orwoll ES, Cauley JA; Osteoporotic Fractures in Men (MrOS) research group. Bone strength measured by peripheral quantitative computed tomography and the risk of nonvertebral fractures: the Osteoporotic in Men (MrOS) Study. J Bone Miner Res, 2011; 26(1): 63-71.

335. Cointry GR, Ferritti JL, Reina PS, Nocciolino LM, Rittweger J, Capozza RF. The pQCT "Bone Strength Indices" (BSIs, SSI). Relative mechanical impact and diagnostic value of the indicators of bone tissue and design quality employed in their calculation in healthy men and pre- and post-menopausal women. J Musculoskelet Neuronal Interact, 2014; 14(1): 29-40.

336. Ashe MC, Khan KM, Kontulainen SA, Guy P, Liu D, Beck TJ, McKay HA. Accuracy of pQCT for evaluating the aged human radius: an ashing, histomorphometry and failure load investigation. Osteoporos Int, 2006; 17(8): 1241-1251.

337. Gordon CL, Webber CE, Nicholson PS. Relation between image-based assessment of distal radius trabecular structure and compressive strength. Can Assoc Radiol J, 1998; 49(6): 390-397.

338. Spadaro JA, Werner FW, Brenner RA, Fortino MD, Fay LA, Edwards WT. Cortical and trabecular bone contribute

339. Thomas SR, Kalkwarf HJ, Buckley DD, Heubi JE. Effective dose of dual-energy X-ray absorptiometry scans in children as a function of age. J Clin Densitom, 2005; 8(4): 415-422.

340. Duckham RL, Frank AW, Johnston JD, Olszynski WP, Kontulainen SA. Monitoring time interval for pQCT-derived bone outcomes in postmenopausal women. Osteoporos Int, 2013; 24(6): 1917-1922.

341. Rinaldi G, Wisniewski CA, Setty NG, Leboff MS. Peripheral quantitative computed tomography: optimization of reproducibility measures of bone density, geometry, and strength at the radius and tibia. J Clin Densitom, 2011; 14(3): 367-373.

342. Sun L, Beller G, Felsenberg D. Quantification of bone mineral density precision according to repositioning errors in peripheral quantitative computed tomography (pQCT) at the radius and tibia. J Musuloskelet Neuronal Interact, 2009; 9(1): 18-24.

343. Swinford RR, Warden SJ. Factors affecting short-term precision of musculoskeletal measures using peripheral quantitative computed tomography (pQCT). Osteoporos Int, 2010; 21(11): 1863-1870.

344. Wong AKO, Beattie KA, Min KKH, Webber CE, Gordon CL, Papaioannou A, Cheung AMW, Adachi JD. A trimodality comparison of volumetric bone imaging technologies. Part I: short-term precision and validity. J Clin Densitom, 2015; 18(1): 124-135.

345. Wong AKO, Beattie KA, Min KKH, Merali Z, Webber CE, Gordon CL, Papaioannou A, Cheung AMW, Adachi JD. A trimodality comparison of volumetric bone imaging

technologies. Part II: 1-yr change, long-term precision, and least significant change. J Clin Densitom, 2015; 18(2): 260-269.

346. Carpenter RD. Finite element analysis of the hip and spine based on quantitative computed tomography. Curr Osteoporos Rep, 2013; 11(2): 156-162.

347. Engelke K, Libanati C, Fuerst T, Zysset P, Genant HK. Advanced CT based in vivo methods for the assessment of bone density, structure, and strength. Curr Osteoporos Rep, 2013; 11: 246-255.

348. Kontulainen SA, Johnston JD, Liu D, Leung C, Oxland TR, McKay HA. Strength indices from pQCT imaging predict up to 85% of variance in bone failure properties at tibial epiphysis and diaphysis. J Musculoskelet Neuronal Interact, 2008; 8(4): 401-409.

349. Liu D, Manske SL, Kontulainen SA, Tang C, Guy P, Oxland TR, McKay HA. Tibial geometry is associated with failure load ex vivo: a MRI, pQCT and DXA study. Osteoporos Int, 2007; 18: 991-997.

350. Weatherhlolt AM, Avin KG, Hurd AL, Cox JL, Marberry ST, Santoni BG, Warden SJ. Peripheral quantitative computed tomography (pQCT) predicts humeral diaphysis torsional mechanical properties with good short-term precision. J Clin Densitom, 2015; 18(4): 551-559.

351. Gorai I, Nonaka K, Kishimoto H, Sakata H, Fujii Y, Fujita T. Cut-off values determined for vertebral fracture by peripheral quantitative computed tomography in Japanese women. Osteoporos Int, 2001; 12: 741-748.

352. Crockett K, Arnold CM, Farthing JP, Chilibeck PD, Johnston JD, Bath B, Baxter-Jones ADG, Kontulainen SA. Bone strength and muscle properties in postmenopausal women with and without a recent distal radius fracture. Osteoporos Int, 2015; 26: 2461-2469.

353. Drey M, Henkel M, Petermeise S, Weib S, Ferrari U, Rottenkolber M, Schmidmaier R. Assessment of bone and muscle measurements by peripheral quantitative computed tomography in geriatric patients. J Clin Densitom, 2018; in press.

354. Dennison EM, Jameson KA, Edwards MH, Denison HJ, Aihie Sayer A, Cooper C. Peripheral quantitative computed tomography measures are associated with adult fracture risk: the Hertfordshire Cohort Study. Bone, 2014; 64: 13-17.

355. Clowes JA, Eastell R, Peel NFA. The discriminative ability of peripheral and axial bone measurements to identify proximal femoral, vertebral, distal forearm and proximal humeral fractures: a case control study. Osteoporos Int, 2005; 16: 1794-1802.

356. Augat P, Fan B, Lane NE, Lang TF, LeHir P, Lu Y, Uffmann M, Genant HK. Assessment of bone mineral at appendicular sites in females with fractures of the proximal femur. Bone, 1998; 22(4): 395-402.

357. Kroger H, Lunt M, Reeve J, Dequeker J, Adams JE, Birkenhager JC, Diaz Curiel M, Felsenberg D, Hyldstrup L, Kotzki P, Laval-Jeantet A-M, Lips P, Louis O, Perez Cano R, Reiners C, Ribot C, Ruegsegger P, Schneider P, Braillon P, Pearson J. Bone density reduction in various measurement sites in men and women with osteoporotic fractures of spine and hip: the European Quantitation of Osteoporosis study. Calcif Tissue Int, 1999; 64: 191-199.

358. Wong AKO. A comparison of peripheral imaging technologies for bone and muscle quantification: a mixed methods clinical review. Curr Osteoporos Rep, 2016; 14: 359-373.

359. Trombetti A, Hars M, Herrmann F, Rizzoli R, Ferrari S. Effect of a multifactorial fall-and-fracture risk assessment and management program on gait and balance performances

and disability in hospitalized older adults: a controlled study. Osteoporos Int, 2013; 24(3): 867-876.

360. Chiara M, Guanluigi G, Pasquale A, Alessandro M, Alice M, Gabriele N, Paolo C, Loredana G, Giovanni T, Franco R, Giulio M, Gianfranco S, Niccolo M, Andrea U. Unexplained falls are frequent in patients with fall-related injury admitted to orthopaedic wards: the UFO study (Unexplained Falls in Older Patients). Curr Gerontol Geriatr Res, 2013; 2013: 928603.

361. Babuska I, Banerjee U, Osborn JE. Generalized finite element methods: main ideas, results, and perspective. Int J Comput Methods, 2004; 1(1): 67-103.

362. Zysset P, Qin L, Lang T, Khosla S, Leslie WD, Shepherd JA, Schousboe JT, Engelke K. Clinical use of quantitative computed tomography-based finite element analysis of the hip and spine in the management of osteoporosis in adults: the 2015 ISCD official positions- Part II. J Clin Densitom, 2015; 18(3): 359-392.

363. Pahr DH, Zysset PK. Finite element-based mechanical assessment of bone quality on the basis of in vivo images. Curr Osteoporos Rep, 2016; 14: 374-385.

364. Neumann A, Lorenz C. Statistical shape model based segmentation of medical images. Comput Med Imgag Graphics, 1998; 22: 133-143.

365. Engelke K, ven Rietbergen B, Zysset P. FEA to measure bone strength: a review. Clinic Rev Bone Miner Metab, 2016; 14: 26-37.

366. Viceconti M, Bellingeri L, Cristofolini L, Toni A. A comparative study on different methods of automatic mesh generation of human femurs. Med Eng Phys, 1998; 20(1): 1-10.

367. Chevalier Y, Pahr D, Zysset PK. The role of cortical shell and trabecular fabric in finite element analysis of human vertebral body. J Biomech Eng, 2009; 131: 111003.

368. Imai K, Ohnishi I, Bessho M, Nakamura K. Nonlinear finite element model predicts vertebral bone strength and fracture site. Spine, 2006; 31: 1789-1794.

369. Keaveny TM. Biomechanical computed tomography-noninvasive bone strength analysis using clinical computed tomography scans. Ann N Y Acad Sci, 2010; 1192: 57-65.

370. Gong H, Zhang M, Fan Y, Kwok WL, Leung PC. Relationships between femoral strength evaluated by nonlinear finite element analysis and BMD, material distribution and geometric morphology. Ann Biom Eng, 2012; 40(7): 1575-1585.

371. Dall'Ara E, Luisier B, Schmidt R, Kainberger F, Zysset P, Pahr D. A nonlinear QCT-based finite element model validation study for the human femur tested in two configurations in vitro. Bone, 2012; 52(1): 27-38.

372. Zhang N, Magland JF, Rajapakse CS, Lam SCB, Wehrli FW. Assessment of trabecular bone yield and post-yield behaviour from high-resolution MRI-based nonlinear finite-element analysis at the distal radius of pre-and postmenopausal women susceptible to osteoporosis. Acad Radiol, 2013; 20(12): 1584-1591.

373. Nawathe S, Juillard F TM. Theoretical bounds for the influence of tissue-level ductility on the apparent-level strength of human trabecular bone. J Biomech, 2013; 46(7): 1293-1299.

374. Brunig M. Nonlinear analysis and elastic-plastic behaviour of anisotropic structures. Finite Element in Analysis and Design, 1995; 20(3): 155-177.

375. Keyak JH, Rossi SA. Prediction of femoral fracture load using finite element models: an examination of stress- and strain-based failure theories. J Biomech, 2000; 33(2): 209-214.

376. Keyak JH, Fourkas MG, Meagher JM, Skinner HB. Validation of an automated method of three-dimensional finite element modelling of bone. J Biomed Eng, 1993; 15(6): 505-5099.

377. Pistoia W, van Rietbergen B, Lochmuller EM, Lill CA, Eckstein F, Ruegsegger P. Estimation of distal radius failure load with micro-finite element analysis models based on three-dimensional peripheral quantitative computed tomography images. Bone, 2002; 30(6): 842-848.

378. Crawford RP, Cann CE, Keaveny TM. Finite element models predict in vitro vertebral body compressive strength better than quantitative computed tomography. Bone, 2003; 33: 744-750.

379. Liebschner MAK, Kopperdahl DL, Resenberg WS, Keaveny TM. Finite element modeling of human thoracolumbar spine. Spine, 2003; 28(6): 559-565.

380. Lu Y, Rosenau E, Paetzold H, Klein A, Puschel K, Morlock MM, Huber G. Stain changes on the cortical shell of vertebral bodies due to spine ageing: a parametric study using a finite element model evaluated by strain measurements. Proc Inst Mech Eng H, 2013; 227(12): 1265-1274.

381. Yao J, Burns JE, Munoz H, Summers RM. Cortical shell unwrapping for vertebral body abnormality detection on computed tomography. Comput Med Imaging Graph, 2014; 38(7): 628-638.

382. Hosseini HS, Clouthier AL, Zysset PK. Experimental validation of finite element analysis of human vertebral collapse under large compressive strains. J Biomech Eng, 2014; 136(4): 041006.

383. Dall'Ara E, Schmidt R, Pahr D, Varga P, Chevalier Y, Patsch J, Kainberger F, Zysset P. A nonlinear finite element model validation study based on a novel experimental technique for inducing anterior wedge-shape fractures in human vertebral bodies in vitro. J Biomech, 2010; 43: 2374-2380.

384. Koivumaki JEM, Thevenot J, Pulkkinen P, Kuhn V, Link TM, Eckstein F, Jamsa T. Ct-based finite element models can be used to estimate experimentally measured failure loads in the proximal femur. Bone, 2012; 50: 824-829.

385. Nishiyama KK, Gilchrist S, Guy P, Cripton P, Boyd SK. Proximal femur bone strength estimated by a computationally fast finite element analysis in a sideways configuration. J Biomech, 2013; 46: 1231-1236.

386. Mizaei M, Alavi F, Allaveisi F, Naeini V, Amiri P. Linear and nonlinear analyses of femoral fractures: computational/experimental study. J Biomech, 2018; 79: 155-163.

387. Keyak JH, Rossil SA, Jones KA, Skinner HB. Prediction of femoral fracture load using automated finite element modeling. J Biomech, 1998; 31: 125-133.

388. Keyak JH. Improved prediction of proximal femoral fracture load using nonlinear finite element models. Med Eng Phys, 2001; 23(3): 165-173.

389. Bessho M, Ohnishi I, Matsuyama J, Matsumoto T, Imai K, Nakamura K. Prediction of strength and strain of the proximal femur by a CT-based finite element method. J Biomech, 2007; 40: 1745-1753.

390. Miura M, Nakamura J, Matsuura Y, Wako Y, Suzuki T, Hagiwara S, Orita S, Inage K, Kawarai Y, Sugano M, Nawata K, Ohtori S. Prediction of fracture load and stiffness of the proximal femur by CT-based specimen specific finite element analysis: cadaveric validation study. BMC Musculoskelet Disord, 2017; 18: 356.

391. Niebur GL, Feldstein M, Yuen JC, Chen TJ, Keaveny TM. High-resolution finite element models with tissue strength asymmetry accurately predict failure of trabecular bone. J Biomech, 2000; 33: 1575-1583.

392. van Rietbergen B, Pistoia W, Ulrich D, Huiskes R, Ruegsegger P. Prediction of trabecular bone failure parameters using a tissue failure criterion and μFE analysis. Compr Simul Model Med, 2000; 1(2): 98-101.

393. Pistoia W, van Rietbergen B, Lochmuller E-M, Lill CA, Eckstein F, Ruegsegger P. Image-based micro-finite-element modeling for improved distal radius strength diagnosis. J Clin Densotom, 2004; 7(2): 153-160.

394. Meuller TL, Christen D, Sandercott S, Boyd SK, van Rietbergen B, Eckstein F, Lochmuller E-M, Muller R, van Lenthe GH. Computational finite element bone mechanics accurately predicts mechanical competence in the human radius of an elderly population. Bone, 2011; 48: 1232-1238.

395. Varga P, Pahr DH, Baumbach S, Zysset PK. HR-pQCT based FE analysis of the most distal radius section provides an improved prediction of Colles' fracture load in vitro. Bone, 2010; 47: 982-988.

396. Varga P, Baumbach S, Pahr D, Zysset PK. Validation of an anatomy specific finite element model of Colles' fracture. J Biomech, 2009; 42: 1726-1731.

397. Varga P, Dall'Ara E, Pahr DH, Pretterklieber M, Zysset PK. Validation of an HR-pQCT-based homogenized finite element approach using mechanical testing of ultra-distal radius sections. Biomech Model Mechanobiol, 2011; 10: 431-444.

398. MacNeil JA, Boyd SK. Bone strength at the distal radius can be estimated from high-resolution peripheral quantitative computed tomography and the finite element method. Bone, 2008; 42: 1203-1213.

399. van Rietbergen B, Ito K. A survey of micro-finite element analysis for clinical assessment of bone strength: the first decade. J Biomech, 2015; 48: 832-841.

400. Christen D, Zwahlen A, Muller R. Reproducibility for linear and nonlinear micro-finite element simulations with density derived material properties of the human radius. J Mech Behav Biomed Mater, 2014; 29: 500-507.

401. Hosseini HS, Dunki A, Fabech J, Stauber M, Vilayphiou N, Pahr D, Pretterklieber M, Wandel J, van Rietbergen B, Zysset PK. Fast estimation of Colles' fracture load of the distal section of the radius by homogenized finite element analysis based on HR-pQCT. Bone, 2017; 97: 65-75.

402. Melton LJ 3rd, Riggs BL, Keaveny TM, Achenbach SJ, Hoffmann PF, Camp JJ, Rouleau PA, Bouxsein ML, Amin S, Atkinson EJ, Robb RA, Khosla S. Structural determinants of vertebral fracture risk. J Bone Miner Res, 2007; 22(12): 1885-1892.

403. Imai K, Ohnishi I, Matsumoto T, Yamamoto S, Nakamura K. Assessment of vertebral fracture risk and therapeutic effects of alendronate in postmenopausal women using a quantitative computed tomography-based nonlinear finite element method. Osteoporos Int, 2009; 20: 801-810.

404. Graeff C, Marin F, Petto H, Kayser O, Reisinger A, Pena J, Zysset P, Glur C-C. High resolution quantitative computed tomography-based assessment of trabecular microstructure and strength estimates by finite-element analysis of the spine, but not

DXA, reflects vertebral status in men with glucocorticoid-induced osteoporosis. Bone, 2013; 52: 568-577.

405. Kopperdahl DL, Aspelund T, Hoffmann PF, Sigurdsson S, Siggeirsdottir K, Harris TB, Gudnason V, Keaveny TM. Assessment of incident spine and hip fractures in women and men using finite element analysis of CT scans. J Bone Miner Res, 2014; 29(3): 570-580.

406. Wang X, Sanyal A, Cawthon PM, Palermo L, Jekir M, Christensen J, Ensrud KE, Cummings SR, Orwoll E, Black DM; Osteoporotic Fractures in Men (MrOS) Research Group, Keaveny TM. Prediction of new clinical vertebral fractures in elderly men using finite element analysis of CT scans. J Bone Miner Res, 27(4): 808-816.

407. Nishiyama KK, Ito M, Harada A, Boyd SK. Classification of women with and without hip fracture based on quantitative computed tomography and finite element analysis. Osteoporos Int, 2014; 25: 619-626.

408. Campbell GM, Gluer CC. Skeletal assessment with finite element analysis: relevance, pitfalls and interpretation. Curr Opin Rheumatol, 2017; 29(4): 402-409.

409. Qasim M, Farinella G, Zhang J, Li X, Yang L, Eastell R, Viceconti M. Patient-specific finite element estimated femur strength as predictor of the risk of hip fracture: the effect of methodological determinants. Osteoporos Int, 2016; 27(9): 2815-2822.

410. Amin S, Kopperdhal DL, Melton LJ 3rd, Achenbach SJ, Therneau TM, Riggs BL, Keaveny TM, Khosla S. Association of hip strength estimates by finite element analysis with fractures in women and men. J Bone Miner Res, 2011; 26(7): 1593-1600.

411. Orwoll ES, Marshall LM, Nielson CM, Cummings SR, Lapidus J, Cauley JA, Ensrud K, Lane N, Hoffmann PR, Kopperdahl DL, Keaveny TM for the Osteoporotic Fractures in

Men (MrOS) Study Group. Finite element analysis of the proximal femur and hip fracture risk in older men. J Bone Miner Res, 2009; 24(3): 475-483.

412. Boutroy S, van Rietbergen B, Sornay-Rendu E, Munoz F, Bouxsein M, Delmas PD. Finite element analysis based on in vivo HR-pQCT imgaes of the distal radius is associated with wrist fracture in postmenopausal women. J Bone Miner Res, 2008; 23(3): 392-399.

413. Melton LJ 3rd, Christen D, Riggs BL, Achenbach SJ, Muller R, van Lenthe GH, Amin S, Atkinton EJ, Khosla S. Assessment forearm fracture risk in postmenopausal women. Osteoporos Int, 2010; 21(7): 1161-1169.

414. Maatta M, Macdonald HM, Mulpuri K, MaKay HA. Deficits in distal radius bone strength, density and microstructure are associated with forearm fractures in girls: an HR-pQCT study. Osteoporos Int, 2015; 26(3): 1163-1174.

415. arr JN, Khosla S, Achenbach SJ, Atkinson EJ, Kirmani S, McCready LK, Melton LJ 3rd, Amin S. Diminished bone strength is observed in adult women and men who sustained a mild trauma distal forearm fracture during childhood. J Bone Miner Res, 2014; 29(10): 2193-2202.

416. Rozental TD, Johannesdottir F, Kempland KC, Bouxesein ML. Characterization of trabecular bone microstructure in premenopausal women with distal radius fractures. Osteoporos Int, 2018; 29: 409-419.

417. Wang J, Stein EM, Zhou B, Nishiyama KK, Yu YE, Shane E, Guo XE. Deterioration of trabecular plate-rod and cortical microarchitecture and reduced bone stiffness at distal radius and tibia in postmenopausal women with vertebral fractures. Bone, 2016; 88: 39-46.

418. Zhu TY, Hung VWY, Cheung W-H, Cheng JCY, Qin L, Leung K-S. Value of measuring bone microarchitecture in fracture discrimination in older women with recent hip fracture: a case-control study with HR-pQCT. Sci Rep, 2016; 6: 34185.

419. Chevalley T, Bonjour JP, van Rietbergen B, Rizzoli R, Ferrari S. Fractures in healthy females followed from childhood to early adulthood are associated with later menarcheal age and with impaired bone microstructure at peak bone mass. J Clin Endocrinol Metab, 2012; 97(11): 4174-4181.

420. Chevalley T, Bonjour JP, van Rietbergen B, Ferrari S, Rizzoli R. Fractures during childhood and adolescence in healthy boys: relation with bone mass, microstructure, and strength. J Clin Endocrinol Metab, 2011; 96(10): 3134-3142.

421. Rudang R, Darelid A, Nilsson M, Mellstrom D, Ohlsson C, Lorentzon M. X-ray-verified fractures are associated with finite element analysis-derived bone strength and trabecular microstructure in young adult men. J Bone Miner Res, 2013; 28(11): 2305-2316.

422. Burt LA, Manske SL, Hanley DA, Boyd SK. Lower bone density, impaired microarchitecture, and strength predict future fragility fracture in postmenopausal women: 5-year follow-up of the Calgary CaMos Cohort. J Bone Miner Res, 2018; 33(4): 589-597.

423. Szulc P, Boutroy S, Chapurlat R. Prediction of fractures in men using bone microarchitecture parameters assessed by high-resolution peripheral quantitative computed tomography- the prospective STRAMBO study. J Bone Miner Res, 2018; 33(8): 1470-1479.

424. Sornay-Rendu E, Boutroy S, Duboeuf F, Chapurlat RD. Bone microstructure assessed by HR-pQCT as predictor of fracture risk in postmenopausal women: the OFELY study. J Bone Miner Res, 32(6): 1243-1251.

425. Biver E, Durosier-Izart C, Chevalley T, van Rietbergen B, Rizzoli R, Ferrari S. Evaluation of radius microstructure and areal bone mineral density improves fracture prediction in postmenopausal women. J Bone Miner Res, 2018; 33(2): 328-337.

426. Ohlsson C, Sundh D, Wallerek A, Nilsson M, Karlsson M, Johansson H, Mellstrom D, Lorentzon M. Cortical bone area predicts incident fractures independently of areal bone mineral density in older men. J Clin Endocrinol Metab, 2017; 102(2): 516-524.

427. Bray F, Ferlay J, Soerjomataram I, Siegel RL, Torre LA, Jemal A. Global cancer statistics 2018: GLOBOCAN estimates of incidence and mortality worldwide for 36 cancers in 185 countries. CA Cancer J Clin, 2018; 68(6): 394-424.

428. Ferlay J, Colombet M, Soerjomataram I, Mathers C, Parkin DM, Pineros M, Znaor A, Bray F. Estimating the global cancer incidence and mortality in 2018: GLOBAN sources and methods. In J Cancer, 2019; 144(8): 1941-1953.

429. Webb PM, Jordan SJ. Epidemiology of epithelial ovarian cancer. Best Pract Res Clin Obstet Gynaecol, 2017; 41: 3-14.

430. Meinhold-Heerlein I, Fotopoulou C, Harter P, Kurzeder C, Mustea A, Wimberger P, Hauptmann S, Sehouli J. The new WHO classification of ovarian, fallopian tube, and primary peritoneal cancer and its clinical implications. Arch Gynecol Obstet, 2016; 293(4): 695-700.

431. Kaku T, Ogawa S, Kawano Y, Ohishi Y, Kobayashi H, Hirakawa T, Nakano H. Histological classification of ovarian cancer. Med Electrron Microsc, 2003; 36(1): 9-17.

432. Berek JS, Bast RC. Epithelial ovarian cancer. In: Kufe DW, Pollock RE, Weichselbaum RR, Bast RC Jr, Gansler TS, Holland JF, Frei E 3rd. Holland-Frei cancer medicine, 6th edition. Hamilton (ON), BC Decker, 2003.

433. Stratton J, Pharoah P, Smith SK, Easton D, Ponder BAJ. A systematic review and meta-analysis of family history and risk of ovarian cancer. Br J Obstet Gynaecol, 1998; 105(5): 493-499.

434. Jervis S, Song H, Lee A, Dicks E, Tyrer J, Harrington P, Easton DF, Jacobs IJ, Pharoah PP, Antoniou AC. Ovarian cancer familial relative risks by tumour subtypes and by known ovarian cancer genetic susceptibility variants. J Med Genet, 2014; 51(2): 108-113.

435. Alsop K, Fereday S, Meldrum C, DeFazio A, Emmanuel C, George J, Dobrovic A, Birrer MJ, Webb PM, Stewart C, Friedlander M, Fox S, Bowtell D, Mitchell G. BRCA mutation frequency and patterns of treatment response in BRCA mutation-positive women with ovarian cancer: a report from the Australian Ovarian Cancer Study Group. J Clin Oncol, 2012; 30(21): 2654-2663.

436. Brody LC, Biesecker BB. Breast cancer susceptibility genes. BRCA1 and BRCA2. Medicine (Baltimore), 1998; 77(3): 208-226.

437. Gorodetska I, Kozeretska I, Dubrovska A. BRCA genes: the role in genome stability, cancer stemness and therapy resistance. J Cancer, 2019; 10(9): 2109-2127.

438. Venkiraraman AR. Cancer suppression by the chromosome custodians, BRCA1 and BRCA2. Science, 2014; 343(6178): 1470-1475.

439. Mullan PB, Quinn JE, Gilmore PM, McWilliams S, Andrews H, Gervin C, McCabe N, Mckenna S, White O, Song YH, Maheswaran S, Liu E, Haber DA. BRCA1 and

GADD45 mediated G2/M cell cycle arrest in response to antimicrotubule agents. Oncogene, 2001; 20(43): 6123-6131.

440. Martinez-Outschoorn UE, Balliet R, Lin Z, Whitaker-Menezes D, Birbe RC, Bombonati A, Pavlides S, Lamb R, Sneddon S, Howell A, Sotgia F, Lisanti MP. BRCA1 mutations drive oxidative stress and glycolysis in the tumor microenvironment: implications for breast cancer prevention with antioxidant therapies. Cell Cycle, 2012; 11(23): 4402-4413.

441. Mansour MA. Ubiquitination: friend and foe in cancer. Int J Biochem Cell Biol, 2018; 101: 80-93.

442. Lee EY, Abbondante S. Tissue-specific tumor suppression by BRCA1. Proc Natl Acad Sci U S A, 2014; 111(12): 4353-4354.

443. Lee MV, Katabathina VS, Bowerson ML, Mityul MI, Shetty AS, Elsayes KM, Balachandran A, Bhosale PR, McCullough AE, Menias CO. BRCA-associated cancers: role of imaging in screening, diagnosis, and management. Radiographics, 2017; 37(4): 1005-1023.

444. Boyd J. Specific keynote: hereditary ovarian cancer: what we know. Gynecol Oncol, 2003; 88(1 Pt 2): S8-10.

445. Nakamura K, Banno K, Yanokura M, Iida M, Adachi M, Masuda K, Ueki A, Kobayashi Y, Nomura H, Hirasawa A, Tominaga E, Aoki D. Features of ovarian cancer in Lynch syndrome (review). Mol Clin Oncol, 2014; 2(6): 909-916.

446. Kuiper RP, Vissers LE, Venkatachalam R, Bodmer D, Hoenselaar E, Goossens M, Haufe A, Kamping E, Niessen RC, Hogervorst FB, Gille JJ, Redeker B, Tops CM, van Gijn ME, van den Ouweland AM, Rahner N, Steinke V, Kahl P, Holinski-Feder E, Morak M, Kloor M, Stemmler S, Betz B, Hutter P, Bunyan DJ, Syngal S, Culver JO, Graham T,

Chan TL, Nagtegaal ID, van Krieken JH, Schackert HK, Hoogerbrugge N, van Kessel AG, Ligtenberg MJ. Recurrence and variability of germline EPCAM deletions in Lynch syndrome. Hum Mutat, 2011; 32(4): 407-14.

447. Harfe BD, Jinks-Robertson S. DNA mismatch repair and genetic instability. Annu Rev Genet, 2000; 34: 359-399.

448. Jascur T, Boland CR. Structure and function of the components of the human DNA mismatch repair system. Int J Cancer, 2006; 119(9): 2030-2035.

449. Li FP, Fraumeni JF Jr. Rhabdomyosarcoma in children: epidemiologic study and identification of a familial cancer syndrome. J Natl Cancer Inst, 1969; 43(6): 1365-1373.

450. Lane DP. Cancer. P53, guardian of the genome. Nature, 1992; 358(6381): 15-16.

451. Tabori U, Baskin B, Shago M, Alon N, Taylor MD, Ray PN, Bouffet E, Malkin D, Hawkins C. J Clin Oncol, 2010; 28(8): 1345-1350.

452. Fernandez-Cuesta L, Oakman C, Falagan-Lotsch P, Smoth KS, Quinaux E, Buyse M, Dolci MS, Azambuja ED, Hainaut P, Dell'orto P, Larsimont D, Francis PA, Crown J, Piccart-Gebhart M, Viale G, Leo AD, Olivier M. Prognostic and predictive value of TP53 mutations in node-positive breast cancer patients treated with anthracycline- or anthracycline/taxane-based adjuvant therapy: results from the BIG 02-98 phase III trial. Breast Cancer Res, 2012; 14(3): R70.

453. Toss A, Tomasello C, Razzaboni E, Contu G, Grandi G, Cagnacci A, Schilder RJ, Cortesi L. Hereditary ovarian cancer: not only BRCA 1 and 2 genes. Biomed Res Int, 2015; 341723.

454. Song H, Dicks E, Ramus SJ, Tyrer JP, Intermaggio MP, Hayward J, Edlund CK, Conti D, Harrington P, Fraser L, Philpott S, Anderson C, Rosenthal A, Gentry-Maharaj A, Bowtell

DD, Alsop K, Cicek MS, Cunningham JM, Fridley BL, Alsop J, Jimenez-Linan M, Hogdall E, Hogdall CK, Jensen A, Kruger Kjaer S, Lubinski J, Huzarski T, Jakubowska A, Gronwald J, Poblete S, Lele S, Sucheston-Campbell L, Moysich KB, Odunsi K, Goode EL, Menon U, Jacobs IJ, Gayther SA, Pharoah PDP. Contribution of germline mutations in the RAD51B, RAD51C, and RAD51D genes to ovarian cancer in the population. J Clin Oncol, 2015; 33(26): 2901-2907.

455. Ramus SJ, Song H, Dicks E, Tyrer JP, Rosenthal AN, Intermaggio MP, Fraser L, Gentry-Maharaj A, Hayward J, Philpott S, Anderson C, Edlund CK, Conti D, Harrington P, Barrowdale D, Bowtell DD, Alsop K, Mitchell G, ACOS Study Group, Cicek MS, Cunningham JM, Fridley BL, Alsop J, Jimenez-Linan M, Poblete S, Lele S, Sucheston-Campbell L, Moysich KB, Sieh W, McGuire V, Lester J, Bogdanova N, Durst M, Hillemanns P, Ovarian Cancer Association Consortium, Odunsi K, Whittemore AS, Karlan BY, Dork T, Goode EL, Menon U, Jacobs IJ, Antoniou AC, Pharoah PDP, Gayther SA. Germline mutations in the BRIP1, BARD1, PALB2, and NBN genes in women with ovarian cancer. J Natl Cancer Inst, 2015; 107(11): djv214.

456. Olsen CM, Nagle CM, Whiteman DC, Ness R, Pearce CL, Pike MC, Rossing MA, Terry KL, Wu AH; Australian Cancer Group Study (Ovarian Cancer); Australian Ovarian Cancer Study Group, Risch HA, Yu H, Doherty JA, Chang-Claude J, Hein R, Nickels S, Wang-Gohrke S, Goodman MT, Carney ME, Matsuno RK, Lurie G, Moysich K, Kjaer SK, Jensen A, Hogdall E, Goode EL, Fridley BL, Vierkant RA, Larson MC, Schildkraut J, Hoyo C, Moorman P, Weber RP, Cramer DW, Vitonis AF, Bandera EV, Olson SH, Rodriguez-Rodriguez L, King M, Brinton LA, Yang H, Garcia-Closas M, Lissowska J, Anton-Culver H, Ziogas A, Gayther SA, Ramus SJ, Menon U, Gentry-Maharaj A, Webb

PM; Ovarian Cancer Association Consortium. Obesity and risk of ovarian cancer subtypes: evidence from the Ovarian Cancer Association Consortium. Endocri Relat Cancer, 2013; 20(2): 251-262.

457. Collaborative Group on Epidemiological Studies of Ovarian Cancer. Ovarian cancer and body size: individual participant meta-analysis including 25157 women with ovarian cancer from 47 epidemiological studies. PLoS Medicine, 2012; 9(4): e1001200.

458. Dixon-Suen SC, Nagle CM, Thrift AP, Pharoah PDP, Ewing A, Pearce CL, Zheng W; Australian Ovarian Cancer Study Group, Chenevix-Trench G, Fasching PA, Beckmann MW, Lambrechts D, Vergote I, Lambrechts S, Van Nieuwenhuysen E, Rossing MA, Doherty JA, Wicklund KG, Chang-Claude J, Jung AY, Moysich KB, Odunsi K, Goodman MT, Wilkens LR, Thompson PJ, Shvetsov YB, Dork T, Park-Simon TW, Hillemanns P, Bogdanova N, Butzow R, Nevanlinna H, Pelttari LM, Leminen A, Modugno F, Ness RB, Edwards RP, Kelley JL, Heitz F, du Bois A, Harter P, Schwaab I, Karlan BY, Lester J, Orsulic S, Rimel BJ, Kjær SK, Høgdall E, Jensen A, Goode EL, Fridley BL, Cunningham JM, Winham SJ, Giles GG, Bruinsma F, Milne RL, Southey MC, Hildebrandt MAT, Wu X, Lu KH, Liang D, Levine DA, Bisogna M, Schildkraut JM, Berchuck A, Cramer DW, Terry KL, Bandera EV, Olson SH, Salvesen HB, Thomsen LCV, Kopperud RK, Bjorge L, Kiemeney LA, Massuger LFAG, Pejovic T, Bruegl A, Cook LS, Le ND, Swenerton KD, Brooks-Wilson A, Kelemen LE, Lubiński J, Huzarski T, Gronwald J, Menkiszak J, Wentzensen N, Brinton L, Yang H, Lissowska J, Hogdall CK, Lundvall L, Song H, Tyrer JP, Campbell I, Eccles D, Paul J, Glasspool R, Siddiqui N, Whittemore AS, Sieh W, McGuire V, Rothstein JH, Narod SA, Phelan C, Risch HA, McLaughlin JR, Anton-Culver H, Ziogas A, Menon U, Gayther SA, Ramus

SJ, Gentry-Maharaj A, Wu AH, Pike MC, Tseng CC, Kupryjanczyk J, Dansonka-Mieszkowska A, Budzilowska A, Rzepecka IK, Webb PM; Ovarian Cancer Association Consortium. Adult height is associated with increased risk of ovarian cancer: a Mendelian randomisation study. Br J Cancer, 2018; 118(8): 1123-1129.

459. Collaborative Group on Epidemiological Studies of Ovarian Cancer, Beral V, Gaitskell K, Hermon C, Moser K, Reeves G, Peto R. Ovarian cancer and smoking: individual participants meta-analysis including 28,114 women with ovarian cancer from 51 epidemiological studies. Lancet Oncol, 2012; 13(9): 946-956.

460. Faber MT, Kjær SK, Dehlendorff C, Chang-Claude J, Andersen KK, Høgdall E, Webb PM, Jordan SJ; Australian Cancer Study (Ovarian Cancer); Australian Ovarian Cancer Study Group, Rossing MA, Doherty JA, Lurie G, Thompson PJ, Carney ME, Goodman MT, Ness RB, Modugno F, Edwards RP, Bunker CH, Goode EL, Fridley BL, Vierkant RA, Larson MC, Schildkraut J, Cramer DW, Terry KL, Vitonis AF, Bandera EV, Olson SH, King M, Chandran U, Kiemeney LA, Massuger LF, van Altena AM, Vermeulen SH, Brinton L, Wentzensen N, Lissowska J, Yang HP, Moysich KB, Odunsi K, Kasza K, Odunsi-Akanji O, Song H, Pharaoh P, Shah M, Whittemore AS, McGuire V, Sieh W, Sutphen R, Menon U, Gayther SA, Ramus SJ, Gentry-Maharaj A, Pearce CL, Wu AH, Pike MC, Risch HA, Jensen A; Ovarian Cancer Association Consortium. Cigarette smoking and risk of ovarian cancer: a pooled analysis of 21 case-control studies. Cancer Causes Control, 2013; 24(5): 989-1004.

461. Gong TT, Wu QJ, Vogtmann E, Lin B, Wang YL. Age at menarche and risk of ovarian cancer: a meta-analysis of epidemiological studies. In J Cancer, 132(12): 2894-2900.

462. Wentzensen N, Poole EM, Trabert B, White E, Arslan AA, Patel AV, Setiawan VW, Visvanathan K, Weiderpass E, Adami HO, Black A, Bernstein L, Brinton LA, Buring J, Butler LM, Chamosa S, Clendenen TV, Dossus L, Fortner R, Gapstur SM, Gaudet MM, Gram IT, Hartge P, Hoffman-Bolton J, Idahl A, Jones M, Kaaks R, Kirsh V, Koh WP, Lacey JV Jr, Lee IM, Lundin E, Merritt MA, Onland-Moret NC, Peters U, Poynter JN, Rinaldi S, Robien K, Rohan T, Sandler DP, Schairer C, Schouten LJ, Sjoholm LK, Sieri S, Swerdlow A, Tjonneland A, Travis R, Trichopoulou A, van den Brandt PA, Wilkens L, Wolk A, Yang HP, Zeleniuch-Jacquotte A, Tworoger SS. Ovarian cancer risk factors by histologic subtype: an analysis from the Ovarian Cancer Cohort Consortium. J Clin Oncol, 2016; 34(24): 2888-2898.

463. Whittemore AS, Harris R, Itnyre J. Characteristics relating to ovarian cancer risk: collaborative analysis of 12 US case-control studies. ii. Invasive epithelial ovarian cancers in white women. Collaborative Ovarian Cancer Group. Am J Epidemiol, 1992; 136(10): 1184-1203.

464. Luan NN, Wu QJ, Gong TT, Vogtmann E, Wang YL, Lin B. Breastfeeding and ovarian cancer risk: a meta-analysis of epidemiologic studies. Am J Clin Nutr, 98(4): 1020-1031.

465. Collaborative Group on Epidemiological Studies on Ovarian Cancer, Beral V, Doll R, Hermon C, Peto R, Reeves G. Ovarian cancer and oral contraceptives: collaborative reanalysis of data from 45 epidemiological studies including 23,257 women with ovarian cancer and 87,303 controls. Lancet, 371(9609): 303-314.

466. Collaborative Group on Epidemiological Studies of Ovarian Cancer, Beral V, Gaitskell K, Hermon C, Moser K, Reeves G, Peto R. Menopausal hormone use and ovarian cancer

risk: individual participant meta-analysis of 52 epidemiological studies. Lancet, 2015; 385(9980): 1835-1842.

467. Henderson JT, Webber EM, Sawaya GF. Screening for ovarian cancer: updated evidence report and systematic review for the US Preventive Services Task Force. JAMA, 2018; 319(6): 595-606.

468. Lewis KE, Lu KH, Klimczak AM, Mok SC. Recommendations and choices for BRCA mutation carriers at risk for ovarian cancer: a complicated decision. Cancers, 2018; 10(2): 57.

469. Nelson HD, Pappas M, Zakher B, Mitchell JP, Okinaka-Hu L, Fu R. Risk assessment, genetic counselling, and genetic testing for BRCA-related cancer in women: a systematic review to update the U.S. preventive services task force recommendation. Ann Intern Med, 2014; 160(4): 255-266.

470. Finch AP, Lubinski J, Moller P, Singer CF, Karlan B, Senter L, Rosen B, Maehle L, Ghadirian P, Cybulski C, Huzarski T, Eisen A, Foulkes WD, Kim-Sing C, Ainsworth P, Tung N, Lynch HT, Neuhausen S, Metcalfe KA, Thompson I, Murphy J, Sun P, Narod SA. Impact of oophorectomy on cancer incidence and mortality in women with a BRCA1 or BRCA2 mutation.

471. Domchek SM, Friebel TM, Singer CF, Evans DG, Lynch HT, Isaacs C, Garber JE, Neuhausen SL, Matloff E, Eeles R, Pichert G, Van t'veer L, Tung N, Weitzel JN, Couch FJ, Rubinstein WS, Ganz PA, Daly MB, Olopade OI, Tomlinson G, Schildkraut J, Blum JL, Rebbeck TR. Association of risk-reducing surgery in BRCA1or BRCA2 mutation carriers with cancer risk and mortality. JAMA, 2010; 304(9): 967-975.

472. Vermeulen RFM, van Beurden M, Korse CM, Kenter GG. Impact of risk-reducing salpingo-oophorectomy in premenopausal women. Climacteric, 2017; 20(3): 212-22 1.

473. Shuster LT, Gostout BS, Grossardt BR, Rocca WA. Prophylactic oophorectomy in premenopausal women and long-term health. Menopause Int, 2008; 14: 111–116.

474. Rocca WA, Ulrich LG. Oophorectomy for whom and at what age? Primum non nocere. Maturitas, 2012; 71: 1–2.

475. Faubion SS, Kuhle CL, Shuster LT, Rocca WA. Long-term health consequences of premature or early menopause and considerations for management. Climacteric, 2015; 18(4): 483-491.

476. Garnero P, Sornay-Rendu E, Chapuy M, Delmas PD. Increased bone turnover in late postmenopausal women is a major determinant of osteoporosis. J Bone Miner Res, 1996; 11: 337-349.

477. Hannon R, Blumsohn A, Naylor K, Eastell R. Response of biochemical markers of bone turnover to hormone replacement therapy: impact of biological variability. J Bone Miner Res, 1998; 13: 1124-1133.

478. Lufkin EG, Wahner HW, O'Fallon WM, Hodgson SF, Kotowicz MA, Lane AW, Judd HL, Caplan RH, Riggs BL. Treatment of postmenopausal osteoporosis with transdermal estrogen. Ann Intern Med, 1992; 117: 1-9.

479. Bjarnason NH, Hassager C, Christiansen C. Postmenopausal bone remodelling and hormone replacement. Climacteric, 1998; 1: 72-79.

480. Torgerson DJ, Bell-Syer SE. Hormone replacement therapy and prevention of nonvertebral fractures: a meta-analysis of randomized controls. JAMA, 2001; 285: 2891-2897.

481. Gambacciani M, Levancini M. Hormone replacement therapy and the prevention of postmenopausal osteoporosis. Prz Menipauzalny, 2014; 13(4): 213-220.

482. Khosla S, Oursler MJ, Monroe DG. Estrogen and the skeleton. Trends Endocrinol Metab, 2012; 23(11): 576-581.

483. Tomkinson A, Reeve J, Shaw RW, Noble BS. The death of osteocytes via apoptosis accompanies estrogen withdrawal in human bone. J Clin Endocrinol Metab, 1997; 82: 3128-3135.

484. Tomkinson A, Gevers EF, Wit JM, Reeve J, Noble BS. The role of estrogen in the control of rat osteocyte apoptosis. J Bone Miner Res, 1998; 13: 1243–1250.

485. Emerton KB, Hu B, Woo AA, Sinofsky A, Hernandez C, Majeska RJ, Jepsen KJ, Schaffler MB. Osteocyte apoptosis and control of bone resorption following ovariectomy in mice. Bone, 2010; 46: 577-583.

486. Marathe N, Rangaswami H, Zhuang S, Boss GR, Pilz RB. Pro-survival effects of 17β-estradiol on osteocytes are mediated by NO/cGMP via differential actions of PKG I and II. J Biol Chem, 2011; 287(2): 978-988.

487. Oursler MJ, Osdoby P, Pyfferoen J, Riggs BL, Spelsberg TC. Avian osteoclasts as estrogen target cells. Proc Natl Acad Sci USA, 1991; 88: 6613–6617.

488. Manolagas SC. Birth and death of bone cells: basic regulatory mechanisms and implications for the pathogenesis and treatment of osteoporosis. Endocr Rev, 2000; 21(2): 115-137.

489. Kameda T, Mano H, Yuasa T, Mori Y, Miyazawa K, Shiokawa M, Nakamaru Y, Hiroi E, Kameda A, Yang NN, Hakeda Y, Kumegawa M. Estrogen inhibits bone resorption by

directly inducing apoptosis of the bone-resorbing osteoclasts. J Exp Med, 1997; 186(4): 489-495.

490. Riggs BL. The mechanisms of estrogen regulation of bone resorption. J Clin Invest, 2000; 106(10): 1203-1204.

491. Huber DM, Bendixen AC, Pathrose P, Srivastava S, Dienger KM, Shevde NK, Pike JW. Androgens suppress osteoclast formation induced by RANKL and macrophage-colony stimulating factor. Endocrinology, 2001; 142: 3800-3808.

492. Srivastava S, Toraldo G, Weitzmann MN, Cenci S, Ross FP, Pacifici R. Estrogen decreases osteoclast formation by down-regulating receptor activator of NF-kB ligand (RANKL)-induced JNK activation. J Biol Chem, 2001; 276: 8836-8840.

493. Eghbali-Fatourechi G, Khosla S, Sanyal A, Boyle WJ, Lacey DL, Riggs BL. Role of RANK ligand in mediating increased bone resorption in early postmenopausal women. J Clin Invest, 2003; 111: 1221-1230.

494. Roggia C, Gao Y, Cenci S, Weitzmann MN, Toraldo G, Isaia G, Pacifici R. Up-regulation of TNF-producing T cells in the bone marrow: a key mechanism by which estrogen deficiency induces bone loss in vivo. Proc Natl Acad Sci U S A, 2001; 98: 13960-13965.

495. Cenci S, Weitzmann MN, Roggia C, Namba N, Novack D, Woodring J, Pacifici R. Estrogen deficiency induces bone loss by enhancing T-cell production of TNF-a. J Clin Invest, 2000; 106: 1229-1327.

496. Kousteni S, Bellido T, Plotkin LI, O'Brien CA, Bodenner DL, Han L, Han K, DiGregorio GB, Katzenellenbogen JA, Katzenellenbogen BS, Roberson PK, Weinstein RS, Jilka RL,

Manolagas SC. Nongenotropic, sex-nonspecific signaling through the estrogen or androgen receptors: dissociation from transcriptional activity. Cell, 2001; 104: 719-730.

497. Kousteni S, Han L, Chen JR, Almeida M, Plotkin LI, Bellido T, Manolagas SC. Kinase-mediated regulation of common transcription factors accounts for the bone-protective effects of sex steroids. J Clin Invest, 2003; 111: 1651-1664.

498. Almeida M, Martin-Millan M, Plotkin LI, Stewart SA, Roberson PK, Kousteni S, O'Brien CA, Bellido T, Parfitt AM, Weinstein RS, Jilka RL, Manolagas SC. Skeletal involution by associated oxidative stress and its acceleration by loss of sex steroids. J Biol Chem, 2007; 282: 27285-27297.

499. Manolagas SC, Almeida M. Gone with the Wnts: beta-catenin, t-cell factor, forkhead box O, and oxidative stress in age-dependent diseases of bone, lipid, and glucose metabolism. Mol Endocrinol, 2007; 21: 2605-2614.

500. Chang J, Wang Z, Tang E, Fan Z, McCauley L, Franceschi R, Guan K, Krebsbach PH, Wang C-Y. Inhibition of osteoblastic bone formation by nuclear factor-kappaB. Nat Med, 2009; 15: 682-689.

501. Sidon L, Ingham S, Clancy T, Clayton R, Clarke A, Jones EA, Lalloo F, Evans DG. Uptake of risk-reducing salpingo-oophorectomy in women carrying a BRCA1 or BRCA2 mutation: evidence for lower uptake in women affected by breast cancer and older women. Br J Cancer, 2012; 106(4): 775-779.

502. Chapman JS, Powell CB, McLennan J, Crawford B, Mak J, Stewart N, Chen L. Surveillance of survivors: follow-up after risk-reducing salpingo-oophorectomy in BRCA 1/2 mutation carriers. Gynecol Oncol, 2011; 122(2): 339-343.

503. Garcia C, Lyon L, Conell C, Littell RD, Powell CB. Osteoporosis risk and management in BRCA1 and BRCA2 carriers who undergo risk-reducing salpingo-oophorectomy. Gynecol Oncol, 2015; 138: 723-726.

504. Cohen JV, Chiel L, Boghossian L, Jones M, Stopfer JE, Powers J, Rebbeck TR, Nathanson KL, Domchek SM. Non-cancer endpoints in BRCA1/2 carriers after risk-reducing salpingo-oophorectomy. Fam Cancer, 2012; 11(1): 69-75.

505. Michelsen TM, Dorum A, Dahl AA. A controlled study of mental distress and somatic complaints after risk-reducing salpingo-oophorectomy in women at risk for hereditary breast ovarian cancer. Gynecol Oncol, 2009; 113: 128-133.

506. Powell CB, Alabaster A, Stoller N, Armstrong MA, Salyer C, Hamilton I, Raine-Bennett T. Bone loss in women with BRCA1 and BRCA2 mutations. Gynecol Oncol, 2018; 148(3): 535-539.

507. Challberg J, Ashcroft L, Lalloo F, Eckersley B, Clayton R, Hopwood P, Selby P, Howell A, Evans DG. Menopausal symptoms and bone health in women undertaking risk reducing bilateral salpingo-oophorectomy: significant bone health issues in those not taking HRT. Br J Cancer, 2011; 105(1): 22-27.

508. Hibler E, Kauderer J, Greene MH, Rodriguez GC, Alberts DS. Bone loss following oophorectomy among high-risk women: an NRG oncology/gynecologic oncology group study. Menopause, 2016; 23(11): 1228-1232.

509. Kotsopoulos J, Hall E, Finch A, Hu H, Murphy J, Rosen B, Narod SA, Cheung AM. Changes in bone mineral density after prophylactic bilateral salpingo-oophorectomy in carriers of a BCRA mutation. JAMA Netw Open, 2019; 2(8): e198420.

510. Fakkert IE, Abma EM, Westrik IG, Lefrandt JD, Wolffenbuttel BH, Oosterwijk JC, Slart RH, van der Veer E, de Bock GH, Mourits MJ. Bone mineral density and fractures after risk-reducing salpingo-oophorectomy in women at increased risk for breast and ovarian cancer. Eur J Cancer, 2015; 51(3): 400-408.

511. Fakkert IE, Teixeira N, Abma EM, Slart RHJA, Mourits MJE, de Bock GH. Bone mineral density and fractures after surgical menopause: systematic review and meta-analysis. BJOG 2017; 124: 1525-1535.

512. American Diabetes Association. Diagnosis and classification of diabetes mellitus. Diabetes Care, 2009; 32(Suppl 1): S62-S67.

513. Maahs DM, West NA, Lawrence JM, Mayer-Davis EJ. Epidemiology of type 1 diabetes. Endocrinol Metab Clin North Am, 2010; 39(3): 481-497.

514. SEARCH for Diabetes in Young Study Group, Liese AD, D'Agostino RB Jr, Hamman RF, Kilgo PD, Lawrence JM, Liu LL, Loots B, Linder B, Marcovina S, Rodriguez B, Standiford D, Williams DE. The burden of diabetes mellitus among US youth: prevalence estimates from the SEARCH for Diabetes in Young Study. Pediatrics, 2006; 118(4): 1510-1518.

515. Writing Group for the SEARCH for Diabetes in Youth Study Group, Dabelea D, Bell RA, D'Agostino RB Jr, Imperatore G, Johansen JM, Linder B, Liu LL, Loots B, Marcovina S, Mayer-Davis EJ, Pettitt DJ, Waitzfelder B. Incidence of diabetes in youth in the United States. JAMA, 2007; 297(24): 2716-2724.

516. DIAMOND Project Group. Incidence and trends of childhood Type 1 diabetes worldwide 1990-1999. Diabet Med, 2006; 23(8): 857-866.

517. WHO Diamond Project Group. WHO multinational project for childhood diabetes. Diabetes Care, 1990; 13(10): 1062-1068.

518. SEARCH Study Group. SEARCH for Diabetes in Youth: a multicentre study of the prevalence, incidence and classification of diabetes mellitus in youth. Control Clin Trials, 2004; 25(5): 458-471.

519. Vehik K, Hamman RF, Lezotte D, Norris JM, Klingensmith G, Bloch C, Rewers M, Dabelea D. Increasing incidence of type 1 diabetes in 0- to 17-yearold Colorado youth. Diabetes care, 2007; 30(3): 503-509.

520. Green A, Gale EAM, Patterson CC. Incidence of childhood-onset insulin-dependent diabetes mellitus: the EURODIAB ACE study. Lancet, 1992; 339(8798): 905-909.

521. EURODIAB ACE Study Group. Variation and trends in incidence of childhood diabetes in Europe. Lancet, 2000; 355(9207): 873-876.

522. Hermann R, Knip M, Veijola R, Simell O, Laine AP, Akerblom HK, Groop PH, Forsblom C, Petterson-Fernholm K, Ilonen J; FinnDiane Study Group. Temporal changes in the frequencies of HLA genotypes in patients with Type 1 diabetes- indication of an increased environmental pressure? Diabetologia 2003; 46(3): 420-425.

523. Kaila B, Dean HJ, Schroeder M, Taback SP. HLA, day care attendance, and socio-economic status in young patients with Type 1 diabetes. Diabet Med, 2003; 20(9): 777-779.

524. Gillespie KM, Bain SC, Barnett AH, Bingley PJ, Christie MR, Gill GV, Gale EA. The rising incidence of childhood type 1 diabetes and reduced contribution of high-risk HLA haplotypes. Lancet, 2004; 364(9446): 1699-1700.

525. Redondo MJ, Fain PR, Eisenbarth GS. Genetics of type 1A diabetes. Recent Prog Horm Res, 2001; 56: 69-89.

526. Mehers KL, Gillespie KM. The genetic basis for type 1 diabetes. Br Med Bull, 2008; 88: 115-129.

527. Virtanen SM, Knip M. Nutritional risk predictors of beta cell autoimmunity and type 1 diabetes at a young age. Am J Clin Nutr, 2003; 78: 1053-1067.

528. Vandewalle CL, Coeckelberghs MI, De Leeuw IH, Du Caju MV, Schuit FC, Pipeleers DG, Gorus FK. Epidemiology, clinical aspects, and biology of IDDM patients under age 40 years. Comparison of data from Antwerp with complete ascertainment with data from Belgium with 40% ascertainment. The Belgian Diabetes Registry. Diabetes Care, 1997; 20(10): 1556-1561.

529. Thunander M, Petersson C, Jonzon K, Fornander J, Ossiansson B, Torn C, Edvardsson S, Landin-Olsson M. Incidence of type 1 and type 2 diabetes in adults and children in Kronoberg, Sweden. Diabetes Res Clin Pract, 2008; 82(2): 247-255.

530. Patterson CC, Dahlquist GG, Gyurus E, Green A, Soltesz G; EURODIAB Study Group. Incidence trends for childhood type 1 diabetes in Europe during 1989–2003 and predicted new cases 2005–20: a multicentre prospective registration study. Lancet, 2009; 373(9680): 2027-2033.

531. Mayer-Davis EJ, Bell RA, Dabelea D, D'Agostino R Jr, Imperatore G, Lawrence JM, Liu L, Marcovina S; SEARCH for Diabetes in Youth Study Group. The many faces of diabetes in American youth: type 1 and type 2 diabetes in five race and ethnic populations: the SEARCH for Diabetes in Youth Study. Diabetes Care, 2009; 32(Suppl 2): S99-S101.

532. Bell RA, Mayer-Davis EJ, Beyer JW, D'Agostino RB Jr, Lawrence JM, Linder B, Liu LL, Marcovina SM, Rodriguez BL, Williams D, Dabelea D; SEARCH for Diabetes in Youth Study Group. Diabetes in non-Hispanic white youth: prevalence, incidence, and clinical characteristics: the SEARCH for Diabetes in Youth Study. Diabetes Care, 2009; 32(Suppl 2): S102-S111.

533. Mayer-Davis EJ, Beyer J, Bell RA, Dabelea D, D'Agostino R Jr, Imperatore G, Lawrence JM, Liese AD, Liu L, Marcovina S, Rodriguez B; SEARCH for Diabetes in Youth Study Group. Diabetes in African American youth: prevalence, incidence, and clinical characteristics: the SEARCH for Diabetes in Youth Study. Diabetes Care, 2009; 32(Suppl2): S112-S122.

534. Lawrence JM, Mayer-Davis EJ, Reynolds K, Beyer J, Pettitt DJ, D'Agostino RB Jr, Marcovina SM, Imperatore G, Hamman RF; SEARCH for Diabetes in Youth Study Group. Diabetes in Hispanic American youth: prevalence, incidence, demographics, and clinical characteristics: the SEARCH for Diabetes in Youth Study. Diabetes Care, 2009; 32(Suppl 2): S123-S132.

535. Liu LL, Yi JP, Beyer J, Mayer-Davis EJ, Dolan LM, Dabelea DM, Lawrence JM, Rodriguez BL, Marcovina SM, Waitzfelder BE, Fujimoto WY; SEARCH for Diabetes in Youth Study. Type 1 and Type 2 diabetes in Asian and Pacific Islander U.S. youth: the SEARCH for Diabetes in Youth Study. Diabetes Care, 2009; 32(Suppl 2): S133-S140.

536. Dabelea D, DeGroat J, Sorrelman C, Glass M, Percy CA, Avery C, Hu D, D'Agostino RB, Jr, Beyer J, Imperatore G, Testaverde L, Klingensmith G, Hamman RF; SEARCH for Diabetes in Youth Study Group. Diabetes in Navajo youth: prevalence, incidence, and

clinical characteristics: the SEARCH for Diabetes in Youth Study. Diabetes Care, 2009; 32(Suppl 2): S141-S147.

537. Soltesz G, Patterson CC, Dahlquist G; EURODIAB Study Group. Worldwide childhood type 1 diabetes incidence- what can we learn from epidemiology? Pediatri Diabetes, 2007; 8(Suppl 6): 6-14.

538. Karvonen M, Pikaniemi M, Pikaniemi J, Kohtamaki K, Tajima N, Tuomilehto J. Sex difference in the incidence of insulin-dependent diabetes mellitus: an analysis of the recent epidemiological data. World Health Organization DIAMOND Project Group. Diabetes Metab Rev, 1997; 13(4): 275-291.

539. Gale EA, Gillespie KM. Diabetes and gender. Diabetologia, 2001; 44(1): 3-15.

540. Weets I, De Leeuw IH, Du Caju MV, Rooman R, Keymeulen B, Mathieu C, Rottiers R, Daubresse JC, Rocour-Brumioul D, Pipeleers DG, Gorus FK; Belgian Diabetes Registry. The incidence of type 1 diabetes in the age group 0–39 years has not increased in Antwerp (Belgium) between 1989 and 2000: evidence for earlier disease manifestation. Diabetes Care, 2002; 25(5): 840-846.

541. Pundziute-Lycka A, Dahlquist G, Nystrom L, Arnqvist H, Bjork E, Blohme G, Bolinder J, Eriksson JW, Sundkvist G, Ostman J; Swedish Childhood Diabetes Study Group. The incidence of Type I diabetes has not increased but shifted to a younger age at diagnosis in the 0–34 years group in Sweden 1983–1998. Diabetologia, 2002; 45(6): 783-791.

542. Kyvik KO, Nystrom L, Gorus F, Songini M, Oestman J, Castell C, Green A, Guyrus E, Ionescu-Tigoviste C, McKinney PA, Michalkova D, Ostrauskas R, Raymond NT. The epidemiology of Type 1 diabetes mellitus is not the same in young adults as in children. Diabetologia, 2004; 47(3): 377-384.

543. Kahn HS, Morgan TM, Case LD, Dabelea D, Mayer-Davis EJ, Lawrence JM, Marcovina SM, Imperatore G; SEARCH for Diabetes in Youth Study Group. Association of type 1 diabetes with month of birth among U.S. youth: The SEARCH for Diabetes in Youth Study. Diabetes Care, 2009; 32(11): 2010-2015.

544. Vaiserman AM, Carstensen B, Voitenko VP, Tronko MD, Kravchenko VI, Khalangot MD, Mechova LV. Seasonality of birth in children and young adults (0–29 years) with type 1 diabetes in Ukraine. Diabetologia, 2007; 50(1): 32-35.

545. McKinney PA, EURODIAB Seasonality of Birth Group. Seasonality of birth in patients with childhood Type I diabetes in 19 European regions. Diabetologia, 2001; 44(Suppl 3): B67-B74.

546. Willis JA, Scott RS, Darlow BA, Lewy H, Ashkenazi I, Laron Z. Seasonality of birth and onset of clinical disease in children and adolescents (0–19 years) with type 1 diabetes mellitus in Canterbury, New Zealand. J Pediatr Endocrinol Metab, 2002; 15(5): 645-647.

547. Laron Z, Shamis I, Nitzan-Kaluski D, Ashkenazi I. Month of birth and subsequent development of type I diabetes (IDDM). J Pediatr Endocrinol Metab, 1999; 12(3): 397-402.

548. Mathieu C, Gysemans C, Giulietti A, Bouillon R. Vitamin D and diabetes. Diabetologia, 2005; 48: 1247-1257.

549. Mohr SB, Garland CF, Gorham ED, Garland FC. The association between ultraviolet B irradiance, vitamin D status and incidence rates of type 1 diabetes in 51 regions worldwide. Diabetologia, 2008; 1391-1398.

550. Mayer EJ, Hamman RF, Gay EC, Lezotle DC, Savitz Da, Klingensmith GJ. Reduced risk of IDDM among breast-fed children. The Colorado IDDM Registry. Diabetologia, 1988; 37: 1625-1632.

551. Bodington MJ, McNally PG, Burden AC. Cow's milk and Type 1 childhood diabetes: No increase in risk. Diabet Med, 1994; 11: 663-665.

552. Norris JM, Beaty B, Klingensmith G, et al. Lack of association between early exposure to cow's milk protein and beta-cell autoimmunity. Diabetes Autoimmunity Study in the Young (DAISY). JAMA, 1996; 276: 609-614.

553. Virtanen SM, Hypponen E, Laara E, Vahasalo P, Kulmala P, Savola K, Rasanen L, Aro A, Knip M, Akerblom HK. Cow's milk consumption, disease-associated autoantibodies and type 1 diabetes mellitus: a follow-up study in siblings of diabetic children. Childhood Diabetes in Finland Study Group. Diabet Med, 1998; 15: 730-738.

554. Virtanen SM, Kenward MG, Erkkola M, Kautiainen S, Kronberg-Kippila C, Hakulinen T, Ahonen S, Uusitalo L, Niinisto S, Veijola R, Simell O, Ilonen J, Knip M. Age at introduction of new foods and advanced beta cell autoimmunity in young children with HLA-conferred susceptibility to type 1 diabetes. Diabetologia, 2006; 49(7): 1512-1521.

555. Ziegler AG, Schmid S, Huber D, Hummel M, Bonifacio E. Early infant feeding and risk of developing type 1 diabetes-associated autoantibodies. JAMA 2003; 290: 1721-1728.

556. Knekt P, Reunanen A, Marniemi J, Leino A, Aromaa A. Low vitamin E status is a potential risk factor for insulin-dependent diabetes mellitus. J Intern Med, 1999; 245: 99-102.

557. Atkinson MA, Bluestone JA, Eisenbarth GS, Hebrok M, Herold KC, Accili D, Pietropaolo M, Arvan PR, Von Herrath M, Markel DS, Rhodes CJ. How does type 1

diabetes develop? The notion of homicide or β-cell suicide revisited. Diabetes, 2011; 60(5): 1370-1379.

558. Atkinson MA, Eisenbarth GS, Michels AW. Type 1 diabetes. Lancet, 2014; 383(9911): 69-82.

559. Atkinson MA. The pathogenesis and natural history of Type 1 diabetes. Cold Spring Harb Perspect Med, 2012; 2(11): a007641.

560. Meier JJ, Bhushan A, Butler AW, Rizza RA, Butler PC. Sustained beta cell apoptosis in patients with long-standing type 1 diabetes: indirect evidence for islet regeneration? Diabetologia, 2005; 48(11): 2221-2228.

561. Eisenbarth GS. Type I diabetes mellitus. A chronic autoimmune disease. N Engl J Med, 1986; 314(21): 1360-1368.

562. Akirav E, Kushner JA, Herold KC. Beta-cell mass and type 1 diabetes: going, going, gone? Diabetes, 2008; 57(11): 2883-2888.

563. Sosenko JM, Skyler JS, Krischer JP, Greenbaum CJ, Mahon J, Rafkin LE, Cuthbertson D, Cowie C, Herold K, Eisenbarth G, Palmer JP, Diabetes Prevention Trial- Type 1 Study Group. Glucose excursions between states of glycemia with progression to type 1 diabetes in the diabetes prevention trial-type 1 (DPT-1) Diabetes. Diabetes, 2010; 59(10): 2386-2389.

564. Ferrannini E, Mari A, Nofrate V, Sosenko JM, Skyler JS. Progression to diabetes in relatives of type 1 diabetic patients: mechanisms and mode of onset. Diabetes, 2010; 59: 679-85.

565. Greenbaum CJ, Beam CA, Boulware D, Gitelman SE, Gottlieb PA, Herold KC, Lachin JM, McGee P, Palmer JP, Pescovitz MD, Krause-Steinrauf H, Skyler JS, Sosenko JM;

Type 1 Diabetes TrialNet Study Group. Fall in C-peptide during first 2 years from diagnosis: evidence of at least two distinct phases from composite type 1 diabetes TrialNet data. Diabetes, 2012; 61(8): 2066-2073.

566. Shah VN, Carpenter RD, Ferguson VL, Schwartz AV. Bone health in type 1 diabetes. Curr Opin Endocrinol Diabetes Obes, 2018; 25(4): 231-236.

567. Palermo A, D'Onofrio L, Buzzetti R, Manfrini S, Napoli N. Pathophysiology of bone fragility in patients with diabetes. Calcif Tissue Int, 2017; 100(2): 122-132.

568. Vestergaard P. Discrepancies in bone mineral density and fracture risk in patients with type 1 and type 2 diabetes- a meta-analysis. Osteoporos Int, 2007; 18(4): 427-444.

569. Weber DR, Haynes K, Leonard MB, Willi SM, Denburg MR. Type 1 diabetes is associated with an increased risk of fracture across the life span: a population-based cohort study using the Health Improvement Network (THIN). Diabetes Care, 2015; 38(10): 1913-1920.

570. Shah VN, Shah CS, Snell-Bergeon JK. Type 1 diabetes and risk for fracture: meta-analysis and review of the literature. Diabet Med, 2015; 32(9): 1134-1142.

571. Gallacher SJ, Fenner JA, Fisher BM, Quin JD, Fraser WD, Logue FC, Cowan RA, Boyle IT, MacCuish. An evaluation of bone density and turnover in premenopausal women with type 1 diabetes mellitus. Diabet Med, 1993; 10: 129-133.

572. Hampson G, Evans C, Petitt RJ, Evans WD, Woodhead SJ, Peters JR, Ralston SH. Bone mineral density, collagen type 1 alpha 1 genotypes and bone turnover in premenopausal women with diabetes mellitus. Diabetologia, 1998; 41: 1314-1320.

573. Tuominen JT, Impivaara O, Puukka P, Rönnemaa T. Bone mineral density in patients with type 1 and type 2 diabetes. Diabetes Care, 1999; 22: 1196-1200.

574. Rachon D, Mysliwska J, Suchecka-Rachoń K, Semetkowska-Jurkiewicz B, Zorena K, Lysiak-Szydłowska W. Serum interleukin-6 levels and bone mineral density at the femoral neck in post-menopausalwomenwithType1diabetes. Diabet Med, 2003; 20: 475-480.

575. Liu EY, Wactawski-Wende J, DonahueRP, Dmochowski J, HoveyKM, Quattrin T. Does low bone mineral density start in post-teenage years inwomen with type 1 diabetes? Diabetes Care, 2003; 8: 2365-2369.

576. Strotmeyer ES, Cauley JA, Orchard TJ, Steenkiste AR, Dorman JS. Middle-aged premenopausal women with type 1 diabetes have lower bone mineral density and calcaneal quantitative ultrasound than nondiabetic women. Diabetes Care, 2006; 29: 306-311.

577. Neumann T, Samann A, Lodes S, Kastner B, Franke S, Kiehntopf M, Hemmelmann C, Lehmann T, Muller UA, Hein G, Wolf G. Glycaemic control is positively associated with prevalent fractures but not with bone mineral density in patients with Type 1 diabetes. Diabet Med, 2011; 28: 872-875.

578. Botushanov N, Yaneva M, Orbetzova M, Botushanova A. Bone mineral density in bulgarian patients with type 1 diabetes mellitus. J Osteopor Phys Act, 2014; 2: 1.

579. Miazgowski T, Pynka S, Noworyta-Zietara M, Krzyzanowska-Swiniarska B, Pikul R. Bone mineral density and hip structural analysis in type 1 diabetic men. Eur J Endocrinol, 2007; 156: 123-127.

580. Slade JM, Coe LM, Meyer RA, McCabe LR. Human bone marrow adiposity is linked with serum lipid levels not T1-diabetes. J Diabetes Complicat, 2012; 26: 1-9.

581. Lunt H, Florkowski CM, Cundy T, Kendall D, Brown LJ, Elliot JR, Wells JE, Turner JG. A population-based study of bone mineral density in women with longstanding type 1 (insulin dependent) diabetes. Diabetes Res Clin Pract, 1998; 40: 31-38.

582. Ingberg CM, Palmer M, Aman J, Arvidsson B, Schvarcz E, Berne C. Body composition and bone mineral density in longstanding type 1 diabetes. J Intern Med, 2004; 255: 392-398.

583. Rakic V, Davis WA, Chubb SA, Islam FM, Prince RL, Davis TM. Bone mineral density and its determinants in diabetes: the Fremantle Diabetes Study. Diabetologia, 2006; 49: 863-871.

584. Hamilton EJ, Rakic V, Davis WA, Chubb SA, Kamber N, Prince RL, Davis TM. Prevalence and predictors of osteopenia and osteoporosis in adults with Type 1 diabetes. Diabet Med, 2009; 26: 45-52.

585. Leidig-Bruckner G, Grobholz S, Bruckner T, Scheidt-Nave C, Nawroth P, Schneider JG. Prevalence and determinants of osteoporosis in patients with type 1 and type 2 diabetes mellitus. BMC Endocr Disord, 2014; 14: 33.

586. Starup-Linde J, Vestergaard P. Biochemical bone turnover markers in diabetes mellitus: a systematic review. Bone 2016; 82: 69-78.

587. Hygum K, Starup-Linde J, Harslof T, Vestergaard P, Langdahl BL. Mechanisms in endocrinology: diabetes mellitus, a state of low bone turnover: a systematic review and meta-analysis. Eur J Endocrinol 2017; 176: R137-R157.

588. Ishikawa K, Fukui T, Nagai T, Kuroda T, Hara N, Yamamoto T, Inagaki K, Hirano T. Type 1 diabetes patients have lower strength in femoral bone determined by quantitative computed tomography: a cross-sectional study. J Diabetes Investig, 2015; 6: 726-733.

589. Verroken C, Pieters W, Beddeleem L, Goemaere S, Zmierczak HG, Shadid S, Kaufman JM, Lapauw B. Cortical bone size deficit in adult patients with type 1 diabetes mellitus. J Clin Endocrinol Metab 2017; 102: 2887-2895.

590. Shanbhogue VV, Hansen S, Frost M, Jorgensen NR, Hermann AP, Henriksen JE, Brixen K. Bone geometry, volumetric density, microarchitecture, and estimated bone strength assessed by HR-pQCT in adult patients with type 1 diabetes mellitus. J Bone Miner Res 2015; 30: 2188-2199.

591. Abdalrahaman N, McComb C, Foster JE, McLean J, Lindsay RS, McClure J, McMillan M, Drummond R, Gordon D, McKay GA, Shaikh MG, Perry CG, Ahmed SF. Deficits in trabecular bone microarchitecture in young women with type 1 diabetes mellitus. J Bone Miner Res 2015; 30: 1386-1393.

592. Kanis JA, McCloskey EV, Johansson H, Cooper C, Rizzoli R, Reginster JY; Scientific Advisory Board of the European Society for Clinical and Economic Aspects of Osteoporosis and Osteoarthritis (ESCEO) and the Committee of Scientific Advisors of the International Osteoporosis Foundation (IOF). European guidance for the diagnosis and management of osteoporosis in postmenopausal women. Osteoporos Int 2013; 24(1): 23-57.

593. Baccaro LF, Conde DM, Costa-Paiva L, Pinto-Neto AM. The epidemiology and management of postmenopausal osteoporosis: a viewpoint from Brazil. Clin Interv Aging 2015; 10: 583-591.

594. Nguyen ND, Frost SA, Center JR, Eisman JA, Nguyen TV. Development of prognostic nomograms for individualizing 5-year and 10-year fracture risk. Osteoporos Int 2008; 19(10): 1431-1444.

595. Kanis JA, Oden A, Johansson H, Borgstrom F, Strom O, McCloskey E. FRAX and its applications to clinical practice. Bone 2009; 44(5): 734-743.

596. Ettinger B, Liu H, Blackwell T, Hoffman AR, Ensrud KE, Orwoll ES; Osteoporotic Fracture in Men (MrOS) Research Group. Validation of FRC, a fracture risk assessment tool, in a cohort of older men: the Osteoporotic Fractures in Men (MrOS) Study. J Clin Densitom 2012; 15(3): 334-342.

597. Wu C, Hans D, He Y, Fan B, Njeh CF, Augat P, Richards J, Genant HK. Prediction of bone strength of distal forearm using radius bone mineral density and phalangeal speed of sound. Bone 2000; 26: 529-533.

598. Jiang H, Yates CJ, Gorelik A, Kale A, Song Q, Wark, JD. Peripheral quantitative computed tomography (pQCT) measures contribute to the understanding of bone fragility in older patients with low-trauma fracture. J Clin Densitom, 2018; 21(1): 140-147.

599. Robinson DL, Jiang H, Song Q, Yates C, Lee PVS, Wark JD. The application of finite element modelling based on clinical pQCT for classification of fracture status. Biomechanics and Modeling in Mechanobiology 2019; 18(1): 245-260.

600. Unnikrishnan GU, Barest GD, Berry DB, Hussein AI, Morgan EF. Effect of specimen-specific anisotropic material properties in quantitative computed tomography-based finite element analysis of the vertebra. J Biomech Eng 2013; 135(10): 101007-101011.

601. Evans AL, Paggiosi MA, Eastell R, Walsh JS. Bone density, microstructure and strength in obese and normal weight men and women in younger and older adulthood. J Bone Miner Res 2015; 30(5): 920-928.

602. Zhang N, Magland JF, Rajapakse CS, Bhagat YA, Wehrli FW. Potential of in vivo MRI-based nonlinear finite-element analysis for the assessment of trabecular bone post-yield properties. Med Phys 2013; 40(5): 052303.

603. MacNeil JA, Boyd SK. Improved reproducibility of high-resolution peripheral quantitative computed tomography for measurement of bone quality. Med Eng Phys, 2008; 30: 792-799.

604. Kawalilak CE, Kontulainen SA, Amini MA, Lanovaz JL, Olszynski WP, Johnston JD. In vivo precision of three HR-pQCT-derived finite element models of the distal radius and tibia in postmenopausal women. BMC musculoskeletal Disorders 2016; 17(1): 1-11.

605. Wehrli FW. Magnetic resonance of calcified tissues. Journal of Magnetic Resonance 2013; 229: 35-48.

606. Leslie WD, Morin SN. Osteoporosis epidemiology 2013: implications for diagnosis, risk assessment, and treatment. Curr Opin Rheumatol 2014; 26(4): 440-446.

607. Sabesan VJ, Valikodath T, Childs A, Sharma VK. Economic and social impact of upper extremity fragility fractures in elderly patients. Aging Clin Exp Res 2015; 27(4): 539-546.

608. Mallmin H, Ljunghall S, Persson I, Naessen T, Krusemo UB, Bergstrom R. Fracture of the distal forearm as a forecaster of subsequent hip fracture: a population-based cohort study with 24 years follow-up. Calcif Tissue Int 1993; 52: 269-272.

609. Johnston JD, McDonald M, Kontulainen SA. Off-axis loads cause failure of the distal radius at lower magnitudes than axial loads: an ex vivo experimental comparison between left and right forearms. J Orthop Res, 2020; in press.

610. Hosseinitabatabaei A, Kawalilak CE, McDonald MP, Kontulainen SA, Johnston JD. HR-pQCT based finite element modeling of distal radius failure load: relationship with ex vivo fall-configuration failure load and in vivo precision error. 2019, Manuscript submitted for publication.

611. Edwards WB, Troy KL. Finite element prediction of surface strain and fracture strength at the distal radius. Medical Engineering & Physics 2012; 34(3): 290-298.

612. Myers ER, Sebeny EA, Hecker AT, Corcoran TA, Hipp JA, Greenspan SL, Hayes WC. Correlations between photon absorption properties and failure load of the distal radius in vitro. Calcified Tissue International 1991; 49: 292-297.

613. Doube M, Klosowski M, Arganda-Carreras I, Cordelières F P, Dougherty R P, Jackson J S, Schmid B, Hutchinson J R, and Shefelbine S J. BoneJ: Free and Extensible Bone Image Analysis in ImageJ. Bone 2010; 47(6): 1076–1079.

614. Colles A. On the fracture of the carpal extremity of the radius. The Edinburgh Medical and Surgical Journal 1814; 10(38): 182-186.

615. Goldfarb CA, Yin Y, Gilula LA, Fisher AJ, Boyer MI. Wrist fractures: what the clinician wants to know. Radiology 2001; 219(1): 11-28.

616. Crenshaw AH. Fractures of shoulder girdle, arm, and forearm. In: Canale ST (Ed.), Campbell's Operative Orthopaedics. Mosby, St Louis; 1998, pp2281-2362.

617. Fernandez DL. Distal radius fracture: the rationale of a classification. Chirurgie De La Main 2001; 20: 411-425.

618. Jupiter JB and Fernandez DL. Comparative classification for fractures of distal end of the radius. The Journal of Hand Surgery 1997; 22: 563-571.

619. Liu XS, Stein EM, Zhou B, Zhang CA, Nickolas TL, Cohen A, Thomas V, McMahon DJ, Cosman F, Nieves J, Shane E, Guo XE. Individual trabecula segmentation (ITS)-based morphological analyses and microfinite element analysis of HR-pQCT images discriminate postmenopausal fragility fractures independent of DXA measurements. J Bone Miner Res 2012; 27(2): 263-272.

620. Luisier B, Dall'Ara E, Pahr DH. Orthotropic HR-pQCT-based FE models improve strength predictions for stance but not for side-way fall loading compared to isotropic QCT-based FE models of human femurs. J Mech Behav Mater 2014; 32: 287-299.

621. Bankoff ADP. Biomechanical Characteristics of the Bone, Human Musculoskeletal Biomechanics Tarun Goswani, IntechOpen; 2012, DOI: 10.5772/19690. Available from: https://www.intechopen.com/books/human-musculoskeletal-biomechanics/biomechanical-characteristics-of-the-bone

622. Ascenzi MG, Chin J, Lappe J, Recker R. Non-osteoporotic women with low-trauma fracture present altered birefringence in cortical bone. Bone 2016; 84: 104-112.

623. Chung KC, Spilson SV. The frequency and epidemiology of hand and forearm fractures in the United States. J Hand Surg Am 2011; 26(5): 908-915.

624. Jerrhag D, Englund M, Magnus KK, Rosengren BE. Epidemiology and time trends of distal forearm fractures in adults – a study of 11.2 million person-years in Sweden. BMC Musculoskelet Disord 2017; 18(1): 240.

625. Cauley JA. Osteoporosis: fracture epidemiology update 2016. Current Opinion in Rheumatology, 2017; 29(2): 150-156.

626. Haentjens P, Johnell O, Kanis JA, Bouillon R, Cooper C, Lamraski G, Vanderschueren D, Kaufman JM, Boonen S; Network on Male Osteoporosis in Europe (NEMO).

Evidence from data searches and life-table analyses for gender-related differences in absolute risk of hip fracture after Colles' or spine fracture: Colles' fracture as an early and sensitive marker of skeletal fragility in white men. Journal of Bone and Mineral Research, 2004; 19(12):1933-1944.

627. Sornay-Rendu E, Boutroy S, Munoz F, Delmas PD. Alterations of cortical and trabecular architecture are associated with fractures in postmenopausal women, partially independent of decreased BMD measured by DXA: the OFELY study. J Bone Miner Res, 2007; 22(3): 425-433.

628. Ulrich D, van Rietbergen B, Laib A, Ruegsegger P. Load transfer of the distal radius from in-vivo high-resolution CT-imaging. J Biomech, 1999; 32(8): 821-828.

629. Gray HA, Taddei F, Zavatsky AB, Cristofolini L, Gill HS. Experimental validation of a finite element model of a human cadaveric tibia. J Biomech Eng, 2008; 130(3): 031016.

630. Morgan EF, Bayraktar HH, Keaveny TM. Trabecular bone modulus-density relationships depend on anatomic site. Journal of Biomechanics, 2003; 36(7): 894-904.

631. Ringle CM, Wende S, Becker J-M. SmartPLS 3. Boenningstedt SmartPLS GmbH. www.smartpls.com. Accessed 24 Jan 2019.

632. Delong ER, Delong DM, Clarke-Pearson DL. Comparing the areas under two or correlated receiver operating characteristics curves: a nonparametric approach. Biometrics, 1988; 44(3): 837-845.

633. Clarke B. Normal bone anatomy and physiology. Clinical Journal of the American Society of Nephrology, 2008; 3(Suppl 3): S131-139.

634. Stagi S, Cavalli L, Cavalli T, de Martino M, Brandi ML. Peripheral quantitative computed tomography (pQCT) for the assessment of bone strength in most of bone affecting conditions in developmental age: a review. Ital J Pediatr, 2016; 42:88.

635. Boyd SK. Site-specific variation of bone micro-architecture in the distal radius and tibia. J Clin Densitom, 2008; 11(3): 424-430.

636. Reina P, Cointry GR, Nocciolino L, Feldman S, Ferretti JL, Rittweger J, Capozza RF. Analysis of the independent power of age-related, anthropometric and mechanical factors as determinants of the structure of radius and tibia in normal adults. A pQCT study. Journal of Musculoskeletal and Neuronal Interactions, 2015; 15(1): 10-22.

637. Van Caenegem E, Taes Y, Wierckx K, Vandewalle S, Toye K, Kaufman J-M, Schreiner T, Haraldsen I, T'Sjoen G. Low bone mass is prevalent in male-to-female transsexual person before the start of cross-sex hormonal therapy and gonadectomy. Bone, 2013; 54(1): 92-97.

638. Saarnio E, Pekkinen M, Itkonen ST, Kemi V, Karp H, Ivaska KK, Risteli J, Koivula M-K, Karkkainen M, Makitie O, Sievanen H, Lamberg-Allardt C. Low free 25-hydroxyvitamin D and high vitamin D binding protein and parathyroid hormone in obese Caucasians. A complex association with bone? PLoS One, 2018; 13(2): e0192596.

639. Marques IDB, Araujo MJCLN, Graciolli FG, dos Reis LM, Pereira RM, Custodio MR, Jorgetti V, Elias RM, David-Neto E, Moyses RMA. Biopsy vs. peripheral computed tomography to assess bone disease in CKD patients on dialysis: differences and similarities. Osteoporosis International, 2017; 28(5): 1675-1683.

640. Schafer AL, Burghardt AJ, Sellmeyer DE, Palermo L, Shoback DM, Majumdar S, Black DM. Postmenopausal women treated with combination parathyroid hormone (1-84) and

ibandronate different microstructural changes at the radius vs. tibia: the PTH and Ibandronate Combination Study (PICS). Osteoporosis International, 2013; 24(10): 2591-2601.

641. Zanchetta MB, Costa F, Longobardi V, Longarini G, Mazure RM, Moreno ML, Vazquez H, Silveira F, Niveloni S, Smecuol E, de la Paz Temprano M, Hwang HJ, Gonzalez A, Maurino EC, Bogado C, Zanchetta JR, Bai JC. Significant bone microarchitecture impairment in premenopausal women with active celiac disease. Bone 2015; 76: 149-157.

642. Famula A, Nowotny-Czupryna O, Czupryna K, Nowotny J. Previous physical activity and body balance in elderly people. Biol Sport, 2013; 30(4): 311-315.

643. Yang PF, Sanno M, Ganse B, Koy T, Bruggemann GP, Muller LP, Rittweger J. Torsion and antero-posterior bending in the in vivo human tibia loading regimes during walking and running. PLoS ONE, 2014; 9(4): e94525.

644. Vilayphiou N, Boutroy S, Szulc P, van Rietbergen B, Munoz F, Delmas PD, Chapurlat R. Finite element analysis performed on radius and tibia HR-pQCT images and fragility fractures at all site in men. Journal of Bone and Mineral Research, 2011; 26(5): 965-973.

645. Nishiyama KK, Macdonald HM, Hanley DA, Boyd SK. Women with previous fragility fractures can be classified based on bone microarchitecture and finite element analysis measured with HR-pQCT. Osteoporosis International, 2013; 24:1733-1740.

646. Bielesz B, Patsch JM, Fischer L, Bojic M, Winnicki W, Weber M, Cejka D. Cortical porosity not superior to conventional densitometry in identifying hemodialysis patients with fragility fracture. PLoS One, 2017; 12(2): e0171873.

647. Papaioannou A, Watts NB, Kendler DL, Yuen CK, Adachi JD, Ferko N. Diagnosis and management of vertebral fractures in elderly adults. Am J Med, 2002; 113(3): 220-228.

648. Van Staa TP, Dennison EM, Leufkens HG, Cooper C. Epidemiology of fractures in England and Wales. Bone, 2001; 29(6): 517-522.

649. Stone KL, Seeley DG, Lui LY, Cauley JA, Ensrud K, Browner WS, Nevitt MC, Cummings SR; Osteoporotic Fractures Research Group. BMD at multiple sites and risk of fracture of multiple types: long-term results from the Study of Osteoporotic Fractures. J Bone Miner Res, 2003; 18(11): 1947-1954.

650. Amiri L, Kheiltash A, Movassaghi S, Moghaddassi M, Seddigh L. Comparison of bone density of distal radius with hip and spine using DXA. Acta Med Iran, 2017; 55(2): 92-96.

651. De Laet C, Oden A, Johnell O, Jonsson B, Kanis JA. The impact of the use of multiple risk factors on case finding strategies: a mathematical framework. Osteoporos Int 2005; 16: 313-318.

652. Kanis JA, Oden A, Johnell O, Johansson H, De Laet C, Brown J, Burckhardt P, Cooper C, Christiansen C, Cummings S, Eisman JA, Fujiwara S, Gluer C, Goltzman D, Hans D, Krieg M-A, La Croix A, McCloskey E, Mellstrom D, Melton 3rd LJ, Pols H, Reeve J, Sanders K, Schott A-M, Silman A, Torgerson D, van Staa T, Watts NB, Yoshimura N. The use of clinical risk factors enhances the performance of BMD in the prediction of hip and osteoporotic fractures in men and women. Osteoporos Int, 2007; 18: 1033–1046.

653. Sornay-Rendu E, Munoz F, Delmas PD, Chapurlat RD. The FRAX tool in French women: How well does it describe the real incidence of fracture in the OFELY cohort? J Bone Miner Res, 2010; 25: 2101–2107.

654. Crandall CJ, Schousboe JT, Morin SN, Lix LM, Leslie W. Performance of FRAX and FRAX-Based Treatment Thresholds in Women Aged 40 Years and Older: The Manitoba BMD Registry. J Bone Miner Res, 2019; 34: 1419–1427.

655. Briot K, Paternotte S, Kolta S, Eastell R, Felsenberg D, Reid DM, Glüer C-C, Roux C FRAX®: Prediction of Major Osteoporotic Fractures in Women from the General Population: The OPUS Study. PLoS ONE, 2014; 8: e83436.

656. Wu Q, Xiao X, Xu Y. Performance of FRAX in Predicting Fractures in US Postmenopausal Women with Varied Race and Genetic Profiles. J Clin Med, 2020; 9(1): 285.

657. Crandall CJ, Schousboe JT, Morin SN, Lix LM, Leslie W. Performance of FRAX and FRAX‐Based Treatment Thresholds in Women Aged 40 Years and Older: The Manitoba BMD Registry. J Bone Miner Res, 2019; 34(8): 1419-1427.

658. Martinez-Morillo M, Grados D, Holgado S. Premenopausal osteoporosis: how to treat? Reumatol Clin, 2012; 8(2): 93-97.

659. Harvey NC, McCloskey E, Kanis JA. Editorial for Joint Bone Spine: Use of FRAX® in men. Joint Bone Spine, 2016; 83(5): 477-478.

660. Evans RK, Negus CH, Centi AJ, Spiering BA, Kraemer WJ, Nindl BC. Peripheral QCT sector analysis reveals early exercise-induced increases in tibial bone mineral density. J Musculoskelet Neuronal Interact, 2012; 12(3): 155-164.

661. Rantalainen T, Nikander R, Daly RM, Heinonen A, Sievanen H. Exercise loading and cortical bone distribution at the tibial shaft. Bone, 2011; 48(4): 786-791.

662. Polidoulis I, Beyene J, Cheung AM. The effect of exercise on pQCT parameters of bone structure and strength in postmenopausal women- a systematic review and meta-analysis of randomized controlled trials. Osteoporos Int, 2012; 23(1): 39-51.

663. Whittemore AS, Gong G, John EM, McGuire V, Li FP, Ostrow KL, Dicioccio R, Felberg A, West DW. Prevalence of BRCA1 mutation carriers among U.S. non-Hispanic Whites. Cancer Epidemiol Biomarkers Prev, 2004; 13(12): 2078-2083.

664. Metcalfe KA, Birenbaum-Carmeli D, Lubinski J, Gronwald J, Lynch H, Moller P, Ghadirian P, Foulkes WD, Klijin J, Friedman E, Kim-Sing C, Ainsworth P, Rosen B, Domchek S, Wagner T, Tung N, Manoukian S, Couch F, Sun P, Narod SA, and the Heredity Breast Cancer Clinical Study Group. Interventional variation in rates of uptake of preventive options in BRCA1 and BRCA2 mutation carriers. Int J Cancer, 2008; 122(9): 2017-2022.

665. Rachner TD, Khosla S, Hofbauer LC. Osteoporosis: now and the future. Lancet, 2011; 377: 1276-1287.

666. Dhainaut A, Hoff M, Syversen U, Haugeberg G. Technologies for assessment of bone reflecting bone strength and bone mineral density in elderly women: an update. Womens Health (Lond), 2016; 12(2): 209-216.

667. Gluer CC. 30years of DXA technology innovations. Bone, 2017; 104: 7-12.

668. Jiang H, Robinson DL, McDonald M, Lee PVS, Kontulainen SA, Johnston JD, Yates CJ, Wark JD. Predicting experimentally-derived failure load at the distal radius using finite element modelling based on peripheral quantitative computed tomography cross sections (pQCT-FE): a validation study. Bone, 2019; 129: 115051.

669. Jiang H, Robinson DL, Yates CJ, Lee PVS, Wark JD. Peripheral quantitative computed tomography (pQCT)-based finite element analysis provides enhanced diagnostic performance in identifying non-vertebral fracture patients compared with dual energy X-ray absorptiometry. Osteoporos Int, 2020; 31(1): 141-151.

670. Hickey M, Trainer A, Braat S, Davey M-A, Krejany E, Wark J. What happens after menopause? (WHAM): protocol for a prospective, multicentre, age-matched cohort trial of risk-reducing bilateral salpingo-oophorectomy in high-risk premenopausal women. BMJ Open, 2017; 7(11): e018758.

671. De Laet C, Oden A, Johnell O, Jonsson B, Kanis JA. The impact of the use of multiple risk factors on case finding strategies: a mathematical framework. Osteoporos Int, 2005; 16(3): 313-318.

672. Collaborative Group on Hormonal Factors in Breast Cancer. Type and timing of menopausal hormone therapy and breast cancer risk: individual participant meta-analysis of the worldwide epidemiological evidence. Lancet, 2019; 394:1159-68.

673. Rebbeck TR, Friebel T, Wagner T, Lynch HT, Garber JE, Daly MB, Isaacs C, Olopade OI, Neuhausen SL, van 't Veer L, Eeles R, Evans DG, Tomlinson G, Matloff E, Narod SA, Eisen A, Domchek S, Armstrong K, Weber BL; PROSE Study Group. Effect of short-term hormone replacement therapy on breast cancer risk reduction after bilateral prophylactic oophorectomy in BRCA1 and BRCA2 mutation carriers: the PROSE Study Group. J Clin Oncol, 2005; 23:7804-10.

674. Li Z, Kuhn G, Schirmer M, Muller R, Ruffoni D. Impaired bone formation in ovariectomized mice reduces implant integration as indicated by longitudinal in vivo micro-computed tomography. PLoS One, 2017; 12(9): e0184835.

675. Kawalilak CE, Johnston JD, Olszynski WP, Kontulainen SA. Characterizing microarchitectural changes at the distal radius and tibia in postmenopausal women using HR-pQCT. Osteoporos Int, 2014; 25(8): 2057-2066.

676. Vermeulen RFM, Korse CM, Kenter GG, Brood-van Zanten MMA, van Beurden M. Safety of hormone replacement therapy following risk-reducing salpingo-oophorectomy: systematic review of literature and guideline. Climacteric, 2019; 22(4): 352-360.

677. Domchek S, Kaunitz AM. Use of systemic hormone therapy in BRCA mutation carriers. Manopause, 2016; 23(9): 1026-1027.

678. Vermeulen RFM, Beurden MV, Kieffer JM, Bleiker EMA, Valdimarsdottir HB, Massuger LFAG, Mourits MJE, Gaarenstroom KN, van Dorst EBL, van der Putten HWHM, Aaronson NK. Hormone replacement therapy after risk-reducing salpingo-oophorectomy minimises endocrine and sexual problems: A prospective study. Eur J Cancer, 2017; 84: 159-167.

679. Chan JL, Senapati S, Johnson LNC DiGiovanni L, Voong C, Butts SF, Domchek SM. Risk factors for sexual dysfunction in BRCA mutation carriers after risk-reducing salpingo-oophorectomy. Menupause, 2019; 26(2): 132-139.

680. Sullivan SD, Sarrel PM, Nelson LM. Hormone replacement therapy in young women with primary ovarian insufficiency and early menopause. Fertil Steril, 2016; 106(7): 1588-1599.

681. Bahar S, Abali R, Guzel S, Bozkurt S, Guzel EC, Aral H, Boran AB. Comparison of the acute alterations in serum bone turnover markers and bone mineral density among women with surgical menopause. Eur J Obstet Gynecol Reprod Biol, 2011; 159(1): 194-197.

682. Peris P, Alvarez L, Monegal A, GuaNabens N, Duran M, Pons F, Martinez de Osaba MJ, Echevarria M, Ballesta AM, Munoz-Gomez J. Biochemical markers of bone turnover after surgical menopause and hormone replacement therapy. Bone, 1999; 25(3): 349-353.

683. Fakkert IE, van der Veer E, Abma EM, Lefrandt JD, Wolffenbuttel BHR, Oosterwijk JC, Slart RHJA, Westrik IG, de Bock GH, Mourits MJE. Elevated bone turnover markers after risk-reducing salpingo-oophorectomy in women at increased risk for breast and ovarian cancer. PLoS One, 2017; 12(1): e0169673.

684. Khosla S, Atkinson EJ, Melton LJ 3rd, Riggs BL. Effects of age and estrogen status on serum parathyroid hormone levels and biochemical markers of bone turnover in women: a population-based study. J Clin Endocrinol Metab, 1997; 82(5): 1522-1527.

685. Gaugris S, Heaney RP, Boonen S, Kurth H, Bentkover JD, Sen SS. Vitamin D inadequacy among post-menopausal women: a systematic review. QJM, 2005; 98(9): 667-676.

686. Janghorbani M, Van Dam RM, Willett WC, Hu FB. Systematic review of type 1 and type 2 diabetes mellitus and risk of fracture. Am J Epidemiol, 2007; 166(5): 485-505.

687. Fuusager GB, Christesen HT, Milandt N, Schou AJ. Glycemia control and bone mineral density in children and adolescents with type 1 diabetes. Pediatr Diabetes, 2019; 20(5): 629-636.

688. Jiang N, Xia W. Assessment of bone quality in patients with diabetes mellitus. Osteoporos Int, 2018; 29(8): 1721-1736.

689. Callegari ET, Garland SM, Gorelik A, Reavley NJ, Wark JD. Predictors and correlates of serum 25-hydroxyvitamin D concentrations in young women: results from the Safe-D study. Br J Nutr, 2017; 118(4): 263-272.

690. Fenner Y, Garland SM, Moore EE, Jayasinghe Y, Fletcher A, Tabrizi SN, Gunasekaran B, Wark JD. Web-based recruiting for health research using a social networking site: an exploratory study. J Med Internet Res, 2012; 14(1): e20.

691. Callegari ET, Reavley N, Garland SM, Gorelik A, Wark JD. Vitamin D status, bone mineral density and mental health in young Australian women: the Safe-D study. J Public Health Res, 2015; 4(3): 594.

692. Weaver CM, Gordon CM, Janz KF, Kalkwarf HJ, Lappe JM, Lewis R, O'Karma M, Wallace TC, Zemel BS (2016). The National Osteoporosis Foundation's position statement on peak bone mass development and lifestyle factors: a systematic review and implementation recommendations. Osteoporos Int, 27(4): 1281-1386.

693. Meier C, Nguyen TV, Center JR, Seibel MJ, Eisman JA. Bone resorption and osteoporotic fractures in elderly men: the dubbo osteoporosis epidemiology study. J Bone Miner Res, 2005; 20(4): 579-587.

694. Madson JOB, Jorgensen NR, Pociot F, Johannesen J. Bone turnover markers in children and adolescents with type 1 diabetes- A systematic review. Pediatr Diabetes, 2019; 20(5): 510-522.

695. Callegari ET, Gorelik A, Garland SM, Chiang CY, Wark JD. Bone turnover marker reference intervals in young females. Ann Clin Biochem, 2017; 54(4): 438-447.

696. Shah VN, Harrall KK, Shah CS, Gallo TL, Joshee P, Snell-Bergeon JK, Kohrt WM. Bone mineral density at femoral neck and lumbar spine in adults with type 1 diabetes: a meta-analysis and review of the literature. Osteoporos Int, 2017; 28(9): 2601-2610.

697. Pan H, Wu N, Yang T, He W. Association between bone mineral density and type 1 diabetes mellitus: a meta-analysis of cross-sectional studies. Diabetes Metab Res Rev, 2014; 30(7): 531-542.

698. Kaur H, Joshee P, Franquemont S, Baumgartner A, Thurston J, Pyle L, Nadeau KJ, Shah VN. Bone mineral content and bone density is lower in adolescents with type 1 diabetes: a brief report from the RESISTANT and EMERALD studies. J Diabetes Complications, 2018; 32(10): 931-933.

699. Halper-Stromberg E, Gallo T, Champakanath A, Taki I, Rewers M, Snell-Bergeon, Frohnert BI, Shah VN. Bone mineral density across the lifespan in patients with type 1 diabetes. J Clin Endocrinol Metab, 2020; 105(3): dgz153.

700. Madsen JOB, Herskin CW, Zerahn B, Jensen AK, Jorgensen NR, Olsen BS, Pociot F, Johannesen J. Unaffected bone mineral density in Danish children and adolescents with type 1 diabetes. J Bone Miner Metab, 2019; 38(3): 328-337.

701. Abdalrahaman N, McComb C, Foster JE, Lindsay RS, Drummond R, McKay GA, Perry CG, Ahmed SF. The relationship between adiposity, bone density and microarchitecture is maintained in young women irrespective of diabetes status. Clin Endocrinol (Oxf), 2017; 87(4): 327-335.

702. Roggen I, Gies I, Vanbesien J, Louis O, De Schepper J. Trabecular bone mineral density and bone geometry of the distal radius at completion of pubertal growth in childhood type 1 diabetes. Horm Res Paediatr, 2013; 79(2): 68-74.

703. Choksi P, Jepsen KJ, Clines GA. The challenges of diagnosing osteoporosis and the limitations of currently available tools. Clin Diabetes Endocrinol, 2018; 29; 4-12.

704. Picardi A, Cipponeri E, Bizzarri C, Fallucca S, Guglielmi C, Pozzilli P. Menarche in type 1 diabetes is still delayed despite good metabolic control. Fertil Steril, 2008; 90(5): 1875-1877.

705. Goshtasebi A, Berger C, Barr SI, Kovacs CS, Towheed T, Davison KS, Prior JC. Adult premenopausal bone health related to reproductive characteristics-population-based data from the Canadian Muticentre Osteoporosis Study (CaMos). Int J Environ Res Public Health, 2018; 15(5): E1023.

706. Zhang Q, Greenbaum J, Zhang WD, Sun CQ, Deng HW. Age at menarche and osteoporosis: a Mendelian randomization study. Bone, 2018; 117: 91-97.

707. Almstedt HC, Cook MM, Bramble LF, Dabir DV, LaBrie JW. Oral contraceptive use, bone mineral density, and bone turnover markers over 12 months in college-aged females. J Bone Miner Metab, 2020; 38(4): 544-554.

708. Kim SJ, Yang W-G, Cho E, Park E-C. Relationship between weight, body mass index and bone mineral density of lumbar spine in women. J Bone Metab, 2012; 19(2): 95-102.

709. Tran F, Stone M, Huang C-Y, Lloyd M, Woodhead HJ, Elliott KD, Crock PA, Howard NJ, Craig ME. Population-based incidence of diabetes in Australian youth aged 10-18 yr: increase in type 1 diabetes but not type 2 diabetes. Pediatr Diabetes, 2014; 15(8): 585-590.

710. Hennessy S, Bilker WB, Berlin JA, Strom BL. Factors influencing the optimal control-to-case ratio in matched case-control studies. Am J Epidemiol, 1999; 149(2): 195-197.

711. Allali F, Mansouri LE, Abourazzak FZ, Ichchou L, Khazzani H, Bennani L, Abouqal R, Hajjaj-Hassouni N. The effect of past use of oral contraceptive on bone mineral density,

bone biochemistry markers and muscle strength in healthy pre and post-menopausal women. BMC Women's Health, 2009; 9: 31.

712. Ott SM, Scholes D, Lacroix AZ, Ichikawa LE, Yoshida CK, Barlow WE. Effects of contraceptive use on bone biochemical markers in young women. J Clin Endocronol Metab, 2001; 86(1): 179-185.

713. Scholes D, Ichikawa L, LaCroix AZ, Spangler L, Beasley JM, Reed S, Ott SM. Oral contraceptive use and bone density in adolescent and young adult women. Contraception, 2010; 81(1): 35.

714. Prior JC, Kirkland SA, Joseph L, Kreiger N, Murray TM, Hanley DA, Adachi JD, Vigna YM, Berger C, Blondeau L, Jackson SA, Tenenhouse A, for the CaMOS Research Group. Oral contraceptive use and bone mineral density in premenopausal women: cross-sectional, population-based data from the Canadian Multicentre Osteoporosis Study. CMAJ, 2001; 165(8): 1023-1029.

715. Herrmann M, Engelke K, Ebert R, Muller-Deubert S, Rudert M, Ziouti F, Jundt F, Felsenberg D, Jakob F. Interactions between muscle and bone- where physic meet biology. Biomolecules, 2020; 10(3): 432.

716. D'Souza DM, Al-Sajee D, Hawke TJ. Diabetic myopathy: impact of diabetes mellitus on skeletal muscle progenitor cells. Front Physiol, 2013; 4: 379.

717. Orlando G, Balducci S, Bazzucchi I, Pugliese G, Sacchetti M. The impact of type 1 diabetes and diabetic polyneuropathy on muscle strength and fatigability. Acta Diabetol, 2017; 54(6): 543-550.

718. Krause MP, Riddell MC, Hawke TJ. Effects of type 1 diabetes mellitus on skeletal muscle: clinical observations and physiological mechanisms. Pediatr Diabetes, 2011; 12(4 Pt1): 345-364.

719. Bethtold S, Dirlenbach I, Raile K, Noelle V, Bonfig W, Schwarz HP. Early manifestation of type 1 diabetes in children is a risk factor for changed bone geometry: data using peripheral quantitative computed tomography. Pediatrics, 2006; 118(3): e627-e634.

720. Maratova K, Soucek O, Matyskova J, Hlavka Z, Petruzelkova L, Obermannova B, Stepanka P, Kolouskova S, Sumnik Z. Muscle functions and bone strength are impaired in adolescents with type 1 diabetes. Bone, 2018; 106: 22-27.

721. Fowlkes JL, Bunn RC, Liu L, Wahl EC, Coleman HN, Cockrell GE, Perrien DS, Lumpkin Jr CK, Thrailkill KM. Runt-repated transcription fractor 2 (RUNX2) and RUNX2-related osteogenic genes are down-regulated throughout osteogenesis in type 1 diabetes mellitus. Endocrinology, 2008; 149(4): 1697-1704.

722. Wu H, Whitfield TW, Gordon JAR, Dobson JR, Tai PWL, van Wijnen AJ, Stein JL, Stein GS, Lian JB. Genomic occupancy of Runx2 with global expression profiling identifies a novel dimension to control of osteoblastogenesis. Genome Biol, 2014; 15(3): R52.

723. Kalaitzoglou E, Popescu I, Bunn RC, Fowlkes JL, Thrailkill KM. Effects of type 1 diabetes on osteoblasts, osteocytes and osteoclasts. Curr Osteoporos Rep, 2016; 14(6): 310-319.

724. Tsentidis C, Gourgiotis D, Kossiva L, Doulgeraki A, Marmarinos A, Galli-Tsinopolou A, Karavanaki K. Higher levels of s-RANKL and osteoprotegerin in children and adolescents with type 1 diabetes mellitus may indicate increased osteoclast signaling and

predisposition to lower bone mass: a multivariate cross-sectional analysis. Osteoporos Int, 2016; 27(4): 1631-1643.

725. Loureiro MB, Ururahy MAG, Freire-Neto FP, Oliveira GHM, Duarte VMG, Luchessi AD, Brandao-Neto J, Hirata RDC, Hirata MH, Maciel-Neto JJ, Arrais RF, Almeida MG, Rezende AA. Low bone mineral density is associated to poor glycemic control and increased OPG expression in children and adolescents with type 1 diabetes. Diabetes Res Clin Pract, 2014; 103(3): 452-457.

726. Motyl KJ, Botolin S, Irwin R, Appledorn DM, Kadakia T, Amalfitano A, Schwartz RC, McCabe LR. Bone inflammation and altered gene expression with type I diabetes early onset. J Cell Physiol, 2009; 218(3): 575-583.

727. Wittrant Y, Gorin Y, Woodruff K, Horn D, Abboud HE, Mohan S, Abboud-Werner SL. High d(+)glucose concentration inhibits RANKL-induced osteoclastogenesis. Bone, 2008; 42(6): 1122-1130.

728. Valcourt U, Merle B, Gineyts E, Viguet-Carrin S, Delmas PD, Garnero P. Non-enzymatic glycation of bone collagen modifies osteoclastic activity and differentiation. J Biol Chem, 2007; 282(8): 5691-5703.

729. Wacholder S, McLaughlin JK, Silverman DT, Mandel JS. Selection of controls in case-control studies. I. Principles. Am J Epidemiol, 1992; 135(9): 1019-1028.

730. Wacholder S, Silverman DT, McLaughlin JK, Mandel JS. Selction of controls in case-control studies. II. Types of controls. Am J Epidemiol, 1992; 135(9): 1029-1041.

731. Kirk B, Zanker J, Duque G. Osteosarcopenia: epidemiology, diagnosis, and treatment-facts and numbers. J Cachexia Sarcopenis Muscle, 2020; 11(3): 609-618.

732. Cruz-Jentoft AJ, Bahat G, Bauer J, Boirie Y, Bruyere O, Cederholm T, Cooper C, Landi F, Rolland Y, Sayer AA, Schneider SM, Sieber CC, Topinkova E, Vandewoude M, Visser M, Zamboni M, and Writing Group for the European Working Group on Sarcopenia in Older People 2 (EWGSOP2), and the Extended Group for EWGSOP2. Age Ageing, 2019; 48(1): 16-31.

Appendices

Appendix 1

Journal of Clinical Densitometry: Assessment & Management of Musculoskeletal Health, vol. 21, no. 1, 140–147, 2018

1094-6950/21:140–147/$36.00
https://doi.org/10.1016/j.jocd.2017.02.003

Peripheral Quantitative Computed Tomography (pQCT) Measures Contribute to the Understanding of Bone Fragility in Older Patients With Low-trauma Fracture

Hongyuan Jiang,[1] Christopher J. Yates,[1,2] Alexandra Gorelik,[3] Ashwini Kale,[1,2] Qichun Song,[1,4] and John D. Wark[1,2]*

[1]Department of Medicine, Royal Melbourne Hospital, University of Melbourne, Parkville, Victoria, Australia; [2]Bone and Mineral Medicine, Royal Melbourne Hospital, Parkville, Victoria, Australia; [3]Melbourne EpiCentre, University of Melbourne and Melbourne Health, Parkville, Victoria, Australia; and [4]Department of Orthopaedics, The Second Affiliated Hospital, Xi'an Jiaotong University, Xi'an, Shaanxi, China

Abstract

Dual-energy X-ray absorptiometry (DXA) as currently used has limitations in identifying patients with osteoporosis and predicting occurrence of fracture. We aimed to express peripheral quantitative computed tomography (pQCT) variables of patients with low-trauma fracture as T-scores by using T-score scales obtained from healthy young women, and to evaluate the potential clinical utility of pQCT for the assessment of bone fragility. Fracture patients were recruited from a fracture liaison service at the Royal Melbourne Hospital. Reference pQCT data were obtained from studies on women's health conducted by our group. A study visit was arranged with fracture patients, during which DXA and pQCT were applied to measure their bone strength. A total of 59 fracture patients were recruited, and reference data were obtained from 78 healthy young females. All DXA variables and most pQCT variables were significantly different between healthy young females and fracture patients ($p < 0.05$), except polar stress-strain index ($p = 0.34$) and cortical bone density ($p = 0.19$). Fracture patients were divided into osteoporosis and non-osteoporosis groups according to their DXA T-scores. Significant differences were observed in most pQCT variables ($p < 0.05$), except trabecular area and cortical density ($p > 0.9$ and $p = 0.5$, respectively). By applying pQCT T-scores, 11 (27%) of patients who were classified as having low or medium risk of osteoporosis on DXA T-scores alone were reclassified as high risk. Results of logistic regression suggested trabecular bone density as an independent predictor of osteoporosis status. More patients can be identified with osteoporosis by applying pQCT T-score variables in older people with low-trauma fracture. Peripheral QCT T-scores contribute to the understanding of bone fragility in this population.

Key Words: DXA; low-trauma fracture; pQCT; T-score.

Received 10/5/16; Revised 01/24/17; Accepted 02/13/17.
Conflict of interest: The authors declare that they have no conflict of interest.
*Address correspondence to: John D. Wark, MBBS, FRACP, PhD, Royal Melbourne Hospital Department of Medicine, University of Melbourne, Parkville, Victoria, Australia. E-mail: jdwark@unimelb.edu.au

Introduction

Fragility fracture, also known as low-trauma fracture (LTF), is a serious complication of osteoporosis. Not only is it associated with significant morbidity and mortality *(1)*, but it is also a major public health problem because of the high associated direct and indirect costs.

The currently used diagnostic criteria for osteoporosis were based on areal bone mineral density (aBMD) determined by dual-energy X-ray absorptiometry (DXA). However, there are limitations when DXA is used to predict fracture risk. Peripheral quantitative computed tomography (pQCT) has some advantages over DXA. It can measure volumetric BMD (vBMD) and separately estimate trabecular and cortical compartments of the bone *(2)*. Peripheral QCT also can measure bone geometry, allowing estimation of bone bending strength *(3)*. Although it is unclear which parameters contribute more to fracture prediction, it is likely that a combination of BMD and geometric parameters will improve fracture prediction compared with single variables.

A T-score, defined as the standard deviation (SD) from the reference mean of young healthy adult women, is used to classify different groups in the diagnostic criteria. Similar to DXA T-scores, a system of pQCT T-scores potentially could be used to diagnose osteoporosis and to predict fracture risk. Therefore, in this study, we aimed to express pQCT variables of patients with LTF as T-scores by using T-score scales obtained from healthy young Australian women, and to evaluate the potential clinical utility of pQCT for the assessment of bone fragility.

Methods

Study Participants

Participants with LTF were recruited from a fracture liaison service at the Royal Melbourne Hospital, which has been shown to improve uptake of osteoporosis intervention guidelines *(4)*. Inclusion criteria included (1) age 50 years or greater; (2) 1 or more LTFs sustained within the past 3 months; and (3) able to attend 1 study visit at the Royal Melbourne Hospital. Exclusion criteria included (1) prior diagnosis of osteoporosis; (2) prolonged (>3 months) use of osteoporosis therapy in the past 2 years; (3) prior therapy with teriparatide or strontium ranelate; (4) unstable doses of hormone replacement therapy; and (5) secondary causes of low bone density, for example, hyperthyroidism, diabetes, severe vitamin D deficiency (serum 25-hydroxyvitamin D < 12.5 nmol/L), and alcoholism.

Reference data were obtained from 2 ongoing studies on women's health conducted by our research group: the Young Female Health Initiative (YFHI) and the Safe-D studies. The YFHI is a comprehensive prospective study of health, lifestyle, and well-being in young Australian females aged 16–25 years *(5)*, and the Safe-D study aims to explore vitamin D and related health in young Australian females aged 16–25 years *(6)*. DXA and pQCT are part of a site visit required for each participant in both studies. Data from the 2 studies were screened to exclude participants aged less than 19 years and those with medical conditions that may affect their bone health. The means and SDs of pQCT variables of adult participants were used as reference data and to determine T-scores for pQCT variables in patients with LTF.

Written informed consent was obtained from each participant before participation. This study has been approved by the Melbourne Health Human Research Ethics Committee (MH 2014.143).

DXA Scanning and Analysis

A fan-beam densitometer (Horizon QDR 4500A, Hologic Inc., Bedford, MA) was used to scan the lumbar spine (LS) and the hip of all participants. All scans were performed in array mode by an experienced operator. The manufacturer's commercial software (version 9.10D) was used to analyze DXA scans and to obtain DXA T-scores of the LS, the femoral neck (FN), the trochanteric region, and the total hip (TH). The reference data used by the commercial software to obtain DXA T-scores were HLK (25-Oct-91), which were mainly based on data of American Caucasian women. The 12-month precision of the scanner for the spine phantom was 0.39% for aBMD and 0.58% for bone mineral content *(7)*.

pQCT Scanning and Analysis

An XCT 3000 pQCT scanner (Stratec Medizintechnik, Pforzheim, Germany) was used by the same experienced operator to scan all participants' tibia. A scout view scan was performed before the CT scan to ensure the correct scanning sites. Scanning sites were the 4% and the 66% site of participants' non-dominant tibia, defined as percentage of the tibia length from the distal to the proximal end. Length was measured from the medial malleolus to the medial condyle at the tibia. The voxel size was $0.4 \times 0.4 \times 2.0$ mm. A threshold of 280 mg/cm^3 was applied to separate bone from soft tissue and a threshold of 710 mg/cm^3 was applied to separate cortical bone from trabecular bone. The coefficient of variation is 0.105 for polar stress-strain index (SSIp), 0.061 for trabecular vBMD (Trb vBMD), and 0.055 for cortical thickness (Thk). Analysis of pQCT data was performed by the same investigator using the Stratec commercial software (version XCT 5.50E).

Individual T-scores of pQCT tibia variables were calculated using the equation:

$$T\text{-}score = \frac{\text{individual value} - \text{reference mean}}{\text{reference SD}}.$$

In the following sections, pQCT T-scores refer to the T-scores of pQCT tibia variables calculated from the means and SDs of the reference pQCT tibia variables. T-scores of pQCT variables with significant difference between patients with and patients without osteoporosis (according to their DXA T-scores) were selected to reclassify the patients. The same cutoff values with DXA T-score classification (i.e., T-score ≥−1.0 defined as low-risk score, T-score between −1.0 and −2.5 defined as moderate, and ≤−2.5 defined as high-risk score for osteoporosis) were applied in the reclassification.

Other Data Collected

Other data collected included age, gender, height, weight, fracture details, risk factors for fracture, and comorbidities (e.g., smoking, alcohol consumption, glucocorticoids use, diagnosis of rheumatoid arthritis, history of previous LTF, and parental history of hip fracture). Fracture risk factor data were determined according to the FRAX description *(8)*.

Statistical Analysis

Univariate analysis was undertaken to compare relationships between demographic and clinical factors and LTF. Participants were divided into an osteoporosis group and a non-osteoporosis group according to their DXA T-scores of LS, FN, or TH using the World Health Organization diagnostic criteria *(9)*. Differences in continuous variables were assessed by 2-sample *t* test or Wilcoxon rank sum test, and by chi-square test for categorical variables. Logistic regression analysis was used to determine the independent associations between osteoporosis status by DXA and pQCT T-scores while adjusting for age, sex, and body mass index (BMI), and further adjusting for fracture risk factors. A further analysis was performed using the same cutoff values of pQCT T-score with those of DXA T-score into 3 groups: normal, moderate, and high risk, corresponding to normal BMD, osteopenia, and osteoporosis based on DXA T-scores, respectively. All statistical analyses were performed using SPSS Statistics 22.0 (SPSS Inc., Chicago, IL). The level of significance was set at 2-sided $p < 0.05$.

Results

Participant Characteristics

A total of 59 participants with LTF were recruited from the fracture liaison service, including 44 females and 15 males (range 51–83 years; mean 65 ± 9 years). A diagnosis of osteoporosis was made using DXA T-score classification, based on World Health Organization T-score criteria at or below −2.5 at 1 or more of the LS, FN, or TH sites. Osteoporosis was diagnosed in 18 (30.5%) patients, whereas the other 41 (69.5%) patients were diagnosed with osteopenia (33, 55.9%) or normal BMD (8, 13.6%). No difference in age, sex, or BMI was observed between participants with and participants without osteoporosis ($p = 0.11$). No difference was found in fracture risk factors as defined in the FRAX algorithm *(10)* and fracture site (all $p > 0.05$). Participant characteristics are summarized in Table 1.

Peripheral QCT Reference Data

After screening for eligibility, data from 330 participants of the YFHI and Safe-D studies were included as reference data. The young females included had a mean age of 23 ± 2 years and a mean BMI of 24.3 ± 5.3 kg/m^2. Means and SDs of pQCT reference data, as well as DXA variables, are shown in Table 2.

Table 1
Characteristics of the Study Participants

	Osteoporosis[a] (n = 18)	Non-osteoporosis[a] (n = 41)	p^b
Age (yr)	68 ± 7	64 ± 10	0.11
Height (m)	1.592 ± 0.099	1.669 ± 0.100	0.01
Weight (kg)	69.9 ± 18.0	83.1 ± 13.5	0.01
BMI (kg/m^2)	27.5 ± 5.9	29.9 ± 4.9	0.15
Sex			0.4
Female	15	29	
Male	3	12	
Smoking	3 (16.7%)	3 (7.3%)	0.4
Alcohol	3 (16.7%)	4 (9.8%)	0.7
Glucocorticoids	1 (5.6%)	3 (7.3%)	>0.9
Rheumatoid arthritis	2 (11.1%)	10 (24.4%)	0.3
Previous LTF	12 (66.7%)	27 (65.9%)	>0.9
Parental hip fracture	2 (11.1%)	5 (12.2%)	>0.9
Fracture site			0.6
Forearm	10	23	
Ankle	3	8	
Humerus	2	5	
Hand	2	3	
Foot	1	2	
Hip	1	1	
Knee	1	1	
Spine	1	0	

[a]Diagnosis of osteoporosis or non-osteoporosis is made according to their DXA T-scores of lumbar spine, femoral neck, or total hip.
[b]*p* for Fisher's exact test in comparison of proportions.

DXA and pQCT Results of Fracture Patients

DXA variables of the LS (L1–L4) were obtained for all participants except for 1 in whom only variables of L1–L3 were obtained, as the analysis software could not detect L4. DXA variables of the hip were not available in another 2 participants because of hip replacement of both sides. Peripheral QCT variables of the tibia were obtained from all participants. Results of DXA and pQCT variables are summarized for all participants in Table 2.

DXA and pQCT variables were compared between reference and patients with LTF. All DXA measures were significantly lower in patients with LTF than in young healthy adults (all $p < 0.001$). All pQCT bone density measures of the tibia, as well as cortical thickness, were significantly lower in fracture patients than in young healthy adults (all $p < 0.05$), whereas trabecular cross-sectional area (Trb CSA) was significantly higher in fracture patients than in young healthy adults ($p < 0.001$). SSIp and cortical cross-sectional area (Crt CSA) had no significant difference between the 2 groups ($p = 0.34$ and $p = 0.19$, respectively). Results of comparison between reference and patients with LTF are shown in Table 2.

Table 2
DXA and pQCT Results and T-scores from Reference and Patients with LTF

Variable	Reference[a]	LTF[a]	95% CI[b]	*p*	T-score of fracture participants[a]
DXA aBMD (g/cm^2)					
Lumbar spine	1.038 ± 0.129	0.952 ± 0.167	(0.036, 0.135)	0.001[c]	−1.00 ± 1.41
Femoral neck	0.864 ± 0.142	0.715 ± 0.115	(0.113, 0.186)	<0.001[c]	−1.78 ± 0.90
Trochanteric region	0.720 ± 0.118	0.677 ± 0.133	(0.002, 0.084)	0.02[c]	−0.79 ± 1.31
Total hip	0.933 ± 0.135	0.853 ± 0.139	(0.038, 0.123)	<0.001[c]	−1.09 ± 1.04
pQCT of the tibia					
SSIp (mm^3)	2256.5 ± 451.1	2183.4 ± 556.1	(−79.5, 225.7)	0.34	−0.16 ± 1.23
Tot vBMD (mg/cm^3)	327.2 ± 41.8	247.4 ± 49.1	(66.3, 93.3)	<0.001	−1.91 ± 1.17
Trb CSA (mm^2)	443.1 ± 63.6	524.7 ± 97.8	(−108.0, −55.2)	<0.001[c]	1.28 ± 1.54
Trb vBMD (mg/cm^3)	248.6 ± 35.1	195.6 ± 39.2	(42.1, 63.9)	<0.001	−1.51 ± 1.12
Crt CSA (mm^2)	285.4 ± 41.5	275.0 ± 57.3	(−5.2, 26.0)	0.19	−0.25 ± 1.38
Crt vBMD (mg/cm^3)	1150.9 ± 26.7	1105.5 ± 42.0	(34.1, 56.7)	<0.001	−1.70 ± 1.57
Crt thk (mm)	4.14 ± 0.62	3.86 ± 0.86	(0.05, 0.51)	0.02	−0.45 ± 1.37

[a]Results expressed as mean ± SD.
[b]95% CI for (Reference—LTF).
[c]*p* for Wilcoxon rank sum test due to non-normal distribution.

DXA T-scores and pQCT variables of the tibia were compared between participants with and participants without osteoporosis diagnosed by DXA. DXA T-scores were significantly lower in patients with osteoporosis than in patients without osteoporosis (Table 3). Most pQCT variables of the tibia were significantly lower in patients with osteoporosis diagnosed by DXA than in patients without osteoporosis diagnosed by DXA (p ranges from <0.001 to 0.02), except Trb CSA ($p > 0.9$) and Crt vBMD ($p = 0.5$). Results of comparisons between patients with and patients without osteoporosis are shown in Table 3.

Reclassification of Fracture Patients

According to the reclassification, in evaluating bone fragility in patients with LTF, single pQCT T-score variables, compared with DXA T-scores, did not identify more patients at high risk, except the T-score for Total vBMD (Tot vBMD), which identified 23 patients at high risk, compared with 18 patients using DXA T-scores alone. Combining all selected pQCT T-score variables identified 7 more patients at high risk than did DXA T-scores alone. Among the 41 DXA-normal or DXA-osteopenia participants, 11 (27%) patients were reclassified from low or medium risk

Table 3
DXA and pQCT Results of Osteoporosis and Non-osteoporosis Participants Diagnosed by DXA T-scores

Variable	Osteoporosis[a]	Non-osteoporosis[a]	95% CI[b]	*p*
DXA T-score				
Lumbar spine	−2.28 ± 1.35	−0.44 ± 1.02	(1.11, 2.58)	<0.001
Femoral neck	−2.62 ± 0.48	−1.39 ± 0.78	(0.90, 1.57)	<0.001
Trochanteric region	−1.88 ± 1.13	−0.28 ± 1.06	(0.95, 2.24)	<0.001
Total hip	−2.04 ± 0.89	−0.66 ± 0.80	(0.88, 1.88)	<0.001
pQCT of the tibia				
SSIp (mm^3)	1691.3 ± 404.2	2400.1 ± 471.3	(464.2, 952.8)	<0.001
Tot vBMD (mg/cm^3)	209.4 ± 40.9	264.1 ± 42.9	(30.9, 78.6)	<0.001
Trb CSA (mm^2)	526.3 ± 144.6	524.2 ± 71.0	(−76.1, 73.0)	>0.9
Trb vBMD (mg/cm^3)	159.2 ± 28.7	211.6 ± 31.9	(35.4, 69.5)	<0.001
Crt CSA (mm^2)	238.1 ± 60.0	291.2 ± 48.5	(20.2, 86.1)	0.003
Crt vBMD (mg/cm^3)	1100.1 ± 37.3	1107.9 ± 44.1	(−14.8, 30.4)	0.5
Crt thk (mm)	3.44 ± 0.86	4.04 ± 0.78	(0.11, 1.09)	0.02

[a]Results expressed as mean ± SD.
[b]95% CI for (Non-osteoporosis—Osteoporosis).

Table 4
Classification of Patients with LTF by Combinations of DXA-T-scores and pQCT T-scores

	DXA T-scores		
	Normal (n = 8)	Osteopenia (n = 33)	Osteoporosis (n = 18)
T-score of SSIp			
Normal	8	33	6
Moderate risk	0	0	11
High risk	0	0	1
T-score of Tot vBMD			
Normal	2	14	1
Moderate risk	3	11	5
High risk	3	8	12
T-score of Trb vBMD			
Normal	5	16	0
Moderate risk	2	16	8
High risk	1	1	10
T-score of Crt CSA			
Normal	5	30	9
Moderate risk	2	3	7
High risk	1	0	2
T-score of Crt Thk			
Normal	4	28	10
Moderate risk	3	5	5
High risk	1	0	3
Combination of pQCT T-scores			
Normal	2	12	0
Moderate risk	3	13	4
High risk	3	8	14

to high risk by combination of pQCT T-scores (Table 4). By applying DXA and pQCT T-scores together, 29 patients were identified as having high risk, which increased the percentage diagnosed with osteoporosis from 30.5% to 49.2% (Table 4).

Logistic Regression Analyses

All pQCT T-score variables had a moderate linear correlation with at least 1 DXA T-score variable ($r \geq 0.6$, $p < 0.001$), except T-scores for Crt vBMD and Trb CSA, which correlated weakly with all DXA T-scores ($r < 0.5$). The logistic regression model (without adjustment for fracture risk factors) suggested that each SD decrease in the T-score of SSIp increased the risk of DXA osteoporosis by 78.6% (odds ratio [OR] 0.214; 95% confidence interval [CI], 0.068–0.671, $p = 0.001$), and each SD decrease of the T-score of Trb vBMD increased the risk of DXA osteoporosis by 79.7% (OR 0.203; 95% CI, 0.057–0.722, $p = 0.003$). These associations remained significant after adjusting for fracture risk factors. Risk of DXA osteoporosis was greater with each SD decrease in this multivariate regression model (OR 0.033; 95% CI, 0.004–0.313, $p < 0.001$ for T-score of SSIp; OR 0.032, 95% CI 0.003–0.391, $p < 0.001$ for T-score of Trb vBMD). Sixty-two percent of the change in osteoporosis status can be explained by this model (Table 5).

Discussion

Peripheral QCT has several advantages over DXA. First, it can measure volumetric vBMD. Compared with DXA, which measures BMD as the bone mineral content in a projected bone area (aBMD), pQCT can monitor BMD in a given volume owing to the volumetric data acquired *(10)*. This is a true physical density (in the unit of mg/cm^3), which is independent of bone size. Second, pQCT can separately estimate trabecular and cortical compartments of bone, whereas DXA can calculate only an average or integral BMD of the whole bone. Trabecular bone is approximately 8 times more metabolically active than cortical bone and changes more quickly over time, and with many diseases and treatments than cortical bone *(11)*. The ability of pQCT to discriminate between trabecular and cortical compartments is potentially advantageous as a previous study showed that cortical and trabecular structures are differentially associated with fragility fracture *(12)*. Finally, pQCT can also measure bone geometry, allowing estimation of bone bending strength. Geometric parameters have a strong correlation with bone failure loads measured experimentally *(13,14)*. In postmenopausal women, bone geometry parameters are significantly different from those in young females *(15)*. SSI assessed by pQCT, which reflects the mechanical competence of human bone, is based on the calculation of geometric parameters and has been recommended as a diagnostic indicator for osteoporosis or

Table 5
T-scores of SSIp and Trb vBMD as Independent Predictors of Osteoporosis Status Determined by DXA T-scores Alone

	Adjusted for age, sex, and BMI		Adjusted for age, sex, BMI, and fracture risk factors	
	p	OR (95% CI)	*p*	OR (95% CI)
SSIp	0.001	0.2137 (0.0680, 0.6711)	0.003	0.0329 (0.0035, 0.3127)
Trb vBMD	0.003	0.2034 (0.0573, 0.7221)	0.007	0.0320 (0.0026, 0.3907)

related bone-weakening diseases *(16–18)*. In a recent study, Cointry et al argued that the mechanical competence of bone was mostly determined by those geometric parameters rather than BMD *(19)*.

In this study, we used pQCT data of young healthy females as reference data, based on which individual pQCT T-scores of the fracture patients were calculated. We applied the same reference data to both female and male fracture patients. According to our data, similar differences were observed in all pQCT variables between men and women, except in Crt vBMD ($p = 0.15$). This is consistent with previous studies of normative pQCT data, although there was a relatively small sample size of male participants in this study. In a study by Langsetmo et al *(20)*, the authors demonstrated the validity of using female reference data for both males and females. Three methods of BMD normalization were compared in age-adjusted regression models, and parallel results for the 3 models were observed. In a literature review by Kanis et al *(21)*, several prospective studies were reviewed and the authors concluded that the same criteria used to diagnose osteoporosis and estimate fracture risk in women can be applied to men.

In our study, significant differences were observed in both pQCT bone density and bone geometry variables between healthy young adults and fracture patients. All vBMD variables were significantly lower in older patients than in young females, which was consistent with differences in bone quantity variables determined by DXA. The difference in Trb vBMD was more apparent than that of Crt vBMD (21.3% vs 3.9%), which suggested that changes in trabecular bone were much faster than those in cortical bone, for example, cortical porosity. Differences in Tot vBMD and Trb vBMD (24.4% and 21.3%, respectively) were generally more apparent than those in aBMD (8.3%, 17.2%, 6.0%, and 8.6% for LS aBMD, FN aBMD, Tro aBMD, and TH aBMD, respectively). This may suggest that pQCT-determined Tot vBMD and Trb vBMD are more sensitive to changes of the tibia in relation to age; however, more data from in-between age groups are needed to validate this hypothesis.

Trb CSA was significantly higher, whereas Crt Thk was significantly lower in older patients than in young adults. These findings were consistent with data of Yuen et al *(22)*. This may be due to the "trabecularization" of the endocortical surface, a process of expansion of the marrow cavity particularly in long bones, leading to aged cortical bone exhibiting morphological similarities to trabecular bone *(23)*. In pQCT analysis of these geometric variables, the Contour Mode defines the outer surface of cortical bone first. Then, the Peel Mode separates cortical bone from trabecular bone by applying a default threshold of 710 mg/cm^3. Because of the "trabecularization" of the endo-cortical bone, less bone volume is defined as cortical bone by the default threshold of analysis software, whereas more bone volume is categorized as trabecular bone. This likely explains the observed changes in bone geometric variables between young adults and fracture patients.

Perhaps surprisingly, no significant difference was observed in SSIp between young adults and older patients with LTF. This is probably because cortical measures are affected to a lesser degree than trabecular measures in this relatively young population with LTF compared with a population with mean age of over 70 or 80 years. SSIp presumably would be decreased if the study population included older people aged over 70 or 80 years. Perhaps this in turn is associated with the fracture types (mostly Colles' fracture) that were observed in our study population. Another possible explanation is that SSIp calculated from the commercial software has some limitations, at least in the observed age group, when used to assess bone fragility. Future research can be focused on other techniques that have been developed in mechanical engineering, such as finite element analysis, to generate more clinically relevant parameters *(24,25)*.

Among the pQCT measures of interest, we found that T-scores of SSIp and Trb vBMD predicted the osteoporosis status (defined by DXA T-scores) of patients with LTF independently of age, sex, and BMI. The model explained 62% of variations of osteoporosis status. This finding confirmed utility of pQCT T-scores in the diagnosis of osteoporosis.

The most significant finding of this study was that more patients with LTF would be identified as high risk (osteoporosis) after introducing pQCT T-scores into the diagnostic criteria for osteoporosis. Although a single pQCT T-score variable (T-score of Tot vBMD) identified more patients at high risk when applied individually compared with DXA T-scores, our study found that most pQCT T-scores when applied alone did not perform better than DXA T-scores in identifying patients at high risk. This finding justified the combination of several pQCT T-scores as well as combination with DXA T-scores. Indeed, when applied in combination with DXA T-scores, 49.2% of patients with LTF would be classified as having osteoporosis (18.7% more than using DXA alone), which therefore could improve the rate of osteoporosis intervention in these older patients. Among the patients who were classified as having low or medium risk by DXA T-scores alone, 11 of 41 (27%) were reclassified as having high risk by applying pQCT T-scores, which was the most significant finding in this study.

Another interesting finding was that although the SSIp T-score was a good predictor for DXA-detected osteoporosis by the logistic regression analysis, its sensitivity in the diagnosis of osteoporosis was poor if the same cutoff values were used with DXA T-scores in our sample. Indeed, most patients had a T-score of SSIp >−2.0 in our sample. One of the reasons was that no significant difference was observed in SSIp between healthy young females and patients with LTF, the reason for which was discussed above. Another reason may be that a cutoff value of −2.5 or less is not applicable for SSIp, at least in a population of patients aged 50–70 years. Future epidemiological studies therefore are needed to describe the distribution of pQCT

T-scores in different age groups and in relation to the prediction of incident fractures.

A limitation of the current study was the small sample size of male participants. A limited number of studies have focused on osteoporosis in men due to the lower incidence of osteoporotic fracture in men than in women. Including male participants is actually one of the strengths of this study; however, data from only 15 male participants were obtained, which limited the feasibility of dividing all participants into groups based on gender. Sex-related differences have been found in bone remodeling of the tibia *(26)*, and results from a population study showed that significant differences existed in pQCT tibia measures (mostly cortical measures) between older men and women *(27)*. However, further analyses showed similar results when only female data were analyzed in this study. Therefore, it would be informative if more data from older males could be obtained and data of males and females could be compared.

In conclusion, DXA has limitations in identifying patients with increased fracture risk as only 30.5% of patients who had sustained LTFs were classified as osteoporotic by DXA T-scores. The use of pQCT T-scores can reclassify 27% (11 out of 41) of patients from low or medium risk to high risk (osteoporosis) and appears to complement the use of DXA T-scores in estimating fracture risk.

Acknowledgments

The authors thank Ms Emma Callegari for the extraction of reference data from the 2 studies on young women's health and Mr Richard Farrugia for coordinating the referral of patients to the fracture liaison service.

References

1. Svedbom A, Hernlund E, Ivergård M, et al. 2013 Osteoporosis in the European Union: a compendium of country-specific reports. Arch Osteoporos 8:137.
2. Fonseca A, Gordon CL, Barr RD. 2013 Peripheral quantitative computed tomography (pQCT) to assess bone health in children, adolescents, and young adults: a review of normative data. J Pediatr Hematol Oncol 35(8):581–589.
3. Cointry GR, Ferretti JL, Reina PS, et al. 2014 The pQCT "Bone Strength Indices" (BSIs, SSI). Relative mechanical impact and diagnostic value of the indicators of bone tissue and design quality employed in their calculation in healthy men and pre- and post-menopausal women. J Musculoskelet Neuronal Interact 14(1):29–40.
4. Yates CJ, Chauchard MA, Liew D, et al. 2015 Bridging the osteoporosis treatment gap: performance and cost-effectiveness of a fracture liaison service. J Clin Densitom 18(2):150–156.
5. Jayasinghe Y, Rangiah C, Gorelik A, et al. 2016 Primary HPV DNA based cervical cancer screening at 25 years: views of young Australian women aged 16–28 years. J Clin Virol 76(Suppl 1):S74–S80. doi:10.1016/j.jcv.2015.10.026.
6. Callegari ET, Reavley N, Garland SM, et al. 2015 Vitamin D status, bone mineral density and mental health in young Australian women: the Safe-D study. J Public Health Res 4(594):152–156.
7. Briggs AM, Perilli E, Parkinson IH, et al. 2010 Novel assessment of subregional bone mineral density using DXA and pQCT and subregional microarchitecture using micro-CT in whole human vertebrae: applications, methods, and correspondence between technologies. J Clin Densitom 13(2):161–174.
8. Kanis JA, Oden A, Johansson H, et al. 2009 FRAX® and its application to clinical practice. Bone 44(5):734–743.
9. WHO Study Group on Assessment of Fracture Risk and its Application to Screening for Post Menopausal Osteoporosis. 1994 Assessment of Fracture risk and its Application it Screening for Post Menopausal Osteoporosis: Report of a WHO Study Group. Geneva: WHO. WHO Technical Series 843.
10. Engelke K, Libanati C, Liu Y, et al. 2009 Quantitative computed tomography (QCT) of the forearm using general purpose spiral whole-body CT scanners: accuracy, precision and comparison with dual-energy X-ray absorptiometry (DXA). Bone 45(1):110–118.
11. Clarke B. 2008 Normal bone anatomy and physiology. Clin J Am Soc Nephrol 3(Suppl 3):S131–S139.
12. Roux JP, Wegrzyn J, Arlot M, et al. 2010 Contribution of trabecular and cortical components to biomechanical behavior of human vertebrae: an ex vivo study. J Bone Miner Res 25(2):356–361.
13. Lochmüller EM, Lill CA, Kuhn V, et al. 2002 Radius bone strength in bending, compression and falling and its correlation with clinical densitometry at multiple sites. J Bone Miner Res 17(9):1629–1638.
14. Muller ME, Webber CE, Bouxsein ML. 2003 Predicting the failure load of the distal radius. Osteoporos Int 14(4):345–352.
15. Stathopoulos KD, Katsimbri P, Atsali E, et al. 2011 Age-related differences of bone mass, geometry and strength in treatment-naïve postmenopausal women. A tibia pQCT study. J Clin Densitom 14(1):33–40.
16. Wong AKO, Beattie KA, Min KKH, et al. 2015 A trimodality comparison of volumetric bone imaging technologies. Part I: short-term precision and validity. J Clin Densitom 18(1):124–135.
17. Ahlborg HG, Johnell O, Turner CH, et al. 2003 Bone loss and bone size after menopause. NEJM 349(4):327–334.
18. Sheu Y, Zmuda JM, Boudreau RM, et al. 2011 Bone strength measured by peripheral quantitative computed tomography and the risk of nonvertebral fractures: the Osteoporotic in Men (MrOS) Study. J Bone Miner Res 26(1):63–71.
19. Cointry GR, Ferretti JL, Reina PS, et al. 2014 The pQCT Bone Strength Indices" (BSIs, SSI). Relative mechanical impact and diagnostic value of the indicators of bone tissue and design quality employed in their calculation in healthy men and pre- and post-menopausal women. J Musculoskel Neuron 14(1):29–40.
20. Langsetmo L, Leslie WD, Zhou W, et al. for the CaMOS Research Group. 2010 Using the same bone density reference database for men and women provides a simpler estimation of fracture risk. J Bone Miner Res 25(10):2108–2114.
21. Kanis JA, Johnell O, Oden A, et al. 2001 Diagnosis of osteoporosis and fracture threshold in men. Calcif Tissue Int 69:218–221.
22. Yuen KW, Kwok TC, Qin L, et al. 2010 Characteristics of age-related changes in bone compared between male and female reference Chinese populations in Hong Kong: a pQCT study. J Bone Miner Metab 28(6):672–681.

23. Zebaze RM, Ghasem-Zadeh A, Bohte A, et al. 2010 Intracortical remodelling and porosity in the distal radius and post-mortem femurs of women: a cross-sectional study. Lancet 375(9727):1729–1736.
24. Carpenter RD. 2013 Finite element analysis of the hip and spine based on quantitative computed tomography. Curr Osteoporos Rep 11(2):156–162.
25. Engelke K, Libanati C, Fuerst T, et al. 2013 Advanced CT based in vivo methods for the assessment of bone density, structure, and strength. Curr Osteoporos Rep 11:246–255.
26. Ruff CB, Hayes WC. 1988 Sex differences in age-related remodelling of the femur and tibia. J Orthop Res 6(6):886–896.
27. Riggs BL, Melton LJ, Robb RA, et al. 2004 Population-based study of age and sex differences in bone volumetric density, size, geometry, and structure at different skeletal sites. J Bone Miner Res 19(12):1945–1954.

Appendix 2

Biomechanics and Modeling in Mechanobiology (2019) 18:245–260
https://doi.org/10.1007/s10237-018-1079-7

ORIGINAL PAPER

The application of finite element modelling based on clinical pQCT for classification of fracture status

Dale L. Robinson[1] · Hongyuan Jiang[2] · Qichun Song[2,3] · Christopher Yates[4] · Peter Vee Sin Lee[1] · John D. Wark[2,5]

Received: 15 April 2018 / Accepted: 17 September 2018 / Published online: 6 October 2018

Abstract
Fracture risk assessment using dual-energy X-ray absorptiometry (DXA) frequently fails to diagnose osteoporosis amongst individuals who later experience fragility fractures. Hence, more reliable techniques that improve the prediction of fracture risk are needed. In this study, we evaluated a finite element (FE) modelling framework based on clinical peripheral quantitative computed tomography (pQCT) imaging of the tibial epiphysis and diaphysis to predict the stiffness at these locations in compression, shear, torsion and bending. The ability of these properties to identify a group of women who had recently sustained a low-trauma fracture from an age- and weight-matched control group was determined and compared to clinical pQCT and DXA properties and structural properties based on composite beam theory. The predicted stiffnesses derived from the FE models and composite beam theory were significantly different ($p < 0.05$) between the control and fracture groups, whereas no meaningful differences were observed using DXA and for the stress–strain indices (SSIs) derived using pQCT. The diagnostic performance of each property was assessed by the odds ratio (OR) and the area under the receiver operating curve (AUC), and both were greatest for the FE-predicted shear stiffness (OR 16.09, 95% CI 2.52–102.56, $p = 0.003$) (AUC: 0.80, 95% CI 0.67–0.93). The clinical pQCT variable total density (ρ_{tot}) and a number of structural and FE-predicted variables had a similar probability of correct classification between the control and fracture groups (i.e. ORs and AUCs with mean values greater than 5.00 and 0.80, respectively). In general, the diagnostic characteristics were lower for variables derived using DXA and for the SSIs (i.e. ORs and AUCs with mean values of 1.65–2.98 and 0.64–0.71, respectively). For all properties considered, the trabecular-dominant tibial epiphysis exhibited enhanced classification characteristics, as compared to the cortical-dominant tibial diaphysis. The results of this study demonstrate that bone properties may be derived using FE modelling that have the potential to enhance fracture risk assessment using conventional pQCT or DXA instruments in clinical settings.

Keywords pQCT · FE modelling · Fracture status · Bone strength

1 Introduction

Osteoporotic fractures are a global health concern amongst the elderly and have been linked to increased hospitalisation, morbidity and mortality (Nazrun et al. 2014; Sattui and Saag 2014; Johnell and Kanis 2006). Areal bone mineral density (aBMD) measured by dual-energy X-ray absorptiometry (DXA) is currently the clinical 'gold standard' for osteoporosis diagnosis, and low BMD has been widely recognised as a risk factor for fracture (Stone et al. 2003; Kanis 2002). However, a large proportion of individuals who are not diagnosed as osteoporotic by DXA still experience low-trauma bone

Electronic supplementary material The online version of this article (https://doi.org/10.1007/s10237-018-1079-7) contains supplementary material, which is available to authorized users.

✉ Peter Vee Sin Lee
pvlee@unimelb.edu.au

[1] Department of Biomedical Engineering, University of Melbourne, Melbourne, VIC 3010, Australia

[2] Department of Medicine, Royal Melbourne Hospital, University of Melbourne, Melbourne, VIC, Australia

[3] Department of Orthopaedics, 2nd Affiliated Hospital, Xi'an Jiaotong University, Xi'an, China

[4] Department of Diabetes and Endocrinology, Royal Melbourne Hospital, Melbourne, VIC, Australia

[5] Bone and Mineral Medicine, Royal Melbourne Hospital, Melbourne, VIC, Australia

fracture (Schuit et al. 2004; Siris et al. 2001); hence, there remains a need to develop new clinical methods that better identify individuals at risk of fracture.

The strength of bone changes with 'bone quality' and is a function of its structural architecture and constituents (Seeman and Delmas 2006; Ammann and Rizzoli 2003). Quantitative computed tomography (QCT) provides measurements of volumetric BMD (vBMD), which is dependent on bone structure and composition. The vBMD derived at each voxel in a QCT scan may be converted into an equivalent Young's modulus (E), and using composite beam theory, the axial, bending and torsional rigidities of the bone may be calculated (Whealan et al. 2000; Morgan et al. 2003). These structural properties have been shown to provide superior fracture risk predictions compared with clinical radiographic criteria (Snyder et al. 2006, 2009). Bone strength metrics such as stress–strain indices for bending (SSI_x and SSI_y) and torsion (SSI_{pol}) have also been used for fracture risk prediction (Erlandson et al. 2012; Duckham et al. 2013, 2014). These indices compare the structural rigidity of cortical bone to an identically shaped bone with physiologically normal cortical density (1200 mg/cm^3) and have been shown to predict 40–80% of variance in the bone failure loads for three-point bending (Lochmüller et al. 2002; Kontulainen et al. 2008) and compression (Lochmüller et al. 2002; Kontulainen et al. 2008; Ashe et al. 2006; Muller et al. 2003). A limitation of the aforementioned structural properties and strength indices is that they neglect three-dimensional (3D) effects, such as transverse shear and volume changes (Poisson effect). Techniques that consider 3D bone loading may offer some improvement in predictions of bone fracture risk, as compared to current methods.

Finite element (FE) models of cadaveric bones created from non-invasive imaging, such as peripheral QCT (pQCT), have demonstrated an excellent ability to predict bone fracture strength for bending and compression, accounting for 70–90% of variance between specimens (Pistoia et al. 2002; Varga et al. 2009; Zysset et al. 2013). Further, FE models derived from HR-pQCT (Nishiyama et al. 2013; Liu et al. 2012) or QCT (Amin et al. 2011) have demonstrated good classification characteristics for identifying fracture status with area under the receiver operating curve (AUC) of 0.69–0.85. However, assessing fracture risk by QCT or HR-pQCT in a clinical setting poses three dilemmas: (1) the long time required to set up and analyse patient-specific FE models (3.5–10 h (Kawalilak et al. 2016)), (2) the large radiation dose associated with QCT, which for a 10-cm 3D scan of L1 and L2 or a 15-cm 3D scan of the proximal femur ranges from 1.5 to 3.0 mSv (Engelke et al. 2008), and (3) the prohibitively high costs involved with either purchasing or scanning with a HR-pQCT system. A novel approach is needed to address these challenges facing the application of FE modelling as an effective tool for clinical assessment of bone properties and fracture risk. In the study described here, we have investigated whether FE modelling derived from tibial pQCT images may provide a solution.

Clinical tibia pQCT imaging typically targets two locations, the trabecular-dominant distal epiphysis (4% site of the tibial length from the distal end) and the cortical-dominant diaphysis (e.g. the 66% site) (Duckham et al. 2013; Rinaldi et al. 2011). To limit radiation dose and scan time, only a single cross section ~2 mm thick is obtained at these two locations. By generating an FE model based upon these cross sections, all of the aforementioned issues would be addressed: the radiation dose and scan time would be minimal and within clinical imaging protocols, and the FE model simplicity would allow its construction to be quick and easily automated. Whilst this FE model would not represent the entire length of bone, it would account for three-dimensional stresses that are neglected when using structural properties or strength indices.

The aims of the current study were to (1) develop an FE model based on clinical pQCT imaging protocols that predicted the compressive, shear, torsional and bending stiffness of tibial epiphysis and diaphysis and (2) to compute and compare the diagnostic characteristics of DXA, pQCT, structural and FE model variables to identify individuals who have recently sustained a low-trauma fracture.

2 Materials and methods

2.1 Study design

This study assessed the ability of FE-predicted stiffness variables derived from pQCT scans of the tibia to distinguish between patients who had recently sustained a low-trauma fracture at another skeletal site (fracture group) and subjects who had no prior fragility fracture history (control group). The properties of the intact tibia were assumed representative of the subject's current skeletal health, which was assumed deficient for the fracture patients. The tibia was considered because it is readily accessed by a pQCT scanner, it is a site that has been well documented to exhibit changes in its micro-architecture due to ageing and osteoporosis (see review by Nishiyama and Shane 2013), and because tibial parameters have been associated with osteoporotic fractures at any skeletal site (Vilayphiou et al. 2011). The classification analysis was repeated for structural properties calculated from composite beam theory, for routine properties used in clinical pQCT imaging and for DXA-derived measurements of aBMD for the total hip and lumbar spine.

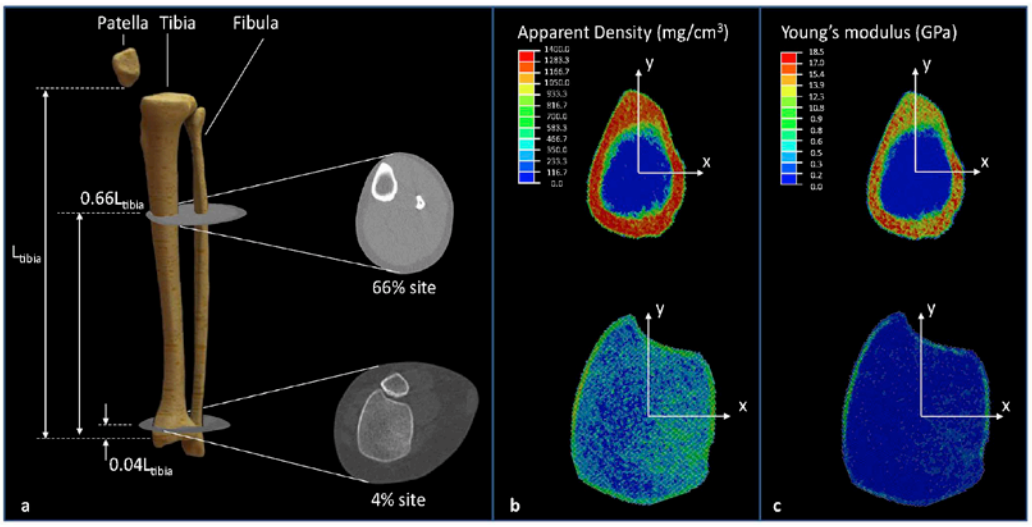

Fig. 1 Diagram of pQCT imaging sites and the mapping of apparent density (ρ_{app}) and Young's modulus. **a** Location of 66 and 4% sites on tibia. L_{tibia}, length of tibia estimated as distance from medial malleolus to inferior apex of patella. Representative pQCT images obtained at the 66 and 4% sites are provided. **b** Contour plot of ρ_{app} at 66 and 4% sites. **c** Contour plot of Young's modulus at 66 and 4% sites. The origin was aligned with the density-weighted centroid of each cross section, and the *x*- and *y*-axes were aligned with the minimum and maximum neutral axes, respectively

2.2 Participants

The fracture group comprised 23 post-menopausal women [age 64.4 ± 8.3 years (mean ± SD)] who had experienced a low-trauma fracture (i.e. a fracture incurred from trauma equivalent to or less than a fall from standing height). Each patient of the fracture group had at least one tibia without fracture, and these patients were scanned within 3 months post-fracture using pQCT and DXA (see "Scanning protocol" section). The control group comprised 23 post-menopausal women (age 64.8 ± 6.8 years) that had no prior history of fracture to the imaged tibia and who had not incurred any previous fragility fractures. Healthy controls were recruited through electronic and paper-based advertisements at the University of Melbourne and the Royal Melbourne Hospital. The control participants were included if they were greater than 50 years of age, had no prior history of medical conditions that may affect bone health (e.g. osteoporosis, hyperthyroidism, diabetes) and if using hormone replacement therapy were receiving a stable dose. Control and fracture group patients were also selected to achieve a height- and weight-match between the groups. All low-trauma fracture patients were recruited through the Royal Melbourne Hospital Fracture Capture program (Yates et al. 2015). Ethics approval for this study was obtained from the Melbourne Health Human Research Ethics Committee [ID MH2014.143]. Patients provided written informed consent before participation.

2.3 pQCT and DXA scanning protocol

A Stratec XCT-3000 pQCT scanner (Medizintechnik, Pforzheim, Germany) running operating software version 6.20 acquired axial cross sections of the tibia. Scans were performed by an experienced technologist according to the XCT-3000 software user's manual. Axial images were obtained at two sites, 4 and 66% of the bone length measured proximally from the distal articular surface (Fig. 1a). A scout scan was used to locate the distal articular surface of the tibia. Each cross section had a slice thickness of 2 mm and a 0.4 mm voxel size. Tibia length (L_{tibia}) was measured manually as the vertical distance from the medial malleolus to the inferior apex of the patella, whilst the knee was flexed at 90°. Daily phantom scans were performed to assess long-term scanner stability, and to date, no alterations of the calibration function have been required.

A fan-beam densitometer (Horizon QDR 4500A, Hologic Inc., Bedford, MA, USA) was used to scan the hip and lumbar spine of each subject. The scans were analysed using the manufacturer's commercial software (version 9.10D) to obtain aBMD measurements for the femoral neck, lumbar spine and total hip. All scans were performed in array mode

by an experienced operator, and the 12-month precision of the scanner for the spine phantom was 0.39% for aBMD and 0.58% for bone mineral content (Briggs et al. 2010).

2.4 pQCT properties

The tibial bone pQCT images were manually segmented using commercially available software (MATLAB; version R2016b Mathworks, Natick, MA, USA), and the Hounsfield unit (H_f) of each voxel was converted to apparent bone mineral density (ρ_{app}) using Eq. 1 (see also Fig. 1b), which was derived for the scanner based on the specifications provided in the open-source software BoneJ (Doube et al. 2010). These segmented data were used to derive standard pQCT variables including: total area (a_{tot}) and total density (ρ_{tot}). The bone stress–strain indices for bending (SSI_x and SSI_y) and torsion (SSI_{pol}) were calculated for each of the 4 and 66% locations (Eqs. 2–3).

$$\rho_{app} = 1.484H_f - 48965, \tag{1}$$

$$SSI_x = \sum \frac{CD_i A_i d_{y,i}^2}{CD_{norm} d_{ymax}}, \quad SSI_y = \sum \frac{CD_i A_i d_{x,i}^2}{CD_{norm} d_{xmax}}, \tag{2}$$

$$SSI_{pol} = \sum \frac{CD_i A_i r_i^2}{CD_{norm} r_{max}}, \tag{3}$$

where ρ_{app} is the apparent bone mineral density; H_f is the Hounsfield unit; CD_i is the cortical bone density; A_i is the area of voxel i; $d_{x,i}$, $d_{y,i}$ and r_i are the horizontal, vertical and radial distances of voxel i from the cortex centroid, respectively; CD_{norm} is the normal physiological density of cortical bone (1200 g/cm^3); and d_{xmax}, d_{ymax} and r_{max} are the maximum x, y and radial distances of a cortical bone voxel from the cortex centroid, respectively. The x- and y-axes were aligned with the minimum and maximum neutral axes, respectively, derived from the cortical bone in each cross section.

2.5 Structural properties

The Young's modulus (E_i) of cortical and trabecular bone was calculated at each voxel i in the segmented pQCT images using Eq. 4, which was derived from mechanical tests performed on small cylindrical bone specimens extracted from the tibia (Morgan et al. 2003) (see also Fig. 1c). Axial and torsional rigidities (EA and GJ, respectively) and the bending rigidity about the x and y-axes (EI_x and EI_y, respectively) were calculated for each cross section using Eqs. 5–8.

$$E_i = 15520\rho_{app,i}^{1.93}, \tag{4}$$

$$EA = \sum E_i a_i, \tag{5}$$

$$GJ = \sum G_i \left(x_i^2 + y_i^2\right) a_i, \tag{6}$$

$$EI_x = \sum E_i y_i^2 a_i; EI_y = \sum E_i x_i^2 a_i, \tag{7}$$

$$\bar{x} = \frac{\sum E_i x_i a_i}{\sum a_i}; \quad \bar{y} = \frac{\sum E_i y_i a_i}{\sum a_i}, \tag{8}$$

where E_i, G_i, $\rho_{app,i}$ and a_i are, respectively, the Young's modulus, shear modulus, apparent density and area of voxel i. For transverse cross sections, G_i was taken as $E_i/2.6$ (Snyder et al. 2006). EA is the axial rigidity, GJ is the torsional rigidity, and EI_x and EI_y are the bending rigidities about the x- and y-axes. The x- and y-axes were aligned to the minimum and maximum neutral axes, respectively, derived using both the cortical and trabecular bone in each cross section. $\bar{x}$ and $\bar{y}$ are the coordinates of the density-weighted centroid for the cross section, and x_i and y_i represent the horizontal and vertical distance between voxel i and the density-weighted centroid.

2.6 FE model properties

Using MATLAB, the segmented pQCT images were extruded by the 2-mm slice thickness to generate a mesh of $0.4 \times 0.4 \times 2$ mm elements (Fig. 2a). Each element was modelled as a linear-elastic material with the respective E_i and G_i set to the values calculated above (see Sect. 2.5), and the mesh was re-sliced in the axial direction into 0.4-mm cubic elements (Fig. 2b). Each voxel mesh was used to create a FE model in the commercial software Abaqus (version 6.11, Simulia, Dassault Systemes, Providence, RI, USA). Although the cubic element size of 0.4 mm was too large to capture the topology of individual trabeculae, which for the distal tibia vary between 0.10 and 0.15 mm (Liu et al. 2010; Thomsen et al. 2005), previous FE models of the femur that represented cortical and trabecular bone with a continuum of elements that incorporated edge lengths greater than 1.5 mm were found to predict experimental bending and compressive strengths, with coefficients of determination (R^2) between 0.85 and 0.90 (Keyak et al. 1997; Koivumäki et al. 2012; Dragomir-Daescu et al. 2011). Hence, the continuum mesh with an element size of 0.4 mm implemented in the current study was assumed sufficient for modelling the contribution of the trabecular and cortical bone to the total stiffness of the 2-mm-thick tibial cross sections.

The origin of the models was set as the density-weighted centroid (Eq. 8), the x- and y-axes were aligned with the minimum and maximum neutral axes, respectively, and the z-axis was normal to the cross section. Four load cases were considered for all FE models; axial compression, shear, torsion and bending (Fig. 3a–d). Axial compression was simulated by a 0.01-mm displacement of the superior surface towards the inferior surface. Shear was simulated by a 0.01-mm displacement of the superior surface in the direction of either the x- or y-axes. Torsion was simulated by a 0.0001 rad rotation of the inferior surface about the z-axis. Bending was simu-

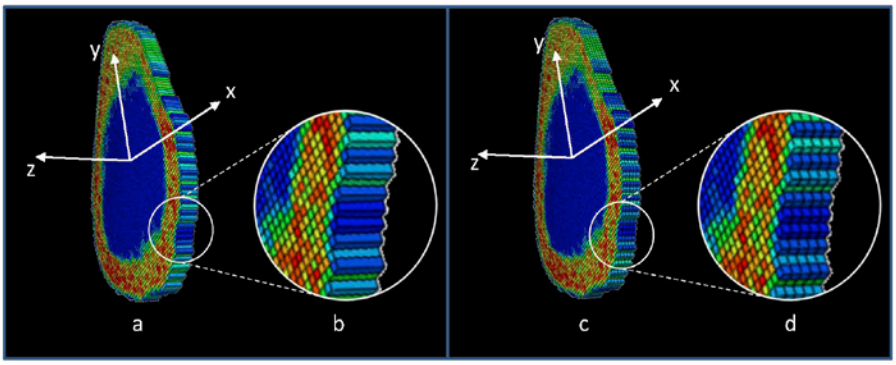

Fig. 2 Diagram of FE model mesh of a representative specimen at the 66% site. Contours corresponding to different Young's moduli are included in each picture. **a** FE model mesh generated by a 2-mm extrusion of the pQCT image. **b** Inset to part a showing the rectangular elements. **c** FE model mesh after re-slicing axially. **d** Inset to part c showing the 0.4-mm cubic elements. The origin of the models was set as the density-weighted centroid (Eq. 8), the *x*- and *y*-axes were aligned with the minimum and maximum neutral axes, respectively, and the *z*-axis was normal to the cross section

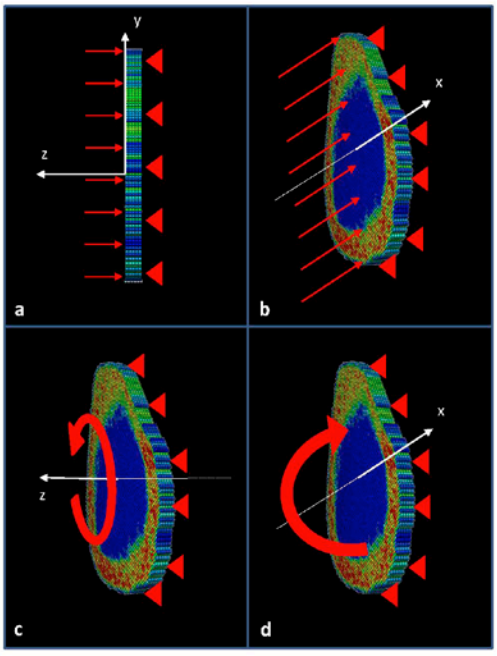

Fig. 3 Diagram of the load cases applied to each cross section. The FE mesh corresponds to a representative specimen at the 66% site, and the contours representing different Young's moduli are included in each picture. **a** Compression load case, corresponding to a 0.01-mm displacement. *Red arrows* applied displacement of 0.01 mm in the negative z direction. *Red triangles* fixed boundary condition applied to surface. **b** Shear load case. Red arrows applied displacement of 0.01 mm in either the positive x direction or positive y direction. **c** Torsion load case. *Red arrow* applied rotation of 0.0001 radians about the z-axis. **d** Bending load case. *Red arrow* applied rotation of 0.0001 radians about either the *x*- or *y*-axis

lated by a 0.0001 rad rotation of the inferior surface about either the *x*- and *y*-axes (i.e. cross-sectional neutral axes). These idealised loading conditions would almost certainly differ from tibial loading in vivo, where compression, shear, torsion and bending occur simultaneously (Yang et al. 2014). Logically, however, a bone that more weakly resists an idealised load has a greater risk of fracture for the combined load case. Indeed, this assumption has been adopted in previous micro-finite element studies, where the strength of the tibia or radius was calculated for idealised axial compression, and used to assess fracture risk (Vilayphiou et al. 2011).

The reaction forces and moments predicted from the simulations were divided by the respective applied displacement or rotation to determine the compressive stiffness (k_{comp}), shear stiffness (k_{shear}), torsional stiffness ($k_{torsion}$) and bending stiffness (k_{bend}) of each cross section. Although strain-based failure criteria in FE models have been previously used to predict bone strength (Pistoia et al. 2002), this was not possible here because results from a mesh convergence study showed the absolute strain predictions from our FE models were unreliable for 0.4-mm cubic elements implemented in a 2-mm-thick cross section (data not shown). In all simulations, the unprescribed degrees-of-freedom of the inferior and superior surfaces were set to zero to account for the resistance of the surrounding bone.

2.7 FE model verification

To verify that the FE model predictions were independent of the FE mesh size, a mesh convergence analysis was performed. For the 4 and 66% sites of a representative fracture subject, the original 0.4-mm cubic elements of the

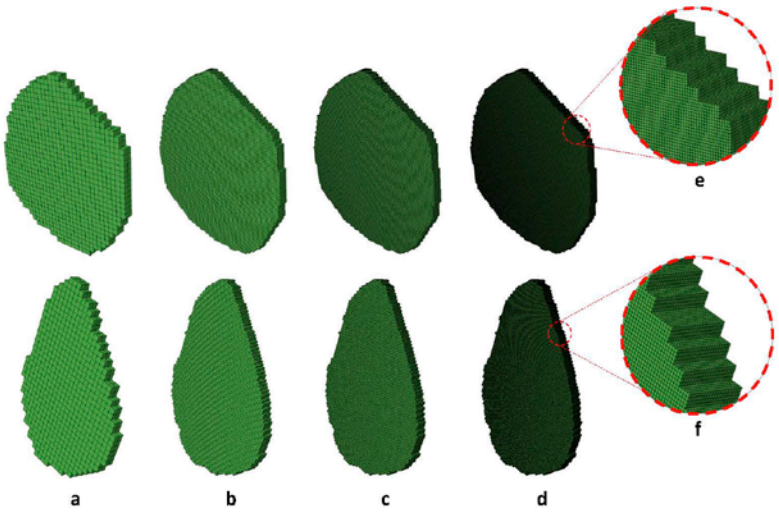

Fig. 4 FE model meshes corresponding to a different cubic element sizes that were used in the verification analysis. The FE models describe a 4% site (top row) and 66% site (bottom row) of a representative participant of the control group. FE models corresponded to cubic element sizes of 1.0, 0.4, 0.2 and 0.1 mm (**a**–**d**, respectively). Close-up views of the FE model mesh with a 0.1-mm cubic element size are shown for the 4 and 66% sites (**e** and **f**, respectively)

FE model were resized to 0.1, 0.2 or 1.0 mm (Fig. 4). The apparent density and, hence, modulus of the elements for each different mesh size were calculated at their respective centroids in MATLAB using a piecewise cubic surface fitted to the density distribution of the original pQCT image. The FE model for each mesh was used to simulate the four load cases, from which the corresponding FE model properties were calculated.

The rigid boundary conditions together with the thin cross sections would generate some stress concentrations in the FE model. However, by applying identical boundary conditions for all FE models, it was assumed that the relative differences in stiffness predicted between the control and fracture group would be consistent regardless of the cross-sectional thickness. To support this reasoning, three FE models of 50-mm-diameter cylindrical tubes of Young's modulus 0.15 GPa, 0.16 GPa and 0.17 GPa were created that were either 2 or 100 mm thick (see Supplementary material Fig. 1) and used to simulate the aforementioned compression, shear, torsion and bending load cases. The relative changes in stiffness predicted as the Young's modulus was varied were identical for each tube thickness (see Supplementary material Table 1), thus confirming that relative differences in FE-predicted bone properties were unlikely to have been affected by cross-sectional thickness.

2.8 Statistical analysis

Significant differences between the control and fracture groups were assessed by a two-sample Kolmogorov–Smirnov test ($p < 0.05$), which makes no assumption about the distribution of the data.

To identify collinearity, variance inflation factors (VIFs) were derived from multivariate linear regressions where the predictors were based on either the pQCT properties (a_{tot}, ρ_{tot}, SSI_x, SSI_y and SSI_{pol}), DXA properties (aBMD lumbar, aBMD femoral neck, aBMD total hip), structural properties (EA, GJ, EI_x and EI_y) or FE model properties (k_{comp}, k_{shear}, $k_{torsion}$ and k_{bend}), and any unrelated property taken as the dependent variable. Age, height and weight were also included in each regression, and collinearity was assumed for a VIF greater than 5.0 (Ringle et al. 2015).

To evaluate the relationship between fracture status and explanatory variables, a binary logistical regression was performed. The fracture status was considered a categorical variable, and each predictor, the pQCT, DXA, structural and FE model properties were considered in independent regressions, with each being adjusted for confounding variables, such as age, height and weight. Regression results were summarised by the odds ratio (OR) per standard deviation decrease in the predictor. For sets of properties found to be collinear, the property with the greatest average OR was included in the classification analysis, whilst the remaining collinear variables were excluded.

Table 1 Descriptive characteristics of the control and fracture groups and details of fracture sites incurred prior to imaging

Variable	Control group (N = 23)	Fracture group (N = 23)	*p* value
Age (years)	64.8 ± 6.8	64.4 ± 8.3	0.593
Height (cm)	162.3 ± 5.5	159.2 ± 8.9	0.096
Weight (kg)	68.1 ± 14.7	66.2 ± 10.8	0.983
BMI (kg/cm^2)	25.9 ± 5.6	26.2 ± 4.3	0.593
L_{tibia} (cm)	35.5 ± 1.6	33.0 ± 3.5	0.096
Fracture site[a]			
Contralateral tibia or fibula	0	5	
Ankle or foot	0	1	
Femur	0	1	
Humerus	0	3	
Radius	0	15	

Significant differences between the groups were assessed by a two-sample Kolmogorov–Smirnov test

L_{tibia} tibia length, *BMI* body mass index

[a]One fracture group patient sustained a fracture at both the radius and contralateral tibia, whilst another sustained both radial and humeral fracture

The ability of the predictors to classify patients as controls or fracture patients was evaluated by constructing receiver operating characteristic (ROC) curves based on each logistical regression. The sensitivity (ability to correctly identify fracture group patients) and specificity (ability to correctly identify control group patients) were determined for each predictor using standard diagnostic formulae (Lalkhen and McCluskey 2008), with optimal values selected based on the Youden's J statistic, which represents the maximum correct classification rate (Youden 1950). The area under the receiver operating curve (AUC) was also calculated for all predictors. All statistical analyses were performed using SPSS (version 24; SPSS Inc., Chicago, IL, USA).

3 Results

Descriptive characteristics of the control and fracture groups are provided in Table 1, where no significant differences were noted between the groups. The FE model verification analysis indicated that for a cubic element size of 1 mm applied to the 4 and 66% sites, the FE model properties (k_{comp}, k_{shear}, $k_{torsion}$ and k_{bend}) varied considerably from their corresponding values computed with a cubic element size of 0.1 mm by − 96.7 to 2.4% (Table 2). However, for smaller cubic element sizes of 0.4 and 0.2 mm, the FE model properties differed from those calculated with a cubic element size of 0.1 mm by 0.2 to 1.4%. These changes were considered minimal and verified that the FE model properties were independent of mesh size for cubic elements less than or equal to 0.4 mm.

The maximum and minimum principal stresses for each load case predicted by the FE models of a representative participant of the control group are provided for the 4 and 66% sites in Fig. 5. At the 4% site, the maximal principal stresses were confined to the thin layer of cortical bone for all load cases. In comparison, at the 66% site the maximal principal strains were located closer to the periosteum for torsion and bending, at both the endosteum for shear, and across the entire cortex for compression. The only exception to these trends was the maximum principal stress predicted for compression, which was largest for trabecular bone at the 4% site and for the low stiffness elements within the medullary cavity at the 66% site. The reaction force or moment for each load case was used to calculate the compression, shear, torsion and bending stiffness for each site (Table 3).

Table 2 FE model variables computed for different cubic element sizes at the 4 and 66% sites of a representative control subject

Site	Cubic element size (mm)	k_{comp}		k_{shear}		$k_{torsion}$		k_{bend}	
		Value (kN/mm)	Diff. (%)	Value (kN/mm)	Diff. (%)	Value (Nm/°)	Diff. (%)	Value (Nm/°)	Diff. (%)
4% site	1	1242.4	0.0	11.3	− 96.7	1213.0	−1.5	67.8	− 96.2
	0.4*	1256.7	1.1	345.1	1.4	1244.8	1.1	1824.4	1.4
	0.2	1245.9	0.2	341.8	0.4	1234.6	0.3	1805.5	0.3
	0.1	1242.9	N/A	340.4	N/A	1231.4	N/A	1799.8	N/A
66% site	1	3814.9	0.6	1115.2	2.4	2940.3	0.0	2704.7	0.4
	0.4*	3818.7	0.7	1100.6	1.1	2957.0	0.5	2719.8	0.9
	0.2	3798.0	0.2	1092.0	0.3	2945.7	0.2	2701.7	0.2
	0.1	3791.5	N/A	1088.9	N/A	2941.0	N/A	2695.2	N/A

Diff. indicates the percentage difference in each stiffness from the value computed with a cubic element size of 0.1 mm

k_{comp} compressive stiffness, k_{shear} shear stiffness, $k_{torsion}$ torsional stiffness, k_{bend} bending stiffness

*Original element size of FE models

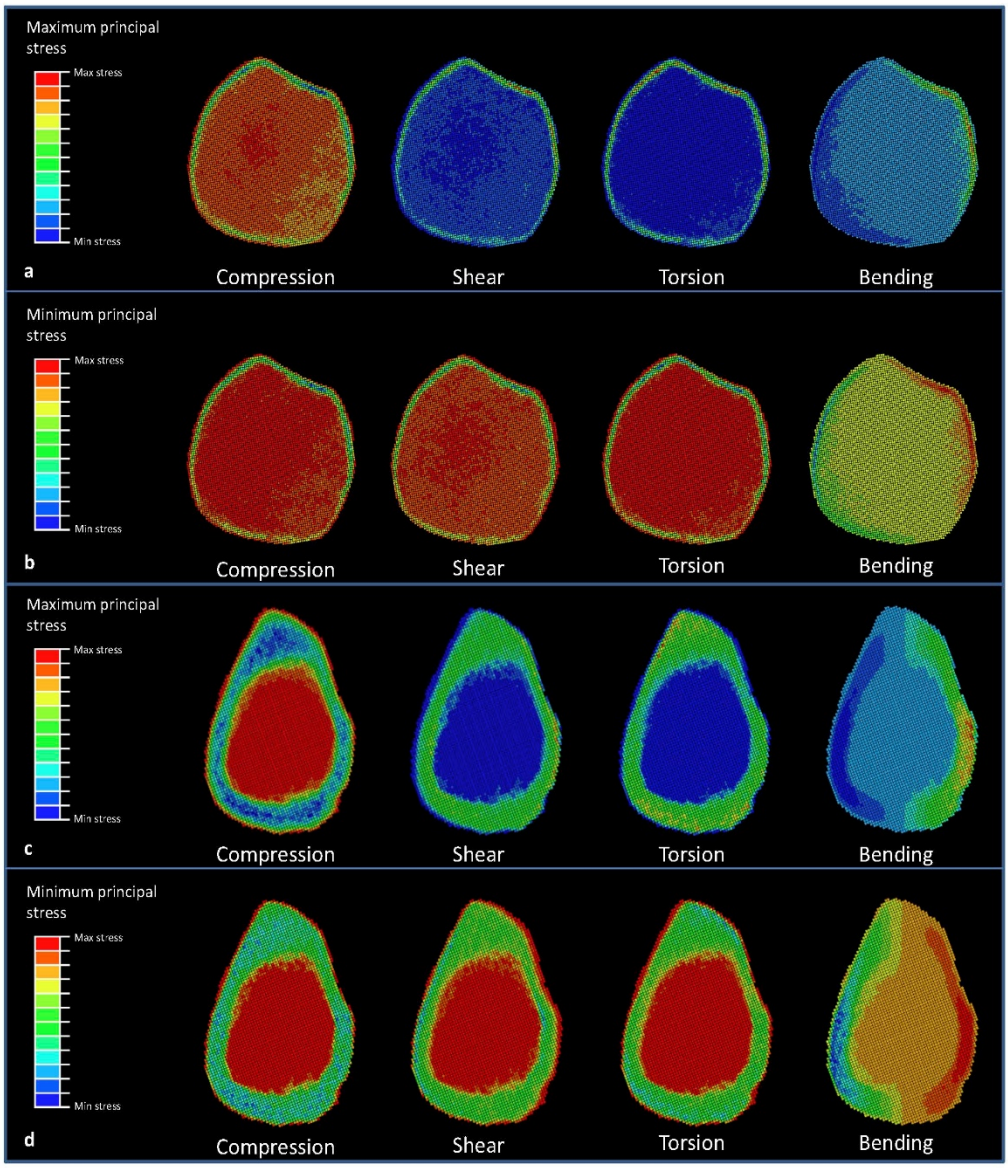

Fig. 5 Principal stresses predicted for compression, shear, torsion and bending predicted by the FE model at the 4 and 66% sites of a representative control participant. **a** Maximum principal stress predicted for each load case at the 4% site. **b** Minimum principal stress predicted for each load case at the 4% site. **c** Maximum principal stress predicted for each load case at the 66% site. **d** Minimum principal stress predicted for each load case at the 66% site. Due to significantly different stresses for each load case, the contours are expressed relative to the maximum and minimum stresses

At the 4% site, all structural and FE model properties differed significantly ($p < 0.05$) between the control and fracture groups (Table 4). Considering the pQCT variables, only ρ_{tot} differed significantly between the two groups at the 4% site ($p = 0.002$). No variables were observed to differ significantly between the controls and fracture group at

the 66% site. There was no significant difference observed between the two groups for the aBMDs derived using DXA. Box and whisker plots of key variables of each imaging modality (i.e. DXA, pQCT, structural and FE model properties) are provided in Fig. 6, which illustrates the distribution of variables between the controls and fracture group.

Based upon the linear multivariate regressions for the DXA, pQCT, structural and FE model properties, the VIFs for age, height and weight were less than 5.0 for all groups and sites (Table 5), indicating there was no collinearity between these variables and the bone properties presented in the current study. For the DXA variables of the control group, aBMD for the femoral neck and total hip each had a VIF greater than 5.0, implying collinearity between these variables. aBMD for the total hip was subsequently included in the classification analysis since it had the greatest average OR (2.98, 95% CI 1.24–7.13; Table 6). At the 4% site of both the control and fracture group, collinearity was observed between all properties within each of the pQCT, structural or FE model modalities (Table 5). Since ρ_{tot}, EA and k_{shear} had the greatest OR for each modality, these were the only variables included in the correlation analysis for the pQCT, structural and FE model properties (Table 6). Similarly, for the pQCT and FE model properties at the 66% site, the respective variables were each found to be collinear, with the SSI_x and $k_{torsion}$ properties included in the classification analysis based upon their greater ORs. However, for the structural properties at the 66% site, only EI_y and GJ were found to be collinear (Table 5). Since GJ had a greater average OR compared to EI_y, it was included in the classification analysis along with the independent variables EA and EI_x.

Considering properties derived at the 4% site and adjusting for age, weight and height, the fracture odds increased most with a decrease in k_{shear} (OR 16.09, 95% CI 2.52–102.56, $p = 0.003$) (Table 6). For variables included in the classification analysis, odds ratios that were significant ($p < 0.05$) with a mean value greater than 5.0 were also observed for the structural property EA and the pQCT property ρ_{tot}. At the 66% site, the odds of fracture were not significantly related to any of pQCT, structural or FE model properties included in the classification analysis. In the case of DXA, the odds ratio was significant for aBMD of the total hip (OR 2.98, 95% CI 1.24–7.13, $p = 0.01$).

The greatest AUC was observed at the 4% site for the FE model property k_{shear} (AUC: 0.81, 95% CI 0.69–0.94). Youden's J statistic was greatest for this variable, indicating the optimal combination of sensitivity and specificity (78.3 and 82.6%, respectively). AUCs of a similar magnitude were observed at the 4% site for the structural property EA (AUC: 0.80, 95% CI 0.67–0.93) and the pQCT property ρ_{tot} (AUC: 0.80, 95% CI 0.67–0.93). The greatest AUC observed for the DXA properties was aBMD for the total hip (AUC: 0.71, 95% CI 0.56–0.86). The AUCs observed at the 66% site provided a poor classification between the controls and fracture group, with mean values between 0.61 and 0.65.

4 Discussion

In this study, an FE model based on pQCT was proposed and its diagnostic ability to identify patients who had recently sustained a low-trauma fracture was compared with structural properties and clinical pQCT and DXA properties. For this analysis, pQCT scans of the tibial epiphysis and diaphysis were obtained for two groups of post-menopausal women; a group who had recently sustained a low-trauma fracture at another skeletal site (fracture group) and an age-matched group with no history of tibial fracture and at the time of this study were considered to be at low risk of incurring a low-trauma fracture (control group). The properties of the intact tibia were assumed to be representative of each subject's current skeletal health, which was hypothesised to be deficient in the fracture group.

Whilst FE models based on individual bone cross sections from pQCT imaging have been previously developed (Kourtis et al. 2008), to our knowledge, this is the first study to (1) use these techniques to assess fracture status in vivo and (2) compare its diagnostic performance with existing fracture risk assessment methods. The FE model property k_{shear} had the greatest OR (16.09; 95% CI 2.52–102.56) and AUC (0.81; 95% CI 0.69–0.94), indicating this variable had the greatest probability to correctly differentiate the fracture group from the control group. The diagnostic characteristics were marginally lower for the structural property EA (OR 10.51; 95% CI 2.07–53.44) (AUC: 0.80; 95% CI 0.67–0.93) and the pQCT property ρ_{tot} (OR 12.86; 95% CI 2.51–65.76) (AUC: 0.80; 95% CI 0.67–0.93). For DXA, aBMD obtained for the total hip had a lower, yet still significant, diagnostic performance (OR 2.98; 95% CI 1.24–7.13) (AUC: 0.71, 95% CI 0.56–0.86). The stress–strain indices used in clinical pQCT imaging had significantly reduced performance compared with the aforementioned variables, with ORs less than 2.02 and an AUC of 0.65, 95% CI 0.49–0.81. The trabecular-dominant distal tibial epiphysis yielded enhanced predictions of fracture status compared with the diaphysis. This suggests that trabecular bone properties are more sensitive than cortical bone properties for identifying fracture risk, a finding supported by others (Melton et al. 2010; Eser et al. 2005).

These findings suggest that simple pQCT measurements (ρ_{tot}) and predictions of bone stiffness obtained using FE modelling may be used to add to the diagnostic accuracy of DXA. Whilst this finding is consistent with others who compared pQCT, HR-pQCT and/or QCT to DXA in fragility and radial fracture assessment (Liu et al. 2012; Boutroy et al. 2008; Jamal et al. 2006; Li et al. 2013), it is acknowledged that DXA is not typically recommended for early

Table 3 Calculation of compressive, shear, torsional and bending stiffness at the 4 and 66% sites for a representative participant of the control group

Load case	4% site		66% site	
	Reaction force or moment	Stiffness	Reaction force or moment	Stiffness
Compression	12,514.5 N	1251.5 kN/mm	38,129.1 N	3812.9 kN/mm
Shear	3430.2 N	343.0 kN/mm	10,984.9 N	1098.5 kN/mm
Torsion	7.1 Nm	1238.0 Nm/°	16.9 Nm	2952.5 Nm/°
Bending	10.4 Nm	1816.9 Nm/°	15.5 Nm	2709.5 Nm/°

Table 4 DXA, pQCT, structural and FE model properties derived for the control and fracture groups

Variable	Control Group (N = 23)	Fracture Group (N = 23)	*p* value
DXA properties			
aBMD lumbar spine (mg/cm^2)	964.8 ± 201.9	874.8 ± 139.8	0.096
aBMD femoral neck (mg/cm^2)	732.9 ± 119.7	679.1 ± 94.6	0.593
aBMD total hip (mg/cm^2)	907.2 ± 167.1	788.3 ± 116.2	0.593

Variable	4% site			66% site		
	Control group (N = 23)	Fracture group (N = 23)	*p* value	Control group (N = 23)	Fracture group (N = 23)	*p* value
pQCT properties						
a_{tot} (mm^2)	1132.8 ± 184.3	1181.3 ± 162.0	0.360	571.9 ± 62.4	552.3 ± 96.9	0.593
ρ_{tot} (mg/cm^3)	279.8 ± 55.2	222.7 ± 38.9	0.002	622.6 ± 100.1	617.2 ± 110.9	0.842
SSI_x (mm^2)	405.5 ± 216.8	317.2 ± 184.9	0.195	1527.9 ± 212.3	1377.3 ± 289.5	0.195
SSI_y (mm^2)	225.9 ± 188.3	143.5 ± 152.8	0.360	879.7 ± 165.9	794.9 ± 175.9	0.195
SSI_{pol} (mm^2)	547.9 ± 360.0	388.8 ± 296.0	0.195	2128.2 ± 330.2	1917.0 ± 407.5	0.360
Structural properties						
EA (10^6 N)	1.8 ± 0.5	1.3 ± 0.4	0.002	5.5 ± 1.0	5.1 ± 1.0	0.195
GJ (N/m)	152.9 ± 38.6	118.2 ± 31.9	<0.001	298.9 ± 60.4	265.7 ± 71.9	0.360
EI_x (N/m)	221.5 ± 57.5	170.9 ± 44.1	<0.001	547.3 ± 102.7	483.6 ± 137.1	0.360
EI_y (N/m)	175.5 ± 44.8	136.1 ± 39.5	0.006	228.3 ± 64.6	205.7 ± 58.8	0.593
Finite element model properties						
k_{comp} (kN/mm)	1148.8 ± 325.1	821.0 ± 233.4	<0.001	3361.7 ± 671.8	3125.6 ± 668.0	0.195
k_{shear} (kN/mm)	318.2 ± 92.6	221.8 ± 64.9	<0.001	963.8 ± 198.4	896.4 ± 197.3	0.195
$k_{torsion}$ (Nm/°)	1279.9 ± 328.8	977.5 ± 273.0	<0.001	2532.1 ± 517.1	2240.4 ± 611.5	0.360
k_{bend} (Nm/°)	1871.4 ± 484.7	1430.2 ± 411.3	<0.001	2386.1 ± 689.6	2144.4 ± 621.5	0.593

Values are specified where applicable for the 4 and 66% sites of the tibia

aBMD areal bone mineral density, a_{tot} total area, ρ_{tot} total density, SSI_x and SSI_y stress–strain indices about the *x*- and y-axes, respectively, SSI_{pol} torsional stress–strain index, *EA* axial rigidity, EI_x and EI_y bending rigidity about the *x*- and y-axes, respectively, *GJ* torsional rigidity, k_{comp} compressive stiffness, k_{shear} shear stiffness, $k_{torsion}$ torsional stiffness, k_{bend} bending stiffness

Significant differences between the groups were assessed by a two-sample Kolmogorov–Smirnov test

post-menopausal women aged less than 60 years, unless they possess a clinical risk factor (Kanis et al. 2013; Cummings et al. 2002). Although the low-trauma fractures sustained by the fracture group patients are a well-established risk factor that improves the sensitivity of fracture prediction using DXA (Kanis et al. 2007), this was not the case for the control subjects, who did not present with any apparent fracture risks. Hence, a reduced fracture risk sensitivity would be expected for the controls using DXA, which would explain its reduced

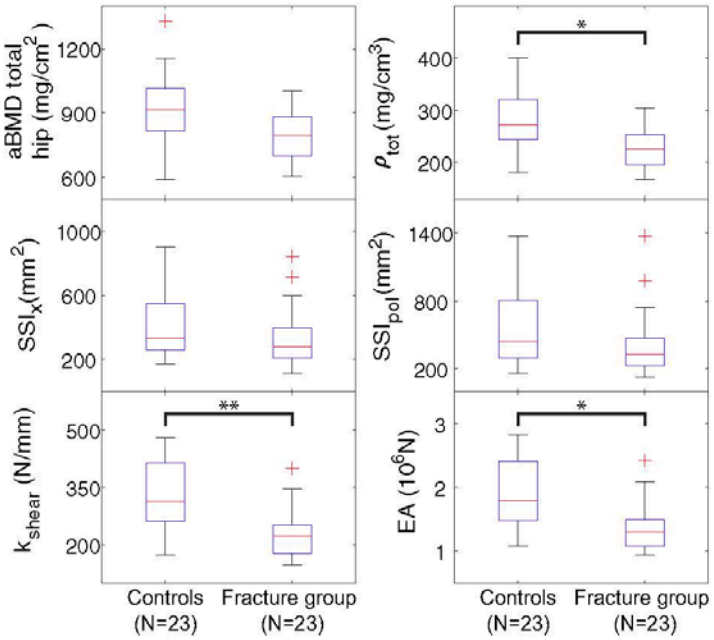

Fig. 6 Box and whisker plot of key pQCT, FE model structural and DXA properties compared between the controls and fracture group. Variables include aBMD total hip, areal bone mineral density measured for the total hip by DXA; ρ_{tot}, total density obtained by pQCT at the 4% site; SSI_x, stress–strain index about the x-axis at the 4% site; SSIpol, polar stress–strain index at the 4% site; k_{shear}, shear stiffness at the 4% site; EA, axial rigidity at the 4% site. The red line represents the median, the edges of the box are the 25th and 75th percentiles, and the whiskers extend to the maximum and minimum of the data. Red crosses indicate outliers in the data. $^{*}p < 0.05$; $^{**}p < 0.001$

diagnostic accuracy compared with the other modalities considered in the current study.

The classification performance obtained for the structural and FE-derived properties also supports previous findings that other bone properties exist that better correlate with fracture properties compared with stress–strain indices (Kontulainen et al. 2008). In this study, the differences between the groups appeared best characterised by differences in the trabecular bone, which may explain the poor diagnostic performance of the stress–strain indices, since they are calculated based solely on the density and distribution of cortical bone. This effect may have also reduced the diagnostic performance of the DXA-derived aBMD measurements, since the imaging sites have proportionally greater amounts of cortical bone compared with the tibial epiphysis.

This study had limitations that are acknowledged. The generalisation of the findings in this study may be limited by the low number of subjects in the control and fracture group. The number of participants was motivated by the intentions of this work, specifically to present the FE modelling framework and to examine whether the classification characteristics of this model appeared to classify fracture risk favourably, albeit for a relative small sample of subjects. In future work, we intend to re-evaluate the classification characteristics of all presented bone properties across a much larger cohort.

The distribution of fracture sites across the fracture group patients was inhomogeneous, with a number of different upper or lower limb fractures observed. These fracture sites were a consequence of the recruitment of low-trauma fracture patients from a fracture liaison service, a cohort which predominately comprise peripheral fractures, as compared to the prevalence of hip and vertebral fractures typically encountered for osteoporotic fracture groups (Premaor et al. 2009; McLellan et al. 2003; Cummings and Melton 2002). However, given that pQCT specifically images the peripheral skeleton, it would be suggested that the prediction of fracture risk based on FE-derived bone properties is ideal for predicting fracture risk in cohorts with increased limb fracture prevalence, as considered in the current study. When further considering the different fracture sites, it is feasible that the seven patients who sustained a low-trauma lower limb fracture may have experienced bone remodelling of their intact tibia due to the loss in mobility and change in loading experienced following the injury. Compared with the bone remodelling cycle of 120–200 days (Eriksen 2010), it is feasible that some remodelling may have taken place from post-fracture to pQCT imaging, which for these patients was on average 64.4 days (range 30–88 days). However, there were no significant differences observed between fracture group patients with and without a lower limb fracture (Supplementary material Table 2), which would support the reasoning that any changes in bone structure due to different post-fracture tibial loadings between subjects were minor and considered unlikely to alter the findings of the current study.

Table 5 Variance inflation factor (VIF) of DXA, pQCT, structural and FE model properties derived for the control and fracture groups

Modality	Variable	VIF	
		Control group ($N = 23$)	Fracture group ($N = 23$)
DXA properties	Age	1.4	1.2
	Height	1.6	1.4
	Weight	2.3	1.5
	aBMD lumbar spine	4.1	1.4
	aBMD femoral neck	11.0	4.0
	aBMD total hip	16.7	3.7

Modality	Variable	VIF, 4% site		VIF, 66% site	
		Control group ($N = 23$)	Fracture group ($N = 23$)	Control group ($N = 23$)	Fracture group ($N = 23$)
pQCT properties	Age	1.9	1.6	1.6	1.4
	Height	2.2	2.1	1.9	1.9
	Weight	2.0	2.3	3.0	1.5
	a_{tot}	5.2	6.9	55.3	44.9
	ρ_{tot}	5.1	6.4	56.7	21.4
	SSI_x	31.8	103.1	18.1	37.8
	SSI_y	83.4	281.5	38.7	20.6
	SSI_{pol}	143.4	671.3	101.8	77.2
Structural properties	Age	1.3	1.4	1.2	1.2
	Height	1.8	1.7	1.6	2.1
	Weight	2.3	1.5	1.7	1.2
	EA	5.6	12.9	2.9	2.7
	GJ	15.1	30.1	8.5	8.2
	EI_x	9.4	32.3	2.3	2.8
	EI_y	13.1	18.3	5.8	5.9
Finite element model properties	Age	2.9	1.4	1.3	1.3
	Height	2.3	1.7	1.6	2.3
	Weight	3.3	1.4	2.1	1.6
	k_{comp}	2298.6	441.6	5398.2	3753.6
	k_{shear}	2301.5	419.6	5311.0	3548.2
	$k_{torsion}$	39.4	80.1	21.3	34.3
	k_{bend}	35.7	56.3	21.5	18.5

Values are specified where applicable for the 4% and 66% imaging sites of the tibia
aBMD areal bone mineral density, a_{tot} total area, ρ_{tot} total density, SSI_x and SSI_y stress–strain indices about the *x*- and y-axes, respectively, SSI_{pol} torsional stress–strain index, *EA* axial rigidity, EI_x and EI_y bending rigidity about the *x*- and y-axes, respectively, *GJ* torsional rigidity, k_{comp} compressive stiffness, k_{shear} shear stiffness, $k_{torsion}$ torsional stiffness, k_{bend} bending stiffness

Another evident issue is whether the fracture status of each subject was truly related to the structural properties at two discrete locations of the intact tibia. Whilst these sites are useful for comparing differences in cortical and trabecular bone structures at a consistent location, their ability to predict skeletal fracture risk relies on the assumption of uniform structural changes throughout the body. In reality, bone loss associated with ageing or osteoporosis is not uniform across the body (Hansen et al. 1995; Arlot et al. 1997). By acquiring pQCT scans at other locations such as the contralateral tibia or the forearms, the extent of the inhomogeneity may be evaluated and possibly used to improve the diagnostic performance of the methods presented in the current study. We note, however, that previous longitudinal data have shown the tibia to be a reasonable predictor for all types of fragility fractures, including vertebrae, ribs or the appendicular skeleton (Vilayphiou et al. 2011).

Table 6 Odds ratio, sensitivity, specificity and area under curve (AUC) of receiver operative characteristic curve derived for DXA, pQCT, structural and FE model properties[a,b]

Imaging modality	Variable	Odds ratio (95% CI)	Sensitivity (%)	Specificity (%)	AUC (95% CI)
DXA properties	aBMD lumbar spine	**1.77 (0.84–3.72)**	**43.48**	**91.30**	**0.64 (0.48–0.81)**
	aBMD femoral neck	1.65 (0.78–3.48)	–	–	–
	aBMD total hip	**2.98 (1.24–7.13)***	**82.61**	**56.52**	**0.71 (0.56–0.86)**

Imaging modality	Variable	4%				66%			
		Odds ratio (95% CI)	Sensitivity (%)	Specificity (%)	AUC (95% CI)	Odds ratio	Sensitivity (%)	Specificity (%)	AUC (95% CI)
pQCT properties	a_{tot}	1.97 (0.88–4.42)	–	–	–	1.07 (0.54–2.15)	–	–	–
	ρ_{tot}	**12.86 (2.51–65.76)****	**73.91**	**78.26**	**0.80 (0.67–0.93)**	1.05 (0.56–1.97)	–	–	–
	SSI_x	1.88 (0.82–4.29)	–	–	–	**2.02 (0.80–5.08)**	**82.61**	**47.83**	**0.65 (0.49–0.81)**
	SSI_y	1.86 (0.84–4.13)	–	–	–	1.63 (0.72–3.69)	–	–	–
	SSI_{pol}	1.93 (0.85–4.37)	–	–	–	1.89 (0.79–4.51)	–	–	–
Structural properties	EA	**10.51 (2.07–53.44)****	**73.91**	**78.26**	**0.80 (0.67–0.93)**	**1.34 (0.62–2.91)**	**39.13**	**91.30**	**0.61 (0.44–0.77)**
	GJ	6.70 (1.62–27.74)*	–	–	–	**1.64 (0.68–3.92)**	**47.83**	**78.26**	**0.63 (0.46–0.79)**
	EI_x	6.44 (1.61–25.81)*	–	–	–	**1.72 (0.70–4.21)**	**65.22**	**60.87**	**0.63 (0.47–0.80)**
	EI_y	5.78 (1.55–21.57)**				–	–	–	
Finite element model properties	k_{comp}	13.46 (2.32–77.97)**	–	–	–	1.33 (0.61–2.87)	–	–	–
	k_{shear}	**16.09 (2.52–102.56)****	**78.26**	**82.61**	**0.81 (0.69–0.94)**	1.31 (0.61–2.81)	–	–	–
	$k_{torsion}$	7.34 (1.69–31.88)**	–	–	–	**1.69 (0.7–4.06)**	**47.83**	**78.26**	**0.63 (0.47–0.79)**
	k_{bend}	6.80 (1.68–27.52)**	–	–	–	1.32 (0.62–2.80)	–	–	–

Values are specified where applicable for the 4% and 66% imaging sites of the tibia

a_{tot} total area, ρ_{tot} total density, SSI_x and SSI_y stress–strain indices about the x- and y-axes, respectively, SSI_{pol} torsional stress–strain index, EA axial rigidity, EI_x and EI_y bending rigidity about the x- and y-axes, respectively, k_{shear} shear stiffness, $k_{torsion}$ torsional stiffness. Bold text, data for variables included in the classification analysis, based on their collinearity assessment and greater odds ratio

[a]Adjusted for age, height and weight

[b]Significance of odds ratio tested with respect to null hypothesis (i.e. classification based on chance)

*$p < 0.05$

**$p < 0.01$

A final limitation was that the loads applied in the FE model would differ from those encountered by tibiae in vivo. For example, the knee joint experiences both forces and bending moments that each change magnitude and direction during daily activities (Kutzner et al. 2010). However, musculoskeletal loadings vary significantly between individuals (Heller et al. 2001; Rohlmann et al. 2014; Kutzner et al. 2010), and obtaining these correct loading combinations for a large number of patients would not be feasible in a clinical setting. Therefore, idealising the loading conditions was the only practical option available and adequately met the aims of our study since the classification analysis only considered differences in bone properties between the control and fracture groups.

In summary, we have demonstrated that FE models of individual pQCT cross sections are likely to enhance diagnosis of fracture status compared with stress–strain indices used in pQCT image and aBMD measurements derived using DXA. Whilst it is feasible to apply these methods in prospective fracture risk diagnosis, caution should be exercised when generalising the findings of our study since it was cross sectional in design and based on outcomes for a small number of relatively young subjects where DXA is known to be less sensitive for fracture risk assessment (Kanis et al. 2013). Hence, longitudinal data for a larger and, ideally, older cohort of patients are needed to confirm the outcomes based on our assessment of fracture status. Nevertheless, we would recommend caution when using pQCT properties such as SSIs for fracture risk prediction because our results suggest more accurate variables are available such as bone properties derived from FE modelling or structural analysis.

Acknowledgements We thank all participants for consenting to provide their pQCT tibia scan data for this study. We duly acknowledge Ashwini Kale for diligently performing all pQCT scans, Richard Farrugia for facilitating patient recruitment and clinic coordination activities and Associate Professor Andrew Bucknill for his strong support of the Royal Melbourne Hospital fracture liaison service. This work was supported by a collaborative PhD scholarship provided by the University of Melbourne and the China Scholarship Council to HJ.

References

Amin S, Kopperdhal DL, Melton LJ, Achenbach SJ, Therneau TM, Riggs BL, Keaveny TM, Khosla S (2011) Association of hip strength estimates by finite-element analysis with fractures in women and men. J Bone Miner Res 26(7):1593–1600

Ammann P, Rizzoli R (2003) Bone strength and its determinants. Osteoporos Int 14(S3):13–18

Arlot ME, Sornay-Rendu E, Garnero P, Vey-Marty B, Delmas PD (1997) Apparent pre- and postmenopausal bone loss evaluated by DXA at different skeletal sites in women: the OFELY cohort. J Bone Miner Res 12(4):683–690

Ashe MC, Khan KM, Kontulainen SA, Guy P, Liu D, Beck TJ, McKay HA (2006) Accuracy of PQCT for evaluating the aged human radius: an ashing, histomorphometry and failure load investigation. Osteoporos Int 17(8):1241–1251

Boutroy S, Van Rietbergen B, Sornay-Rendu E, Munoz F, Bouxsein ML, Delmas PD (2008) Finite element analysis based on in vivo HR-PQCT images of the distal radius is associated with wrist fracture in postmenopausal women. J Bone Miner Res 23(3):392–399

Briggs AM, Perilli E, Parkinson IH, Wrigley TV, Fazzalari NL, Kantor S, Wark JD (2010) Novel assessment of subregional bone mineral density using DXA and PQCT and subregional microarchitecture using micro-CT in whole human vertebrae: applications, methods, and correspondence between technologies. J Clin Densitom 13(2):161–174

Cummings SR, Melton LJ (2002) Osteoporosis I: epidemiology and outcomes of osteoporotic fractures. Lancet 359(9319):1761–1767

Cummings SR, Bates D, Black DM (2002) Clinical use of bone densitometry: scientific review. JAMA 288(15):1889–1897

Doube M, Kłosowski M, Arganda-Carreras I, Cordelières FP, Dougherty RP, Jackson JS, Schmid B, Hutchinson JR, Shefelbine SJ (2010) BoneJ: free and extensible bone image analysis in ImageJ. Bone 47(6):1076–1079

Dragomir-Daescu D, Op Den Buijs J, McEligot S, Dai Y, Entwistle RC, Salas C, Melton LJ, Bennet KE, Khosla S, Amin S (2011) Robust QCT/FEA models of proximal femur stiffness and fracture load during a sideways fall on the hip. Ann Biomed Eng 39(2):742–755

Duckham RL, Frank AW, Johnston JD, Olszynski WP, Kontulainen SA (2013) Monitoring time interval for PQCT-derived bone outcomes in postmenopausal women. Osteoporos Int 24(6):1917–1922

Duckham RL, Baxter-Jones ADG, Johnston JD, Vatanparast H, Cooper D, Kontulainen S (2014) Does physical activity in adolescence have site-specific and sex-specific benefits on young adult bone size, content, and estimated strength? J Bone Miner Res 29(2):479–486

Engelke K, Adams JE, Armbrecht G, Augat P, Bogado CE, Bouxsein ML, Felsenberg D, Ito M, Prevrhal S, Hans DB, Lewiecki EM (2008) Clinical use of quantitative computed tomography and peripheral quantitative computed tomography in the management of osteoporosis in adults: the 2007 ISCD official positions. J Clin Densitom 11(1):123–162

Eriksen EF (2010) Cellular mechanisms of bone remodeling. Rev Endocr Metab Disord 11(4):219–227

Erlandson MC, Kontulainen SA, Chilibeck PD, Arnold CM, Faulkner RA, Baxter-Jones ADG (2012) Former premenarcheal gymnasts exhibit site-specific skeletal benefits in adulthood after long-term retirement. J Bone Miner Res 27(11):2298–2305

Eser P, Frotzler A, Zehnder Y, Denoth J (2005) Fracture threshold in the femur and tibia of people with spinal cord injury as determined by peripheral quantitative computed tomography. Arch Phys Med Rehabil 86(3):498–504

Hansen MA, Overgaard K, Christiansen C (1995) Spontaneous postmenopausal bone loss in different skeletal areas—followed up for 15 years. J Bone Miner Res 10(2):205–210

Heller MO, Bergmann G, Deuretzbacher G, Dürselen L, Pohl M, Claes L, Haas NP, Duda GN (2001) Musculo-skeletal loading conditions at the hip during walking and stair climbing. J Biomech 34(7):883–893

Jamal SA, Gilbert J, Gordon C, Bauer DC (2006) Cortical PQCT measures are associated with fractures in dialysis patients. J Bone Miner Res 21(4):543–548

Johnell O, Kanis JA (2006) An estimate of the worldwide prevalence and disability associated with osteoporotic fractures. Osteoporos Int 17(12):1726–1733

Kanis JA (2002) Osteoporosis III: diagnosis of osteoporosis and assessment of fracture risk. Lancet 359(9321):1929–1936

Kanis JA, Oden A, Johnell O, Johansson H, De Laet C, Brown J, Burckhardt P, Cooper C, Christiansen C, Cummings S, Eisman JA, Fujiwara S, Glüer C, Goltzman D, Hans D, Krieg MA, La Croix A,

McCloskey E, Mellstrom D, Melton LJ, Pols H, Reeve J, Sanders K, Schott AM, Silman A, Torgerson D, Van Staa T, Watts NB, Yoshimura N (2007) The use of clinical risk factors enhances the performance of BMD in the prediction of hip and osteoporotic fractures in men and women. Osteoporos Int 18(8):1033–1046

Kanis JA, McCloskey EV, Johansson H, Cooper C, Rizzoli R, Reginster JY (2013) European guidance for the diagnosis and management of osteoporosis in postmenopausal women. Osteoporos Int 24(1):23–57

Kawalilak CE, Kontulainen SA, Amini MA, Lanovaz JL, Olszynski WP, Johnston JD (2016) In vivo precision of three HR-PQCT-derived finite element models of the distal radius and tibia in postmenopausal women. BMC Musculoskelet Disord 17(1):1–11

Keyak JH, Rossi SA, Jones KA, Skinner HB (1997) Prediction of femoral fracture load using automated finite element modelling. J Biomech 31(2):125–133

Koivumäki JEM, Thevenot J, Pulkkinen P, Kuhn V, Link TM, Eckstein F, Jämsä T (2012) Ct-based finite element models can be used to estimate experimentally measured failure loads in the proximal femur. Bone 50(4):824–829

Kontulainen SA, Johnston JD, Liu D, Leung C, Oxland TR, McKay HA (2008) Strength indices from PQCT imaging predict up to 85% of variance in bone failure properties at tibial epiphysis and diaphysis. J Musculoskelet Neuronal Interact 8(4):401–409

Kourtis LC, Carter DR, Kesari H, Beaupre GS (2008) A new software tool (VA-BATTS) to calculate bending, axial, torsional and transverse shear stresses within bone cross sections having inhomogeneous material properties. Comput Methods Biomech Biomed Eng 11(5):463–476

Kutzner I, Heinlein B, Graichen F, Bender A, Rohlmann A, Halder A, Beier A, Bergmann G (2010) Loading of the knee joint during activities of daily living measured in vivo in five subjects. J Biomech 43(11):2164–2173

Lalkhen AG, McCluskey A (2008) Clinical tests: sensitivity and specificity. Contin Educ Anaesth Crit Care Pain 8(6):221–223

Li N, Li X, Xu L, Sun W, Cheng X, Tian W (2013) Comparison of QCT and DXA: osteoporosis detection rates in postmenopausal women. Int J Endocrinol. https://doi.org/10.1155/2013/895474

Liu XS, Zhang XH, Sekhon KK, Adams MF, McMahon DJ, Bilezikian JP, Shane E, Guo XE (2010) High-resolution peripheral quantitative computed tomography can assess microstructural and mechanical properties of human distal tibial bone. J Bone Miner Res 25(4):746–756

Liu XS, Stein EM, Zhou B, Zhang CA, Nickolas TL, Cohen A, Thomas V, McMahon DJ, Cosman F, Nieves J et al (2012) Individual trabecula segmentation (ITS)-based morphological analyses and microfinite element analysis of HR-PQCT images discriminate postmenopausal fragility fractures independent of DXA measurements. J Bone Miner Res 27(2):263–272

Lochmüller E-M, Lill CA, Kuhn V, Schneider E, Eckstein F (2002) Radius bone strength in bending, compression, and falling and its correlation with clinical densitometry at multiple sites. J Bone Miner Res 17(9):1629–1638

McLellan AR, Gallacher SJ, Fraser M, McQuillian C (2003) The fracture liaison service: success of a program for the evaluation and management of patients with osteoporotic fracture. Osteoporos Int 14(12):1028–1034

Melton LJ, Christen D, Riggs BL, Achenbach SJ, Müller R, Van Lenthe GH, Amin S, Atkinson EJ, Khosla S (2010) Assessing forearm fracture risk in postmenopausal women. Osteoporos Int 21(7):1161–1169

Morgan EF, Bayraktar HH, Keaveny TM (2003) Trabecular bone modulus-density relationships depend on anatomic site. J Biomech 36(7):897–904

Muller ME, Webber CE, Bouxsein ML (2003) Predicting the failure load of the distal radius. Osteoporos Int 14(4):345–352

Nazrun AS, Tzar MN, Mokhtar SA, Mohamed IN (2014) A systematic review of the outcomes of osteoporotic fracture patients after hospital discharge: morbidity, subsequent fractures, and mortality. Ther Clin Risk Manag 10:937–948

Nishiyama KK, Shane E (2013) Clinical imaging of bone microarchitecture with HR-PQCT. Curr Osteoporos Rep 11(2):147–155

Nishiyama KK, Macdonald HM, Hanley DA, Boyd SK (2013) Women with previous fragility fractures can be classified based on bone microarchitecture and finite element analysis measured with HR-PQCT. Osteoporos Int 24(5):1733–1740

Pistoia W, van Rietbergen B, Lochmüller E-M, Lill CA, Eckstein F, Rüegsegger P (2002) Estimation of distal radius failure load with micro-finite element analysis models based on three-dimensional peripheral quantitative computed tomography images. Bone 30(6):842–848

Premaor MO, Pilbrow L, Tonkin C, Adams M, Parker RA, Compston J (2009) Low rates of treatment in postmenopausal women with a history of low trauma fractures: results of audit in a fracture liaison service. QJM 103(1):33–40

Rinaldi G, Wisniewski CA, Setty NG, LeBoff MS (2011) Peripheral quantitative computed tomography: optimization of reproducibility measures of bone density, geometry, and strength at the radius and tibia. J Clin Densitom 14(3):367–373

Ringle CM, Wende S, Becker J-M (2015) SmartPLS 3. Boenningstedt SmartPLS GmbH. www.smartpls.com. Accessed 9 July 2018

Rohlmann A, Pohl D, Bender A, Graichen F, Dymke J, Schmidt H, Bergmann G (2014) Activities of everyday life with high spinal loads. PLoS ONE 9(5):1–10

Sattui SE, Saag KG (2014) Fracture mortality: associations with epidemiology and osteoporosis treatment. Nat Rev Endocrinol 10(10):592–602

Schuit SC, van der Klift M, Weel AEA, de Laet CED, Burger H, Seeman E, Hofman A, Uitterlinden A, van Leeuwen JPT, Pols HA (2004) Fracture incidence and association with bone mineral density in elderly men and women: the Rotterdam study. Bone 34(1):195–202

Seeman E, Delmas PD (2006) Bone quality—the material and structural basis of bone strength and fragility. N Engl J Med 354(21):2250–2261

Siris ES, Miller PD, Barrett-Connor E, Faulkner KG, Wehren LE, Abbott TA, Berger ML, Santora AC, Sherwood LM (2001) Identification and fracture outcomes of undiagnosed low bone mineral density in postmenopausal women: results from the national osteoporosis risk assessment. JAMA 286(22):2815–2822

Snyder BD, Hauser-Kara DA, Hipp JA, Zurakowski D, Hecht AC, Gebhardt MC (2006) Predicting fracture through Benign skeletal lesions with quantitative computed tomography. J Bone Jt Surg 88–A(1):55–70

Snyder BD, Cordio MA, Nazarian A, Kwak SD, Chang DJ, Entezari V, Zurakowski D, Parker LM (2009) Noninvasive prediction of fracture risk in patients with metastatic cancer to the spine. Clin Cancer Res 15(24):7676–7683

Stone KL, Seeley DG, Lui L-Y, Cauley JA, Ensrud K, Browner WS, Nevitt MC, Cummings SR (2003) BMD at multiple sites and risk of fracture of multiple types: long-term results from the study of osteoporotic fractures. J Bone Min. Res 18(11):1947–1954

Thomsen JS, Laib A, Koller B, Prohaska S, Mosekilde L, Gowin W (2005) Stereological Measures of trabecular bone structure: comparison of 3D micro computed tomography with 2d histological sections in human proximal tibial bone biopsies. J Microsc 218(2):171–179

Varga P, Baumbach S, Pahr D, Zysset PK (2009) Validation of an anatomy specific finite element model of Colles' fracture. J Biomech 42(11):1726–1731

Vilayphiou N, Boutroy S, Szulc P, Van Rietbergen B, Munoz F, Delmas PD, Chapurlat R (2011) Finite element analysis performed on

radius and tibia HR-PQCT images and fragility fractures at all sites in men. J Bone Miner Res 26(5):965–973
Whealan KM, Kwak SD, Tedrow JR, Inoue K, Snyder BD (2000) Non-invasive imaging predicts failure load of the spine with simulated osteolytic defects. J Bone Joint Surg Am 82(9):1240–1251
Yang PF, Sanno M, Ganse B, Koy T, Brüggemann GP, Müller LP, Rittweger J (2014) Torsion and antero-posterior bending in the in vivo human tibia loading regimes during walking and running. PLoS ONE 9(4):e94525
Yates CJ, Chauchard MA, Liew D, Bucknill A, Wark JD (2015) Bridging the osteoporosis treatment gap: performance and cost-effectiveness of a fracture liaison service. J Clin Densitom 18(2):150–156
Youden WJ (1950) Index for rating diagnostic tests. Cancer 3(1):32–35
Zysset PK, Dall' Ara E, Varga P, Pahr DH (2013) Finite element analysis for prediction of bone strength. Bonekey Rep 2(AUGUST):1–9

Appendix 3 pQCT precision data

The radius and the tibia of each participant were scanned by two qualified technologists, and the first technologist again. All scans were analysed by them separately. All scans and analysis were performed in line with the standard protocol detailed in Section 3.4. Inter-rater and intra-rater reliability are summarised in Table A3.1. Precision error and least significant changes for each pQCT-FEA variable are summarised in Table A3.2.

Table A3.1 Inter-rater and intra-rater reliability of pQCT-FEA variables

Limb	Site	Variable	Inter-rater reliability	Intra-rater reliability
Radius (n = 9 except for * where n = 8)	4%	k_{comp}	0.770	0.849
		k_{shear}	0.800	0.877
		$k_{torsion}$	0.913	0.918
		k_{bend}	0.951	0.918
	66%	k_{comp}	0.957	0.983 *
		k_{shear}	0.953	0.982 *
		$k_{torsion}$	0.982	0.980 *
		k_{bend}	0.974	0.971 *
Tibia (n = 10)	4%	k_{comp}	0.998	0.997
		k_{shear}	0.998	0.997
		$k_{torsion}$	0.998	0.998
		k_{bend}	0.999	0.999
	66%	k_{comp}	0.999	0.999
		k_{shear}	0.999	0.999
		$k_{torsion}$	0.999	0.999
		k_{bend}	0.998	0.999

Table A3.2 Precision errors and least significant changes of pQCT-FEA variables

Limb	Site	Variable	RMS-SD	RMS-%CV	LSC-SD	LSC-%CV
Radius	4%	k_{comp}	18.13	21.4	50.23	0.593
		k_{shear}	4.23	18.7	11.72	51.7
		$k_{torsion}$	6.99	14.5	19.35	40.1
		k_{bend}	6.44	13.3	17.83	36.9
	66%	k_{comp}	15.37	8.7	42.58	24.2
		k_{shear}	4.67	9.6	12.94	26.7
		$k_{torsion}$	3.68	10.3	10.2	28.6
		k_{bend}	6.33	12.7	17.53	35.3
Tibia	4%	k_{comp}	24.32	1.7	67.38	4.8
		k_{shear}	7.15	1.9	19.82	5.3
		$k_{torsion}$	40.99	1.9	113.54	5.4
		k_{bend}	39.14	1.6	108.41	4.5
	66%	k_{comp}	24.30	0.8	67.32	2.1
		k_{shear}	7.13	0.8	19.76	2.3
		$k_{torsion}$	45.35	1.1	125.63	3.0
		k_{bend}	61.71	1.5	170.92	4.1

RMS-SD: root mean square of standard deviation, **RMS-%CV**: root mean square of coefficient of variation (expressed in %), **LSC-SD**: least significant change in standard deviation, **LSC-%CV**: least significant change in coefficient of variation. RMS-SD and LSC-SD are expressed in the unit of the corresponding variables, which are kN/mm, kN/mm, Nm/deg and Nm/deg for k_{comp}, k_{shear}, $k_{torsion}$ and k_{bend}, respectively.